




University of
Stavanger

Faculty of Science and Technology

MASTER'S THESIS

Study program/ Specialization: Petroleum Engineering/ Well Engineering	Spring semester, 2015 <u>Open</u> / Restricted access
Writer: Albert Vafin	 (Writer's signature)
Faculty supervisor: Mesfin Agonafir Belayneh External supervisor: Oddbjørg V. Greiner	
Thesis title: Simulation - based assessment of drilling riser and its application for the Kara Sea region	
Credits (ECTS): 30	
Key words: Kara Sea, drilling riser design, riser analysis, OrcaFlex and ANSYS simulation.	Pages: 101 + enclosure: 67 and 4 on CD Stavanger: 22.06.2015

ABSTRACT

Drilling in Arctic offshore conditions is a very challenging for the oil industry. With an increase in drilling operations in these harsh environments, drilling riser requirements and limits have become more critical due to uncertainties involved in response prediction.

Hence, during planning phase, a riser assessment should be performed with the objective of selecting the right riser in terms of size, material type and grade. The main purposes of the riser analysis are to define an operational window with regards to the environmental and applied loadings that a riser can tolerate without being failed.

This Master thesis is dedicated to the assessment and analysis of the drilling riser for the application in the Kara Sea region.

The riser is assessed in accordance with ISO 13624, API RP 16Q and DNV-OS-F201 standards, whose comparison and main features are also described in the thesis.

The analysis consists of two different design loadings - static and dynamic. The design environmental loads include the wind, sea currents, and waves which are combined with the drilling rig heave, pitch, roll motions for connected (drilling) and disconnected (non-drilling) design cases to ensure that the implemented riser design is capable to withstand the most severe loads and is reliable to be used for the drilling in the Kara Sea particularly.

The dynamic and static simulations of various riser configurations are carried out by means of OrcaFlex and ANSYS software respectively. During simulations in OrcaFlex, diverse loading scenarios are considered, varying the design wave height and their corresponding periods. The analysis is also conducted with regard to several different densities of the drilling fluid. Drilling risers are analyzed and compared based on API and ISO requirements for allowable limits of the Von-Mises stress, effective tension, and maximum upper and lower flex/ball joint angles.

After gaining an understanding of risers' behavior in dynamic conditions, numerical modeling is established. A finite-element analysis in ANSYS 15.0 software is used to simulate and analyze two operational scenarios namely, normal and extreme (worst-case) conditions in the Kara Sea.

Based on the results of the analysis, this thesis work provides conclusions of the acquired findings, reasonable recommendations for the drilling riser design in arctic conditions of the Kara Sea and also indicate a potential future research areas.

ACKNOWLEDGMENTS

I would like gratefully appreciate my scientific supervisor Mesfin Agonafir Belayneh for his support and continuous help during writing of the Master's thesis. Moreover, he has helped me not only in supervising this work but also during the entire period of the Master Degree program. His patience, immense knowledge, engagement and dedicated approach on the courses of Advanced Drilling Technology and Engineering and Completion Engineering made the lectures highly accessible for me and the atmosphere was at a friendly and advanced level.

I am also thankful very much to my external supervisor Oddbjørg V. Greiner for her guidance and comments in writing this master thesis. She provided me with good and constructive feedback.

CONTENTS

ABSTRACT	II
ACKNOWLEDGMENTS.....	III
CONTENTS	IV
LIST OF FIGURES.....	VII
NOMENCLATURE	X
1. INTRODUCTION	1
1.1. Background and Problem Statement	1
1.2. Thesis Objectives.....	3
2. STANDARDS AND REGULATIONS	4
2.1. API RP 16Q.....	4
2.2. ISO 13624.....	4
2.3. COMPARISON of API RP 16Q and ISO 13624 STANDARDS	5
2.4. DNV-OS-F201.....	7
3. DESCRIPTION OF DRILLING SYSTEM	11
3.1. Surface Equipment of Riser Drilling System	12
3.1.1. Motion-compensating equipment.....	12
3.1.2. Tensioning system.....	12
3.2. Drilling Riser	13
3.2.1. Low-pressure Drilling Riser.....	13
3.2.2. Buoyancy Modules.....	14
3.2.3. Kill/Choke, Booster and Hydraulic lines	14
3.3. Lower Riser Stack	15
3.3.1. Lower Marine Riser Package (LMRP).....	15
3.3.2. Blow-Out Preventer (BOP)	15
4. FUNDAMENTAL MECHANICS OF RISER.....	17
4.1. Influence of Pressure, Tension, and Weight on the System	17
4.1.1. Internal Forces in a Submerged Body	17
4.2. Stresses in Riser.....	21
4.2.1. Radial, Hoop and Axial Stresses	21

4.2.2. Shear stress	23
4.2.3. Bending stress	24
4.3. Von-Mises Failure Criteria	25
4.4. Design Limits	26
4.5. Hydrodynamic Loads	27
4.5.1. Currents	27
4.5.2. Vortex Induced Vibrations (VIV)	28
4.5.2.1. Flow Regimes	29
4.5.2.2. VIV Mitigation Techniques	30
4.5.3. Morison's Equation	32
4.6. Sea Ice Impact	36
CHAPTER 5. ENVIRONMENTAL CONDITIONS IN THE KARA SEA	38
5.1. Geographical Location	38
5.2. Climate.....	39
5.3. Wind	40
5.4. Hydrological Conditions.....	40
5.4.1. Waves	40
5.4.2. Currents	40
5.4.3. Water Temperature.....	41
5.5. Sea Ice Conditions and Icebergs.....	42
CHAPTER 6. SIMULATION TOOLS AND ANALYSIS OF DRILLING RISER.....	43
6.1. Simulation in OrcaFlex Software	43
6.1.1. Coordinate Systems.....	44
6.1.2. Discretized Model of Line.....	45
6.1.3. Static and Dynamic Analysis	46
6.1.3.1. Static Analysis	47
6.1.3.2. Dynamic Analysis.....	47
6.2. Modeling.....	48
6.2.1. Drilling Rig Modeling.....	49
6.2.1.1. SDR "GSF Development Driller II" Specification. General Description.....	49
6.2.1.2. Model Creation	51
6.2.2. Drilling Riser System Modeling	57
6.2.2.1. 21 inch Drilling Riser Configuration.....	57
6.2.2.2. 16 inch Drilling Riser Configuration.....	60
6.2.3. Input Data for Environmental Conditions.....	62
6.2.4. Additional Considerations and Assumptions	64
6.3. Analysis Results and Discussions.....	66

6.3.1. Effect of the wave height on the effective tension with regard to various drilling fluids	67
6.3.2. Effect of the wave height on the Von-Mises stress with regard to various drilling fluid densities	68
6.3.3. Effect of the wave height on the maximum upper flex ball/joint angle with regard to various drilling fluid densities	71
6.3.4. Effect of the wave height on the maximum lower flex ball/joint angle with regard to various drilling fluid densities	72
6.4. Simulation in ANSYS Software	75
6.4.1. General Description.....	75
6.4.2. Engineering Data.....	76
6.4.3. Model Setup	77
6.4.3.1. Geometry of Model.....	77
6.4.3.2. Meshing	78
6.4.4. Description of Loads	78
6.4.5. Analysis Results and Discussions	88
7. SUMMARY AND CONCLUSIONS.....	97
REFERENCES	100
APPENDIX A.....	102
APPENDIX B.....	104
APPENDIX C.....	108
APPENDIX D.....	110
APPENDIX E.....	114
E1. Current Profile.....	114
E2. Design of Waves	114
APPENDIX F	117
APPENDIX G	133
G1. Load calculations for 21 inch riser at the conditions of waves with height of 8 m ...	133
G2. Load calculations for 16 inch riser at the conditions of waves with height of 2.5 m.....	142
G3. Load calculations for 16 inch riser at the conditions of waves with height of 8 m ...	151

LIST OF FIGURES

Figure 1-1. Loads on the drilling riser system.....	2
Figure 3-1. Standard drilling system with the marine riser.....	11
Figure 3-2. Motion-compensating equipment.....	12
Figure 3-3. Main components of the drilling riser.....	13
Figure 3-4. Complete riser joint.....	14
Figure 3-5. Complete BOP stack.....	16
Figure 4-1. Forces acting on an immersed facility.....	17
Figure 4-2. Internal and external forces acting on a riser segment.....	19
Figure 4-3. Tri-axial stress field.....	21
Figure 4-4. Stresses over the segment of thick walled cylinder.....	22
Figure 4-5. Stress distribution across the wall of the cylinder.....	23
Figure 4-6. Bending moment acting on an elementary segment.....	24
Figure 4-7. Von-Mises failure envelope for various Design Factors in 2D plane.....	27
Figure 4-8. Flow regimes of fluid over cylinder.....	30
Figure 4-9. Hydrodynamic and aerodynamic devices for reduction the vortices shedding.....	32
Figure 4-10. Immersed cylindrical pipe under wave action.....	34
Figure 4-11. Drag coefficient as a function of Reynolds Number for spheres, transverse cylinders, and face-on discs.....	35
Figure 4-12. Mass coefficient as a function of D/L.....	35
Figure 5-1. Map of the Kara Sea regions and boundaries.....	38
Figure 5-2. Depth distribution in the Kara Sea.....	39
Figure 5-3. Surface currents distribution in the Kara Sea.....	41
Figure 5-4. Probability (%) of occurrence an iceberg within a year.....	42
Figure 6-1. Coordinate systems in OrcaFlex.....	44
Figure 6-2. Directions with regard to global axes.....	45
Figure 6-3. Model of the actual riser and discretized model of the line.....	45
Figure 6-4. Illustration of various types of the spring-damper systems.....	46
Figure 6-5. Front and top view of SDR “GSF Development Driller II”.....	50
Figure 6-6. Model illustration.....	51
Figure 6-7. Front view to SDR “GSF Development Driller II”.....	53
Figure 6-8. Side view to SDR “GSF Development Driller II”.....	53
Figure 6-9. Top view to SDR “GSF Development Driller II”.....	54
Figure 6-10. 3D view to SDR “GSF Development Driller II”.....	54
Figure 6-11. Front view to SDR “GSF Development Driller II”.....	55
Figure 6-12. Side view to SDR “GSF Development Driller II”.....	55
Figure 6-13. Top view to SDR “GSF Development Driller II”.....	56
Figure 6-14. 3D view to SDR “GSF Development Driller II”.....	56
Figure 6-15. The configuration of the 21 inch riser (on the left) and the model in OrcaFlex program (on the right).....	59
Figure 6-16. The configuration of the 16 inch riser (on the left) and the model in OrcaFlex program (on the right).....	61
Figure 6-17. Distribution of the current velocity over the sea water depth.....	63
Figure 6-19. Maximum Effective Top Tension for 16 inch and 21 inch aluminum risers.....	68
Figure 6-20. Maximum Von-Mises Stress (1025 kg/m ³).....	69
Figure 6-21. Maximum Von-Mises Stress (1438 kg/m ³).....	70

Figure 6-22. Maximum Von-Mises Stress (1678 kg/m ³)	70
Figure 6-23. Maximum Von-Mises Stress (2037 kg/m ³)	70
Figure 6-24. Maximum Upper Flex Ball/Joint Angle (1025 kg/m ³)	71
Figure 6-25. Maximum Upper Flex Ball/Joint Angle (1438 kg/m ³)	71
Figure 6-26. Maximum Upper Flex Ball/Joint Angle (1678 kg/m ³)	72
Figure 6-27. Maximum Upper Flex Ball/Joint Angle (2037 kg/m ³)	72
Figure 6-29. Maximum Lower Flex Ball/Joint Angle (1438 kg/m ³)	73
Figure 6-30. Maximum Lower Flex Ball/Joint Angle (1678 kg/m ³)	73
Figure 6-31. Maximum Lower Flex Ball/Joint Angle (2037 kg/m ³)	74
Figure 6-32. Scheme of the Static Structural Analysis.....	75
Figure 6-33. Materials Set-up at Engineering Data section.....	76
Figure 6-34. The 21 inch drilling riser model in Autodesk Inventor (on the left) and a partially shown 3D model with created mesh in ANSYS (on the right)	77
Figure 6-35. Illustration of the top view to the 21 inch drilling riser	78
Figure 6-36. Drag, Mass and Total Force of wave	82
Figure 6-37. Distribution of Drag, Mass and Total Force of wave over the water depth	83
Figure 6-38. Average velocity of the current over the water depth.....	86
Figure 6-39. Distribution of the Drag Force over the water depth	87
Figure 6-40. Von-Mises stress distribution in the 21 inch steel riser at the wave height of 2.5 m	89
Figure 6-41. Von-Mises stress distribution in the 21 inch steel riser at the wave height of 8 m ..	90
Figure 6-42. Von-Mises stress distribution in the 21 inch aluminum riser at the wave height of 2.5 m	91
Figure 6-43. Von-Mises stress distribution in the 21 inch aluminum riser at the wave height of 8 m	92
Figure 6-44. Von-Mises stress distribution in the 16 inch steel riser at the wave height of 2.5 m	93
Figure 6-45. Von-Mises stress distribution in the 16 inch steel riser at the wave height of 8 m ..	94
Figure 6-46. Von-Mises stress distribution in the 16 inch aluminum riser at the wave height of 2.5 m	95
Figure 6-47. Von-Mises stress distribution in the 16 inch aluminum riser at the wave height of 8 m	96
Figure F-1. Effective tension of steel risers at the wave height of 1 m and period of 3 s	117
Figure F-2. Effective tension of steel risers at the wave height of 2 m and period of 5 s	117
Figure F-3. Effective tension of steel risers at the wave height of 3 m and period of 5 s	117
Figure F-4. Effective tension of steel risers at the wave height of 4 m and period of 6 s	118
Figure F-5. Effective tension of steel risers at the wave height of 5 m and period of 6 s	118
Figure F-6. Effective tension of steel risers at the wave height of 5 m and period of 7 s	118
Figure F-7. Effective tension of steel risers at the wave height of 6 m and period of 7 s	119
Figure F-8. Effective tension of steel risers at the wave height of 7 m and period of 7 s	119
Figure F-9. Effective tension of steel risers at the wave height of 8 m and period of 8 s	119
Figure F-10. Effective tension of steel risers at the wave height of 8 m and period of 9 s	120
Figure F-11. Effective tension of steel risers at the wave height of 9 m and period of 8 s	120
Figure F-12. Effective tension of steel risers at the wave height of 10 m and period of 9 s	120
Figure F-13. Effective tension of aluminum risers at the wave height of 1 m and period of 3 s	121
Figure F-14. Effective tension of aluminum risers at the wave height of 2 m and period of 5 s	121
Figure F-15. Effective tension of aluminum risers at the wave height of 3 m and period of 5 s	121
Figure F-16. Effective tension of aluminum risers at the wave height of 4 m and period of 6 s	122
Figure F-17. Effective tension of aluminum risers at the wave height of 5 m and period of 6 s	122
Figure F-18. Effective tension of aluminum risers at the wave height of 5 m and period of 7 s	122

Figure F-19. Effective tension of aluminum risers at the wave height of 6 m and period of 7 s	123
Figure F-20. Effective tension of aluminum risers at the wave height of 7 m and period of 7 s	123
Figure F-21. Effective tension of aluminum risers at the wave height of 8 m and period of 8 s	123
Figure F-22. Effective tension of aluminum risers at the wave height of 8 m and period of 9 s	124
Figure F-23. Effective tension of aluminum risers at the wave height of 9 m and period of 8 s	124
Figure F-24. Effective tension of aluminum risers at the wave height of 10 m and period of 9 s	124
.....	124
Figure F-25. Von-Mises stress of steel risers at the wave height of 1 m and period of 3 s	125
Figure F-26. Von-Mises stress of steel risers at the wave height of 2 m and period of 5 s	125
Figure F-27. Von-Mises stress of steel risers at the wave height of 3 m and period of 5 s	125
Figure F-28. Von-Mises stress of steel risers at the wave height of 4 m and period of 6 s	126
Figure F-29. Von-Mises stress of steel risers at the wave height of 5 m and period of 6 s	126
Figure F-30. Von-Mises stress of steel risers at the wave height of 5 m and period of 7 s	126
Figure F-31. Von-Mises stress of steel risers at the wave height of 6 m and period of 7 s	127
Figure F-32. Von-Mises stress of steel risers at the wave height of 7 m and period of 7 s	127
Figure F-33. Von-Mises stress of steel risers at the wave height of 8 m and period of 8 s	127
Figure F-34. Von-Mises stress of steel risers at the wave height of 8 m and period of 9 s	128
Figure F-35. Von-Mises stress of steel risers at the wave height of 9 m and period of 8 s	128
Figure F-36. Von-Mises stress of steel risers at the wave height of 10 m and period of 9 s	128
Figure F-37. Von-Mises stress of aluminum risers at the wave height of 1 m and period of 3 s	129
Figure F-38. Von-Mises stress of aluminum risers at the wave height of 2 m and period of 5 s	129
Figure F-39. Von-Mises stress of aluminum risers at the wave height of 3 m and period of 5 s	129
Figure F-40. Von-Mises stress of aluminum risers at the wave height of 4 m and period of 6 s	130
Figure F-41. Von-Mises stress of aluminum risers at the wave height of 5 m and period of 6 s	130
Figure F-42. Von-Mises stress of aluminum risers at the wave height of 5 m and period of 7 s	130
Figure F-43. Von-Mises stress of aluminum risers at the wave height of 6 m and period of 7 s	131
Figure F-44. Von-Mises stress of aluminum risers at the wave height of 7 m and period of 7 s	131
Figure F-45. Von-Mises stress of aluminum risers at the wave height of 8 m and period of 8 s	131
Figure F-46. Von-Mises stress of aluminum risers at the wave height of 8 m and period of 9 s	132
Figure F-47. Von-Mises stress of aluminum risers at the wave height of 9 m and period of 8 s	132
Figure F-48. Von-Mises stress of aluminum risers at the wave height of 10 m and period of 9 s	132
.....	132
Figure G-1. Drag, Mass and Total Force of wave	136
Figure G-2. Distribution of Drag, Mass and Total Force of wave over the water depth	137
Figure G-3. Average velocity of the current over the water depth	140
Figure G-4. Distribution of the Drag Force over the water depth	141
Figure G-6. Distribution of Drag, Mass and Total Force of wave over the water depth	146
Figure G-7. Average velocity of the current over the water depth	149
Figure G-8. Distribution of the Drag Force over the water depth	150
Figure G-9. Drag, Mass and Total Force of wave	154
Figure G-10. Distribution of Drag, Mass and Total Force of wave over the water depth	155

NOMENCLATURE

Latin characters

A_e	external cross-section of the riser segment/ cylinder/ facility;
A_i	internal cross-section of the riser segment/ cylinder;
B_n	net positive buoyancy (lift force);
C	damping matrix;
C_D	drag coefficient;
C_M	mass or inertia coefficient;
D	outer diameter of the riser;
DL	dogleg severity;
D_o	outer diameter of the pipe;
$D_{i\ k/c}$	internal diameter of the kill/choke line;
$D_{i\ mb}$	internal diameter of the mud booster line;
d_m	density of the drilling mud;
d_w	density of the sea water;
E	Young's modulus or the Modulus of Elasticity;
<i>Exponent</i>	Power Law exponent;
F_a	applied axial load;
f_{bt}	buoyancy loss and tolerance factor;
f_D	drag force;
f_H	hydrodynamic force;
f_I	inertia force;
f_u	tensile strength;
$f_{u,temp}$	temperature reduction factor for the tensile strength;
f_{wt}	submerged weight tolerance factor;
f_y	yield stress;
$f_{y,temp}$	temperature reduction factor for the yield stress;
g	gravity acceleration;
h	height of the internal fluid column;
$H_{LMRP+BOP}$	height of LMRP + BOP Stack;
H_m	height of the drilling mud column;
H_{sw}	sea water depth;
H_{S+T}	height of storm surge + tide;

H_{wh}	height of the wellhead;
H_w	height of the sea water column;
$h_{RKB-MSL}$	distance from RKB to mean sea level;
h_{RKB-ML}	distance from RKB to mud line;
h_{TR-MSL}	distance from tensioner ring to mean sea level;
I	second moment of the area;
K	global stiffness matrix;
L_r	riser length;
$L_{r,sub}$	submerged riser length;
M	bending moment/mass matrix;
M_k	plastic bending moment resistance;
m	mass of a unit length of the riser;
m_A	additional mass;
N	number of tensioners supporting the riser;
n	number of tensioners subjected to failure;
P	function of external loads;
$p_a = p_i$	internal pressure in the cylinder;
$p_b = p_e$	external pressure in the cylinder;
p_b	burst resistance;
p_d	maximum design pressure at the surface during normal operations;
p_c	collapse resistance;
p_{ld}	local internal design pressure;
p_{li}	local incidental pressure;
p_{min}	minimum internal pressure;
p_e	external pressure;
p_i	internal pressure;
R	radius of curvature;
R_f	reduction factor to account for fleet angle and mechanical efficiency,
r	inner radius of the cylinder;
S_f	current velocity at the sea surface;
S_b	current velocity at the sea bottom;
T	applied torque;
T_e	effective tension;
T_k	plastic axial force resistance;

T_{SRmin}	minimum slip ring tension;
T_{min}	minimum required top tension;
T_{true}	true tension;
T_{tw}	axial tension on the riser segment;
t	thickness of the wall;
t_l	wall thickness of the riser excluding allowance for fabrication and corrosion;
u	velocity of the fluid particle past the riser;
\dot{u}	constant acceleration of the fluid;
W_s	submerged weight of the riser without contents;
w_a	apparent weight/ equivalent system weight;
w_e	weight of the displaced fluid;
w_i	weight of the internal fluid;
w_t	weight of the immersed riser segment;
x	displacement;
\dot{x}	velocity;
\ddot{x}	acceleration;
y	distance to the center of the pipe;
Z_f	water surface level;
Z_b	the sea bottom level.

Greek characters

α_c	parameter taking into account strain hardening and wall thinning;
α_U	material strength factor;
γ_m	resistance factor of material;
γ_{SC}	safety class resistance factor;
η	uniform factor for combined loading;
ρ	density of the fluid;
ρ_i	density of the internal fluid;
ρ_m	weight density of the drilling fluid;
ρ_{steel}	steel density;
ρ_w	weight density of the sea water;
τ	shear stress;
σ_a	axial stress;
σ_b	bending stress;

σ_r	radial stress;
σ_θ	tangential stress;
σ_{vme}	Von-Mises stress.

Abbreviations

ALS	Accidental Limit State;
ASTM	American Society for Testing and Materials;
API	American Petroleum Institute;
BOP	Blow-Out Preventer;
DNV	Det Norske Veritas;
DTL	Dynamic Tension Limit;
FLS	Fatigue Limit State;
HSE	Health Safety and Environment;
ISO	International Organization for Standardization;
LF	Low Frequency;
LFJ	Lower Flex Joint;
LMRP	Lower Marine Riser Package;
MODU	Mobile Drilling Unit;
MSL	Mean Sea Level;
NORSOK	Norsk Sokkels Konkuranseposisjon;
RAO	Response Amplitude Operator;
RKB	Rotary Kelly Bushing;
SLS	Serviceability Limit State;
SMYS	Specific Minimum Yield Stress;
SMTS	Specific Minimum Tensile Strength;
SSDR	Semisubmersible Drilling Rig;
ULS	Ultimate Limit State;
UFJ	Upper Flex Joint;
VIV	Vortex-Induced Vibrations;
WF	Wave Frequency.

1. INTRODUCTION

Currently the number of offshore wells around the world is increasing. Therefore, the drilling operations require the use of a drilling riser in the system. The drilling riser system is exposed to the sea waves and currents, which apply load on the riser as well.

Understanding the loadings is the main engineering task in order to have the Mechanical Structural Integrity. Thoroughly designed and analyzed systems with all possible loading scenarios during the whole lifetime of the well are very important. Thus, the risk of Health Safety and Environment (HSE) issues can be mitigated and unnecessary expenditures are reduced.

The offshore field development tends to move into the deep waters of more than 10.000 feet and also into arctic fields development with harsh environments. Hence, a Subsea Drilling System has to be reliable for the entire cycle of drilling operation in these challenging conditions.

This thesis presents the simulation-based studies of the drilling riser with regard to the Kara Sea. The simulation was performed using a well-known software such as OrcaFlex and ANSYS. During simulation, several loading scenario have considered in order to investigate the response of riser.

1.1. Background and Problem Statement

During offshore drilling operations, the drilling riser is used to connect the surface equipment on the Mobile Drilling Unit with a subsea well. This key component of the system is subjected to various loadings as a result of the internal and external pressures, vibrations, tensions, temperatures, and many others.

Internal and external pressure loads are generally caused by hydrostatic pressures of the drilling fluid and sea water respectively. [1]

Risers, in large water depths and strong current environments, are prone to vibrations created by the vortices shed from the structure. This Vortex-Induced Vibrations (VIV) may damage the riser and limit its fatigue life, with the potential to cause costly and environmentally damaging. It is an important design consideration when drilling in high current environments.

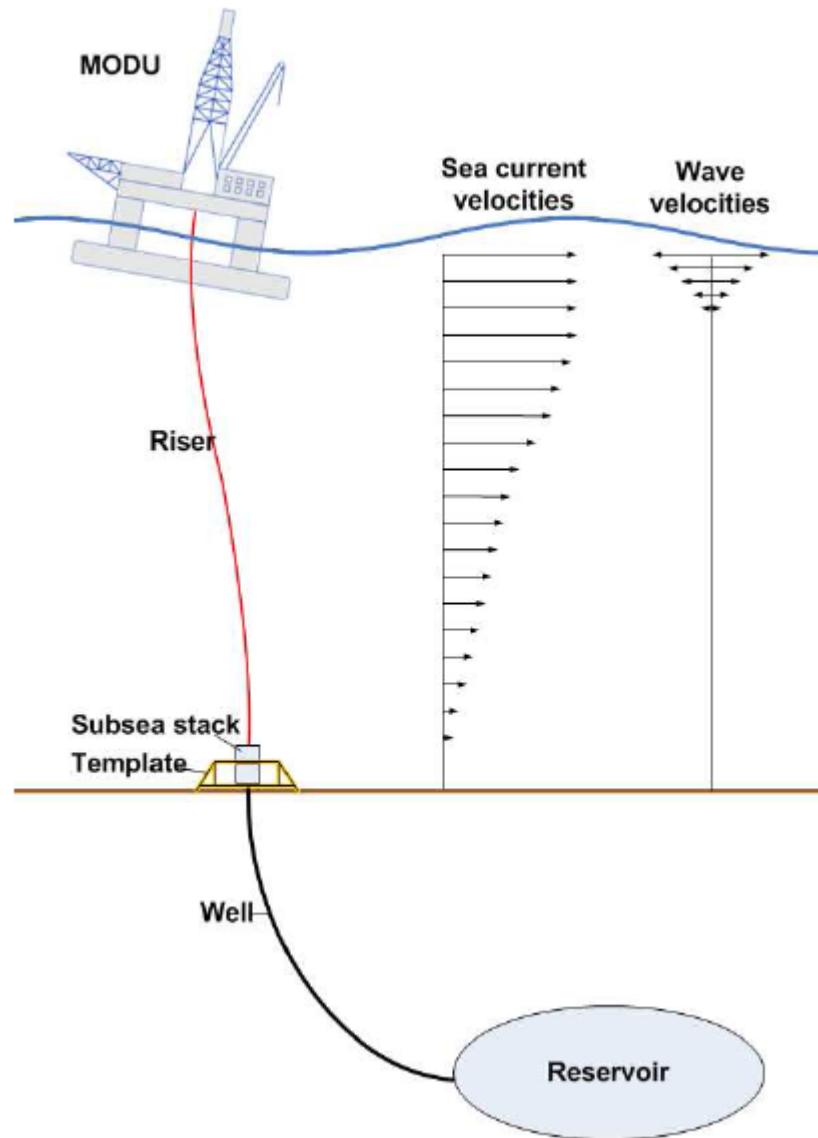


Figure 1-1. Loads on the drilling riser system (DNV, 2011)

In the worst-case scenario, the wellhead fatigue and problems with the riser can lead to a severe damage. Therefore, it is a great importance to assess the mechanics of the riser system under several loading scenarios before the construction.

This thesis addresses issues such as:

- Effect of the wave height on the effective tension with regard to various drilling fluids
- Effect of the wave height on the Von-Mises stress with regard to various drilling fluid densities
- Effect of the wave height on the maximum upper flex ball/joint angle with respect to various drilling fluid densities

- Effect of the wave height on the maximum lower flex ball/joint angle with respect to various drilling fluid densities

1.2. Thesis Objectives

The scope of the thesis is limited to analytical and numerical study of the drilling riser. The main objective of the thesis is to do assessment of the drilling riser. However, the subtasks can be divided into the following:

- Literature studies on the drilling riser (riser types and structures, and the theory on collapse/tensile/burst/elongation etc.);
- Revision of various drilling systems with application of riser and specification;
- Revision of standards and regulations used to select and analyze riser systems;
- Studying the mechanics of the drilling riser under various loading scenario (hydrostatic/current/sea wave etc.);
- Performing numerical simulation studies of drilling risers based on various operational conditions in the Kara Sea;
- Implementation of sensitivity analysis with respect to material properties, dimension, drilling fluid densities.

2. STANDARDS AND REGULATIONS

Offshore equipment should be designed and operated according to the regulations and rules. These are developed based on fundamental principles and the generalized offshore experience of manufacturers, contractors, and operators. Therefore, the selection, design, maintenance and operation of marine drilling riser system for mobile offshore drilling units are specified in the international standards, such as ISO 13624, API RP 16Q and DNV-OS-F201. However, the specifications and rules have to be adjusted and continuously improved for the diverse operating conditions, which can vary, for instance, from deep-water areas to the extremely challenging and harsh arctic environments.

2.1. API RP 16Q

The API PR 16Q standard is released in different versions covering all aspects related to design, fabrication and operation of the drilling riser and its components.[1] The following API recommended guidelines and specifications are applicable to the drilling riser system:

- API PR 16Q – *“Recommended Practice for Design, Selection, Operation and Maintenance of Marine Drilling Riser Systems”*
- API SPEC 16F – *“Specification for Marine Drilling Riser Equipment”*
- API SPEC 16R – *“Specification for Marine Drilling Riser Couplings”*
- API RP 2RD – *“Design of Risers for Floating Production Systems (FPSs) and Tension-Leg Platforms (TLPs)”*
- API Technical Report 16TR1

In addition, this standard has been served as the premise for the ISO 13624 standard.

2.2. ISO 13624

ISO 13624 has been developed under the title *“Petroleum and natural gas industries – Drilling and production equipment”* and comprises the following two parts [2]:

- ISO 13624-1 – *“Design and operation of marine drilling riser equipment”* – the first part provide with the description of main components used to assemble the riser system as

well as the limiting and operational conditions that should be satisfied for the marine drilling riser system.

- ISO 13624-2 – “*Deepwater drilling riser methodologies, operations, and integrity (Technical Report)*” – the second part is developed with intention to supplement a content of the first part, and comprises additional methodologies, worked examples and specifications for the riser assessment.

The drilling riser system in ISO 13624 comprises the tensioning system, excluding the diverter, and all riser equipment between the upper flex joint (UFJ) and the bottom of wellhead welded on the outer part of conductor casing. Moreover, the application of the first part of ISO 13624 is constrained by operations with a subsea BOP stack installed on the sea bottom. [2]

2.3. COMPARISON of API RP 16Q and ISO 13624 STANDARDS

In general, the standards are very similar as ISO 13624 is based on API RP 16Q. The design of the drilling riser in API PR 16Q and ISO 13624-1 standards is recommended to be performed for three operational modes, which the riser can experience throughout drilling operations. The riser can be operated in drilling, non-drilling and riser disconnected mode. The modes are dependent of the loads on the system and operating conditions. In the thesis, the analysis of the drilling riser is implemented regarding normal and worst case conditions, i.e. the drilling and non-drilling modes. [1, 2]

Table 2-1. Comparison of design specifications for marine drilling riser in API RP 16Q and ISO 13624 [1, 2]

Design parameter	Riser connected			Riser disconnected
	Drilling		Non-drilling	
	API PR 16Q	ISO 13624		
Mean upper flex/ball jt. angle	2,0°	1° to 1,5°	N/A	N/A
Max. upper flex/ball jt. angle	4,0°	5,0°	90% available (or contact with moonpool edge)	90% available (or contact with moonpool edge)
Mean lower flex/ball jt. angle	2,0°	2,0°	N/A	N/A
Max. lower flex/ball jt. angle	4,0°	5,0°	90% available	N/A
Stress criteria:				
- Method “A” –	0,40 σ_y	0,40 σ_y	0,67 σ_y	0,67 σ_y

allowable stress				
- Method "B" – allowable stress	0,67 σ_y	0,67 σ_y	0,67 σ_y	0,67 σ_y
- Sign. dyn. stress range:				
@ SAF < 1,5	69 MPa (10 ksi)	69 MPa (10 ksi)	N/A	N/A
@ SAF > 1,5	15/ SAF	15/ SAF	N/A	N/A
Minimum top tension	T_{min}	T_{min}	T_{min}	N/A
Dynamic tension limit	DTL	DTL	DTL	N/A
Maximum tension setting	90% DTL	90% DTL	90% DTL	N/A

In Table 2-1, the most evident difference in design specifications is the limitations for upper and lower flex joint angles. This is specified to reduce the risk of the joint's wear and riser failure. In addition, the clearance in the moonpool area should be considered for the upper ball joint angle when using ISO 13624-1. [2]

The maximum allowable stress is determined for most of water depths by a method A as 40% and 67% of yield stress, for the drilling mode and for the non-drilling mode respectively. However, for deep-water areas the method B should be applied, where the maximum allowable stress is 67% of yield stress for both of the considering modes. These should be done to investigate that the system is robust to undergo all the maximum design loadings while maintaining the maximum lower the allowed stress. [1, 2]

The standards are based upon the Von-Mises failure criteria, which is discussed in Chapter 4.4.

According to the guidelines, the riser should be kept under a minimum tension, ensuring the stability of the riser string. The top tension is required to be set so that to preclude buckling of the riser even at the failure of some tensioners. For calculation of minimum top tension, exactly the same formula is used in API PR 16Q and ISO 13624-1. [1, 2]

$$T_{min} = \frac{T_{SRmin} N}{R_f (N - n)} \quad (2.1)$$

where

$$T_{SRmin} = W_s f_{wt} - B_n f_{bt} + A_i (d_m H_m - d_w H_w) \quad (2.2)$$

T_{SRmin} minimum slip ring tension;

N number of tensioners supporting the riser;

R_f reduction factor to account for fleet angle and mechanical efficiency, (0.95 for drilling and 0.9 for non-drilling);

n	number of tensioners subjected to failure (at least equal to one);
W_s	submerged weight of the riser without contents;
f_{wt}	submerged weight tolerance factor, minimum is 1.05 unless accurately weighed;
B_n	net positive buoyancy (lift force);
f_{bt}	buoyancy loss and tolerance factor, maximum is 0.96 unless accurately measured;
A_i	internal cross sectional area of riser, including auxiliary lines;
d_m	density of drilling mud;
H_m	height of drilling mud column;
d_w	density of sea water;
H_w	height of sea water column;

This is important to outline that ISO standard recommends to maintain the top tension at a reliable level above the minimum tension calculated by API in normal operations to account for the changes in dynamic tension that may lead to reduction of the riser tension below the minimum required value.

As the drilling riser system comprises many various components, which are made from diverse materials, there are some other codes and regulations to be mentioned for the riser design.

2.4. DNV-OS-F201

Det Norske Veritas (DNV) has developed DNV-OS-F201, DNV-OSS-302 and DNV-RP-F206 specifications that can be applied to design and analyze the dynamic riser systems.

DNV-OS-F201 is discussed in this sub-chapter, as it is relevant for pipes with ratio of $t/D < 45$ and drilling risers fall into this classification. [3]

According to the specification, the drilling riser should be designed to withstand any overpressure of internal and external fluids. As discussed in Chapter 4.4, the overpressure of internal fluid may lead to burst and overpressure of external fluid may cause collapse of the riser.

For these purposes the burst and collapse criteria are established.

Burst criteria [3]:

$$(p_{li} - p_e) \leq \frac{p_b(t_1)}{\gamma_m \gamma_{SC}} \quad (2.3)$$

where

$$p_{li} = (p_d + \rho_i gh) + 0.1p_d; \quad (2.4)$$

$$p_b(t_1) = \frac{2}{\sqrt{3}} \frac{2t}{D - t_1} \min\left(f_y; \frac{f_u}{1.15}\right) \quad (2.5)$$

and

$$t_1 = \frac{D}{\frac{4}{\sqrt{3}} \frac{\min\left(f_y; \frac{f_u}{1.15}\right)}{\gamma_m \gamma_{SC} (p_{li} - p_e)} + 1} \quad (2.6)$$

$p_b(t_1)$	burst resistance;
p_{li}	local incidental pressure;
p_e	external pressure;
γ_m	resistance factor of material;
γ_{SC}	safety class resistance factor;
p_d	maximum design pressure at the surface during normal operations;
ρ_i	density of the internal fluid;
h	height of the internal fluid column;
g	gravity acceleration;
D	outer diameter of the riser;
t_1	wall thickness of the riser excluding allowance for fabrication and corrosion;
$f_y = (SMYS - f_{y,temp})\alpha_U$	yield stress;
$f_u = (SMTS - f_{u,temp})\alpha_U$	tensile strength;
$SMYS$	specific minimum yield stress;
$f_{y,temp}$	temperature reduction factor for the yield stress;
$SMTS$	specific minimum tensile strength;
$f_{u,temp}$	temperature reduction factor for the tensile strength;
α_U	material strength factor (0.96 for normal condition, or 1.0 if additional requirement ensuring increased confidence in material strength is satisfied);

In Table 2-2, values for γ_m and γ_{SC} are specified. ULS, ALS, SLS, and FLS are abbreviations of Ultimate, Accidental, Serviceability, and Fatigue Limit State, accordingly. [3]

Material resistance factor y_m		Safety class resistance factor y_{SC}		
ULS&ALS	SLS&FLS	Low	Normal	High
1.15	1.0	1.04	1.14	1.26

Table 2-2. Resistance factors of material and class resistance. [3]

Collapse criteria [3]:

$$(p_e - p_{\min}) \leq \frac{p_c(t_1)}{\gamma_m \gamma_{SC}} \quad (2.7)$$

where

p_{\min} minimum internal pressure;

$p_c(t_1)$ collapse resistance, which can be determined from the equation:

$$(p_c(t) - p_{el}(t))(p_c^2(t) - p_p^2(t)) = p_c(t)p_{el}(t)p_p f_0(t) \frac{D}{t} \quad (2.8)$$

Working stress design (WSD) criterion [3]:

DNV-OS-F201 is based on the Working Stress Design criterion for combined loading which can be utilized for risers with $t/D < 30$. The uniform factor is used herein instead of previous load effect and resistance factors. The criteria is subdivided into two options, for risers exposed to net internal overpressure [3]:

$$\left\{ \left(\frac{M}{M_k} \sqrt{1 - \left(\frac{p_{ld} - p_e}{p_b(t_2)} \right)^2} \right) + \left(\frac{T_e}{T_k} \right)^2 \right\}^2 + \left(\frac{p_{ld} - p_e}{p_b(t_2)} \right)^2 \leq \eta^2 \quad (2.9)$$

and for risers exposed to net overpressure of the external fluid, it should fulfill:

$$\left\{ \left(\frac{M}{M_k} \right) + \left(\frac{T_e}{T_k} \right)^2 \right\}^2 + \left(\frac{p_{ld} - p_e}{p_b(t_2)} \right)^2 \leq \eta^4 \quad (2.10)$$

where

M bending moment;

$M_k = f_y \alpha_c (D - t_2)^2$ plastic bending moment resistance;

$p_{ld} = p_d + \rho_i g h$	local internal design pressure;
T_e	effective tension;
$T_k = f_y \alpha_c \pi (D - t_2) t_2$	plastic axial force resistance;
η	uniform factor for combined loading;
α_c	parameter taking into account strain hardening and wall thinning, defined as:

$$\alpha_c = (1 - \beta) + \beta \frac{f_u}{f_y} \quad (2.11)$$

$$\beta = \begin{cases} (0.4 + q_h) & \text{for } \frac{D}{t_2} < 15 \\ (0.4 + q_h) \left(60 - \frac{D}{t_2} \right) / 45 & \text{for } 15 < \frac{D}{t_2} < 60 \\ 0 & \text{for } \frac{D}{t_2} > 60 \end{cases} \quad (2.12)$$

$$q_h = \begin{cases} \frac{(p_{ld} - p_e) 2}{p_b(t_2) \sqrt{3}} & \text{for } p_{ld} > p_e \\ 0 & \text{for } \textit{else} \end{cases} \quad (2.13)$$

Table 2-3 and Table 2-4 present the uniform factor for WSD criterion and the specification for the respective safety class.

Low	Normal	High
0.83	0.79	0.75

Table 2-3. Uniform factor. [3]

Safety Class	Definition
Low	The failure supposes low probability of human injury and minor environmental and economic impact.
Normal	For conditions where failure implies probability of human injury, high environmental pollution or very significant economic or political impact.
High	For operational conditions where failure implies high probability of human injury, high environmental pollution or very significant economic or political impact.

Table 2-4. Specification of safety classes. [3]

3. DESCRIPTION OF DRILLING SYSTEM

In this chapter, a standard drilling system with a marine riser is described. This gives a general review of the drilling operations and key elements of the drilling riser system. Drilling an offshore well is performed in several stages. Initially, drilling operation is commenced by running a temporary guide base to the sea floor. Then a 36" hole opener is run to drill a 36" wellbore which returns cuttings to the seabed. The first casing string, called as the conductor, is cemented in place. The permanent guide structure is run with the conductor. Afterwards a 26" hole is drilled for the 20" surface casing and the wellhead housing is run. The riser with the BOP stack at the end is connected to the wellhead. The drilling continues by means of the drilling riser, as the subsequent operation requires mud return to the rig. There are three main stages in the well construction and during production phases [4]:

- Drilling
- Completion
- Workover

A standard drilling system with a marine riser is presented in Figure 3-1.

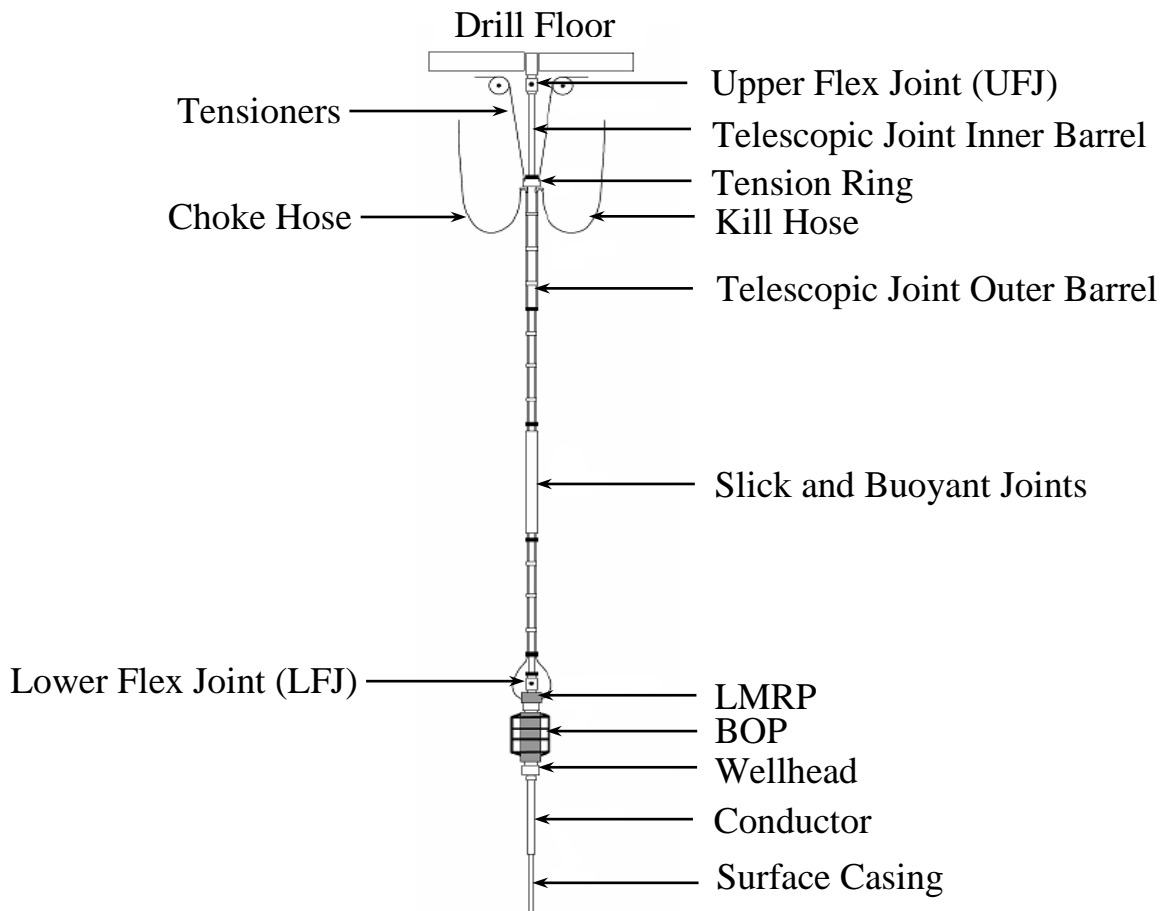


Figure 3-1. Standard drilling system with the marine riser [5]

3.1. Surface Equipment of Riser Drilling System

3.1.1. Motion-compensating equipment

The motion-compensating equipment (Figure 3-2) is a main component of floating drilling rigs compensating for the rig's pitch/heave and other motions. The equipment comprises riser, and guideline and pod-line tensioners as well as the drill string compensator. [6]

The drill string compensator, placed between the Kelly bushing and travelling block, allows to keep constant weight on the bit while the rig moves axially. [6]

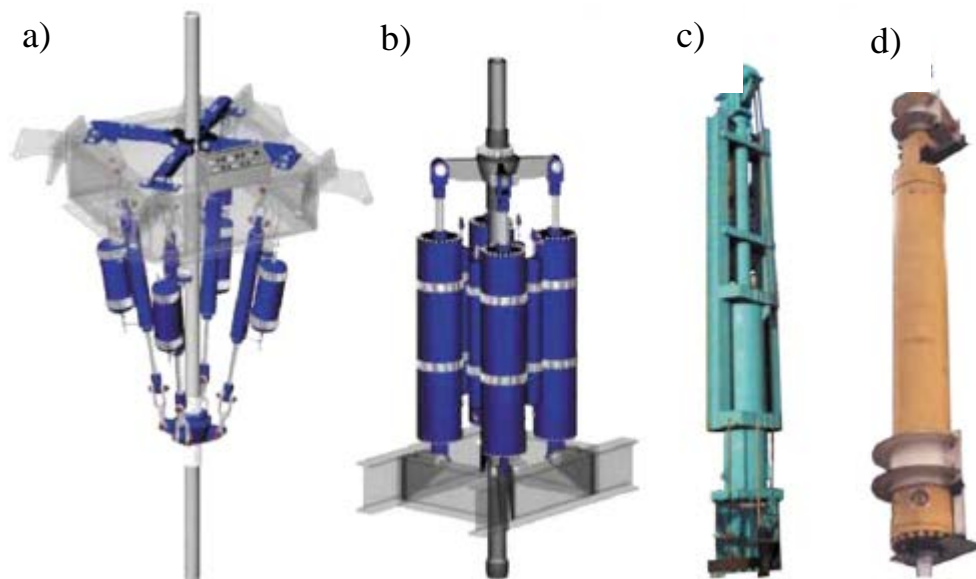


Figure 3-2. Motion-compensating equipment [6]

a – downward facing riser tensioning system, b – upward facing riser tensioning system, c – deepwater development system, d – active compensation system.

3.1.2. Tensioning system

A slip joint, or also called as a telescopic joint, is designed to compensate vertical movements, rolling and pitching of rig. It comprises an outer pipe with manifold lines, the inner tube, and a sealing assembly consisting of a working and emergency seal and an adapter serving to connect the inner pipe to the diverter block.

Riser tensioners are attached to the outer pipe of the telescopic joint with a wire rope cable. The cables help to maintain a constant tension on the riser, preventing it from buckling, during heave movements of a drilling rig.

3.2. Drilling Riser

3.2.1. Low-pressure Drilling Riser

A standard drilling riser, or a low-pressure drilling riser, is a large diameter conduit composed of several pipes with a diameter of 400-500 mm. Its main function is to connect surface equipment with a subsea well. It has an atmospheric pressure inside the central tube as open at the top end. Therefore, the internal pressure cannot surpass due to the drilling mud weight. [7]

The standard drilling riser is shown in Figure 3, which consists of the following elements:

The spider is a tool, which is installed in the rotary table on the drill deck to keep the riser during running operations. [6]

The gimbal is a tool that is placed in the rotary table under the spider. It smoothly distributes the loadings induced by pitch/roll motions of the drilling rig, on the riser system.

A flex joint is used under the riser telescopic connection in order to reduce tension in the riser. In some cases, they may be mounted at the top of the riser between the drill deck and telescopic joint to reduce the loads transmitted to the riser while rig's movements. [6]

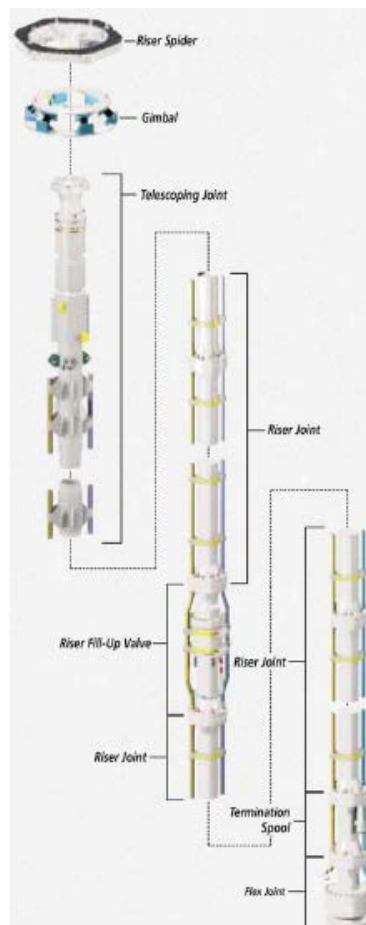


Figure 3-3. Main components of the drilling riser [6]

Riser joints (Figure 3-4) are the major components used to build up the riser. The joints includes a central pipe with the diameter of 21 in. which are welded to the nipple elements having a locking device for connecting the sections together, as well as sealing elements for sealing the joint sections. The pipe flange is mounted at the nipple-end to support the riser in the installation operations. A typical riser joint has a length of 9.14 – 15.24 m. (30 – 50 ft.). The section can be 75 ft. long for the purpose of more efficient operations. [6]



Figure 3-4. Complete riser joint [6]

3.2.2. Buoyancy Modules

The buoyancy equipment is connected to the drilling riser to reduce the weight of the riser system. The riser can be covered over the whole length by buoyancy modules. The modules are filled with a syntactic foam. A small section of the riser near the surface is usually not equipped with buoyancy modules to reduce hydrodynamic impact of loads in the area with prevailing great wave forces. At the bottom, the riser is also not covered with buoyancy joints as it increases the cost of foam due to increasing its density with depth. [6]

Air-containers have sometimes been used in the foretime. These had the certain advantages because the buoyancy could be controlled and optimized prior to each drilling operation, but the process of installation was more complex.

3.2.3. Kill/Choke, Booster and Hydraulic lines

A kill and choke lines are external pipes, which are installed on the outside of the riser. These are used to circulate fluid into and out of the wellbore in case of a gas kick, respectively. These manifold lines are typically fabricated to withstand a pressure of 15 ksi. [6]

A booster line is attached to the outer surface of the main riser pipe to inject the fluid just above the Lower Marine Riser Package (LMRP) for better cuttings evacuation.

A small-diameter hydraulic line is used for hydraulic supply to the Blow-Out Preventer (BOP). [6]

3.3. Lower Riser Stack

3.3.1. Lower Marine Riser Package (LMRP)

The Lower Marine Riser Package is an equipment used to connect the drilling riser with the BOP stack, and comprises control pods, a riser adapter, and the Lower Flex Joint (LFJ). The LMRP allows disconnection of the riser from the BOP in the event of an emergency.

3.3.2. Blow-Out Preventer (BOP)

The BOP stack enables pressure well control. In the event of the primary barrier failure (mud column), a formation influx takes place during drilling, one or more BOPs are activated to seal off the annulus, or wellbore, in order to “shut-in” the well. Afterwards a heavier mud is pumped into the wellbore to re-install primary well control. Mud is pumped down the drill string, up the annulus, through the choke line at the base of the BOP stack, and then up the high-pressure manifold lines on the riser and out the choke manifold until the well pressure is controlled and the inflow of formation fluids is circulated out of the well. Once the well is filled with a “kill mud” from the bottom to the top, the well is back in balance and has been “killed.” Operations may proceed with the integrity of the well re-established. [8]

A typical stack arrangement, as shown in Figure 3-5, has various ram preventers in the lower part and the annular preventers in the top assembly. The configuration of the stack preventers has to be chosen so that to provide maximum pressure integrity, safety and flexibility in case of an emergency. [9]

- Variable Bore (Pipe) Rams enable to seal off around the drill pipe, preventing annular flow between the outside of the drill string and the borehole, but do not restrict flow inside the drill pipe.
- Blind Rams (also called as sealing rams) allow closing and sealing off the well in the absence of the drill string.
- Shear Rams are designed with intention to shear through the casing or drill string with steel blades.
- Blind Shear Rams (also called as shear seal rams) are high-pressure activated rams used to cut through the drill string and close off the well.

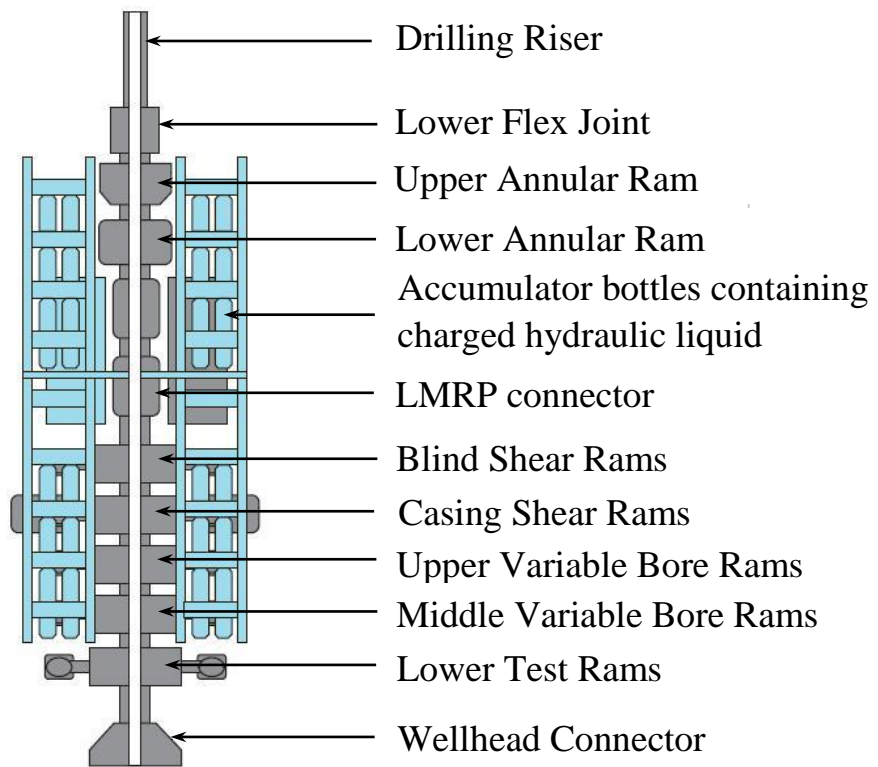


Figure 3-5. Complete BOP stack [10]

4. FUNDAMENTAL MECHANICS OF RISER

In this chapter, the basic mechanics of drilling riser is outlined. This is a significant prerequisite for the analysis to be performed in Chapter 6 of the thesis.

4.1. Influence of Pressure, Tension, and Weight on the System

Riser system is exposed to pressure, tension and weight variations as it extends from the seafloor to the mobile drilling unit where it is attached to the motion-compensating equipment and tensioning system. Therefore, various technical factors, which may have impact on buckling and failure of the riser, should be taken into account prior to modeling of loads. The following sub-chapters describe the loads associated with the tension calculation. [7]

4.1.1. Internal Forces in a Submerged Body

In the assessment of the internal forces acting on a submerged part of body, the issue is to take into consideration is the pressure field. Figure 4-1 presents a part of an immersed facility with the acting forces. [7]

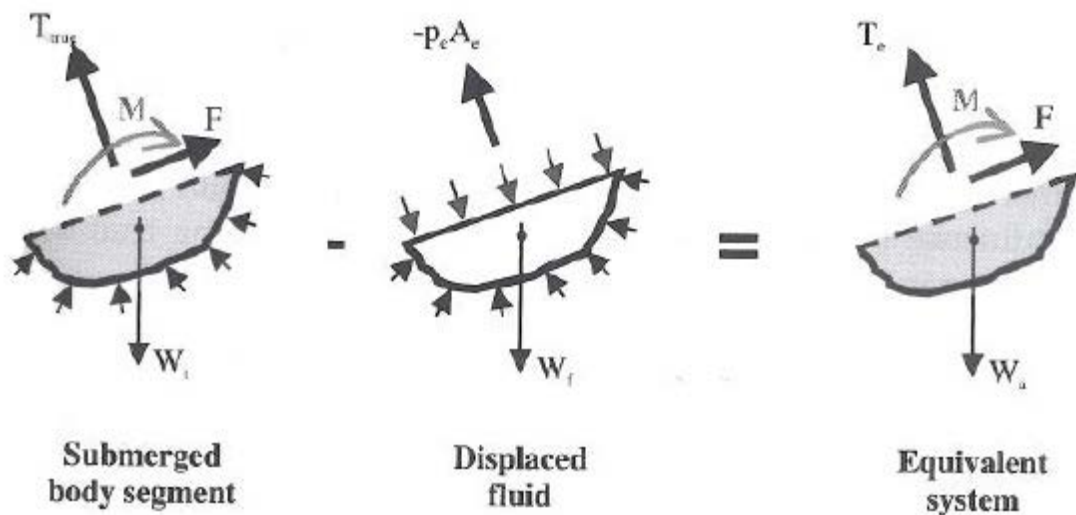


Figure 4-1. Forces acting on an immersed facility [7]

The external forces acting on the downside of the body cannot be calculated by means of Archimedes' Law. In spite of this, the superposition principle enables the internal pressure field to be found easily. Archimedes' Law is utilized in order to avoid complex calculations. The enclosed pressure field acting on the displaced fluid is established for Archimedes' Law

application, the middle picture in Figure 4-1. It is then possible to subtract all these forces from the forces acting on the facility, thus eliminating the pressure field on the downside of the fluid segment. However, the counteracting force $p_e A_e$ should be remained due to the pressure field acting on the body segment. A right-hand picture in Figure 4-1 presents the equal system of acting forces and moments as a result of the superposition application. The shear force F and the moment M are identical for the body segment as for the equivalent system. The effective tension is associated with the internal tension, known as the true tension, as following [7]:

$$T_e = T_{true} - (-p_e A_e) = T_{true} + p_e A_e \quad (4.1)$$

where

T_e effective tension;

T_{true} true tension;

p_e pressure in the fluid;

A_e cross-section of the facility;

The apparent weight W_a can be defined as the weight of the immersed body, also known as the true weight, minus the weight of the displaced fluid, written as the next equation:

$$W_a = W_t - W_f \quad (4.2)$$

The previous conclusions can be reconsidered with respect to the riser under pressure conditions. There is no contact of the fluid at the ends of the riser, i.e. the closed state of the pressure field is not satisfied according to Archimedes' Law. If a curved section of a riser is presented with the internal pressure of fluid p_i and external pressure of fluid p_e . The moments and shear forces have been excluded out of the system for simplification, but the previous arguments are not influenced by that. A curved riser segment with length of δs will be under the true tension T_{tw} in the riser wall, riser weight, and the internal and external fluid pressure. [7]

The closed pressure field acts on the inside fluid in balance with the weight of the fluid inside riser. The pressures acting around the riser wall are in equilibrium with the internal pressure field of the fluid but acting in opposite to them direction. Therefore, the axial pressures are omitted adding the two force systems and using the principle of superposition. Nevertheless, the axial force in the fluid inside the riser is remained. Thus, the equations of the effective tension and apparent weight can be written as follows [7]:

$$T_e = T_{tw} + (-p_i A_i) \quad (4.3)$$

$$w_a = w_t - w_i \quad (4.4)$$

where

- T_e effective tension;
- T_{tw} true tension in the riser wall;
- p_i pressure from the fluid inside the riser;
- A_i cross-section of the riser segment;
- w_a apparent weight;
- w_t weight of the immersed riser segment;
- w_i weight of the internal fluid;

The same method can be applied when external pressure is known, as present in Figure 4-2. All side-pressures are excluded adding the systems of forces acting on the riser segment and the fluid inside the riser and then subtracting the system of forces acting on the displaced fluid. [7]

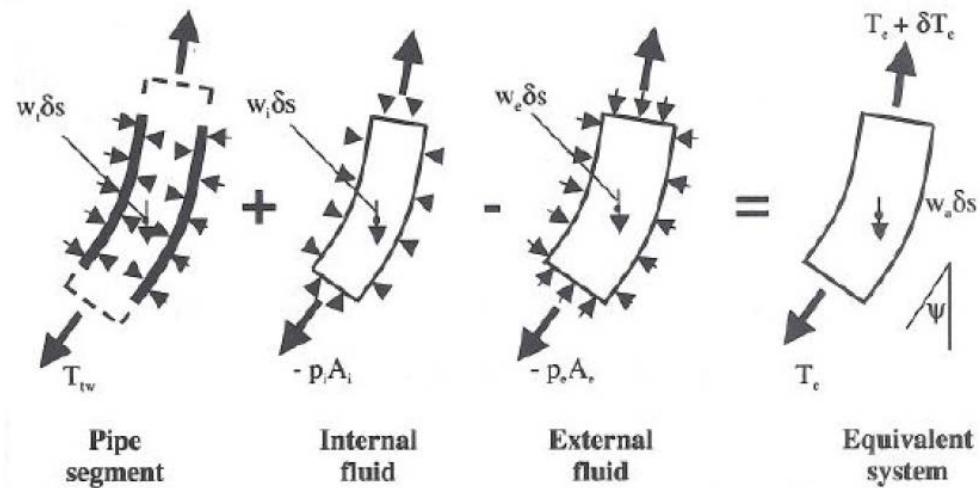


Figure 4-2. Internal and external forces acting on a riser segment [7]

The final equations for the effective tension and apparent weight are the following:

$$T_e = T_{tw} + (-p_i A_i) - (-p_e A_e) \quad (4.5)$$

$$w_a = w_t - w_i - w_e \quad (4.6)$$

where

- T_e effective tension;
- T_{tw} axial tension on the riser segment;

p_i	pressure from the fluid inside the riser;
A_i	internal cross-section of the riser segment;
p_e	pressure from the fluid outside the riser;
A_e	external cross-section of the riser segment;
w_a	weight of the equivalent system;
w_t	weight of the immersed riser segment;
w_i	weight of the internal fluid;
w_e	weight of the displaced fluid;

Assume an element with length of δs and the angles approach zero, reconsideration of forces in the vertical direction becomes:

$$\begin{aligned}\frac{dT_e}{ds} &= w_a \cdot \cos\psi \\ \frac{dT_e}{ds} &= \frac{dT_e}{dx} = w_a\end{aligned}\quad (4.7)$$

Based on the previous derived arguments, the general concept for calculation the effective tension and apparent weight of more complicated riser systems can be defined. However, the equations in this concept are reconsidered with condition of static equilibrium for each constituent element systems. Thus, there is no need for the circular cross-sectional area of the pipe, constant density of the material and its elasticity as well as angle deflections of the riser. This tends to consider the equations in more generic conditions. The equations for the effective tension and apparent weight and their physical definition are transformed into the following [7]:

$$T_e = \sum T_{tw} + \sum (-p_i A_i) - \sum (-p_e A_e) \quad (4.8)$$

$$W_a = \sum w_t - \sum w_i - \sum w_e \quad (4.9)$$

The physical definition of the effective tension can then be concluded as: “*Effective tension is the sum of the vertical force in the riser system, comprising inner fluids, less the vertical force in a column of the displaced fluid (tension is positive)*”. [7]

Therefore, these important conclusions allow calculations of more complex riser systems with nonstandard shape patterns, combination of pipes with fluid inside in movement and so on.

4.2. Stresses in Riser

This chapter presents the various stress fields occurring in the internally and externally pressurized riser under the tension.

4.2.1. Radial, Hoop and Axial Stresses

The pipe, shown in Figure 4-3, is pressurized with internal pressure P_i and with external pressure P_o . The inner radius of the pipe is r and wall thickness is t . There is also axially applied load F . The right-hand sketch shows a segment of pipe showing the generated stress due to the loadings, namely, σ_x , σ_y , and σ_z forming the triaxial stress field.

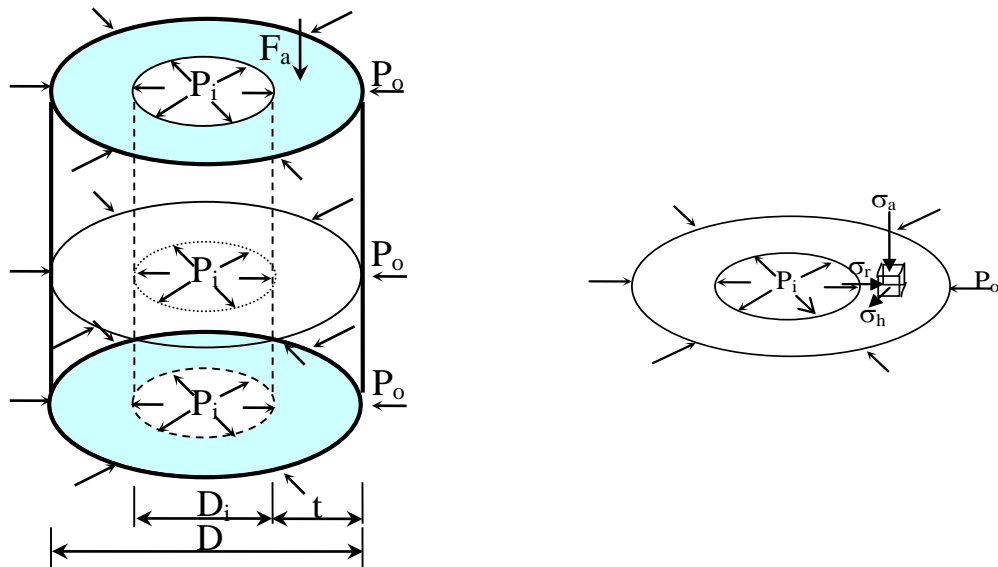


Figure 4-3. Tri-axial stress field

Consider a uniform pressure is applied to a circular thick-walled pipe. In order to consider this as a thick wall cylinder the criterion should satisfy that $t > 0.1 \cdot r$. Figure 4-4 presents the stress fields over the wall of the pipe in three directions. The stresses are known as the tangential stress σ_r acting circumferentially of the pipe, the axial stress σ_a acting in axial direction to the pipe, and the radial stress σ_r acting normally to the pipe wall. The knowledge of these stresses is necessary in order to perform design safe operational limits. [4]

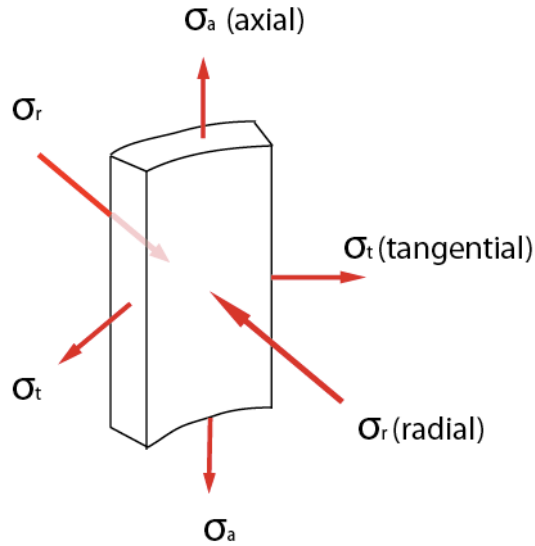


Figure 4-4. Stresses over the segment of thick walled cylinder [4]

The solutions of stress fields distribution over the segment can be derived by combining the following conditions, namely the equation of equilibrium (Newton Law), compatibility relations (geometrical relationship), constitutive relation of the stress-strain-temperature (Hooke's Law) and taking into account suitable boundary condition. These equations are named after a French engineer, Lamé', who solved the problem.

Radial stress [11]

$$\sigma_r = \frac{p_a \cdot a^2 - p_b \cdot b^2}{b^2 - a^2} - \frac{a^2 \cdot b^2}{(b^2 - a^2) \cdot r^2} (p_a - p_b) \quad (4.10)$$

Hoop stress [11]

$$\sigma_\theta = \frac{p_a \cdot a^2 - p_b \cdot b^2}{b^2 - a^2} + \frac{a^2 \cdot b^2}{(b^2 - a^2) \cdot r^2} (p_a - p_b) \quad (4.11)$$

Axial stress [11]

If the axial force is applied to the pipe the force (tension or compression) causes the axial stress. When the tubing is under the tension, the axial stress is equal to the axial force over the cross-sectional area of the pipe. [11] Figure 4-5 illustrates the stress distribution across the wall of the cylinder, which is loaded with inner pressure, P_a greater than the outer pressure P_b .

$$\sigma_a = \frac{F_a}{A} + \frac{p_a \cdot a^2 - p_b \cdot b^2}{b^2 - a^2} \quad (4.12)$$

where

- $p_a = p_i$ internal pressure in the cylinder;
- $a = A_i$ internal cross-sectional area of the cylinder;
- $p_b = p_e$ external pressure in the cylinder;
- $b = A_e$ external cross-sectional area of the cylinder;
- F_a applied axial load;
- r inner radius of the cylinder;

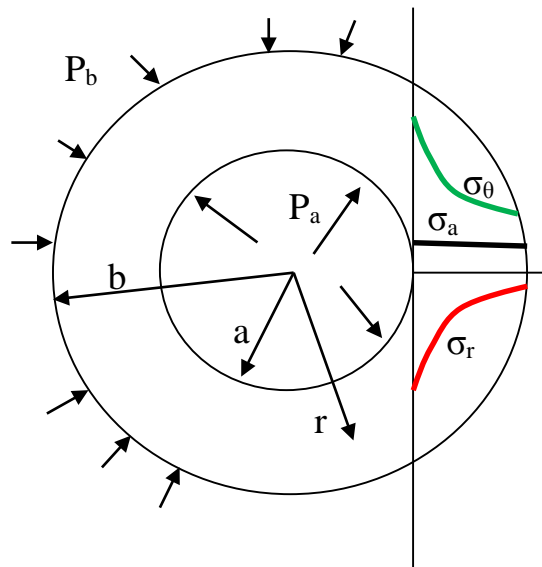


Figure 4-5. Stress distribution across the wall of the cylinder

4.2.2. Shear stress

For the thin walled cylinder with applied torque, the induced shear is approximated as [12]:

$$\tau = \frac{T}{2\pi \cdot r^2 t} \quad (4.13)$$

where

- T applied torque;
- r internal radius of the cylinder;
- t thickness of the wall;

4.2.3. Bending stress

Drilling doglegs and buckling can generate the bending stress field in the riser. The riser is exposed to a bending moment as well. Both effects are important to take into account during analysis. In order to derive the expression for the bending stress the theory of a beam is used. The maximum bending stress (σ_b) caused by the dogleg and is occurred at the outer diameter of the pipe.

$$\sigma_b = \frac{M}{I} y \quad (4.14)$$

where

M bending moment;

I second moment of the area;

y distance to the center of the pipe;

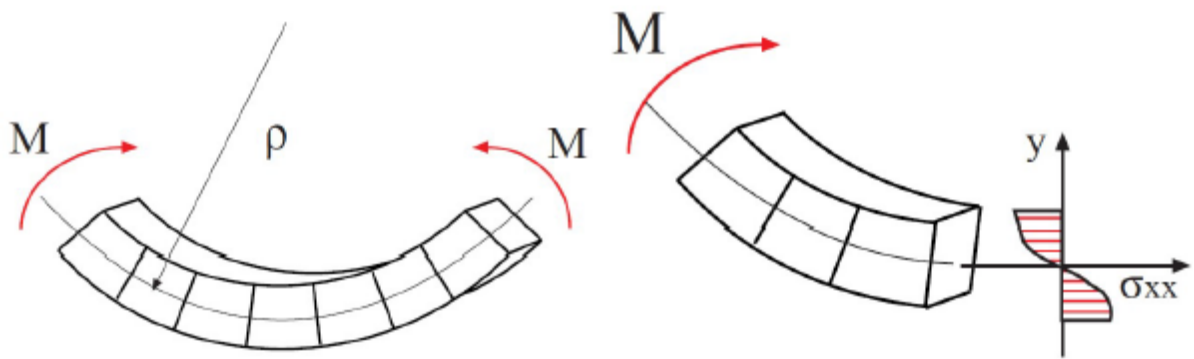


Figure 4-6. Bending moment acting on an elementary segment

$$\sigma_b = \sigma_{DL} = \pm \frac{ED}{2R} = \pm (\pi \cdot E \cdot D \cdot L \cdot D_o) / 432000 \quad (4.15)$$

where

E Young's modulus or the Modulus of Elasticity;

DL dogleg severity, degree/100ft;

R radius of curvature;

D_o outer diameter of the pipe;

+ pipe in tensile (on the outside of the bend);

- pipe in compression (on the inside of the bend);

Adding bending stress to the equation of the axial stress the maximum axial stress becomes:

$$\sigma_{a \max} = \sigma_a + \sigma_{DL} \quad (4.16)$$

The minimum axial stress can be calculated as follows:

$$\sigma_{a \min} = \sigma_a - \sigma_{DL} \quad (4.17)$$

4.3. Von-Mises Failure Criteria

The combined stresses may cause yielding of a material. Thus, the stresses in the walls of a riser needs to be computed in order to assess the condition of riser, whether the loading cause failure or not. Nowadays the most accurate and practical criterion for ductile materials is derived based on the maximum distortion energy criterion, which is also known as Von – Mises failure criteria. The combination of the three major stresses (axial, radial, and hoop stress) and the shear stress induced by applied moment is based on the initial yield limit. In general form for triaxial stresses the Von – Mises criteria is presented as [11]:

$$\sigma_{VME} = \sqrt{\frac{1}{2} \left\{ (\sigma_{\theta} - \sigma_r)^2 + (\sigma_r - \sigma_a)^2 + (\sigma_a - \sigma_{\theta})^2 \right\} + 3\tau^2} \quad (4.18)$$

where

σ_{vme} Von-Mises stress;

σ_{θ} tangential stress;

σ_r radial stress;

σ_a axial stress;

τ shear stress;

It is worth to note that the shear stress can be neglected in the equation if there is no applied torque. [11]

$$\sigma_{VME} = \sqrt{\frac{1}{2} \left\{ (\sigma_{\theta} - \sigma_r)^2 + (\sigma_r - \sigma_a)^2 + (\sigma_a - \sigma_{\theta})^2 \right\}} \quad (4.19)$$

Yielding occurs once the Von-Mises stress is equal to the yield strength of the riser material. Therefore, the limited conditions of yielding for riser are determined by setting the Von-Mises stress to the yield stress for the material. According to the API RP 16Q and ISO 13624 [1, 2], the 67% of yield stress will be taken into account during design.

The riser will be in reality subjected to moments that causes the bending stress. This should be included in the axial stresses while calculating the Von-Mises stress. The criterion is required to be verified at the outer surface with the maximum bending stress and at the inner surface, where the bending occurs at its minimum. The fundamental criterion will be then rewritten including the bending stress, σ_b .

$$\sigma_{VME} = \sqrt{\frac{1}{2} \left\{ (\sigma_\theta - \sigma_r)^2 + (\sigma_r - (\sigma_a + \sigma_b))^2 + ((\sigma_a + \sigma_b) - \sigma_\theta)^2 \right\} + 3\tau^2} \quad (4.20)$$

4.4. Design Limits

For designing purpose, the following condition should be considered:

$$\sigma_{VME}^{Design} = \max \left| \sigma_{VME}^{inner}; \sigma_{VME}^{outer} \right| \quad (4.21)$$

The tri-axial stress intensity design factor is given by [28]

$$SF = \frac{\sigma_y}{\sigma_{VME}} = \frac{\sqrt{2}\sigma_y}{\sqrt{(\sigma_\theta - \sigma_r)^2 + (\sigma_r - \sigma_a)^2 + (\sigma_a - \sigma_\theta)^2}} \quad (4.22)$$

There are four loads, which determine the combined stress limits in tubing, such as the internal and external pressure, the real axial force, and the torque. For simplification the presentation of the limits, the pressure difference ($P_i - P_o$) is calculated. A positive differential pressure represents a “Burst” mode. A negative differential pressure represents a “Collapse” mode.

The limits curve calculated by the Von-Misses yield condition represents where the tube would begin to yield.

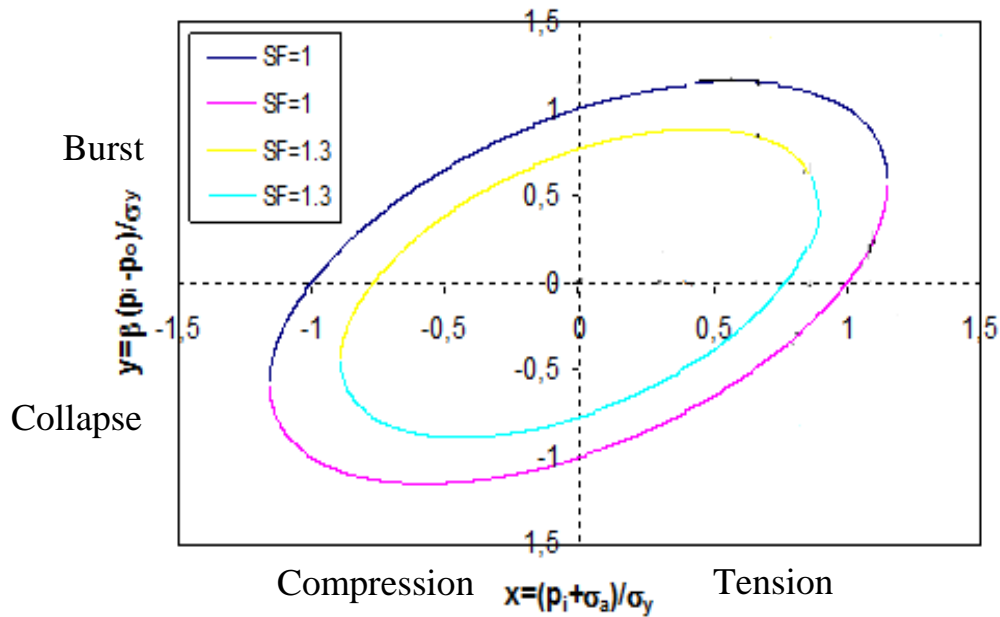


Figure 4-7. Von-Mises failure envelope for various Design Factors in 2D plane

4.5. Hydrodynamic Loads

The hydrodynamic actions of waves and currents on the drilling riser needs to be discuss prior to simulation in OrcaFlex and ANSYS software.

The waves and currents generate loads on the entire riser system below the water surface. The impact of these loads and load values can be determined by means of statistical analysis, using the potential size of the wave and extrapolating to the design waves.

The offshore drilling in deep water conditions is particularly influenced by current effects and therefore measurement of currents is required for having clear picture of operational conditions of the riser. In addition, the currents influence the riser by the drag force. Hence, the riser must withstand the impact of large currents at the same time as large waves occur. [13]

The Petroleum Safety Authority has developed a standard that all sea structures should satisfy the requirement of 100-year wave + 100-year wind + 10-year current. A 100-year wave means that there is one percent probability of surpass per annum. [13]

4.5.1. Currents

External forces induced by currents along the whole length of the riser below the sea line can significantly change the deflection of the riser system and influence the riser tension and optimum position of drilling vessel to minimize deterioration from rotating of the drill string. The curvature of the riser is dependent of the distribution of internal fluid weight, the top

position of the riser with respect to horizontal position of the bottom, the riser tension, and the greatness and direction of the drag and lift forces lengthwise the riser. In general, the current forces may change direction and magnitude with depth irregularly. Moreover, the actual drag/mass coefficients and function of induced force can only be determined representing a very complicated structural loading scenario. As a result, it is extremely challenging task to calculate the precise shape of the riser deflection even though the current profile is investigated. Nevertheless, practical experience has indicated that the riser deflects usually near the top and bottom of the riser string at the maximum angle, which is measured by the top and bottom installed angle-measurement devices.

If the profile is necessary to be calculated over the length of the riser string for engineering purposes, computer software as Orca Flex, which includes an algorithm for building the riser and current profiles, can be used. The riser and current profiles can be valuable for initial position of the dynamic positioning system on the floating drilling rig, as suitable position reference can be restricted in deep-water areas. In addition, the effect of inertia increases the time for the riser to achieve a new steady-state quasi-static form after a change in vessel position. This is observed in deep-waters when the bottom angle of the riser is utilized as a position reference signal. [14]

4.5.2. Vortex Induced Vibrations (VIV)

The vortex-induced vibrations or VIV are motions caused anytime on a blunt body, which is subjected to an external flow of fluid producing vortices around this body at its natural frequency. Vibrations caused by the periodic distribution of vortices are the most frequently found in the practice of construction engineering. The external flow around a bluff cylinder can be explained perfectly utilizing the theory of potential flow at low spread of the Reynolds number. However, the potential theory is not applicable in case of increased the Reynolds number, as boundary layers get detached from the walls of the cylinder. The main reason of this effect is that the fluid around the pipe creates the boundary layers, where viscous forces occur in the area of separation of the boundary layer flow and the layer of fluid next to the hard surface of the pipe.

The risers are particularly sensitive to VIV in deep-water applications comparing to the use in shallow-water areas due to the following factors:

- currents in deep-waters are in general more strong than in shallow-water areas;
- the natural frequency of the riser is lowered with increasing its length and therefore a required magnitude of flow to initiate vortex shedding is reduced as well;
- there are no structures on the drilling platform adjoining to the riser to which it could be attached as the mobile drilling units utilized in deep-water drilling are floating type of platforms;

Substantial currents excite a natural mode of the bending, which is much greater than the basic bending mode of the riser in deep water drilling operations. The velocity (and direction) of currents in deep-water areas changes in general with depth, so there is a possibility that numerous modes of the drilling riser can be provoked into vortex vibrations. Hence, the prediction of the riser behavior concerning VIV becomes more complicated opposed to the short riser systems used in shallow waters.

4.5.2.1. Flow Regimes

Various flow regimes of fluid around the circular cylinder are presented in the Figure 4-8. As shown on Figure, at very small Reynolds number, $Re < 5$, inertial effects are insignificant and the pressures, behind the cylinder at the end of the stream, recover almost to the same initial conditions. Hence, the fluid flow can be described by the theory of potential flow and initiation of vortex shedding is not observed at these values of Reynolds number. A couple of stable vortices are induced immediately at the right side of the cylinder with increased number of Reynolds. With further increase of the Reynolds number, the vortices extend while one of the vortices detaches away and a periodically fluctuated vortex path is generated. The laminar flow of vortex path is occurring up to Re values of 150, and gets into turbulent flow if the Re values equal or higher than 300. Afterwards the vortex path transforms into a fully turbulent state at the distance of approximately 50 diameters of the cylinder downstream. The Re numbers in the diapason of 300 to $3 \cdot 10^5$ is known as a subcritical range, since it is occurred before initiation of the turbulent boundary layer at Re of $3 \cdot 10^5$. However, the vortices path is occurred in turbulent mode with established frequency for subcritical diapason. [15-17]

Vortex shedding happens at a much lower point downstream of the cylinder, at the laminar-turbulent transition range. Vortex shedding forms disarranged flow and the drag declines quickly. The vortex street is recovered only at supercritical values of the $Re > 3 \cdot 10^5$, as boundary layer gets into turbulent mode over again.

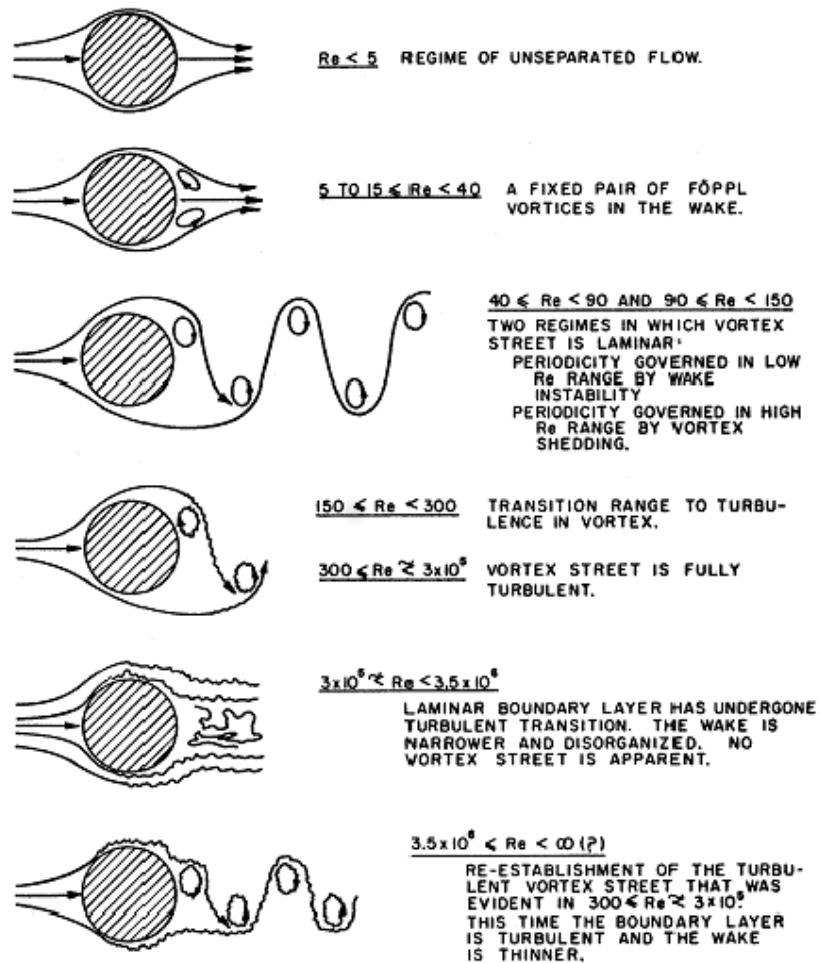


Figure 4-8. Flow regimes of fluid over cylinder [18]

4.5.2.2. VIV Mitigation Techniques

The riser for deep-water application can fail to satisfy the fatigue requirements due to inadequate design for vortex-induced vibrations. Mitigation VIV is therefore becomes the main task to prevent destruction of the riser and high-costly expenditures. There are many diverse methods in order to reduce VIV oscillation of the riser. The most widely used techniques are: [19]

1. Increasing structural damping.

This approach enables to increase the structural damping or mass of the riser so that the hazardous oscillations of the riser system will be gradually diminished. Increase of damping can be obtained by different means, as:

- Attachment of external dampers.
- Use of materials with sufficiently high damping such as rubber, sand, wood, etc.
- Composite materials like concrete can be included in place of steel constructions.

2. Preventing resonance.

VIV can be suppressed if we ensure the natural frequency not matching the frequency of vortex shedding of the structure. This can be achieved by using wires or braces to increase the structural stiffness of the riser. However, the technique becomes impractical solution when it is applied for either complex or large structures.

3. Installation of suppression devices.

The use of vortex suppression devices is the most practical option to be chosen for VIV mitigation. Nevertheless, it is a challenging task to design, test and analyze the suitable device.

M.M. Zdravkovich subdivided suppression devices into three main groups [20]:

- Surface Protrusions

They influence the separation of shear layers and separated lines. The typical examples of this device are studs, fins, strakes, wires, etc. They can be further split into two types:

a) Omni-Directional Devices are the type with no preferred direction as the expression “omni-directional” indicates. Helical strakes represent the most used VIV suppression devices in the group of omnidirectional devices.

b) Uni-Directional Devices. The devices in this group are very effective at one optimal direction but less effective at others.

- Shrouds

Shrouds mitigate VIV by interacting with the entrainment layers. These devices are attached completely around the riser. Axial rods, perforated rods, gauze, and axial slats are the best examples of this type.

Marine fairings are classified into this category.

- Near-wake Stabilizers

For the group the best examples can serve the devices, such as guiding, splitter, and saw-tooth plates, slits cut, base-bleed, vanes along the riser etc.

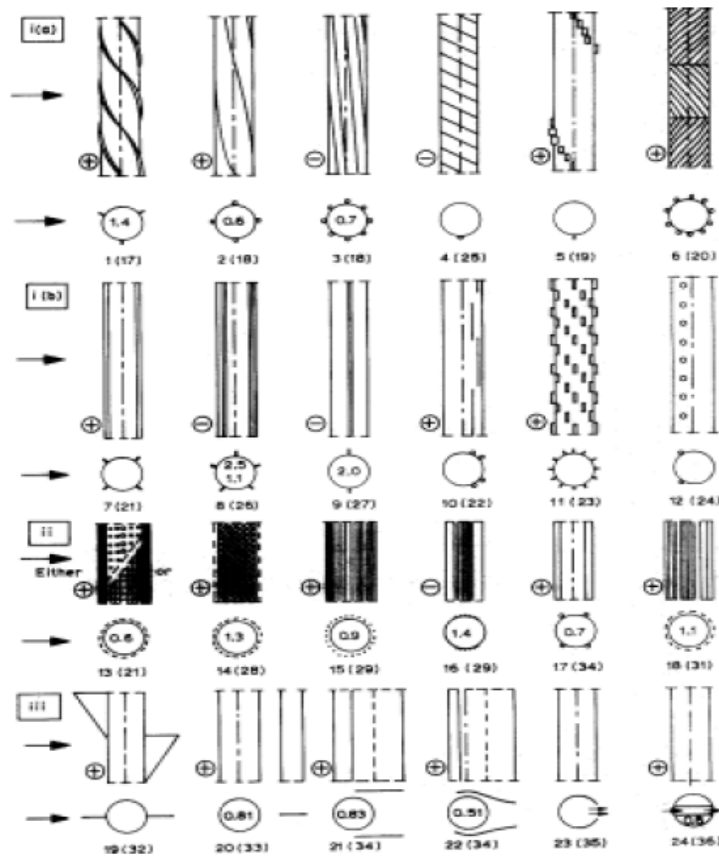


Figure 4-9. Hydrodynamic and aerodynamic devices for reduction the vortices shedding [20]

4.5.3. Morison's Equation

The Morison's equation can be used to find the combined impact of wave and current loads on the structures with a cylindrical shape like the drilling riser. It has been deemed contentious for many years due to a non-linear drag term in the equation. The equation allows the hydrodynamic forces to be calculated with reasonable precision, considering the diameter of the riser smaller as opposed to the length of waves. The trip theory is applied for calculation forces per unit length of the riser in a two-dimensional plane. The hydrodynamic force in the Morison's formula combines two components – a drag force, due to the fluid flow velocity, and an inertia force, because of the flow acceleration. [7]

$$f_H = f_D + f_I \quad (4.23)$$

where

f_H hydrodynamic force;

f_D drag force;

f_I inertia force;

The laboratory experiments have investigated for the flow in a steady state the drag term changes with the square of the fluid flow past the riser. For the drilling riser, exposed to the flow in normal direction to its axis, the drag force per unit length of the riser can be approximated with the following expression [7]:

$$f_D = \frac{1}{2} \cdot \rho \cdot C_D \cdot D \cdot u \cdot |u| \quad (4.24)$$

where

ρ density of the fluid;

C_D non-dimensional drag coefficient determined from the experiments;

D outer diameter of the riser;

u velocity of the fluid particle past the riser;

If the riser moves laterally with a velocity v under acting forces, it should be taken into account in the determination of the drag force. It is done by including the relative velocity in the expression for the drag force calculation [7]:

$$f_D = \frac{1}{2} \cdot \rho \cdot C_D \cdot D \cdot (u - v) \cdot |u - v| \quad (4.25)$$

The laboratory tests have also been performed to examine the lifting force. This force is caused by the fact that the velocity of fluid particles in the eddy currents is higher on the downstream side compared to the upstream side. Hence, the pressure is a minimum on the downstream side, which resulting in a lifting force in the current direction. The approximate expression for the lift force per unit length of the riser can be written as [7]:

$$f_L = \frac{1}{2} \cdot \rho \cdot C_L \cdot D \cdot u \cdot |u| \quad (4.26)$$

where C_L is the dimensionless lifting coefficient determined from the tests and the other components are the same as in the expression of the drag force.

For the risers which satisfy the requirement $D/L < 1/5 = 0.2$, the fluid nearby the riser will be dragged along the flow. Therefore, we get an additional mass, which is accelerated. The resulting mass force per unit length of the riser can be expressed as [13]:

$$f_M = f_I = (m + m_A) \cdot \dot{u} = \left(\rho \cdot \frac{\pi D^2}{4} \right) \cdot C_M \cdot \dot{u} \quad (4.27)$$

where

$$m = \left(\rho \cdot \frac{\pi D^2}{4} \right) \quad \text{mass of a unit length of the riser;}$$

m_A additional mass;

ρ density of the fluid;

D outer diameter of the riser;

$C_M = C_I = (1 + m_A/m)$ non-dimensional mass or inertia coefficient;

\ddot{u} constant acceleration of the fluid;

For the riser under the action of waves, a combined effect of acceleration and velocities should be taken into consideration. If the acceleration is assumed constant over the riser, i.e. $D/L < 1/5$, the Morison's equation can be presented in the form as follows [13]:

$$f(z, t) = f_M + f_D = \left(\rho \cdot \frac{\pi D^2}{4} \right) \cdot C_M \cdot \ddot{u} + \frac{1}{2} \cdot \rho \cdot C_D \cdot D \cdot u \cdot |u| \quad (4.28)$$

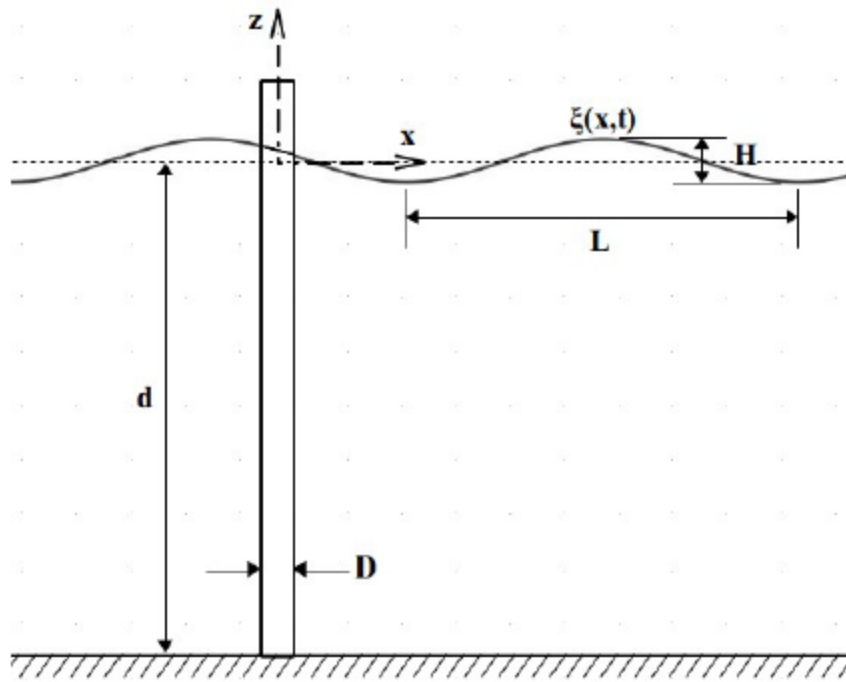


Figure 4-10. Immersed cylindrical pipe under wave action [13]

This is worth to mention that this force is the sum of the drag force and the mass force. However, the total force from waves on the whole riser system is:

$$F(t) = \int_{-d}^{surface} f(z, t) dz = \int_{-d}^{\xi} f_M(z, t) dz + \int_{-d}^{\xi} f_D(z, t) dz \quad (4.29)$$

The coefficients of drag and mass should be defined for each particular case. The drag coefficient is a function of several parameters, such as, roughness of the riser surface and Reynolds number for the fluid flow. That means that the higher roughness on the surface, the greater the drag coefficient will be and hence greater force on the riser. Since it also is much dependent on the Reynolds number (which in turn a function of velocity), the coefficient will vary with the water depth as the velocity changes. The figure below shows the drag coefficient as a function of Reynolds number for various structural shapes. [13]

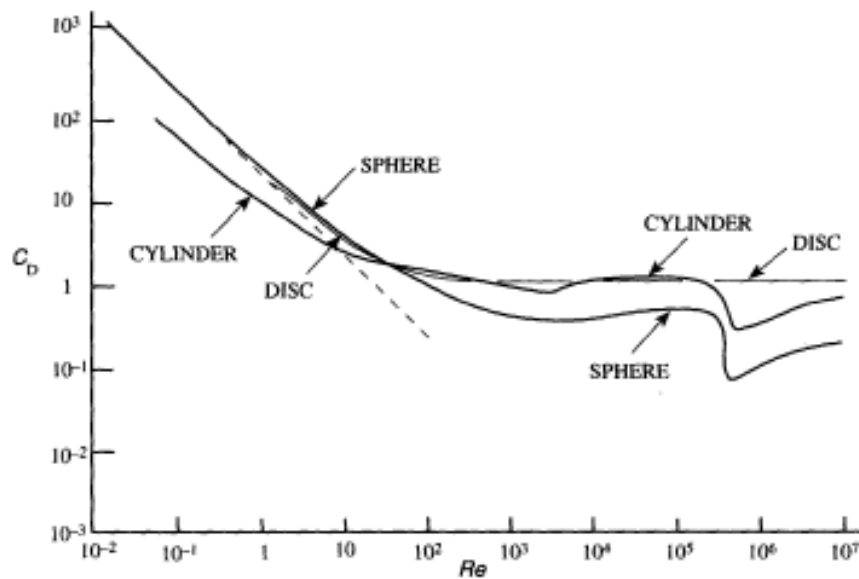


Figure 4-11. Drag coefficient as a function of Reynolds Number for spheres, transverse cylinders, and face-on discs [13]

The mass coefficient is also a dimensionless number and is dependent on the relation D/L , where D is the diameter of the riser and L is the wavelength. Note the Morison criteria $D/L < 0.2$. The figure below shows the mass coefficient as a function of D/L .

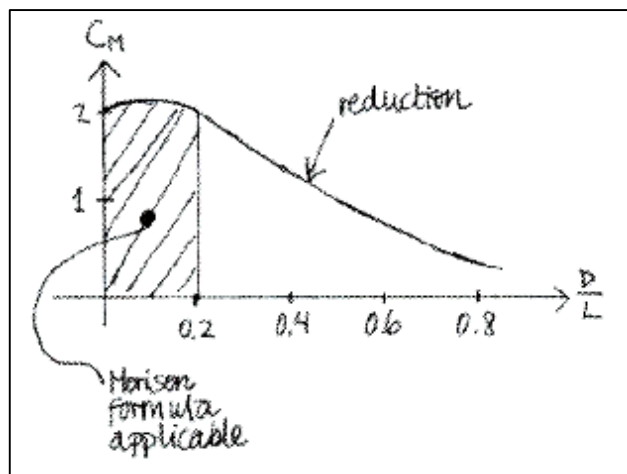


Figure 4-12. Mass coefficient as a function of D/L [21]

There are various standards to find values for the drag coefficient based on different requirements, for instance, NORSOK Standard N-003.

“For surface piercing framed structures consisting of tubular slender members extreme hydrodynamic actions on unshielded circular cylinders are calculated by Morison’s equation on the basis of drag and inertia coefficients equal to

$$C_D = 0.65 \text{ and } C_M = 1.6 \text{ for smooth members}$$

$$C_D = 1.05 \text{ and } C_M = 1.2 \text{ for rough members}$$

These values are applicable for $(u_{max} \cdot T_i)/D > 30$

where

u_{max} the maximum horizontal particle velocity at storm mean water level under the wave crest;

T_i the intrinsic wave period;

D the leg diameter at the storm mean water level;

NORSOK Standard N-003”

However, the drag coefficient can be assumed constant over the entire riser structure, which may result in higher loads than realistic. Following coefficients can be taken for calculation of the total force acting on the riser:

- If the drag term mainly dominate, the drag coefficient is equal to $C_D = 1$.
- If the mass term will dominate, the mass coefficient is equal to $C_M = 2$.
- If both of the forces are considered, the drag coefficient is $C_D = 1.05$ and the mass coefficient is $C_M = 1.20$.

4.6. Sea Ice Impact

The ice presents significantly dangerous threat to the mobile drilling unit. [1]

Ice at sea may be originally formed on either land (glacier) or at the sea. In general, ice formed on land exists as floating pieces of ice whereas ice formed at sea may be in the form of drifting ice floes. Additionally, ice is also classified by age and by thickness, size, surface area, and elevation above water (Bowditch, 1977).

If possible, operations should be avoided in the presence of sea ice as drifting ice floes may induce severe loads on the MODU and its dynamic position-keeping system. Moreover, moving ice chunks are hazardous in particular because they can come near the vessel undetected by radar due to their small sizes.

A drillship's hull can protect the riser against the action of small broken-up pieces of the ice. However, ice may be pushed under the vessel by a sufficient combined impact of the wave, current and/or wind. An "ice ledges" around the moon pool can deflect ice from entering the moon pool and affecting the riser. [1]

In general, the drilling risers installed on semisubmersibles are less protected against the ice at sea. Special skirts or round-shaped columns, which extend below the ice zone, can effectively protect the riser. [1]

CHAPTER 5. ENVIRONMENTAL CONDITIONS IN THE KARA SEA

5.1. Geographical Location

The Kara Sea is situated at the margin of the Arctic Ocean Basin in the northern part, bordering on the Barents Sea (Yugorsky Shar, Karskie Vorota (Kara Gate) and Matochkin Shar Straits, and between the northern end of Novaya Zemlya and Franz Josef Land Archipelago) in the west and the Laptev Sea (Vikitsky, Shokalsky and Krasnaya Armiya (Red Army) Straits) in the east. [22]

The western border of the Kara Sea starts from Kolzat Cape ($81^{\circ} 08' N 65^{\circ} 13' E$) to Cape Zhelaniya ($76^{\circ} 57' N 68^{\circ} 36' E$), hereinafter passing the eastern shores of the Novaya Zemlya islands, the western border of the Matochkin Shar Strait, from the Serebryany Cape (Silver Cape) to Stolbovoy Cape, the western border of the Kara Gate Strait, from Kusov Noss Cape to Rogaty Cape, along the eastern shore of the Vaigach Island, and the western boundary of the Yugorsky Shar Strait from Bely Noss Cape (White Nose) up to Greben Cape; the northern border of the sea extends from the Kolzat Cape to Arctic Cape ($81^{\circ} 16' N 95^{\circ} 43' E$) Severnaya Zemlya Island, the Komsomolsky Island; the eastern boundary runs along the northwestern coast of the Severnaya Zemlya Island and the eastern borders of the Krasnaya Armiya, Shokalsky, and Vilkitsky Straits; the southern border – mainland coast from the Bely Noss Cape to Pronchishev Cape. [23]

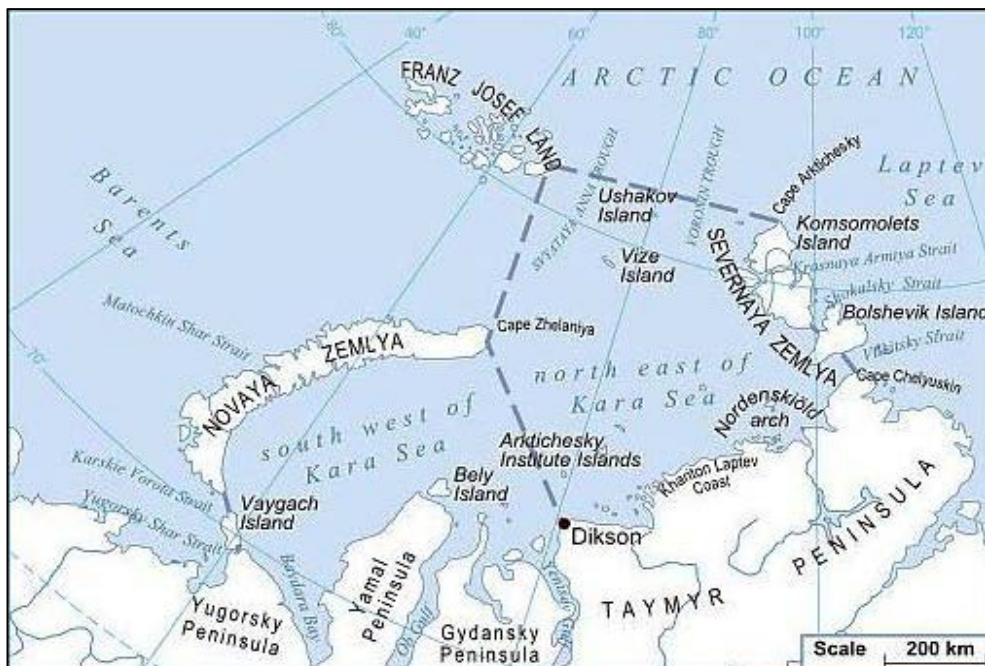


Figure 5-1. Map of the Kara Sea regions and boundaries [22]

The largest bays that form a strongly irregular coastline and get deeply to the shore of mainland are Baidaratskaya, Gydanskaya, Ob Bays and the Yenisey Gulf. According to the oceanographic conditions, the Kara Sea is usually subdivided into two parts, northeastern and southwestern. The dashed line passing from Zhelaniya Cape to Dikson Island is a border of the Kara Sea regions as shown in Figure 5-1. [24]

The total area of the Kara Sea is approximately 883 000 km², with a mean water depth of 111 m and the maximum depth reaches 600 m in the Svyataya Anna Trough and Voronin Trough. The Kara Sea has less than one percent of the total area occupied by the deep-water regions (deeper than 500 m). The sea water volume is 98 000 km³. The Kara Sea is roughly 1500 kilometers long and 800 kilometers wide in the northern part of the sea. [24]

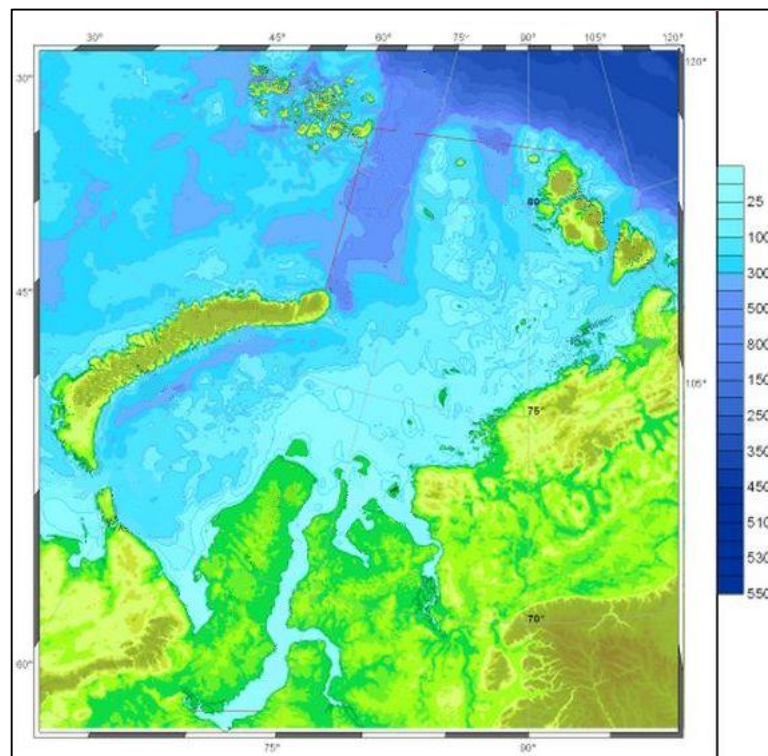


Figure 5-2. Depth distribution in the Kara Sea [23]

5.2. Climate

The arctic climate is prevailing in the Kara Sea region with a cold and dry air. The air masses are drier and colder in winter whereas they are relatively warmer in summer time. The air temperature in the region keeps constant below 0 °C for 9 – 10 months in the north and for 7 – 8 months a year in the south. The period from December to March is considered as the coldest with the average monthly temperature of -14 – (-28) °C. The minimum observed temperature

during winter is $-48\text{ }^{\circ}\text{C}$. The summer is short and lasts from June to September, with mean air temperature is not higher than $7\text{ }^{\circ}\text{C}$. During the summer the temperature in the region may approach up to $16\text{ }^{\circ}\text{C}$. [24]

Also, during the summer time fogs are often observed.

5.3. Wind

The very fast Bora wind blowing with speed of up to 40 m/s is formed on the Novaya Zemlya, Severnaya Zemlya and Franz Josef Land Archipelago. [24]

Strong storms are often accompanied by blizzards in winter and snow squalls in summer. The western part of the sea is mostly exposed to the storms impact. [23]

5.4. Hydrological Conditions

5.4.1. Waves

The Kara Sea region is opened to very fast and frequent winds which lead to developing significantly high waves. Besides that, the size of waves is dependent of the wind speed and its duration. The amount of ice at the sea also influences the wave size as it defines the length of the wind fetch. Therefore, the most powerful waves are registered in the time with small amount of sea ice during the end of summer to the beginning of autumn. [25]

The most frequently occurred waves have the mean height of $1,5$ to $2,5\text{ m}$. The Kara Sea is not characterized by very high waves, which exceed 3 m , but the maximum observed wave height is approximately 8 to 10 m . The most severe waves occur in the areas that are usually not covered with ice, such as northwestern and southwestern parts of the sea. In general, the shallow-water areas in the center of the sea are described by smaller waves, which become more steep and short in storms. The wave heights are reduced by sea ice in the northern parts. [22, 24]

5.4.2. Currents

The system of currents in the Kara Sea is comparatively stable with surface and deep water movements. These sea water movements are associated with the river runoff, water exchange with the Barents Sea and Laptev Sea, and water circulation in the Arctic Basin. The river runoff does not affect the speed of currents but keeps the water flow steady. As it can be

seen in Figure 5-3, there are two main cycles moving counterclockwise along northeastern and southwestern regions of the sea. [22]



Figure 5-3. Surface currents distribution in the Kara Sea [22]

In general, the currents driven with the wind prevail in the shallow-water areas. The speed and direction of sea currents vary with depth. The water movement is considered to be stable in the summer period. As a result, it forms a cyclic movement in the southwestern region of the sea including a comparably cold East-Novozemelsky Current flowing southward along the east coasts of Novaya Zemlya and a comparatively warm Yamal Current flowing northeastward from the Kara Gate Strait. [22]

The speed of currents is rather small but can increase significantly with strong and long lasting winds. Near surface maximum speed of current vary from 80 to 100 cm/s. [24]

5.4.3. Water Temperature

Since the Kara Sea is located in the high latitudes and covered by ice almost the whole year, it is heated up poorly and this leads to a low water temperatures. The surface temperature of water decreases from the south-west part to the north-east part of the sea. The sea surface temperature gradually increases only in the southern regions. [25]

In winter, the water layer under the ice has the temperature similar to the freezing point of water. In the shallow-water areas, the water masses become almost homogeneous from the seabed up to the surface, reaching the temperature of $-1,8^{\circ}\text{C}$. [23]

In summer (in the beginning of July), the sea water is warmed up slowly. The temperature of water reaches its maximum by the end of August when the sea becomes free of

ice. In the coastal areas, the surface temperature of water rises up to 6 °C to 8 °C. In the central region of the sea, the surface water temperature is about 2 °C to 4 °C whereas in the western sea region, the water temperature at the sea is approximately 2 °C. [24]

5.5. Sea Ice Conditions and Icebergs

The ice covers 7/10 to 9/10 of the total area of the Kara Sea for 8 to 10 months a year. Generally, an early formation of ice starts in October in the southern areas of the sea and in September in the north. The ice covers almost the entire sea from October to May. The coastal areas are considered as the fast zones of ice formation. In these zones the land-fast ice splits up into separate floes in the summer time. The sea is completely free of ice typically in the southwestern part and in the coastal northeastern regions of the sea during the summer. [24]

The ice distribution during the summer, autumn, winter and spring season is dependent of the winds. The ways of ice movement is principally from north-east to south-west. [25]

It is worth to note that the ice cover consist of various types and ages of the sea ice. In the north of the sea, a thickness of a multi-year ice reaches about 2,5 m, thickness of a first-year ice approaches up to 1,8 m and young-ice up to 0,3 m covering fissures. [24]

The ice types in the Kara Sea can also be divided by the way of ice cover development as following [25]:

- Primary Ice (forming as a first one);
- Secondary Ice (forming under the Primary Ice);
- Overlying Ice (forming at the top of the ice cover);
- Agglomerated or Broken-up Ice.

Icebergs usually drift near the west coast of the Severnaya Zemlya and the northeast coast of Novaya Zemlya Archipelago. A map of the annual probability of encountering an iceberg with a grid cell resolution of 100×100 km is presented in the Figure 5-4. In the southern coastal regions icebergs have not been observed as it can be seen from the picture. [24]

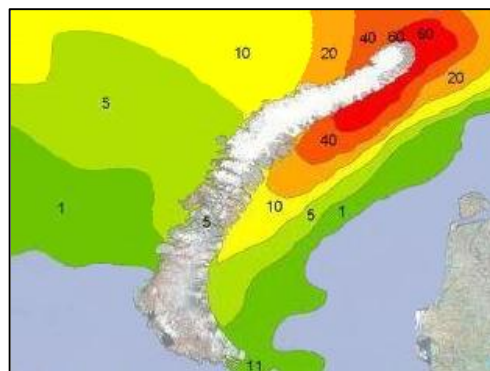


Figure 5-4. Probability (%) of occurrence an iceberg within a year [26]

CHAPTER 6. SIMULATION TOOLS AND ANALYSIS OF DRILLING RISER

The analysis and assessment of the drilling riser for application in the Kara Sea will be performed by means of computer software, such as OrcaFlex and ANSYS. These are powerful tools, which can design and simulate a desired riser systems along with loadings. In this thesis work, the selected riser will be assessed in accordance with ISO 13624, API RP 16Q and DNV-OS-F201 standards by taking into account operational conditions and all possible loading scenarios.

6.1. Simulation in OrcaFlex Software

In this work of the riser assessment, OrcaFlex is considered as the basic program used to simulate the drilling riser behavior at the conditions of the Kara Sea. This chapter presents description of the theory behind the program and modeling of the mobile drilling unit with the riser system. The latest version 9.8a of OrcaFlex Manual is used in a great extent to write this chapter.

According to OrcaFlex Manual, the software can be used for analysis of various marine systems, in particular the drilling risers, at static and dynamic conditions. The software is based on fundamental methods of three-dimensional (3D) finite element with concentrated mass to make calculations more effective and facilitate a mathematical formulation. [27]

The modeling process can be split into few steps. A model of the mobile drilling vessel with the marine riser system is created at first. A full and precise model will be described in the further chapters. Then environmental conditions should be specified, such as wind, waves, current, water temperature, and many others. Afterwards a preferred analysis is chosen and the simulation is run. As a result of the simulation, a suitable data can be extracted for a subsequent analysis. [27]

In the next sub-chapters the basic principle, which is behind OrcaFlex, as well as static and dynamic tools will be discussed.

6.1.1. Coordinate Systems

First and foremost it is worth to note that the different types of coordinate systems are used in OrcaFlex software.

As illustrated on Figure 6-1, the global system of axes GXYZ has the directions GX, GY and GZ, where the Z-axis should have positive direction upwards. The system reference is typically arranged at the water surface in the vessel and riser modeling although the position can be changed by the user. [27]

Each object in the model has its own local system of axes, which usually denoted by Lxyz. The reference of the local coordinate system is placed at the chosen fixed point but it changes the space orientation depending on the position of object. The origin and local axes are also specified for the sea bottom to define its shape. [27]

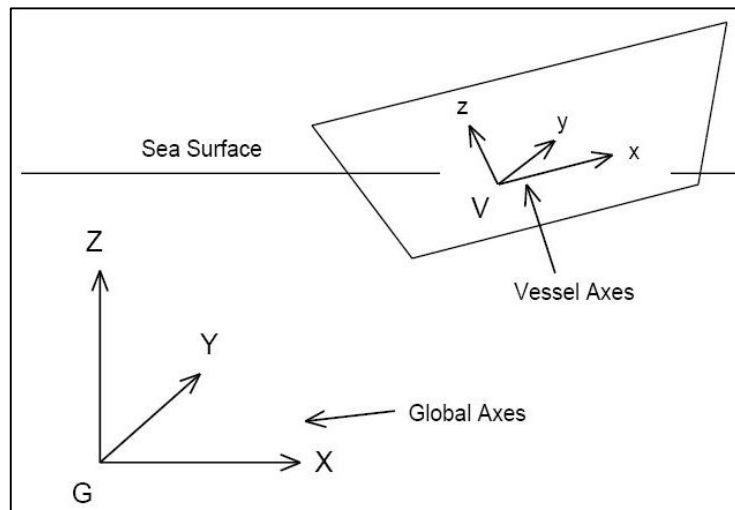


Figure 6-1. Coordinate systems in OrcaFlex [27]

In OrcaFlex the directions and headings are defined by using the azimuth angle of the direction, measured from the x-axis to the y-axis anticlockwise, as presented in the Figure 6-2.

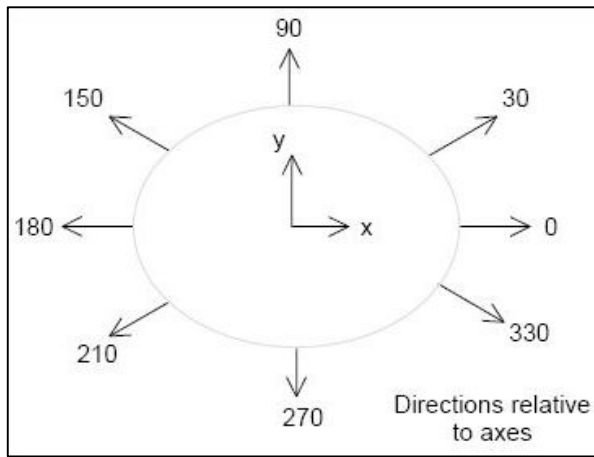


Figure 6-2. Directions with regard to global axes [27]

The propagation of waves, current and wind is defined by using their directions of progression with regard to global axes. The direction of the vessel Vx -axis is used to specify vessel headings. For instance, if the vessel heading is in the direction of Vx -axis in Figure 6-2, a wave direction of 0° implies that the wave is propagating from stern towards bow.

6.1.2. Discretized Model of Line

An actual drilling riser is represented in OrcaFlex as a line model that can be used in program calculations. The discretized line model is comprised of massless segments with torsional and axial properties as well as nodes, which model the properties of actual riser segments such as weight, mass, buoyancy, drag forces and many others. [27]

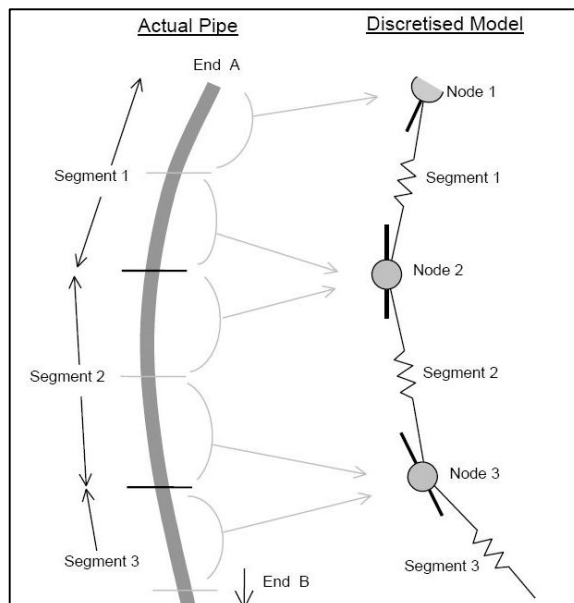


Figure 6-3. Model of the actual riser and discretized model of the line [27]

As shown in Figure 6-3, the nodes are modeled as short rods with properties, which are calculated as the properties of half-length segments at both of the sides of the node. Forces and moments are also applied at the nodes.

Figure 6-4 gives more detailed representation of the line model, including three various types of spring-damper systems that actually model the line properties. [27]

The axial spring-damper at the center of each segment is used to model the axial stiffness and damping of the line. It also applies an opposite and equal effective tension to the nodes at either side of the segment. [27]

The rotational spring-damper system is placed at both of the sides of the node to represent the bending properties of the line. This system allows modeling with various bending stiffness along the length of the line model. [27]

Besides two described systems the damping and torsional stiffness of the line are represented by the torsional spring-damper system if torsion is considered in the model. Otherwise, if torsion is not considered then this system is not included at the middle of the segment and the halves of the segment are twisted freely with regard to each other. [27]

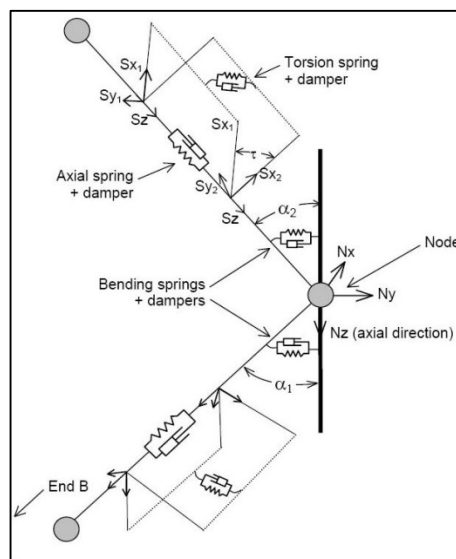


Figure 6-4. Illustration of various types of the spring-damper systems [27]

6.1.3. Static and Dynamic Analysis

A large part in the analysis of the riser system is devoted to the calculations of forces and moments. These calculations are carried out in five steps as follows [27]:

- Tension forces;
- Bending moments;

- Shear forces;
- Torsion moments (if included);
- Finally total load.

The analysis can be run once the model is built up and the correct environmental conditions are specified in the model. In OrcaFlex the analysis is comprised of two main parts, a static analysis and a subsequent dynamic analysis.

6.1.3.1. Static Analysis

The static analysis is carried out to find the position of the drilling riser when it is in an equilibrium state with loads acting from the riser system itself such as mass, buoyancy, weight etc. The equilibrium position is calculated by an iteration method from the initial point of the riser system, which is defined by the input parameters. It is assumed that the line ends are fixed in order to calculate the position of each line. Then the resultant force and moment from the system is determined. A new position of the entire riser system can be found afterwards. This process is repeated until the resultant force is equal to zero. The equilibrium configuration of the system is then used as an initial position for the dynamic simulation/analysis. This is important to note that the analysis takes into account the loads acting from the wind and current but not loads acting from the waves. [27]

6.1.3.2. Dynamic Analysis

The dynamic analysis enables simulation of the system movements over a particular period of time. The movement can be further used in finding the forces, moments and displacements in the system under the specified load. For smooth transition from static to full dynamic motion there is a build-up time when the wave and vessel movements are ramped up from zero to the full level. Once the simulation is completed a tool called View Profile allows having a quick look on how the system behaves over the specified period. [27]

The dynamic analysis in OrcaFlex is based on solving a basic equation of motion, which is given as [27]:

$$M\ddot{x} + C\dot{x} + Kx = P \quad (6.1)$$

where

M mass matrix;

C damping matrix;

K global stiffness matrix;

P function of external loads;

\ddot{x}, \dot{x}, x acceleration, velocity, and displacement, respectively.

The calculation of the equation can be done by two different schemes. The explicit integration and implicit integration scheme work in the same principle, computing the new geometry of the system at every time step. [27]

The explicit scheme applies forward Euler with a constant time. Once the initial positions are found from the static analysis all forces and moments that act on each node and body in the system, are calculated. Then the results are used to compute the special local equation of motion for each node and body in the line model. [27]

$$M\ddot{x} = P - C\dot{x} - Kx \quad (6.2)$$

The equation is further solved for the acceleration at the start of the time step. Then the configuration of the nodes and free bodies are found at the end of the time step, using forward Euler method of integration. This process is repeated over the simulation time. [27]

The implicit scheme of integration performs the calculation of moments and forces etc. in the same principle as the previous scheme. However, it applies the “generalized- α ” method of integration so that the basic equation of motion is solved at the end of the time step. [27]

6.2. Modeling

Modeling of the drilling riser is performed so that the simulation of the reality is implemented as accurate as possible in the program. However, the modeling requires particular limitations associated with assumptions and simplifications in order to carry out the calculations; hence, it will affect the reality in the model. Therefore, it is a particularly worth to note that the physical properties of the riser and environmental conditions should be transferred accurately in the transition from the reality to program model.

The drilling riser model is built up as a vertical beam subjected to waves and sea currents, from a modeling point of view. The upper boundary conditions of the riser are motions of the drilling platform. The rig motions are dependent of the rig design, wind and wave impact. In this thesis the model of the riser system is created on the basis of the drilling riser that can be used in the conditions of the Kara Sea. Therefore, a semi-submersible drilling rig of Transocean, called “GSF Development Driller II”, is chosen to be used in the analysis. In the next sub-chapters the model of drilling platform with the riser system will be described.

6.2.1. Drilling Rig Modeling

6.2.1.1. SSDR “GSF Development Driller II” Specification. General Description.

The “GSF Development Driller II” is a semi-submersible drilling rig capable to perform operations in ultra-deep water and harsh environments. The rig’s design can be configured to keep the vessel at the station by either Dynamic Positioning or by Anchoring. The deck areas and variable deck load capacities provide significant flexibility for exploration drilling or for subsea development projects. Station keeping in the dynamic positioning mode is achieved by eight efficient, variable speed, fixed blade thrusters. The general description of specification is presented in table 6-1.

Parameter	Description
	<u>Dimensions</u>
Length	114 m (375 feet)
Width	88 m (288 feet)
Height	8,5 m (28 feet)
Maximum Water Depth	2286 m (7.500 feet)
Maximum Drilling Depth	11430 m (37.500 feet)
	<u>Drilling Equipment</u>
Derrick Height	70 m (228 feet)
Derrick Length	16 m (52 feet)
Base Width	17 m (57 feet)
Hookload Capacity (maximum rated static hook load)	907000 kg (2.000.000 lbs)
	<u>BOP & Subsea Equipment</u>
BOP Rams	Hydril Compact 18-3/4 inch, 103, 4 MPa (15.000 psi) pressure capability; 6 x ram preventer; (2 x doubles + 2 x singles).
BOP Annulars	2 x Hydril GX 18-3/4 inch, 10.000 psi pressure capability annular preventer
Marine Riser	Kvaerner Clip 21 in., min yield 36.000 psi, 22,8 m (75 feet) long per joint.
Moonpool Length	40,2 m (132 feet)
Moonpool Width	7,6 m (25 feet)
	<u>Station Keeping / Propulsion System</u>
DP System	Kongsberg Simrad SDPM DP-2+
Thrusters	8 x ABB Compact Azipod 4.300 hp, azimuthing nozzled fixed blade thruster (2 x per corner)
Mooring System	8 Bodewes electric 1.150 hp drum winches with 8 x Bridon Dyform mooring lines consisting of 3200 m (10.500 feet) of 3.5 inch wire-line and 8 x 3.240 ft. of 3.25 inch stud link chain, with 8 x 14.75 ft. Vryhof Stevpris MK5 anchors.

Table 6-1. Specification of SSDR “GSF Development Driller II”

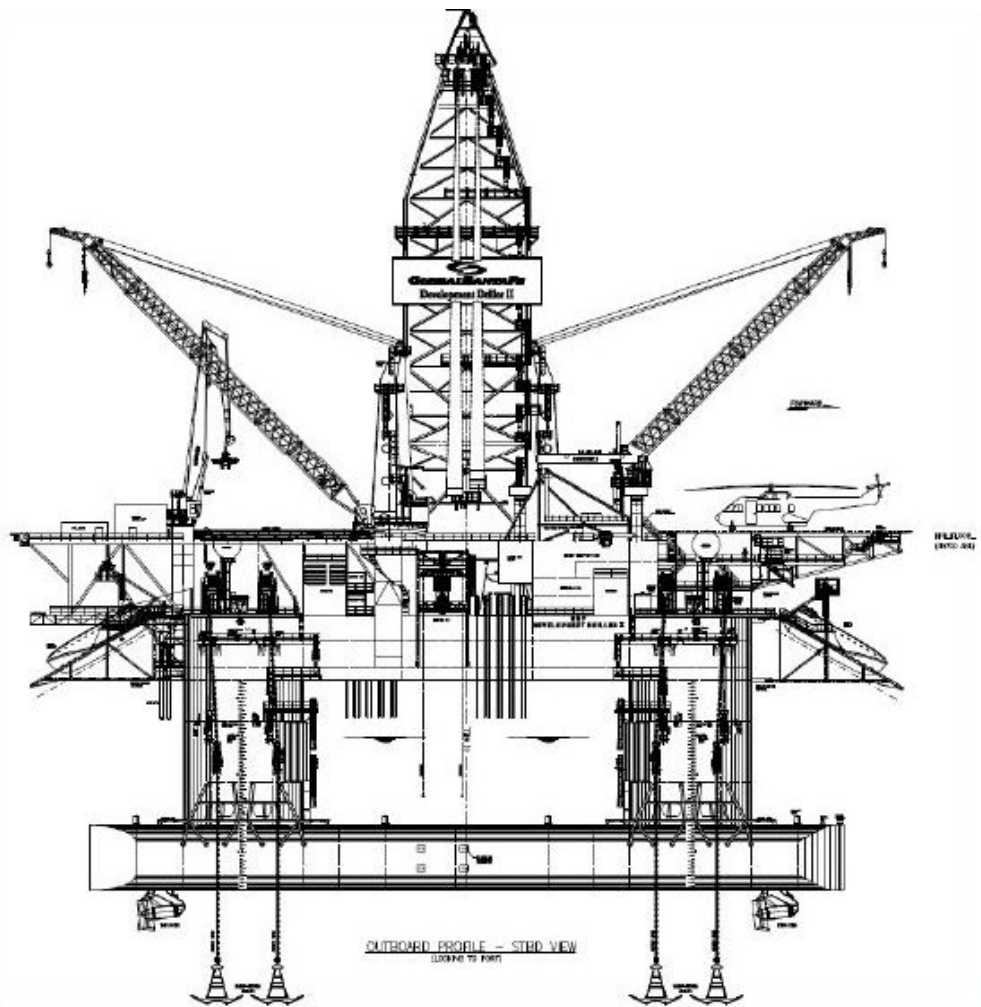
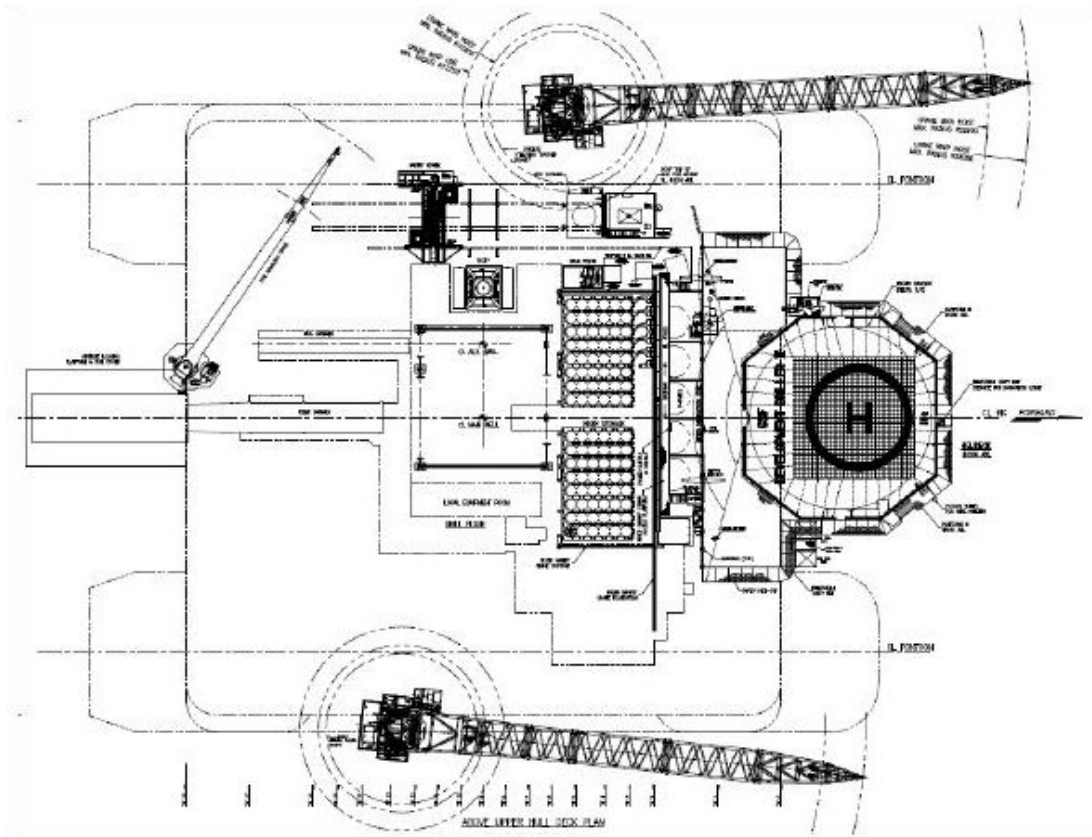


Figure 6-5. Front and top view of SDR "GSF Development Driller II"

6.2.1.2. Model Creation

The mobile drilling unit is modeled by using tool called Vessel, which enables modeling of the MODU's motion on the basis of RAO, QTF and other diffraction parameters. The modeling of floating drilling rig demands a lot of data to specify its properties. The Vessel data form is used to specify a particular data, such as the position of the drilling rig and the method of rig's motions calculation. [27] All data used for platform dimensions is taken from the website of Transocean and rig's specification described in the previous chapter.

Reference System and Platform Drawing

The position of drilling platform is defined with regard to a right-handed local system of coordinates V_{xyz} , which was discussed in the chapter 6.1.1.

The origin in the model is chosen at the center of the rig. However, it can be specified at the bow on the keel or at any other place, as it is simply the starting point on the platform to which all the type data refer. [27]

A surge, sway and heave for the platform must be defined in the directions of V_x , V_y and V_z axes, respectively. It is important to note that the RAOs direction must therefore be applied to these directions as well. [27]

The connection point of the drilling riser on the platform is then defined relative to these local axes. Hence, this point moves with those axes as the platform rotates and moves with regard to the global axes, and OrcaFlex computes these movements automatically. [27]

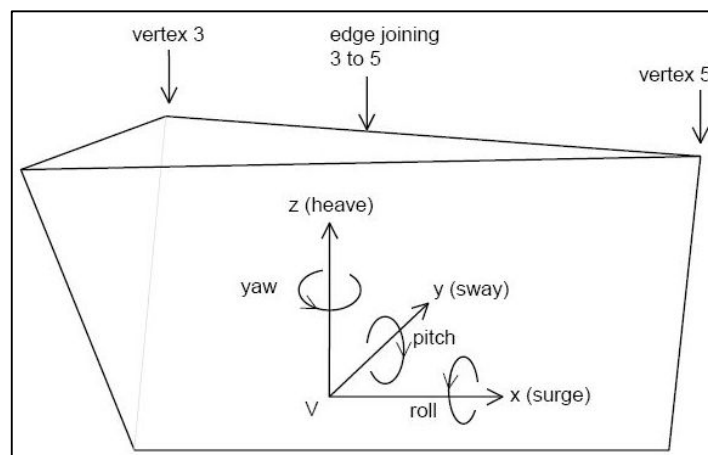


Figure 6-6. Model illustration [27]

The drilling rig is built up as a wire frame of specified vertices and edges. First, the positions of vertices are defined by specifying their coordinates with regard to the platform axes V_{xyz} . Then each pair of vertices is connected by the lines that form the edges.

The derrick on the drilling rig is drawn by setting the specified diameter to the derrick's edges in order to build-up a frame structure consisting of the cylinders or bars. It is worth to notice that if the edge diameter is set to '~' then the derrick will be built as a filled in shape.

A crane, catwalk, helideck, and other equipment that are specific to the rig are drawn in the same principle as discussed before. Therefore, it is possible to draw any rig-specific wire frame, using vertices, edges and pen (possible in a different color) that you specify on the vessel's data form.

Shaded Drawing

The drilling rig is shown, by default, in a shade 3D views of the model using a solid, filled-in shape on the basis of the vertices and edges. A solid surface for the shaded graphics representation is generated from the wire frame data. The 3D drawing enable to perform a simple visual check of the rig structure, and it can also be utilized to check the interference between lines in the model. [27] As with all points on the rig, the drawing coordinates are defined with regard to the local platform axes V_{xyz} , presented in Figure 6-6 above.

Motions Setup

The floating drilling rig is exposed to various types of motion that can be categorized into two groups – the motions with a low frequency (LF), also called as slow drift motions, which occur due to waves or due to rig thrusters, and motions with a wave frequency (WF) which occur due to response to wave loads. In OrcaFlex two vessel motions, such as Primary Motion and Superimposed Motion, exist to enable a separate modeling of these motions in some case. When both of the motions are present they are applied simultaneously, with the wave frequency motion being superimposed on the low frequency motion. [27]

As an example, consider a rig being driven under power along a specified course. Primary motion will be used for the case when the rig moves steadily along its course in the absence of waves. However, the primary motion is enhanced by wave-generated motion when waves are present. That would be modeled in OrcaFlex as the superimposed motion defined by displacement RAOs. OrcaFlex superimposes this latter motion on the primary motion in order to get the total combined motion of the rig. [27]

When a new vessel type is created, it is defined by initial default data, which corresponds to a particular vessel with a length of 103 m. This data should be replaced with a real data for the drilling rig we are modeling. However, due to lack of the data for rig modeling it is possible to

use the default data set of the vessel. As the drilling rig is similar to the default data setting so OrcaFlex automatically scales the vessel type data to specified rig length.

The results of the modeling of SSSR “GSF Development Driller II” are shown in the following Figures 6-7 to 6-14.

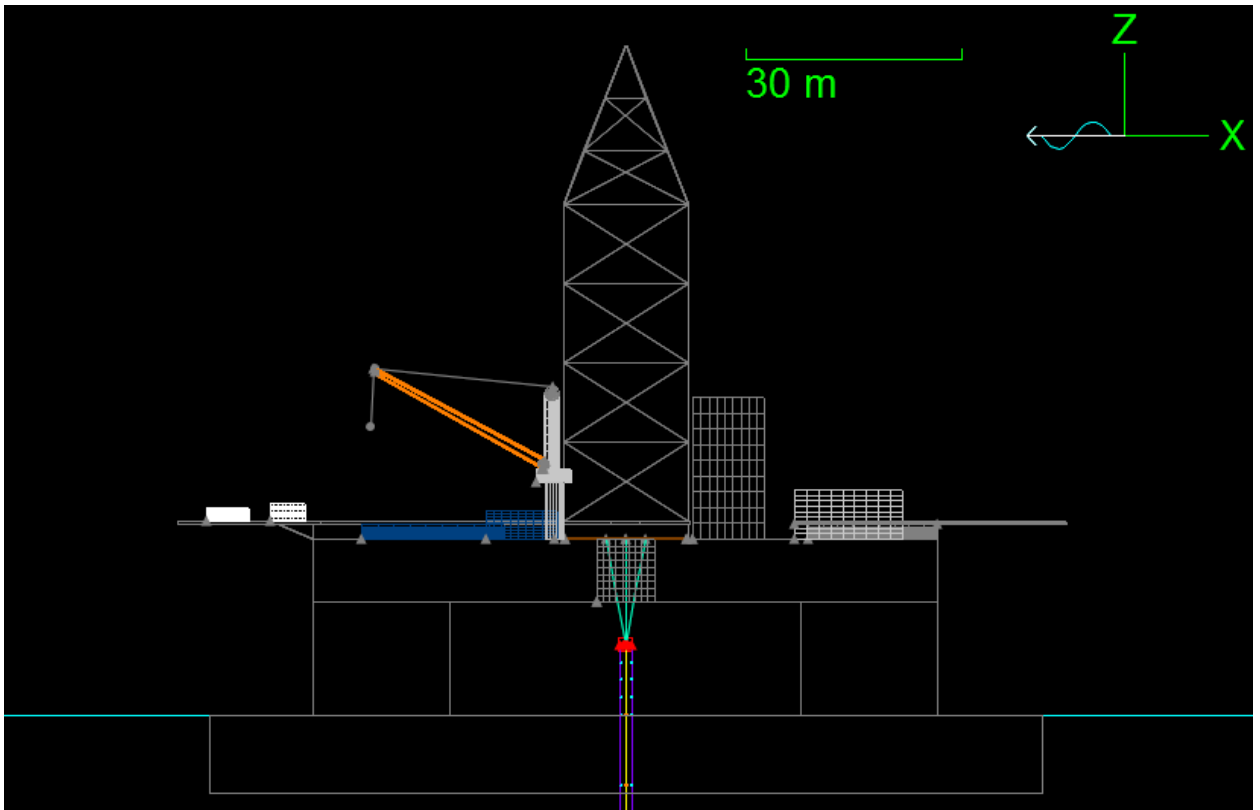


Figure 6-7. Front view to SSSR “GSF Development Driller II”

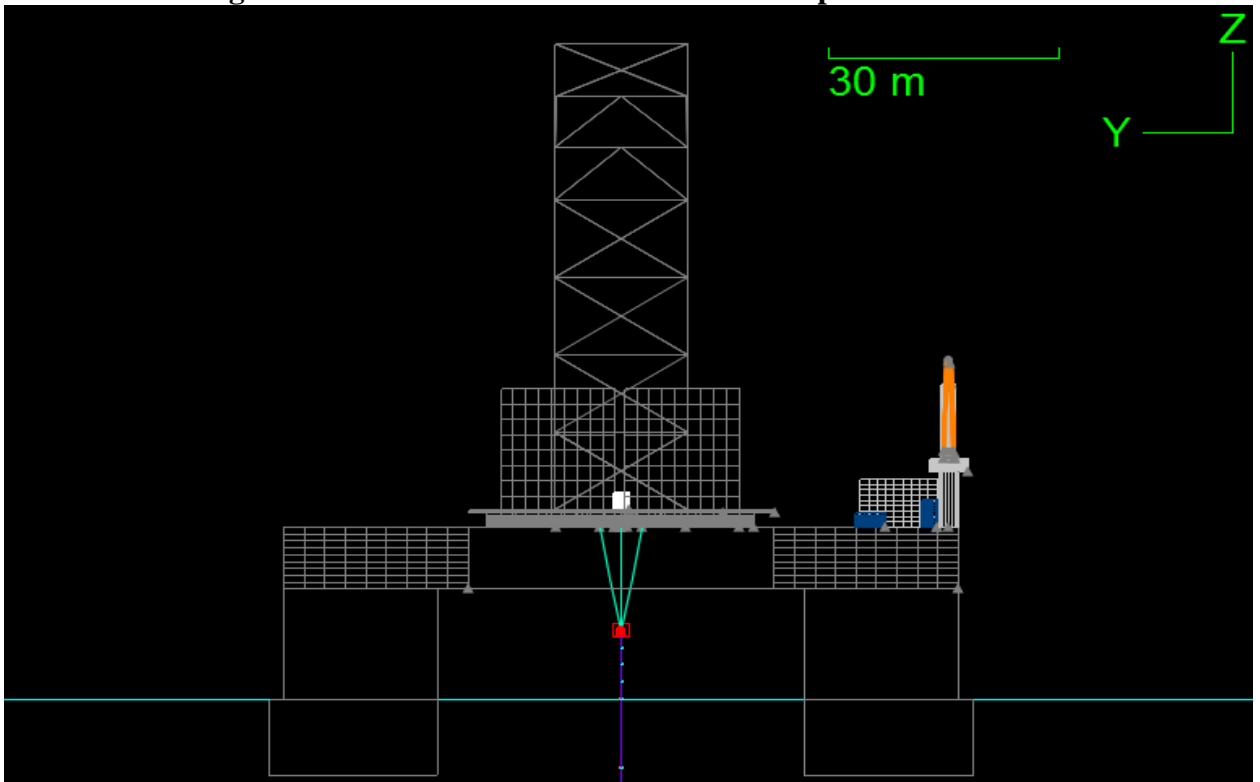


Figure 6-8. Side view to SSSR “GSF Development Driller II”

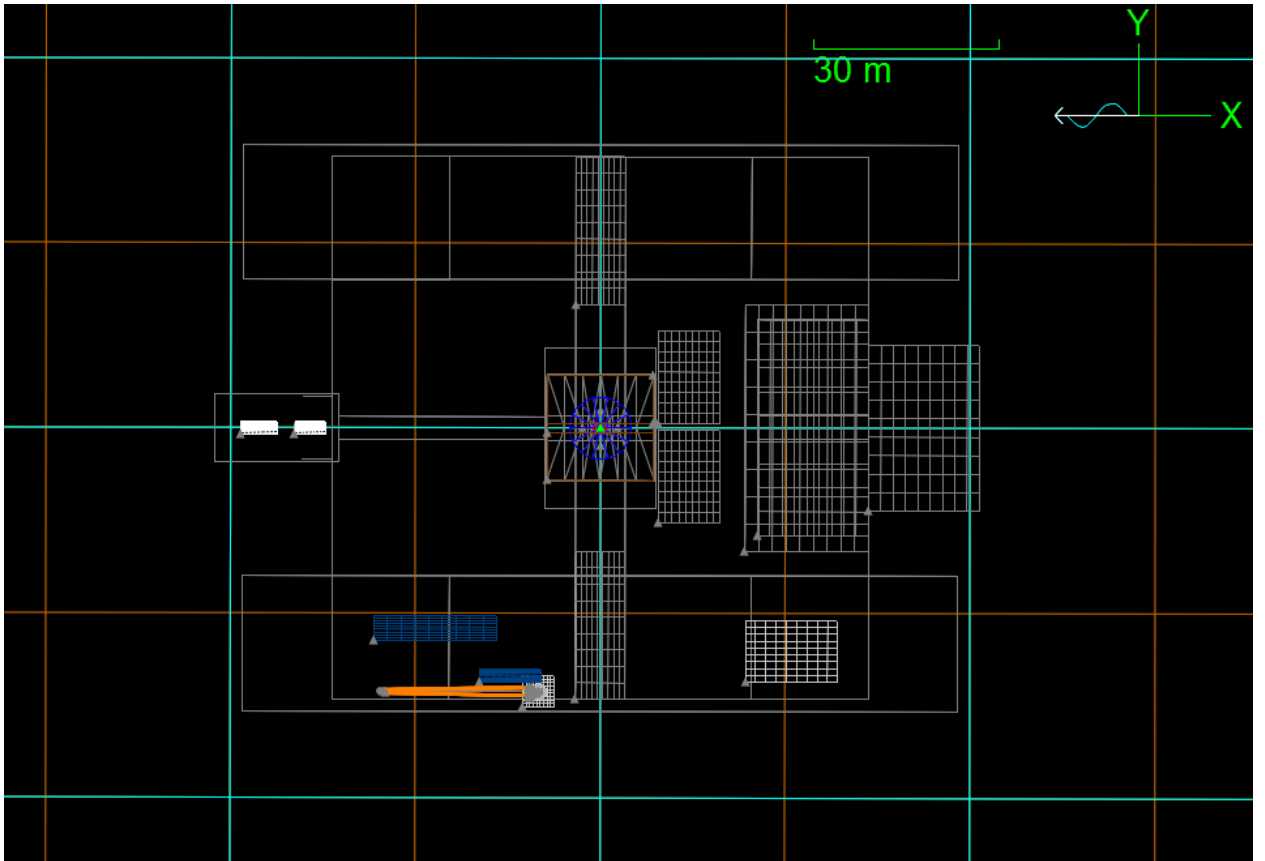


Figure 6-9. Top view to SSDR “GSF Development Driller II”

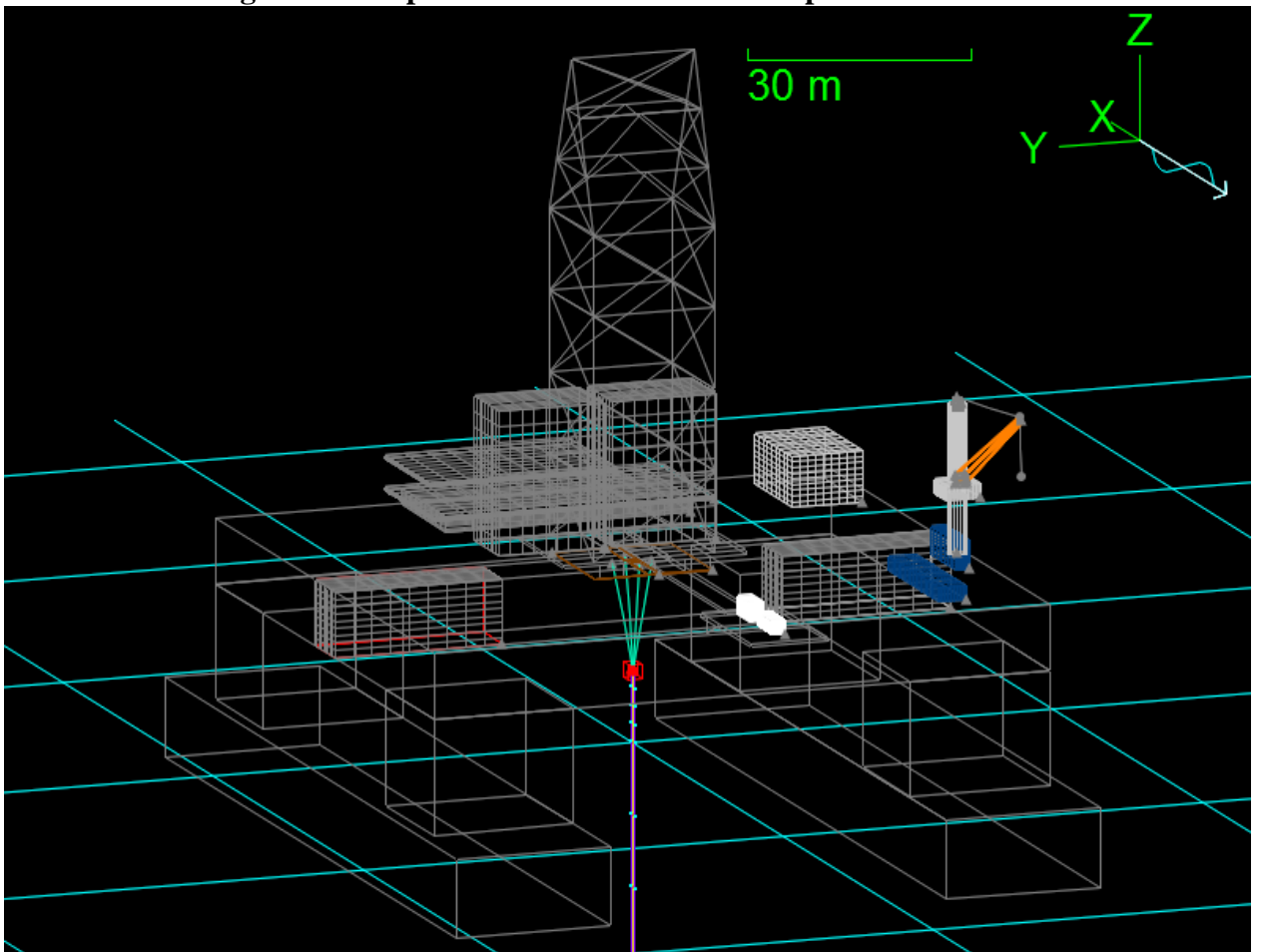


Figure 6-10. 3D view to SSDR “GSF Development Driller II”

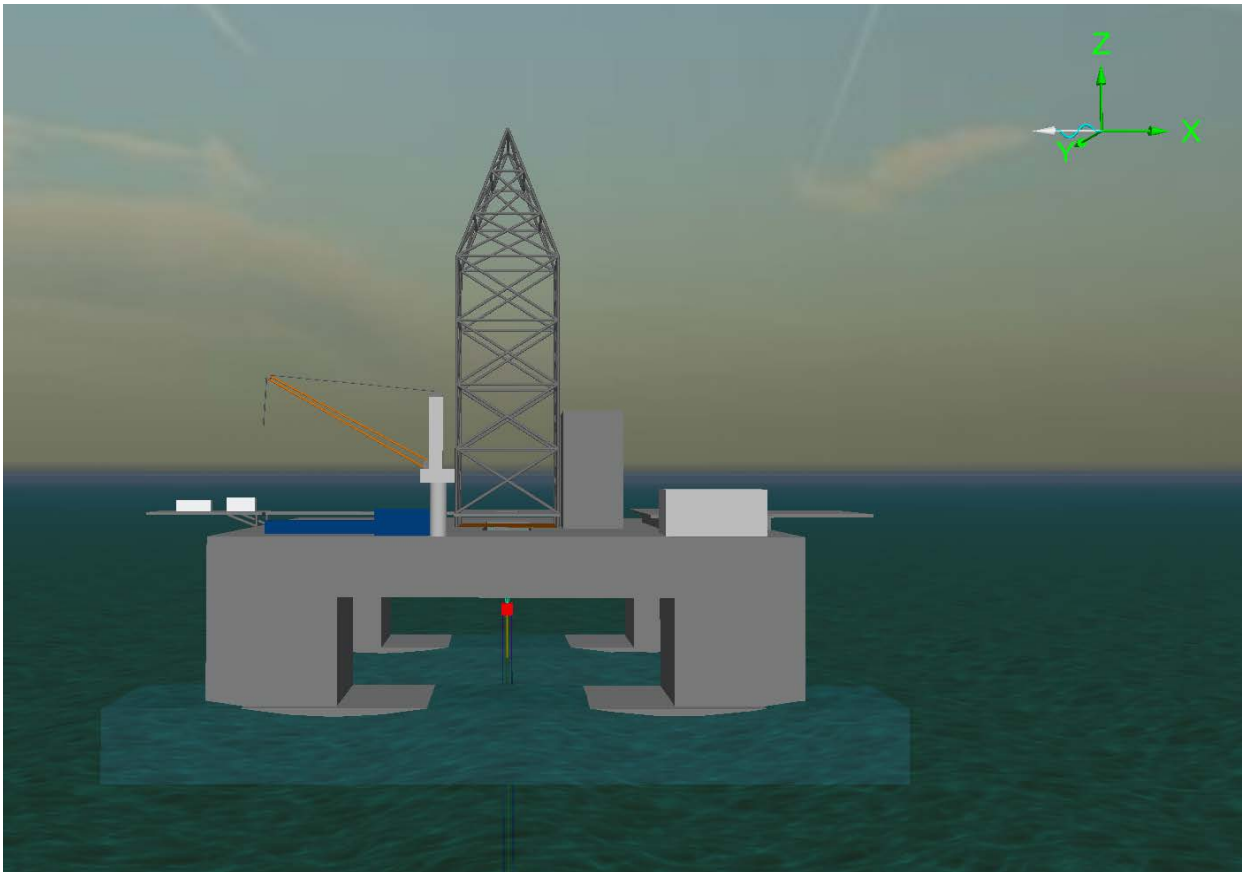


Figure 6-11. Front view to SDR “GSF Development Driller II”

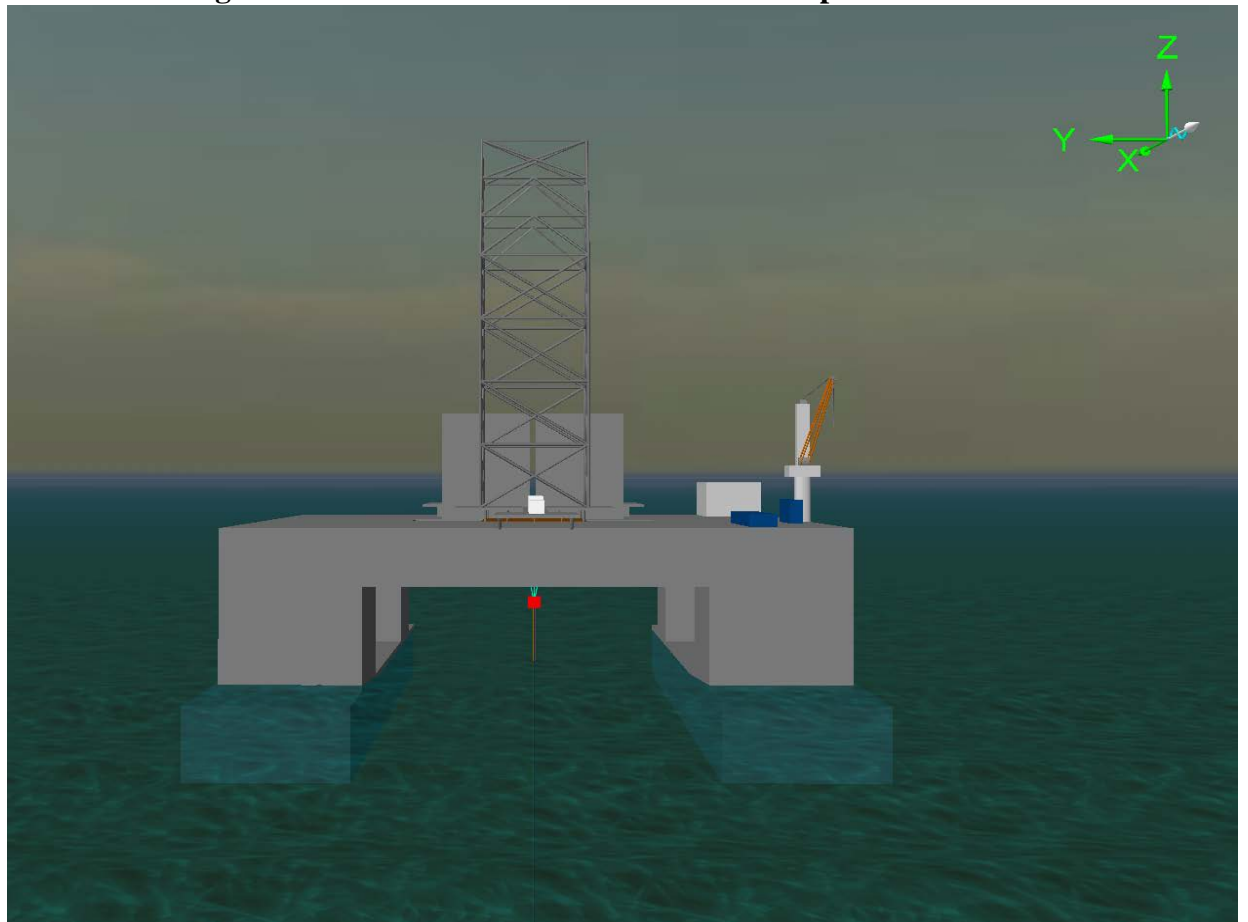


Figure 6-12. Side view to SDR “GSF Development Driller II”

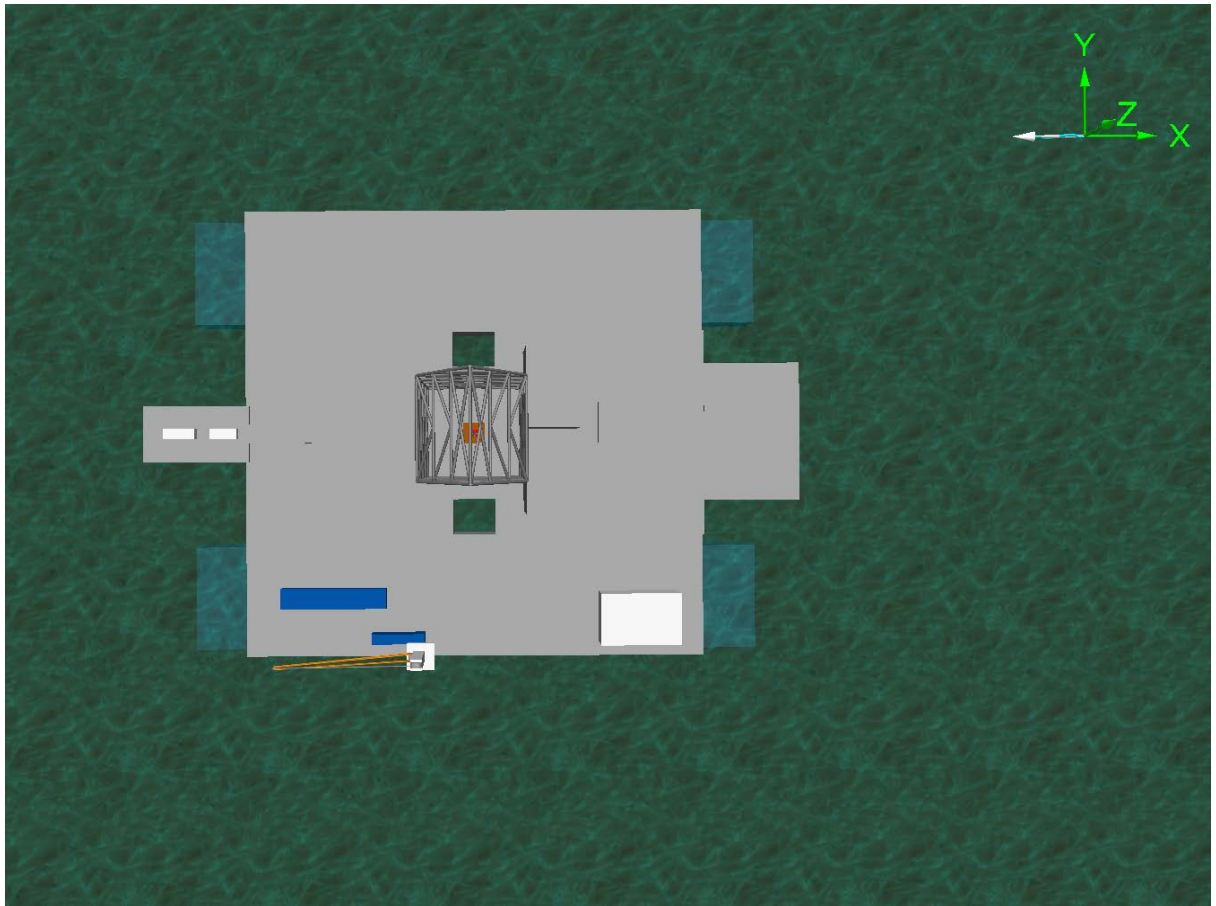


Figure 6-13. Top view to SDR "GSF Development Driller II"

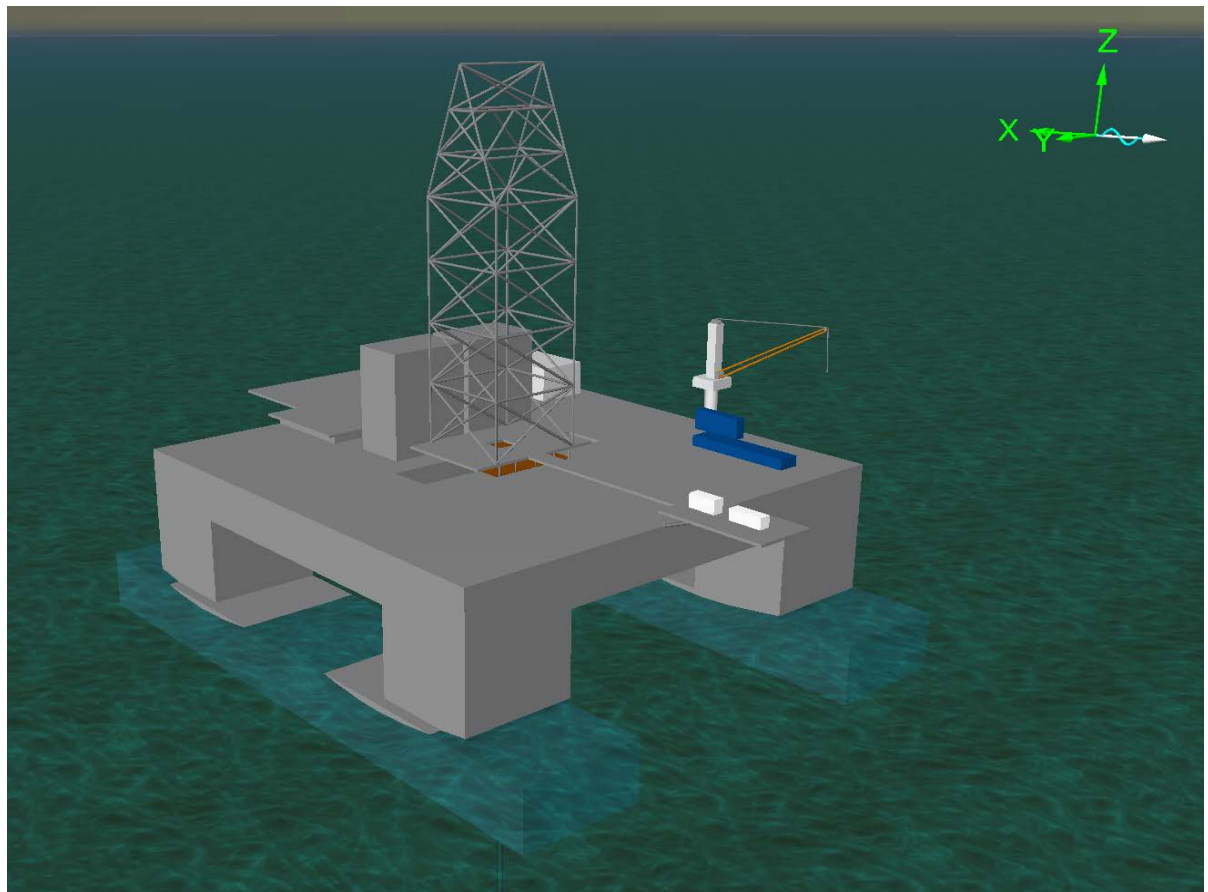


Figure 6-14. 3D view to SDR "GSF Development Driller II"

6.2.2. Drilling Riser System Modeling

From a structural point of view, the model of a typical drilling riser is presented as a beam with the applied tension force at its top end and which is approximately straight at all times. The drilling riser is free to move in the vertical direction at the top end as the upper boundary conditions are not fixed. However, in this thesis the riser model, comprising of the top tensioning equipment, auxiliary lines, LMRP, and BOP stack installed at the wellhead, is therefore becomes more complicated.

The various components of the riser system will be modeled as either a flexible body or a rigid body. It is very important to note that the weight of components should be calculated in air and water, and the correct values should be taken for the riser modeling. The drag and mass coefficients as well as the corresponding drag diameter for the bare riser joints will be included in the model during the dynamic analysis. The model creation and input data used for the drilling riser system in the analysis will be described in this chapter.

In this work the drilling riser simulation will be carried out for two different risers. A conventional drilling riser with the diameter of 21 inch will be used in the first configuration of the riser system whereas the second configuration will include a slim riser with the diameter of 16 inch. Both of the riser system configurations will be analyzed for application in the identical conditions of the Kara Sea, i.e. at the water depth of 100 m, all possible wave heights, and in the presence of constant sea current and wind. Moreover, the modeling of each riser configuration will be conducted for different materials, which can be used for the riser manufacturing, such as steel and aluminum. Configurations of the riser systems used in the analysis will be presented in the following sub-chapters.

6.2.2.1. 21 inch Drilling Riser Configuration

The main aim of the 21 inch riser analysis is to choose the riser configuration which will be reliable and safe, i.e. within the limits for the stress and flex/ball joint angle (as well as other criteria described in Chapter 2), in order to implement the drilling operations in arctic conditions of the Kara Sea.

The drilling riser used in the model is considered for application at the water depth of 100 m according to the mean water depth in the Kara Sea region, which was described in the chapter 5.1. The riser system is kept in tension by the tensioners installed on the semi-submersible drilling rig of Transocean, “GSF Development Driller II”, which the modeling and the description of specification are presented in the chapter 6.2.1. The maximum available

tensioners' capacity on the rig is 1360 tons (3.000 kips) at a full stroke of 15 m. The elevation of upper flex/ball joint above the mean sea level is approximately 27.5 m.

The drilling operations are assumed to be executed with a drilling mud of different densities, such as 8.55 ppg (1.025 s.g.), 12 ppg (1.438 s.g.), 14 ppg (1.678 s.g.), and the heaviest one is 17 ppg (2.037 s.g.). As the heavy density fluid may create a significant internal overpressure a new riser, designed for application in arctic conditions, should be checked for the burst failure, which is described according to DNV-OS-F201 in Chapter 2.4.

The configuration of the conventional 21 inch riser shown in Figure 6-15 is supposed to consist of 4 riser joints, each of them with length of 75 feet. The assembly comprises only bare riser joints without any installed buoyancy modules since the water depth in the area is not deep. This is also done with intention to reduce cost of operations due to expensive syntactic foam used in the buoyancy modules as well as to reduce the hydrodynamic impact of waves and current forces, which are maximum at the top section of the riser system (the wave and current velocity profiles will be presented later). Moreover, the use of bare riser joints over the whole length of the riser makes an on-site installation process less complicated and therefore more efficient.

The total length of the riser system, which stretches from the connection of the UFJ to the seabed, can be adjusted by changing the length of the telescopic joint. The top connection of the riser assembly is attached to bottom end of telescopic joint outer barrel and lower end of the riser system is connected to the LMRP at the height of approximately 10 m above sea floor (this is roughly considered as the total height of LMRP with BOP stack installed at the wellhead).

The drilling riser with its auxiliary lines may have some rotations since the upper flex joint has a nonlinear rotational stiffness that will therefore lower the bending moment of the top end of the assembly as opposed to a fixed end connection of the riser. The lower flex/ball joint works with the same properties of the rotational stiffness as applied to the upper flex joint. The data used for properties of UFJ and LFJ is obtained from the previous works on the riser simulation in Orcaflex.

The grade of the riser material to be used is ASTM A36 steel alloy, which has a minimum tensile stress of 400 Mpa (58 ksi) and a minimum yield strength of 250 Mpa (36 ksi) as specified in ASTM standard for pipe with grade A36 steel (on the basis of ASTM Specification). The second option is to choose aluminum alloy as the material for the 21 inch riser and to perform the analysis in the same order as for the steel riser. The minimum yield strength of aluminum is 90 Mpa (13 ksi). In order to be within the Von-Mises stress limit the wall thickness for the riser is calculated according to the requirement on burst check in DNV accounting for the drilling mud of 17 ppg inside the riser. The main pipe of the riser has a wall

thickness of 22.2 mm (0.875 in). The properties of the riser joints and auxiliary lines are obtained from rig's specifications and presented in Tables 6-2, 6-3.

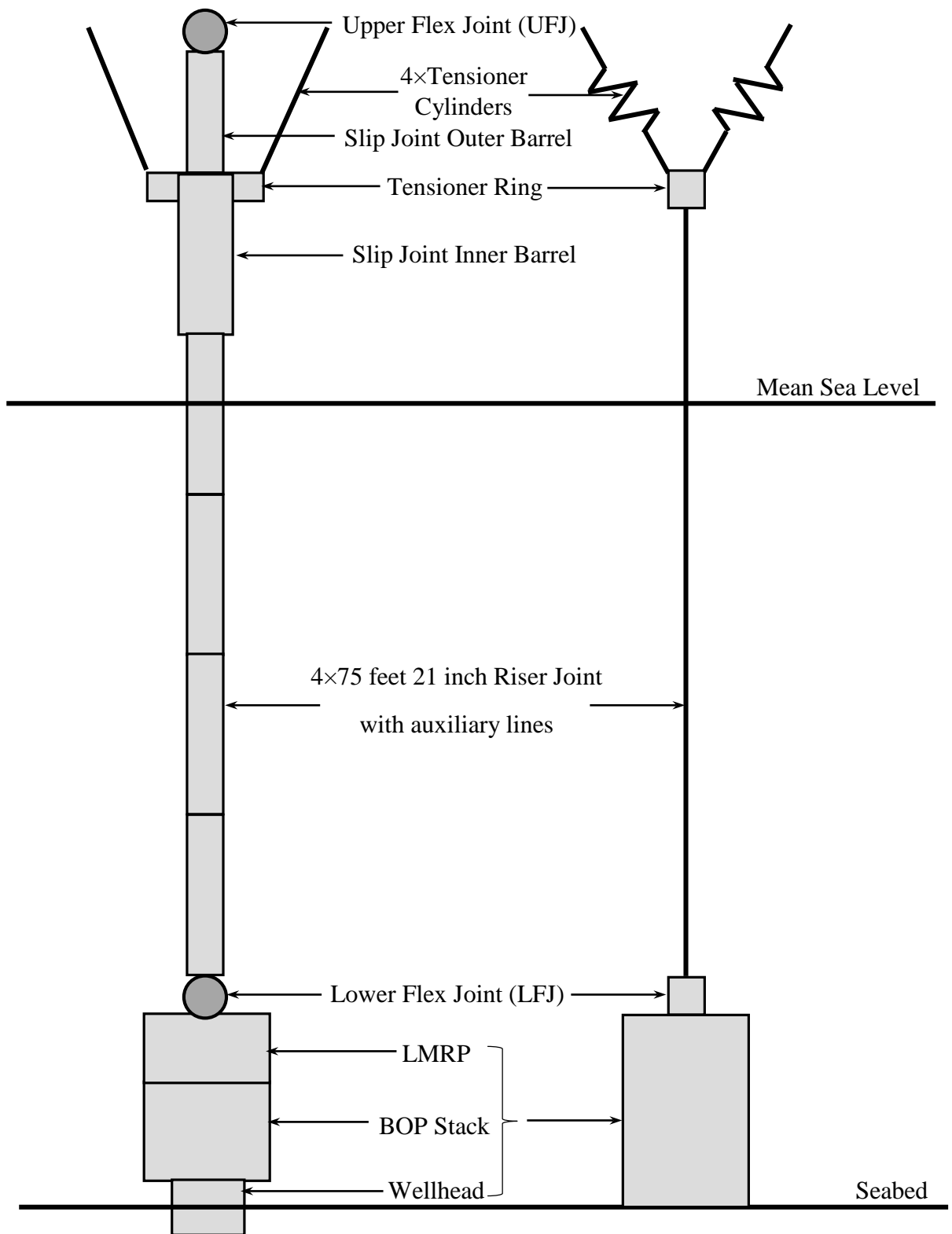


Figure 6-15. The configuration of the 21 inch riser (on the left) and the model in OrcaFlex program (on the right)

Parameter	Dimension	Description
Riser Type	-	75 ft bare riser
Outer Diameter	in/ m	21/ 0.533
Inner Diameter	in/ m	19.25/ 0.489
Wall Thickness	in/ m	0.875/ 0.022
Length per Joint	m	22.86
Dry Weight	ton	6.33

Table 6-2. Specification for the 21 inch riser joint (steel and aluminum)

Auxiliary Line Type	Outer Diameter (in/ m)	Inner Diameter (in/ m)	Wall Thickness (in/ m)	Number of Lines
Choke Line	6.5/ 0.165	4.5/ 0.1143	1/ 0.0254	1
Kill Line	6.5/ 0.165	4.5/ 0.1143	1/ 0.0254	1
Hydraulic Line	2.88/ 0.0073	2.32/ 0.059	0.28/ 0.007	1
Booster Line	5/ 0.127	4/ 0.1016	0.5/ 0.0127	1

Table 6-3. Specification for auxiliary lines of 21 inch riser (steel and aluminum)

It should be taken into account that the auxiliary lines such as hydraulic, choke & kill lines, and booster line add an additional weight to the main riser pipe.

6.2.2.2. 16 inch Drilling Riser Configuration

The configuration of 16 inch drilling riser is considered to be operated in the Kara Sea at the same water depth of 100 m. The analysis of the riser is performed by using the semi-submersible drilling rig “GSF Development Driller II” with the same capability of the tensioning system that was mentioned in the previous sub-chapter but the required minimum top tension should be recalculated in this case.

The range of drilling mud densities is taken the same as used for drilling operations with 21 inch riser. The burst failure check of the riser should also be carried out with the heaviest density of the drilling fluid.

As illustrated in Figure 6-16 the configuration of the 16 inch slim riser to be analyzed is similar to the previous conventional riser configuration since it is comprised of 4 bare riser joints, with length of 75 feet each.

So far as the connection of the drilling rig’s telescopic joint fit for the 21” conventional riser a conical adapter should be in reality installed at the top end of the 16” slim riser in order to connect the riser assembly with the bottom end of telescopic joint outer barrel. However, as the 16” riser properties are considered to be weaker it is possible to make an assumption that the top

connection of the riser will be suitable to the connection at the bottom end of telescopic joint outer barrel.

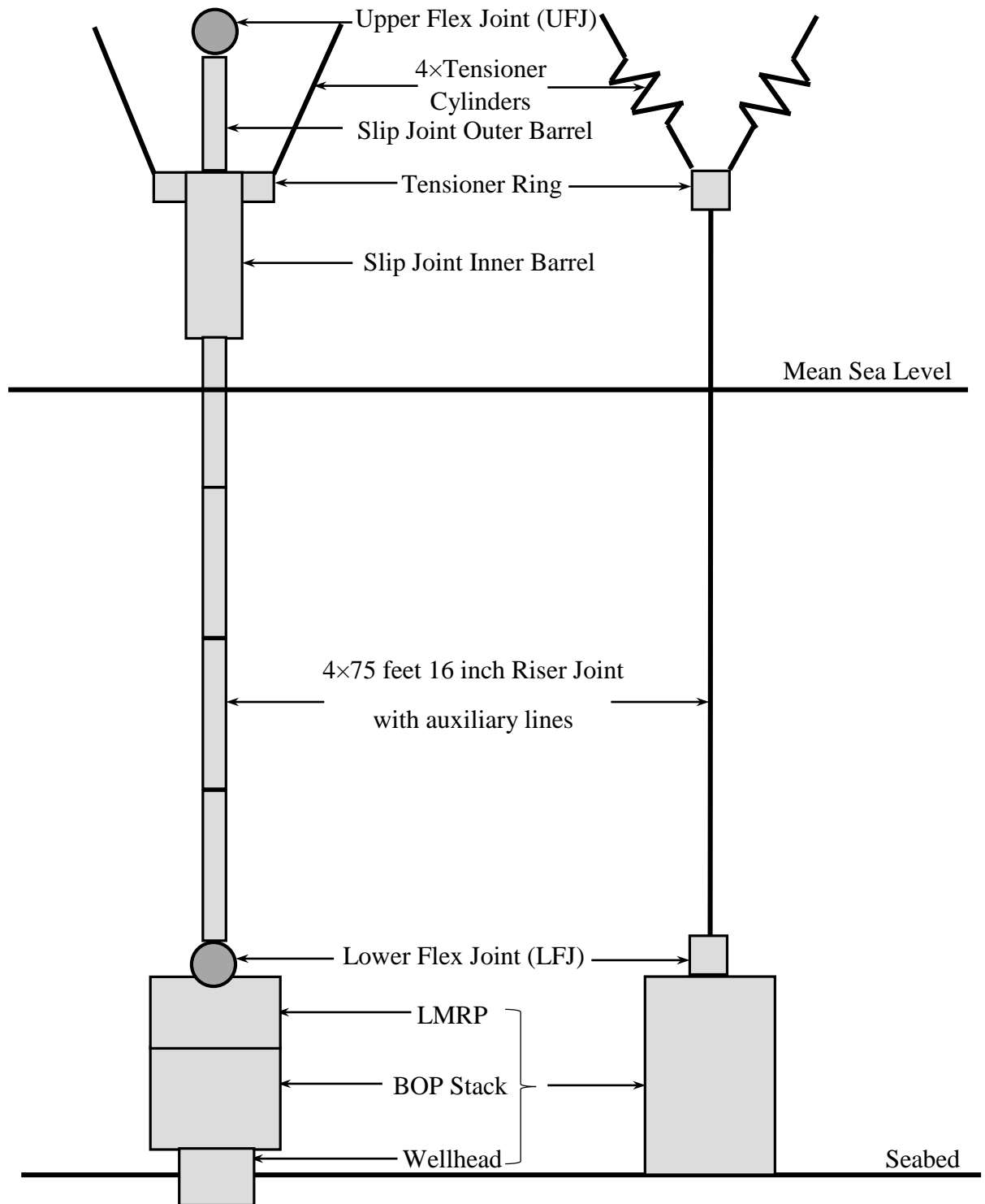


Figure 6-16. The configuration of the 16 inch riser (on the left) and the model in OrcaFlex program (on the right)

The lower end connection of the riser assembly is also attached to the LMRP at the height of 10 m above sea floor as in the case of 21 inch riser assembly. The wall thickness of the main

riser pipe is assumed to be equal to 19 mm (0.75 in) based on the rig's specification and requirement of DNV burst check using the drilling mud of 17 ppg, same as for the conventional riser.

For analysis of the 16 inch riser the same properties of nonlinear rotational stiffness for the upper flex/ball joint and lower flex/ball joint are retained from the 21 inch riser analysis.

Two options for the riser material are considered to be used in the analysis of slim riser such as ASTM A36 steel alloy and aluminum. Both of the material is kept the same properties as in the analysis of 21 inch riser previously.

The detailed description of properties of riser joints and auxiliary lines is taken from the specifications and given in Table 6-4, 6-5.

Parameter	Dimension	Description
Riser Type	-	75 ft bare riser
Outer Diameter	in/ m	16/ 0.406
Inner Diameter	in/ m	14.5/ 0.368
Wall Thickness	in/ m	0.75/ 0.019
Length per Joint	m	22.86
Dry Weight	ton	4.14

Table 6-4. Specification for the 16 inch riser joint (steel and aluminum)

Auxiliary Line Type	Outer Diameter (in/ m)	Inner Diameter (in/ m)	Wall Thickness (in/ m)	Number of Lines
Choke Line	5/ 0.127	3.75/ 0.095	0.625/ 0.016	1
Kill Line	5/ 0.127	3.75/ 0.095	0.625/ 0.016	1
Hydraulic Line	3.5/ 0.089	3/ 0.076	0.25/ 0.0065	1
Booster Line	4/ 0.102	3.25/ 0.083	0.375/0.0095	1

Table 6-5. Specification for auxiliary lines of 16 inch riser (steel and aluminum)

6.2.3. Input Data for Environmental Conditions

The environmental data of the area, where the riser is supposed to be operated, should be carefully examined prior to the modeling and analysis of the riser since it is a critical factor affecting the hydrodynamic forces acting on the riser system. It is more preferable to obtain all data of environmental conditions from respectful and trustful sources such as environmental and meteorological institutes which perform detailed surveys and observations of a particular area of interest.

As discussed in the previous chapters of the thesis the drilling riser should be assessed and chosen with regard to the Kara Sea conditions. A set of the environmental data for this work

was found after thorough studies of some international standards, observations of a research institute and books, which can be a reliable source of information on the Kara Sea area.

Drilling operations are assumed to be performed in the presence of wind with a speed of approximately 40 m/s that is taken as the fastest observed wind velocity. The wind direction is assumed to be from the bow to stern of the rig. [24]

The current profile is obtained by means of the Power Law in OrcaFlex using the maximum speed at surface as 1.0 m/s and the current speed at sea bottom as 0.2 m/s. [24, 27] The Power Law equation used in calculations and table of current velocities with respect to water depth are presented in Appendix E. The current speed profile, which is shown in Figure 6-17, will be used during simulation of both 21 inch and 16 inch riser. The movement of current does not vary with water depth and it is applied in one direction from the bow to stern of the drilling rig, i.e. 180° according to the direction relative to global axes. A tide of the sea is also supposed to be included in the current profile used for simulation.

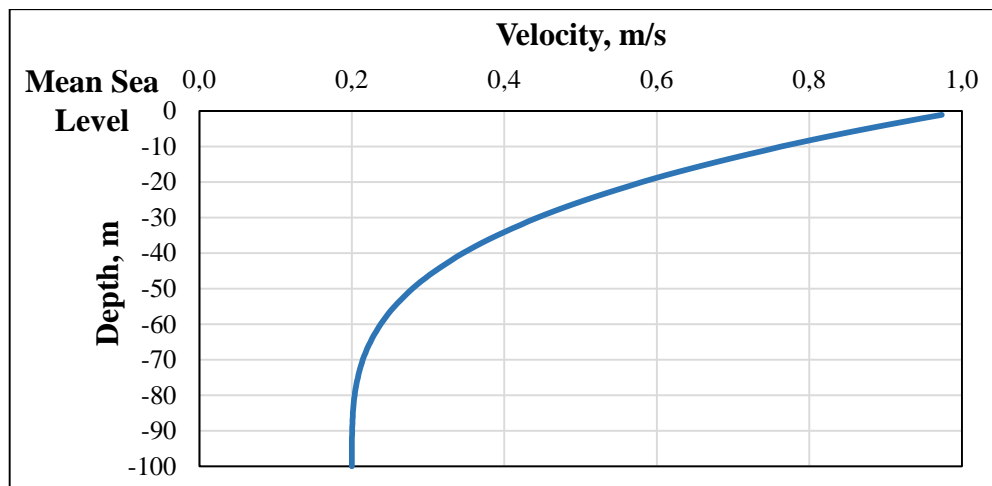


Figure 6-17. Distribution of the current velocity over the sea water depth

A set of data for waves will also be established to be applied in the model. Since the real data were not found for the wave conditions it was considered to apply a guideline from NORSOK N-003, which mentions a simplified method to define a design wave. The suitable wave height H_{100} , which corresponds to a 100 year wave (i.e. an annual probability of exceedance is equal to 10^{-2}), can be defined as a significant wave height H_s multiplied by 1.9 (NORSOK, 2007). Also, according to the method mentioned in the standard the wave period is varied within the range:

$$\sqrt{6.5H_{100}} \leq T \leq \sqrt{11H_{100}} \quad (6.3)$$

To simulate the loading scenarios, a set of design wave periods can now be calculated by using the previously described method from NORSOK N-003. (see Appendix E2) A range of design wave heights is set due to an insufficient data for significant wave heights in the area of the Kara Sea. As a result, the wave conditions can be simulated to represent the operational conditions of the drilling riser.

The propagation direction of waves is assumed to be in the same direction as the sea current and wind, contemporaneously (i.e. 180° direction relative to global axes).

Hence, the input data for waves is established to simulate a satisfactory representation of sea conditions for the riser analysis and results are presented in Table 6-6.

Wave Height, H (m)	T₁ (s)	T₂ (s)
1	3	-
2	5	-
3	5	-
4	6	-
5	6	7
6	7	-
7	7	-
8	8	9
9	8	-
10	9	10

Table 6-6. Design wave heights with associated periods

6.2.4. Additional Considerations and Assumptions

The drilling riser analysis is performed with regard to operational and worst-case scenarios, i.e. the drilling and non-drilling modes.

According to ISO 13624-1 and API RP16Q standards the riser should always be kept under the minimum required top tension during the simulation, ensuring the riser system stability. Moreover, the tension should accommodate for dynamic effects by setting slightly higher values for tensioners. The minimum top tension is calculated and applied for four tensioners as modeled in the program. For simplification purposes each tensioner in the model represents three real tensioners on board of the drilling rig. The tension is varied for each drilling riser configuration being a function of weight, internal and external pressure of fluid at the bottom of the riser. The calculations according to standards (see Chapter 2) are given in detail in Appendix D and the results are presented in Table 6-7.

Riser Configuration	Drilling Fluid Density (kg/m³)	Total Tension (N)	Number of Tensioners	Tensioner Setting (N)
21 inch steel riser	1025	533153.9	4	133288.5
	1438	648725		162181.3
	1678	715885		178971.3
	2037	816345.2		204086.3
16 inch steel riser	1025	315317.9		78829.5
	1438	382187.5		95546.9
	1678	421046.4		105261.6
	2037	479172.8		119793.2
21 inch aluminum riser	1025	182377.7		45594.4
	1438	297948.9		74487.2
	1678	365108.9		91277.2
	2037	465569		116392.3
16 inch aluminum riser	1025	107277.6		26819.4
	1438	174147.2		43536.8
	1678	213006.1		53251.5
	2037	271132.5		67783.1

Table 6-7. Tensioner settings

In order to simplify the simulation, the drilling rig is assumed to be kept without any movement by anchors neglecting the drift-off and drive-off of the rig.

The total simulation is run for 30 seconds that enables to account for one wave period in build-up stage. This is also implemented to reduce the transient effects since at least one wave period for the build-up stage is required in the OrcaFlex program. The wave development is verified for this specific sea state. The rest of wave periods for main simulation time are considered to be sufficient for this project to get into a steady state condition for simulations taking a regular wave as an option. The time step is selected to vary with a time of 0.1 second.

6.3. Analysis Results and Discussions

The modelled riser configurations discussed in Chapter 6.2.2 was performed to examine the response and performance of 21 inch and 16 inch riser during drilling operations at arctic conditions of the Kara Sea. The limitations of meteorological and oceanographic conditions for each drilling riser were obtained by simulation of several different design wave heights. This is also done with intention to investigate what are the capabilities of various risers to implement operations in a safe and efficient manner at the specified water depth of 100 m.

In this chapter, the simulation results of 21 inch conventional and 16 inch slim riser will be described in terms of design parameters such as the effective tension, maximum upper and lower flex/ball joint angles, and Von-Mises stress. In addition, these parameters will be considered with regard to risers of diverse materials such as steel and aluminum. All decisions and recommendations for the operation will be defined according to limitation criterions from API RP 16Q, ISO 13624-1 and DNV-OS-F201 standards which are described in Chapter 2 of the thesis.

For comparison of risers the drilling mud weight density will be used with range from the lightest one of 8.55 ppg (i.e. seawater with density of 1025 kg/m^3) to the heaviest density of 17 ppg (2037 kg/m^3).

The drilling riser will always be exposed to an internal overpressure, even if the seawater is used as the drilling fluid, due to the fact that the height of the drilling fluid column inside the riser is higher than the seawater column outside (the top connection of the riser is located at 27.5 m above the mean sea level for this particular case). According to DNV-OS-F201 the burst check calculations, which are presented in Appendix A, were performed for all risers. All riser configurations with different material properties are designed without any risk for the burst of the main riser pipe since the minimum required wall thickness is much lower than the proposed thickness of the riser wall taken from specifications.

The analysis results are shown through Figures 6-18 to 6-31 and the remaining outcomes can be found in Appendix F. From all factors that were mentioned previously it can be noticed at once that drilling fluid densities and riser materials have great influence on all parameters that should be fulfilled according to guidelines in the analysis of the drilling riser.

The 21 inch conventional riser has shown better capabilities as opposed to the 16 inch slim drilling riser and therefore the 21 inch riser gives competitive advantages during drilling in the Kara Sea.

6.3.1. Effect of the wave height on the effective tension with regard to various drilling fluids

The effective top tension results are presented in Figure 6-18 and Figure 6-19 since tensile limits for all configurations of the drilling riser have great values it is not shown in these Figures. However, the calculation results of allowable limits for the effective tension are presented in Table 6-8.

Riser Configuration	Tensile Limit (kN)
21 inch steel riser	5915,7
16 inch steel riser	3883
21 inch aluminum riser	2130
16 inch aluminum riser	1398

Table 6-8. Allowable limits for the effective tension of various riser configurations

As it can be observed that the effective tension is dependent of the wave height, and increasing with increasing wave heights during simulation. Moreover, the effective top tension depends on the drilling fluid density used in operations. The tension is lower with light drilling fluid and gets higher when utilizing heavy drilling fluid.

The top tension will always be applied to the drilling riser. For reduction of large angles at the flex/ball joints the top tension can be set higher provided that the effective tensile doesn't cross the tensile limit and also the Von-Mises stress doesn't cross the stress limit. The applied top tension also in turn will lead to increase in the bottom effective tension and axial stress.

In addition, it should be noticed that the apparent weight of LMRP and BOP stack was not specified in the model. In reality the variations in the bottom effective tension will be transferred to the lower flex/ball joint initially, then to LMRP/BOP stack, and to wellhead finally. The wellhead will therefore be exposed to tension which can be very high depending on the bottom effective tension. Thus, this dynamic loading can cause the wellhead fatigue and assessment may need to be carried out prior to operations.

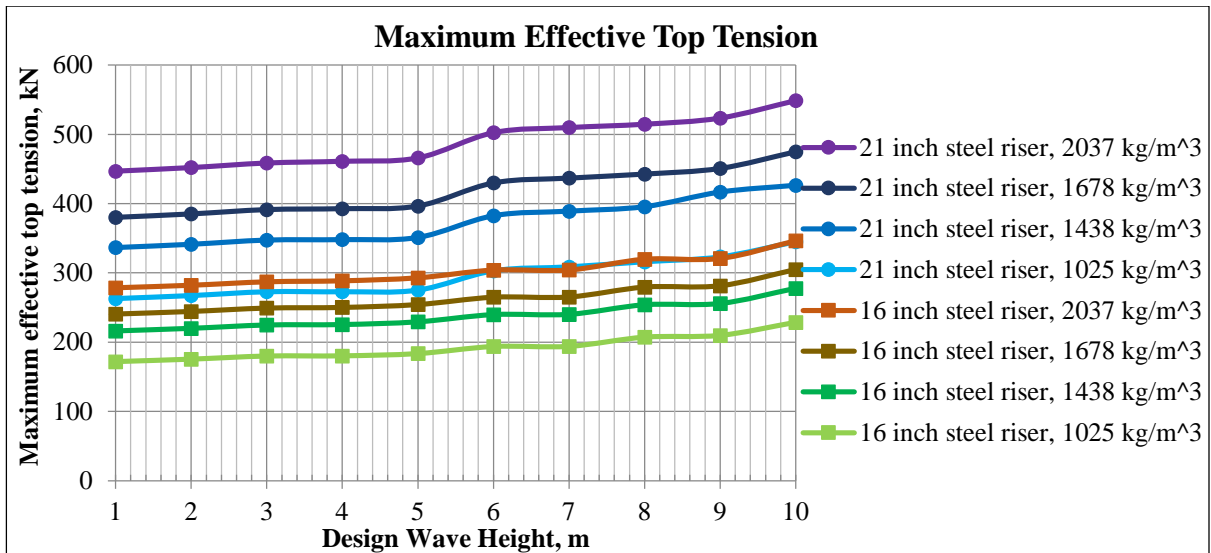


Figure 6-18. Maximum Effective Top Tension for 16 inch and 21 inch steel risers

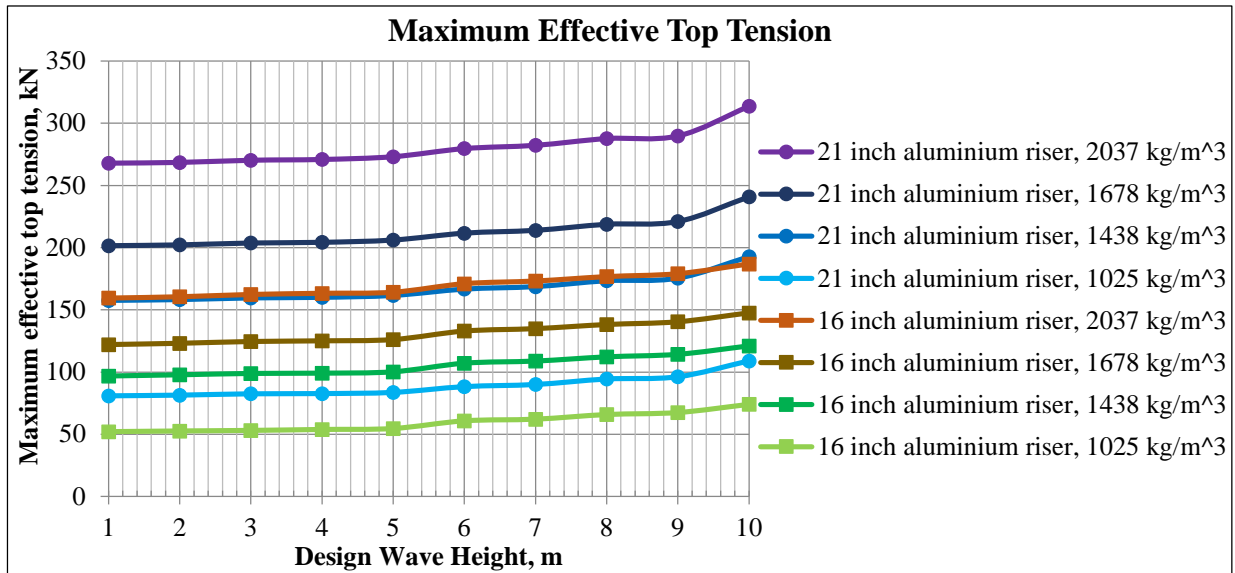


Figure 6-19. Maximum Effective Top Tension for 16 inch and 21 inch aluminum risers

6.3.2. Effect of the wave height on the Von-Mises stress with regard to various drilling fluid densities

The results of the Von-Mises stress in risers for various drilling fluid densities are depicted from Figure 6-20 until Figure 6-23. It is worth to note that the Von-Mises stress is significantly increasing for 16 inch and 21 inch steel risers during simulation of waves with height of 6 and 7 m. Upon discussions with my scientific supervisor and people with a great expertise in OrcaFlex software we came to know that this effect is occurred due to a resonance of the drilling riser.

As it has already been noted the 21 inch conventional riser has better mechanical properties (e.g. moment of inertia for bending and cross-sectional area for tension) than the 16 inch slim riser, despite that both have the same pipe grade A36 steel alloy in the first option and

aluminum alloy as the second option of the riser material, and as a result the conventional riser has lower stresses for all types of the drilling fluid. As it can be seen from the Figures, the combined effect of stresses (Von-Mises stress) in steel risers are already crossing the allowed limit for stresses when simulating the wave height of 6 to 7 m and using drilling fluids with density of 12 to 17 ppg. The Von-Mises stress in aluminum risers are crossing the allowable limit during simulating the wave height of 4 to 5 m and using drilling fluids with density of 8.55 to 17 ppg. Therefore this is not an auspicious option to increase the top tension due to large angles of the drilling riser. As described in Chapter 4.3 the Von Mises stress is the fundamental criteria combining the axial, radial, and hoop stress. The drilling operations performed with heavy drilling fluid in deep-water areas tend to induce hoop stress in the risers. Thus, keeping the rig offsets under control is thought to be more favorable option for reduction of riser angles. However, if the mentioned methods do not give any positive changes and the situation gets into the worst case scenario, the riser must be disconnected.

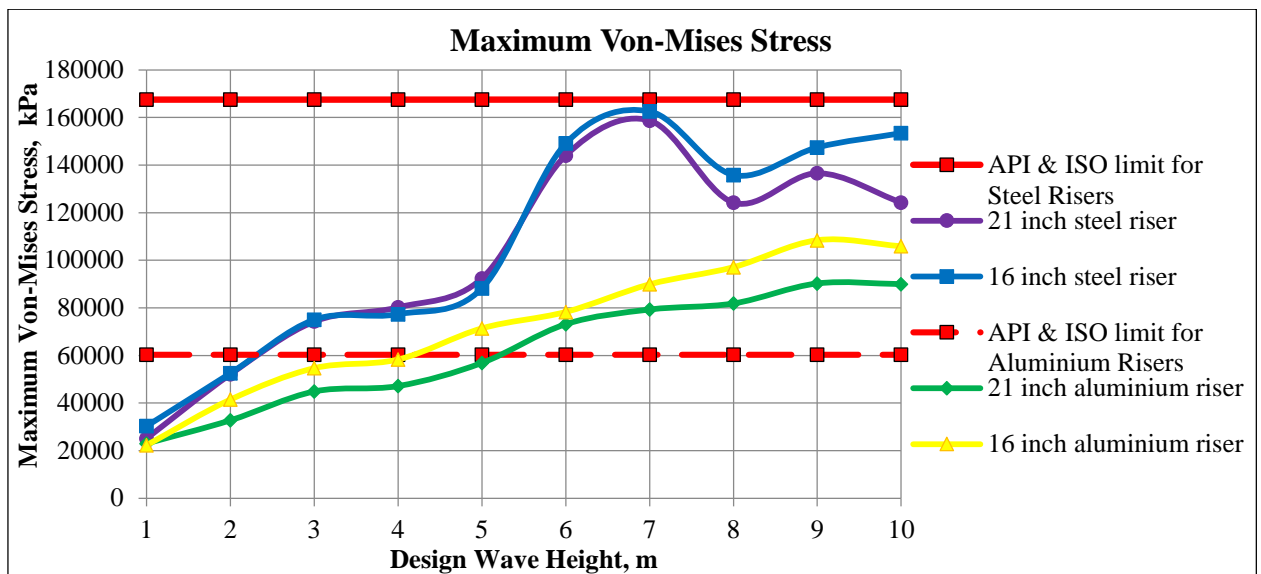


Figure 6-20. Maximum Von-Mises Stress (1025 kg/m³)

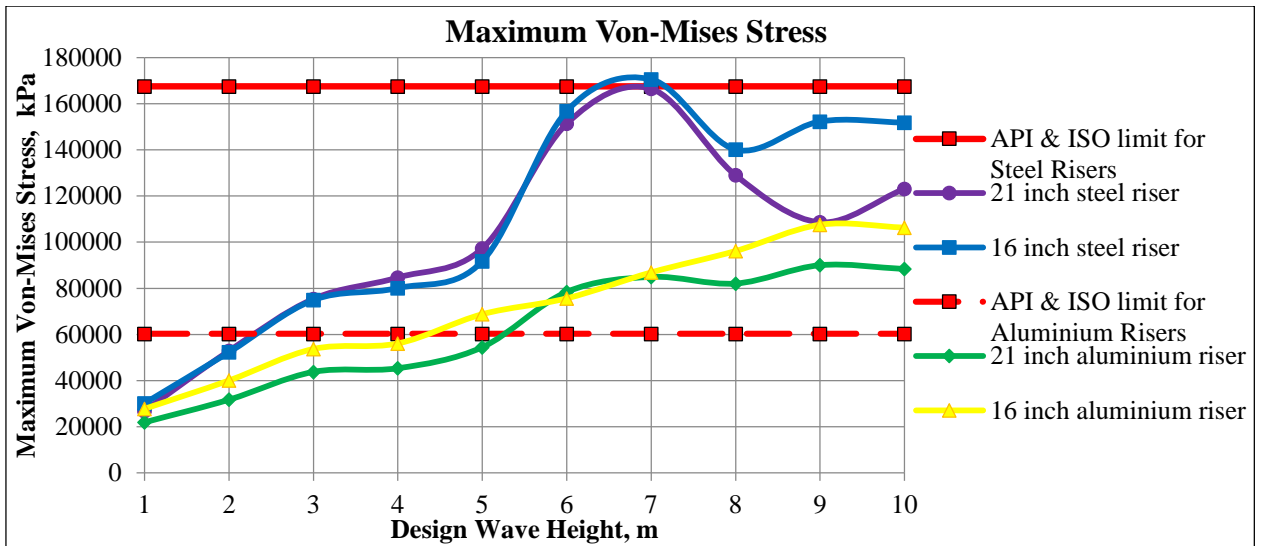


Figure 6-21. Maximum Von-Mises Stress (1438 kg/m³)

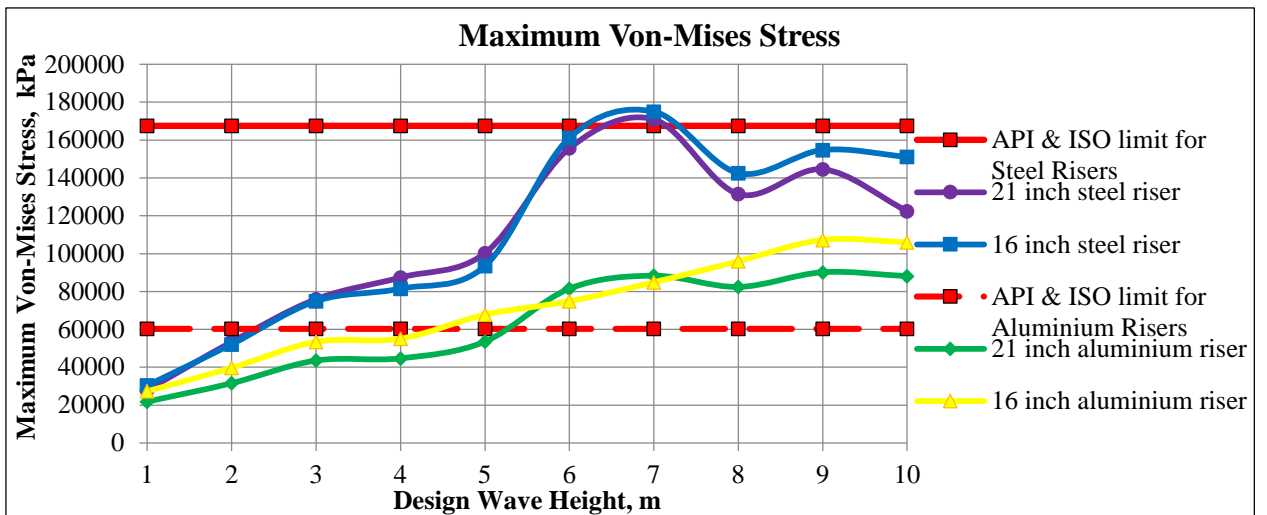


Figure 6-22. Maximum Von-Mises Stress (1678 kg/m³)

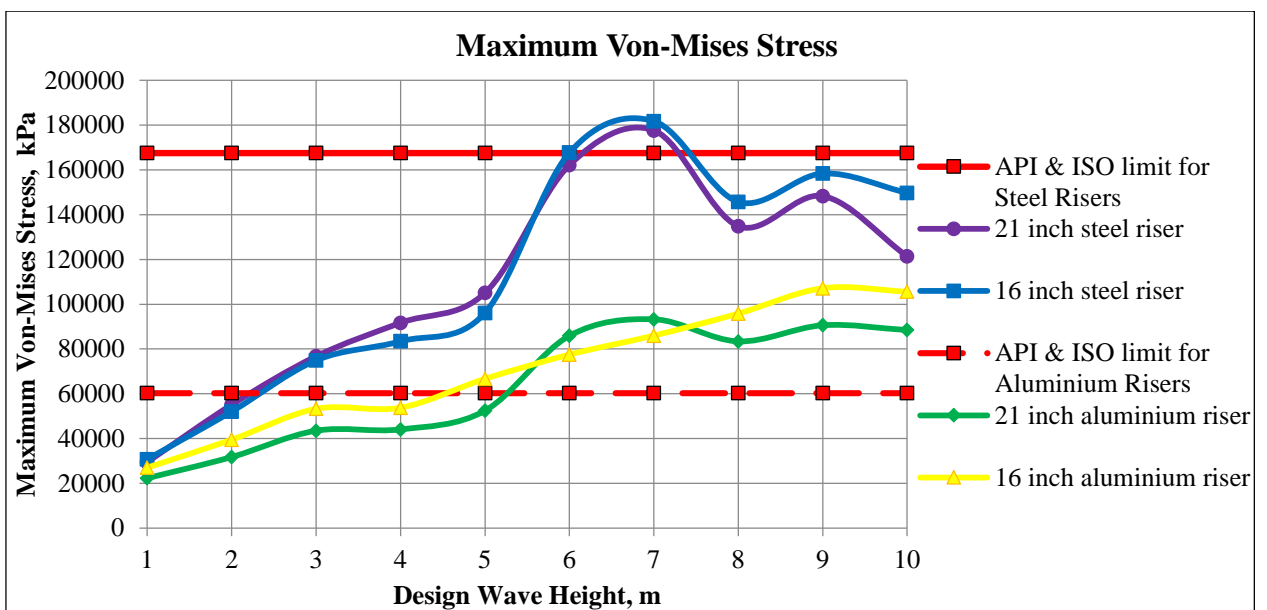


Figure 6-23. Maximum Von-Mises Stress (2037 kg/m³)

6.3.3. Effect of the wave height on the maximum upper flex ball/joint angle with regard to various drilling fluid densities

From Figure 6-24 to Figure 6-27, it can be noticed that the maximum angles for upper flex/ball joint give the satisfactory outcomes since the riser angles fulfill the API and ISO requirements for allowable inclinations of the riser. However, the 16 inch aluminum riser with heavy drilling fluids (12, 14 and 17 ppg) is not capable to operate in extreme conditions with wave heights of 9 to 10 m. Also, it is clear that maximum upper flex/ball joint angle is increasing with increasing wave height.

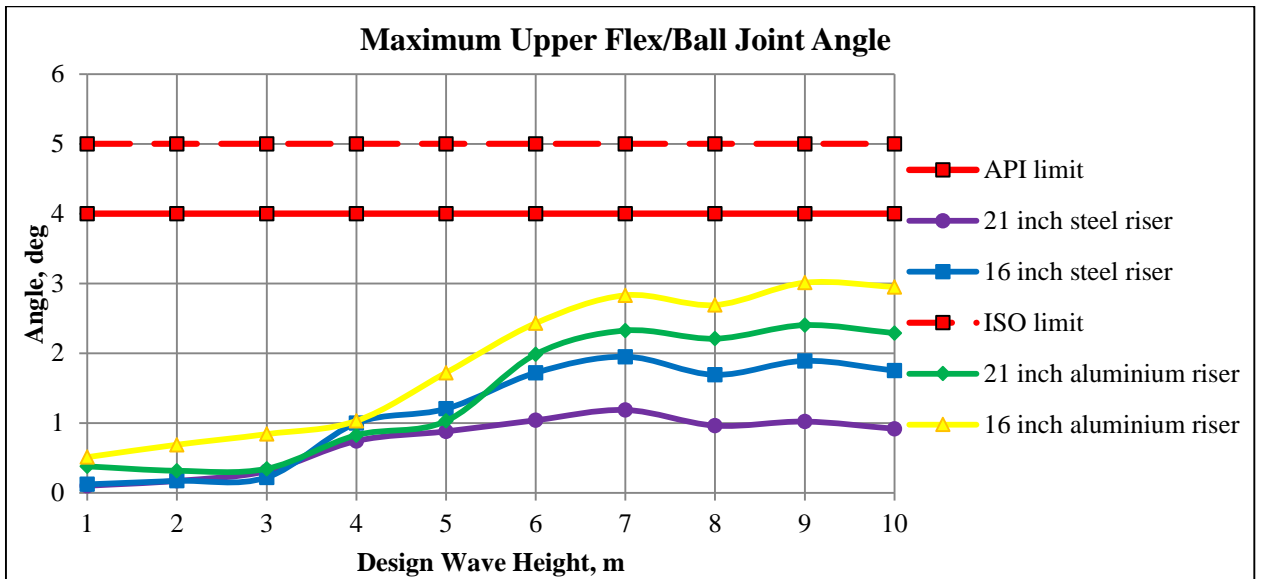


Figure 6-24. Maximum Upper Flex Ball/Joint Angle (1025 kg/m³)

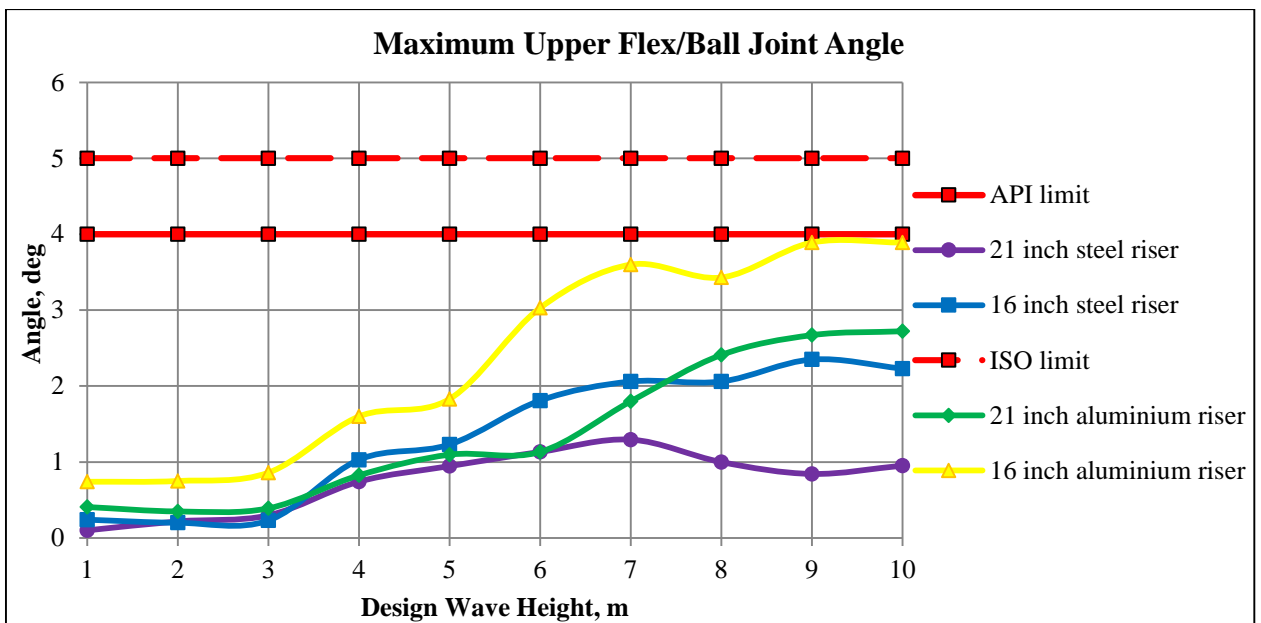


Figure 6-25. Maximum Upper Flex Ball/Joint Angle (1438 kg/m³)

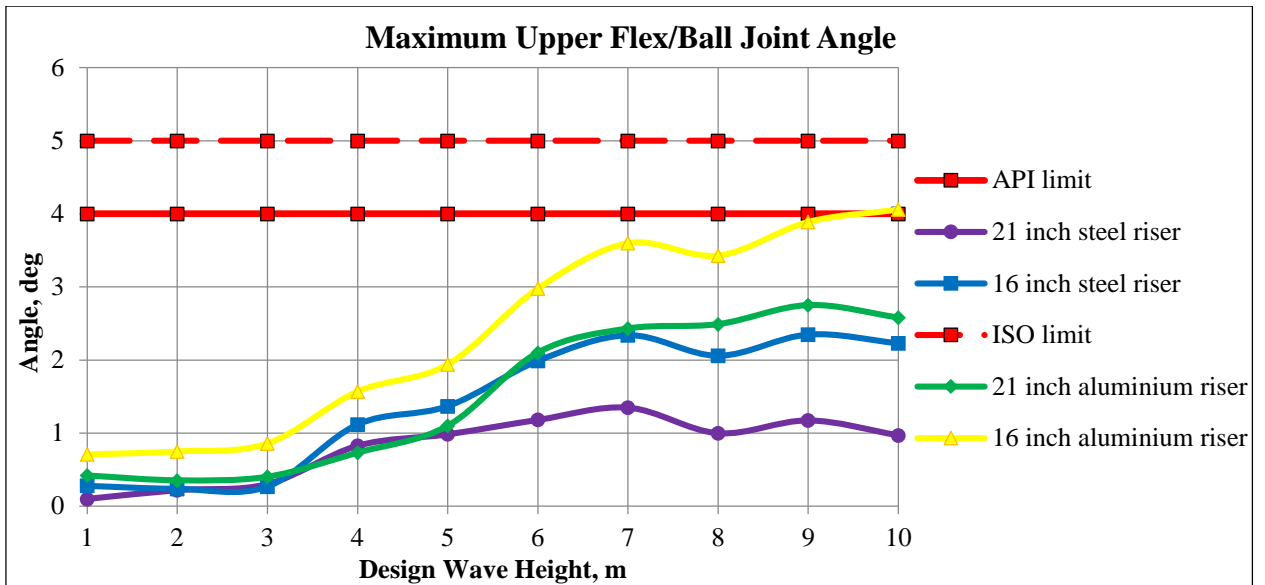


Figure 6-26. Maximum Upper Flex Ball/Joint Angle (1678 kg/m³)

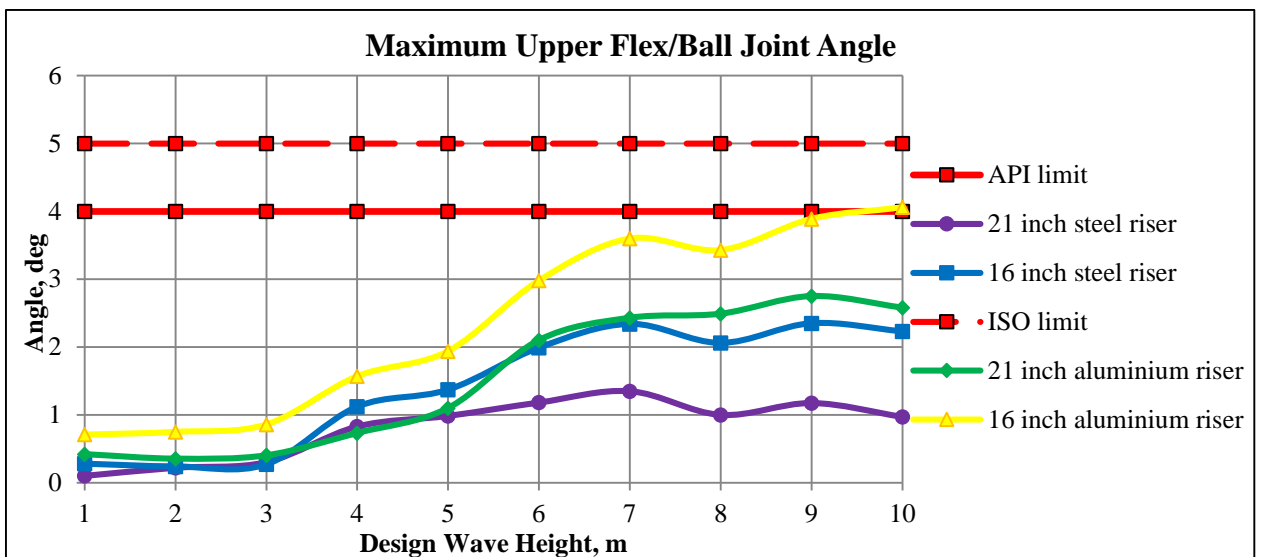


Figure 6-27. Maximum Upper Flex Ball/Joint Angle (2037 kg/m³)

6.3.4. Effect of the wave height on the maximum lower flex ball/joint angle with regard to various drilling fluid densities

The maximum angles for lower flex/ball joint of various riser systems are shown in Figure 6-24 to Figure 6-27. It can be seen from these Figures that the results are satisfactory since angles of the riser inclination fulfill the requirements of API and ISO standards. Only the 16 inch aluminium riser with light drilling fluids (8.55 and 12 ppg) is not suitable for operations in extreme conditions with wave heights of 9 to 10 m as in case of maximum upper flex/ball joint angle. However, the 16 inch aluminium riser becomes more stable as expected when using the heavier drilling fluid (14 and 17 ppg) and the maximum angle of lower flex/ball joint gets lower so that its value does not cross the allowable API limit.

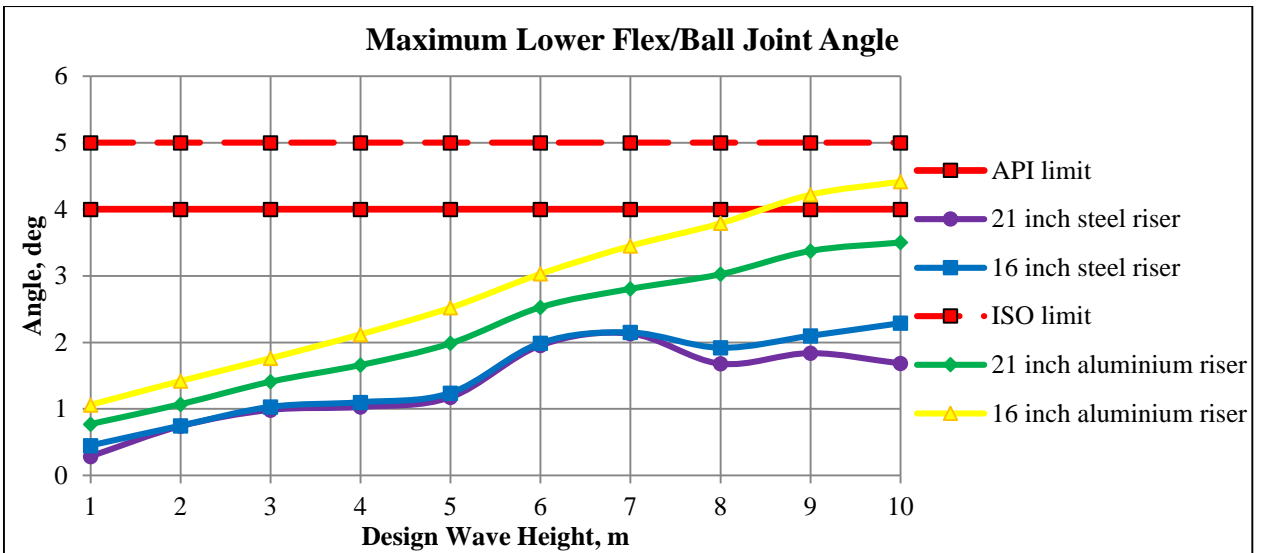


Figure 6-28. Maximum Lower Flex Ball/Joint Angle (1025 kg/m³)

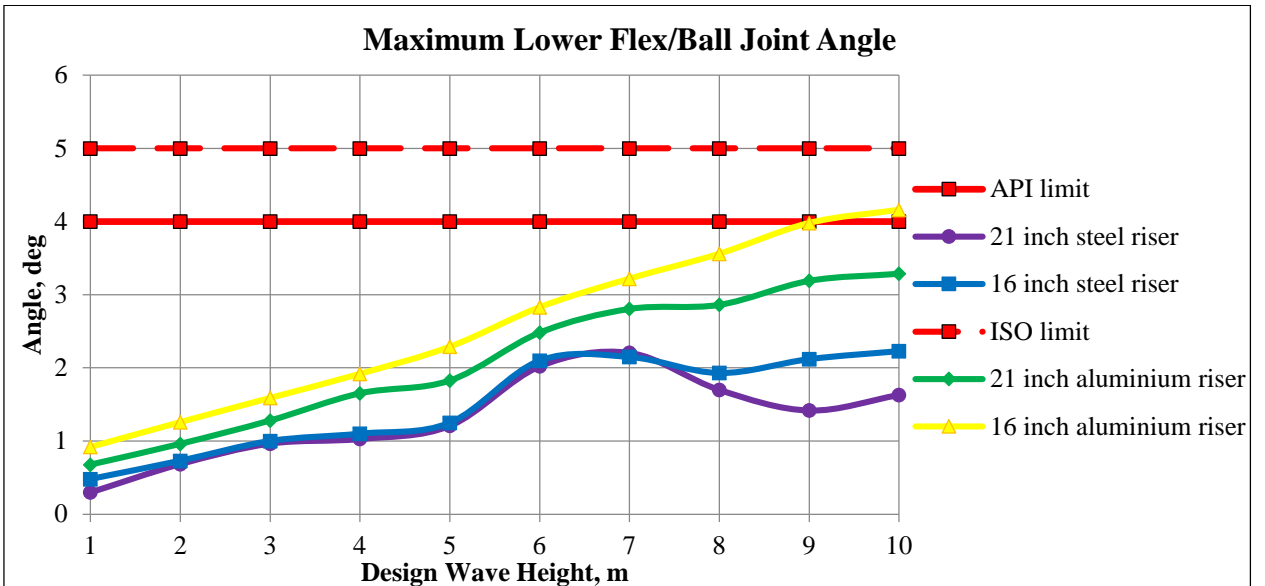


Figure 6-29. Maximum Lower Flex Ball/Joint Angle (1438 kg/m³)

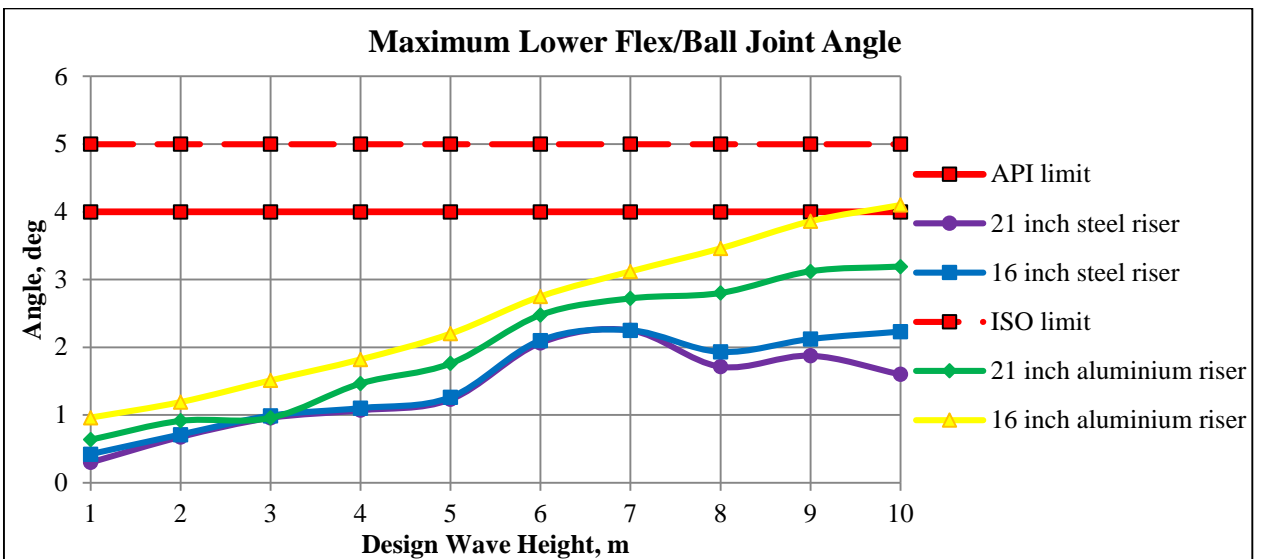


Figure 6-30. Maximum Lower Flex Ball/Joint Angle (1678 kg/m³)

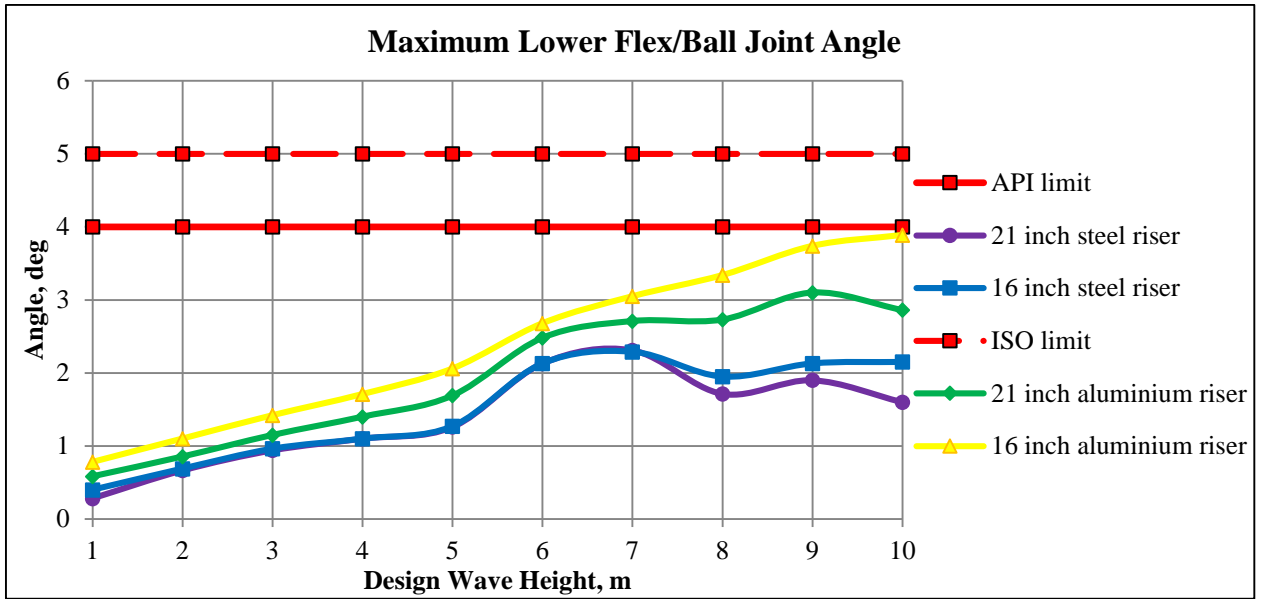


Figure 6-31. Maximum Lower Flex Ball/Joint Angle (2037 kg/m³)

6.4. Simulation in ANSYS Software

The ANSYS program is considered to be utilized in the thesis with a main purpose to study static loads acting on the drilling riser. As described in Chapter 6.1.3.1 OrcaFlex does not enable to include wave forces during static simulation ANSYS is used to apply all possible loads simultaneously taking into account wave forces. ANSYS Workbench 15.0 has a powerful tool which is called Static Structural Analysis and which allows rapid solving of challenging engineering tasks. This tool may also provide with relevant data on stresses and deformations in the drilling riser as results of simulation.

The ANSYS tools are based on a well-known finite element method to model the behavior of the drilling riser under the action of specified wave, current and tension forces.

The modeling procedure can be subdivided into several stages. A simplified model of the drilling riser is created initially. A full description of the model creation will be presented in the following chapter. Then ambient environment should be specified as similar as possible to the conditions of the Kara Sea area. Afterwards all loads are calculated manually and applied to the riser. Finally, the simulation can be run to examine the response of the riser and stresses and deformations caused by loads.

6.4.1. General Description

The model in ANSYS is established describing step-by-step each element in the scheme as shown in Figure 6-31.

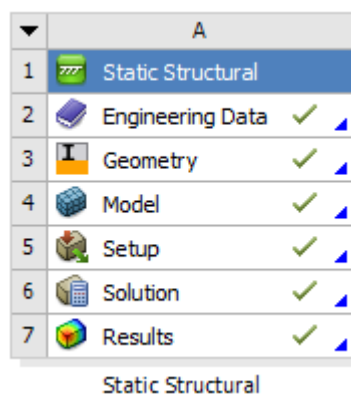


Figure 6-32. Scheme of the Static Structural Analysis

Engineering Data – the data base of materials is used at this stage in order to specify the properties of the riser material in the model.

Geometry – a 3D element structure is created representing the drilling riser.

Model – the most complicated part of the Finite Element Analysis, involving the materials assignment for the riser; creation of the mesh and its adjustment; description of loads, boundary conditions and environment; and finally solution and evaluation of results.

Therefore, prior to the analysis of outcomes, each section in the scheme of Static Structural Analysis should be optimized and implemented according to a maximum accuracy of calculations and computational capabilities of the ANSYS software.

6.4.2. Engineering Data

Materials used for the drilling riser should correspond to the design requirements when specifying their properties in the program. As describe in Chapter 6.2.2 two types of material such as A36 structural steel and aluminum alloy are considered for the drilling riser. Thus, materials are determined in ANSYS by the stress-strain data, density, and other properties.

Outline of Schematic A2: Engineering Data				
	A	B	C	D
1	Contents of Engineering Data		Source	Description
2	Material			
3	Aluminum Alloy	<input type="checkbox"/>	General_Materials.xml	General aluminum alloy. Fatigue properties come from MIL-HDBK-5H, page 3-277.
4	Structural Steel	<input type="checkbox"/>	General_Materials.xml	Fatigue Data at zero mean stress comes from 1998 ASME BPV Code, Section 8, Div 2, Table 5-110.1
*	Click here to add a new material			

Figure 6-33. Materials Set-up at Engineering Data section

6.4.3. Input Data for Environmental Conditions

The input data for the environment used in ANSYS model is presented in Table 6-9.

Parameter	Value	Dimension
Air density	1	kg/m^3
Water density	1025	kg/m^3
Kinematic viscosity	$1.35 \cdot 10^{-6}$	m^2/s
Water temperature	2	$^{\circ}C$

Table 6-9. Input data for the environment

The environmental conditions were specified in the model similar to the Kara Sea region for the summer period since drilling operations can only be carried out during the open water season.

6.4.3. Model Setup

6.4.3.1. Geometry of Model

The modeling of the riser structure in ANSYS was performed on the basis of a detailed three-dimensional (3D) element model. The 3D model was created in the software called Autodesk Inventor Professional and was imported into the *Geometry* section of the project afterwards.

For simplification purposes the riser model was built as a beam or pipe which is approximately vertical at all times. In order to study the only behavior of the main riser pipe the auxiliary lines were neglected. All dimensions for various riser configurations were taken the same as describe as in OrcaFlex software (see Chapter 6.2.2).

Finally, two different models were established since 16 inch and 21 inch riser configurations were examined and assessed in the previous Chapter 6.1.

Figure 6-33 shows an example of the 21 inch drilling riser model in Autodesk Inventor and ANSYS software.

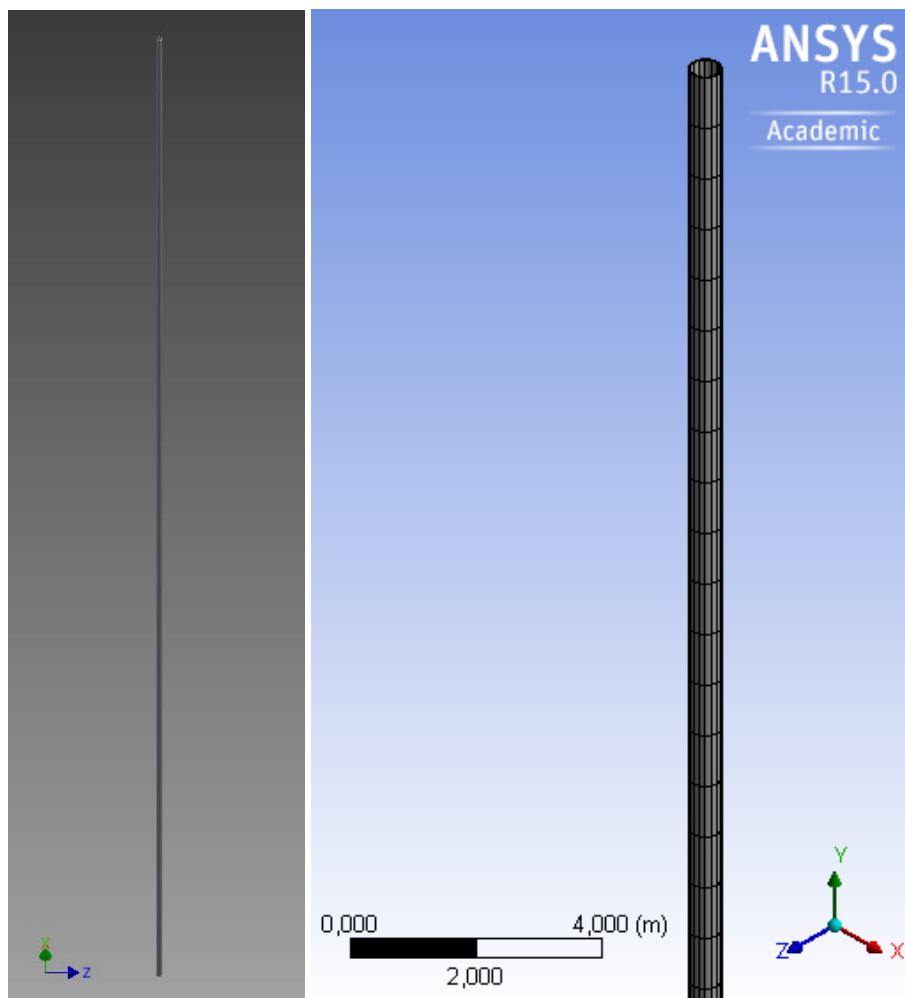


Figure 6-34. The 21 inch drilling riser model in Autodesk Inventor (on the left) and a partially shown 3D model with created mesh in ANSYS (on the right)

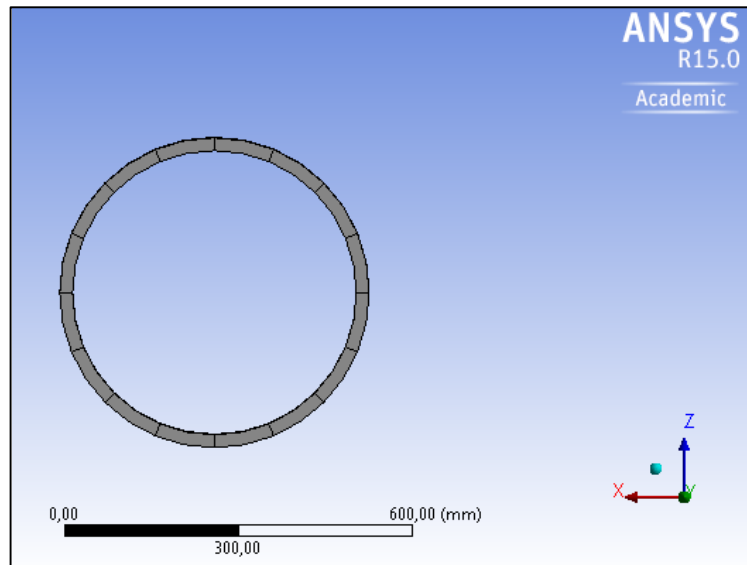


Figure 6-35. Illustration of the top view to the 21 inch drilling riser

6.4.3.2. Meshing

The mesh was applied to the riser model with length of 1 m each cell for all riser configurations. As a result the model is comprised of 1600 elements on the basis of 11280 nodes' coordinates. The relevance of meshing is chosen to be equal -100 for simulation since a higher resolution is not available in an academic version of ANSYS.

6.4.4. Description of Loads

This section is devoted to thorough description of loads' calculations caused by current and waves. The calculations are based on the theory discussed in Chapter 4.5.3.

In this part of the thesis it is suggested to consider two options for waves' height. The first option is the wave with height of 2.5 m since this wave height is the most frequently occurred in the Kara Sea. The second option is proposed to be the wave with height of 8 m as the maximum observed wave height in the Kara Sea region.

The configuration of the 21 inch drilling riser operated at the wave height of 2.5 m is taken as an example for calculations of wave and current forces.

Input Data

Parameter	Designation	Value	Dimension
Wave height	H	2.5	m
Wave amplitude	ξ_0	1.25	m
Period	T	5	s
Water depth	d	100	m
Outer diameter of the riser	D	0.533	m
Water density	ρ	1025	kg/m^3
Standard gravity	g	9.81	m/s^2
Drag coefficient	C_D	1.05	
Mass coefficient	C_M	1.2	

Calculations

1. Wave amplitude:

$$\xi_0 = \frac{H}{2} = 1.25 \text{ m} \quad (6.4)$$

2. Wave length:

$$L = \frac{g \cdot T^2}{2\pi} = 39.1 \text{ m} \quad (6.5)$$

3. Angular velocity:

$$\omega = \frac{2\pi}{T} = 1.3 \text{ s}^{-1} \quad (6.6)$$

4. $k = \frac{2\pi}{L} = 0.161 \quad (6.7)$

5. Checking deep water criterion:

$$\frac{d}{L} = 2.55 > 0.5 \text{ - deep water area} \quad (6.8)$$

6. Checking conditions for Morison's equation:

$$\frac{D}{L} = 0.014 < 0.2 \quad (6.9)$$

$$\frac{H}{L} = 0.064 \leq 0.14 \text{ - non - breaking waves} \quad (6.10)$$

$$\frac{a}{D} < 0.2 \rightarrow a < 0.11 \quad (6.11)$$

Assuming that the motion amplitude (a) for the drilling riser is negligible the Morison equation can be used safely to calculate the forces.

7. Calculating the Keulegan-Carpenter number to check which term will dominate in the Morison equation:

$$N_{KC} = \frac{\pi \cdot H}{D} = 4.7\pi \quad (6.12)$$

Hence, both the drag and mass term will be taken into account in the equation.

8. The Morison equation can be written as follows:

$$f(z, t) = f_M + f_D = \left(\rho \cdot \frac{\pi D^2}{4} \right) \cdot C_M \cdot \dot{u} + \frac{1}{2} \cdot \rho \cdot C_D \cdot D \cdot u \cdot |u| \quad (6.13)$$

$$F(t) = F_M(t) + F_D(t) = \int_{-d}^{surface} f(z, t) dz = \int_{-d}^{\xi_0} f_M(z, t) dz + \int_{-d}^{\xi_0} f_D(z, t) dz \quad (6.14)$$

$$F(t) = \int_{-d}^{\xi_0} \left(\rho \cdot \frac{\pi D^2}{4} \right) \cdot C_M \cdot \dot{u} dz + \int_{-d}^{\xi_0} \frac{1}{2} \cdot \rho \cdot C_D \cdot D \cdot u \cdot |u| dz \quad (6.15)$$

The maximum force in the mass term is found at maximum acceleration but the maximum force in the drag term is found at maximum velocity. These maximum values cannot be added together since the velocity is based on a sinus function and the acceleration is based on a cosines function. That means that they are out of phase (90 degrees) and it is not possible to have the maximum velocity and maximum acceleration simultaneously. The equation can be solved using a graphical method when each contributing term is plotted on a timeline and the maximum force is found graphically.

9. For deep water zone the horizontal velocity and acceleration can be presented as the following:

$$u = \frac{\xi_0 g k}{\omega} e^{kz} \cdot \sin(\omega t), \quad \dot{u} = \xi_0 g k e^{kz} \cdot \cos(\omega t) \quad (6.16) (6.17)$$

Therefore

$$\begin{aligned}
F_M(t) &= \int_{-d}^{\xi_0} \left(\rho \cdot \frac{\pi D^2}{4} \right) \cdot C_M \cdot u dz = \int_{-d}^{\xi_0} \left(\rho \cdot \frac{\pi D^2}{4} \right) \cdot C_M \cdot \xi_0 g k e^{kz} \cdot \cos(\omega t) dz = \\
&= \left(\rho \cdot \frac{\pi D^2}{4} \right) \cdot C_M \cdot \xi_0 g k \cdot \cos(\omega t) \left[\frac{e^{kz}}{k} \right]_{-d}^{\xi_0} = \\
&= \left(\rho \cdot \frac{\pi D^2}{4} \right) \cdot C_M \cdot \xi_0 g \cdot \cos(\omega t) \left[e^{k\xi_0} - e^{-kd} \right]
\end{aligned} \tag{6.18}$$

and

$$\begin{aligned}
F_D(t) &= \int_{-d}^{\xi_0} \frac{1}{2} \cdot \rho \cdot C_D \cdot D \cdot u \cdot |u| dz = \int_{-d}^{\xi_0} \frac{1}{2} \cdot \rho \cdot C_D \cdot D \cdot \left(\frac{\xi_0 g k}{\omega} e^{kz} \right)^2 \cdot \sin(\omega t) |\sin(\omega t)| dz = \\
&= \frac{1}{2} \cdot \rho \cdot C_D \cdot D \cdot \left(\frac{\xi_0 g k}{\omega} \right)^2 \cdot \sin(\omega t) |\sin(\omega t)| \int_{-d}^{\xi_0} e^{2kz} dz = \\
&= \frac{1}{2} \cdot \rho \cdot C_D \cdot D \cdot \left(\frac{\xi_0 g k}{\omega} \right)^2 \cdot \sin(\omega t) |\sin(\omega t)| \left[\frac{e^{2kz}}{2k} \right]_{-d}^{\xi_0} = \\
&= \frac{1}{4} \cdot \rho \cdot C_D \cdot D \cdot k \cdot \left(\frac{\xi_0 g}{\omega} \right)^2 \cdot \sin(\omega t) |\sin(\omega t)| \left[e^{2k\xi_0} - e^{-2kd} \right]
\end{aligned} \tag{6.19}$$

Finally, the expression for the total force calculation can be presented in the next form:

$$\begin{aligned}
F_{Total}(t) &= F_M(t) + F_D(t) = \left(\rho \cdot \frac{\pi D^2}{4} \right) \cdot C_M \cdot \xi_0 g \cdot \cos(\omega t) \left[e^{k\xi_0} - e^{-kd} \right] + \\
&+ \frac{1}{4} \cdot \rho \cdot C_D \cdot D \cdot k \cdot \left(\frac{\xi_0 g}{\omega} \right)^2 \cdot \sin(\omega t) |\sin(\omega t)| \left[e^{2k\xi_0} - e^{-2kd} \right]
\end{aligned} \tag{6.20}$$

10. All derived expressions can now be plotted for a 5.5 s (and 10.5 s for illustration) wave period and the maximum force impact can be found afterwards.

It is important to notice that the integration is performed up to ξ_0 . This is a conservative simplification because in reality the maximum force occurs in a place between the wave crest and still water level for a given time period. That implies that to be theoretically correct the equation have to be solved for maximum force with variable upper-integration limit, varying from 0 to ξ_0 .

11.

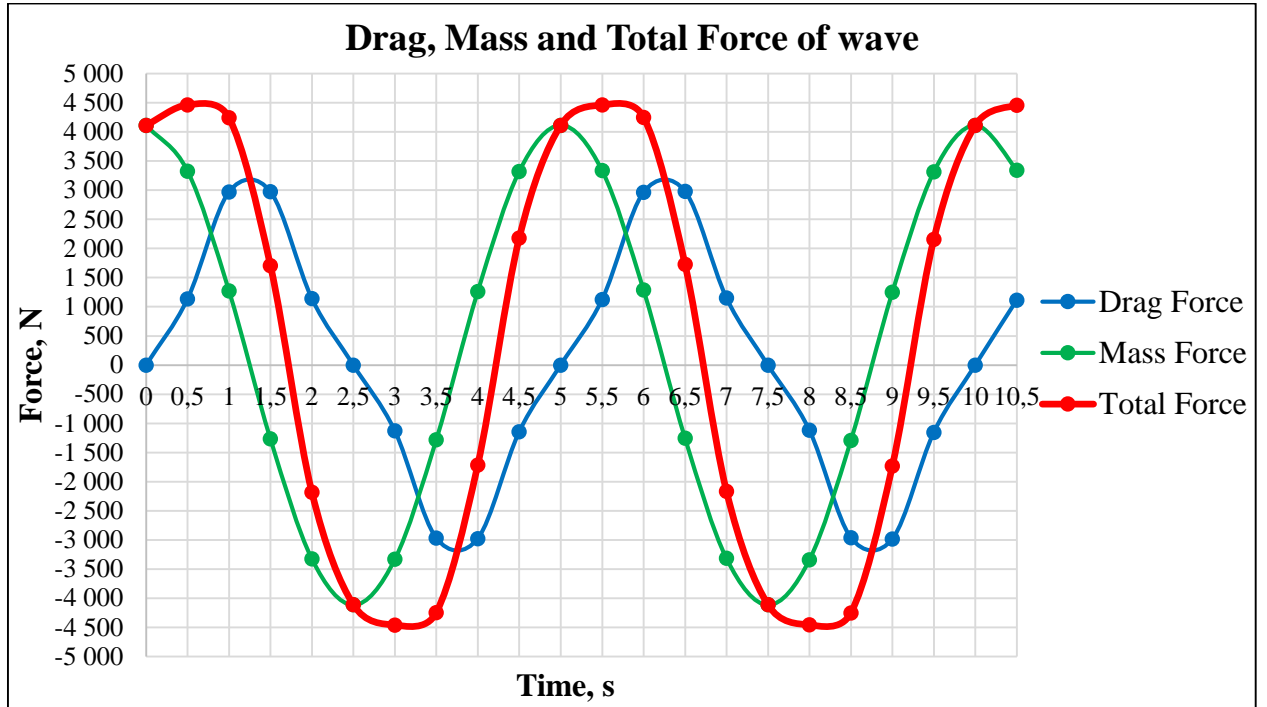


Figure 6-36. Drag, Mass and Total Force of wave

The drag, mass and total forces are shown in Figure 6-35 as a function of time. It can be observed from Figure the forces express negative values as well but the only positive values should be taken into account.

$$F_{Total} = 4500 \text{ N is at the maximum when } t \approx 0.7 \text{ s.}$$

12.

However, the maximum total force should also be defined and plotted as a function of the water depth. The water depth (z) varies from the top point at the wave crest ($\xi_0 = 1.25 \text{ m}$) to the depth at which the maximum total force has any observed impact ($F_{Total}(t = 0.7 \text{ s})$ is approximately equal to 0). The step of depth variation is chosen to be equal to 1 m since the size of the cell in the ANSYS model is specified as 1 m.

$$F_{Total}(t = 0.7, z) = F_M(t = 0.7, z) + F_D(t = 0.7, z) = \left(\rho \cdot \frac{\pi D^2}{4} \right) \cdot C_M \cdot \xi_0 g e^{kz} \cdot \cos(\omega t) + \frac{1}{2} \cdot \rho \cdot C_D \cdot D \cdot k \cdot \left(\frac{\xi_0 g k}{\omega} e^{kz} \right)^2 \cdot \sin(\omega t) \sin(\omega t) \quad (6.21)$$

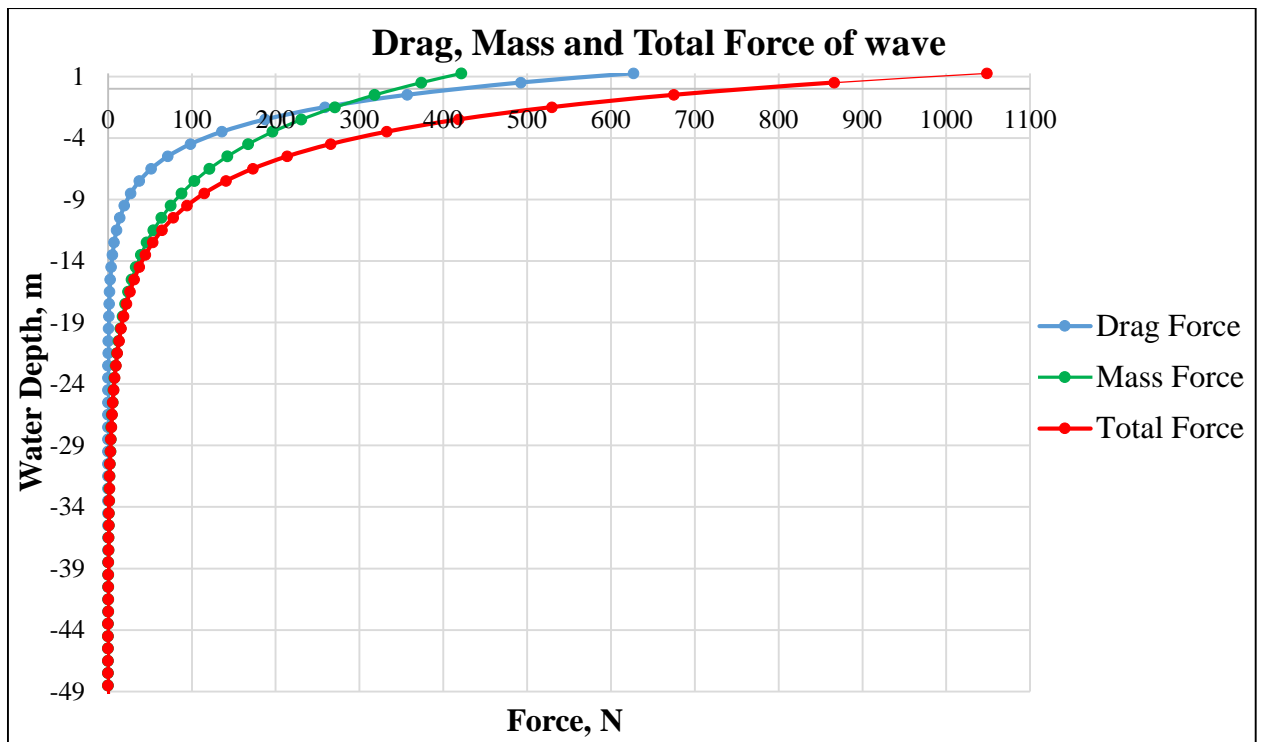


Figure 6-37. Distribution of Drag, Mass and Total Force of wave over the water depth

For remaining riser configurations and various wave heights the detailed calculations of forces are presented in Appendix G and Excel file on DVD.

Since the drilling riser is also exposed to the sea current therefore current forces should be determined in order to apply them on the riser structure in the ANSYS model. For calculation of forces acting on the riser at a constant current the only drag term is taken into consideration in the Morison equation. The distribution of the current velocity over the water depth can be found by the Power Law equation used in OrcaFlex (see Appendix E and Chapter 6.2.3).

Input Data

Parameter	Designation	Value	Dimension
Current velocity at the surface	S_0	1	m/s
Current velocity at the sea bottom	S_b	0.2	m/s
Water depth	d	100	m
Outer diameter of the riser	D	0.533	m
Water density	ρ	1025	kg/m^3
Standard gravity	g	9.81	m/s^2
Drag coefficient	C_D	1.05	
Power Law Exponent	<i>Exponent</i>	0.3	

Calculations

1. Current velocity:

$$S(z) = S_b + (S_f - S_b) \times ((z - z_b) / (z_f - z_b))^{1/Exponent} \quad (6.22)$$

where z varies from 0 to 90 m as the bottom end of the riser is located 10 m above the seabed.

2. Average velocity of the current:

$$S_{average} = \frac{S_n + S_{n+1}}{2} \quad (6.23)$$

3. Finally the drag force can be calculated using the following equation:

$$F_{Total} = F_D = \int_{z'-\Delta z}^{z'} f_D(z, t) dz = \int_{z'-\Delta z}^{z'} \frac{1}{2} \cdot \rho \cdot C_D \cdot D \cdot u \cdot |u| dz = \frac{1}{2} \cdot \rho \cdot C_D \cdot D \cdot u^2 \cdot \Delta z \quad (6.24)$$

where $u = S_{average}$

The step of the water depth variation (Δz) is equal to 1 m due to the cell length (1 m) in the mesh created on the riser structure.

4. The calculation results are presented in Table 6-10.

Water Depth, z	Δz	Current Velocity, $S(z)$	Average Velocity of the Current, $S_{average}$	Drag Force, F_D
m	m	m/s	m/s	N
0	-	1,000	-	-
-1	1	0,974	0,987	279
-2	1	0,948	0,961	265
-3	1	0,923	0,935	251
-4	1	0,898	0,910	238
-5	1	0,874	0,886	225
-6	1	0,851	0,863	213
-7	1	0,828	0,840	202
-8	1	0,806	0,817	191
-9	1	0,784	0,795	181
-10	1	0,763	0,774	172
-11	1	0,742	0,753	163
-12	1	0,722	0,732	154
-13	1	0,703	0,713	146
-14	1	0,684	0,693	138
-15	1	0,665	0,675	131
-16	1	0,647	0,656	124
-17	1	0,630	0,639	117

-18	1	0,613	0,621	111
-19	1	0,596	0,605	105
-20	1	0,580	0,588	99
-21	1	0,565	0,572	94
-22	1	0,549	0,557	89
-23	1	0,535	0,542	84
-24	1	0,520	0,528	80
-25	1	0,507	0,514	76
-26	1	0,493	0,500	72
-27	1	0,480	0,487	68
-28	1	0,468	0,474	64
-29	1	0,455	0,462	61
-30	1	0,444	0,450	58
-31	1	0,432	0,438	55
-32	1	0,421	0,427	52
-33	1	0,411	0,416	50
-34	1	0,400	0,405	47
-35	1	0,390	0,395	45
-36	1	0,381	0,386	43
-37	1	0,371	0,376	41
-38	1	0,363	0,367	39
-39	1	0,354	0,358	37
-40	1	0,346	0,350	35
-41	1	0,338	0,342	34
-42	1	0,330	0,334	32
-43	1	0,323	0,327	31
-44	1	0,316	0,319	29
-45	1	0,309	0,312	28
-46	1	0,303	0,306	27
-47	1	0,296	0,299	26
-48	1	0,290	0,293	25
-49	1	0,285	0,288	24
-50	1	0,279	0,282	23
-51	1	0,274	0,277	22
-52	1	0,269	0,272	21
-53	1	0,265	0,267	20
-54	1	0,260	0,262	20
-55	1	0,256	0,258	19
-56	1	0,252	0,254	18
-57	1	0,248	0,250	18
-58	1	0,244	0,246	17
-59	1	0,241	0,243	17
-60	1	0,238	0,239	16
-61	1	0,235	0,236	16
-62	1	0,232	0,233	16
-63	1	0,229	0,230	15

-64	1	0,227	0,228	15
-65	1	0,224	0,225	15
-66	1	0,222	0,223	14
-67	1	0,220	0,221	14
-68	1	0,218	0,219	14
-69	1	0,216	0,217	14
-70	1	0,214	0,215	13
-71	1	0,213	0,214	13
-72	1	0,211	0,212	13
-73	1	0,210	0,211	13
-74	1	0,209	0,210	13
-75	1	0,208	0,208	12
-76	1	0,207	0,207	12
-77	1	0,206	0,206	12
-78	1	0,205	0,206	12
-79	1	0,204	0,205	12
-80	1	0,204	0,204	12
-81	1	0,203	0,203	12
-82	1	0,203	0,203	12
-83	1	0,202	0,202	12
-84	1	0,202	0,202	12
-85	1	0,201	0,202	12
-86	1	0,201	0,201	12
-87	1	0,201	0,201	12
-88	1	0,201	0,201	12
-89	1	0,201	0,201	12
-90	1	0,200	0,200	12

Table 6-10. Drag force calculations

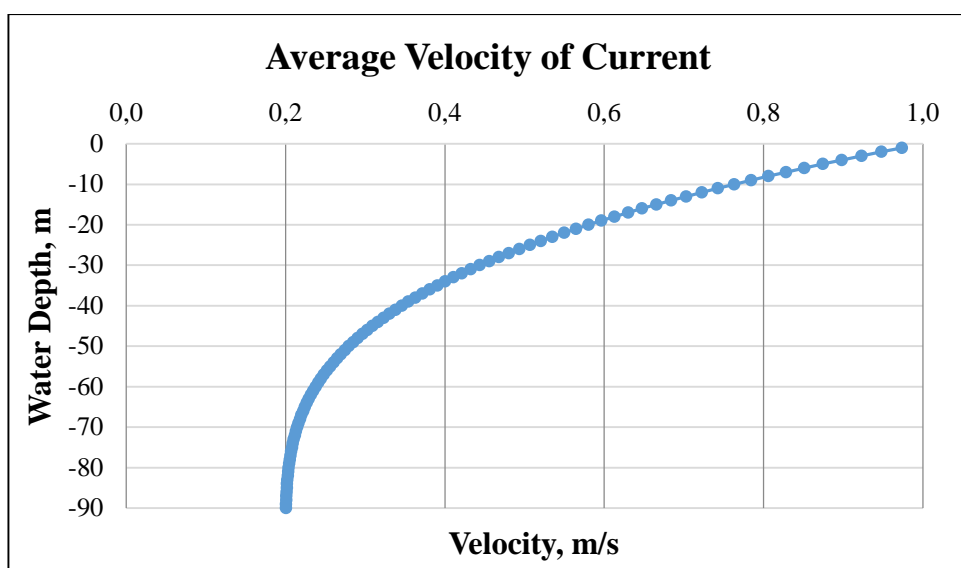


Figure 6-38. Average velocity of the current over the water depth

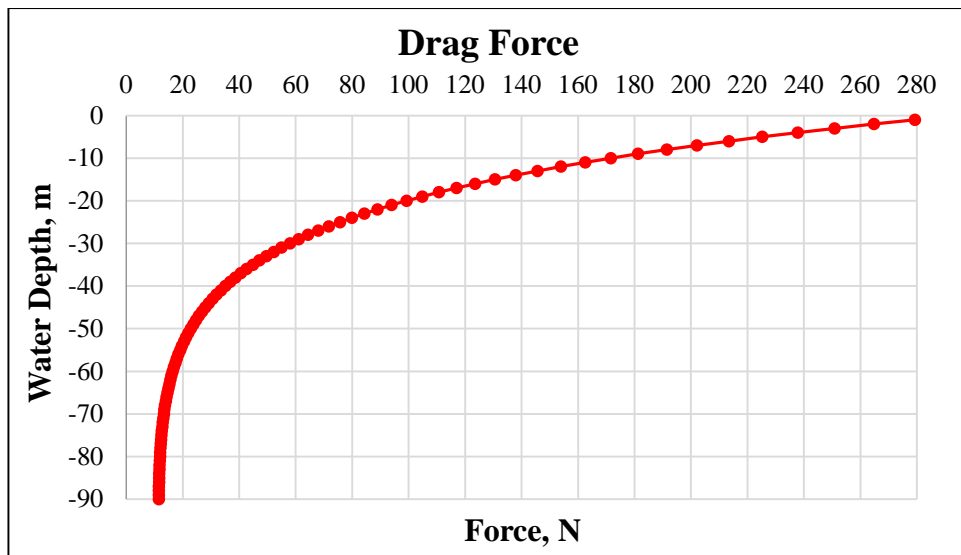


Figure 6-39. Distribution of the Drag Force over the water depth

The detailed calculations of the drag force for the case of 16 inch riser can be found in Appendix G and Excel file on DVD.

Therefore, all forces acting on the drilling riser are calculated and can be applied to the riser structure in ANSYS. First wave forces are applied to a middle of each cell along the length of the riser and then current forces are applied in the same principle. In order to investigate the maximum impact of loads on the riser all forces are chosen to act in the same direction (in positive direction of the x -axis).

The effect of wind forces on the drilling riser is not taken into account in the model since it has given a negligible impact during simulation in OrcaFlex.

The pressure exerted by the drilling fluid inside the riser should be taken into consideration. Thus, it was decided to choose the heaviest drilling fluid with the density of 2037 kg/m^3 (17 ppg) because it may induce large hoop stresses in the riser walls.

The external pressure acting on the drilling riser was also included in the model. Since the riser is submerged by 90 m into the water the pressure of external fluid is applied to a 90 m part of the riser out of the whole its length.

The top tension for various riser configurations is taken based on calculations of the minimum required top tension, which are described in detail in Appendix D and Chapter 6.2.4.

The top boundary condition for the drilling riser is taken as the rig displacement, which is equal to 0 since the drift off and drive off motions were assumed to be negligible. As describe in Chapter 6.2.2 the riser is connected to the LMRP by Lower Flex Joint; therefore, the bottom boundary condition of the riser model is fixed in all directions.

6.4.5. Analysis Results and Discussions

Two configurations of the drilling riser were simulated in ANSYS to examine the performance and behavior of both 16 inch and 21 inch riser at static conditions. The design wave heights were selected to represent normal (2.5 m) and extreme (8m) operational conditions. By applying different materials it will be ascertained what are the limiting properties for the riser material to perform operations safely at the designed water depth of 100 m.

The results of simulations are shown in Figures 6-39 through 6-46.

The fundamental Von-Mises stress of the 16 inch and 21 inch riser is compared since it gives a clear picture of stresses caused by loads on the drilling riser. In the first option both 16 inch and 21 inch riser have the same grade of the material as A36 structural steel; however, the 16 inch slim riser has higher stresses in all situations, as anticipated. The same conclusion as in the previous case can be made for the option of 16 inch and 21 inch aluminum risers. The 16 inch and 21 inch aluminum risers are not safe to be operated in the presence of waves with height of 8 m as the maximum anticipated Von-Mises stress for these riser configurations is higher than the allowable limit (60.3 MPa) for the stresses. However, if the situation tends to reach the worst-case scenario (non-drilling mode) the riser can be disconnected and drilling rig can be moved to a safe location.

All steel risers have performed well during simulations and appear more robust than aluminum riser configurations. From the thesis concern and economical point of view the 16 inch steel riser is suggested for drilling operations in the Kara Sea.

It is also important to emphasize that simulations were carried out at static conditions in ANSYS software and at dynamic conditions in OrcaFlex. Therefore, analysis results obtained from ANSYS cannot be compared directly with outcomes gained out of analysis after simulations in OrcaFlex.

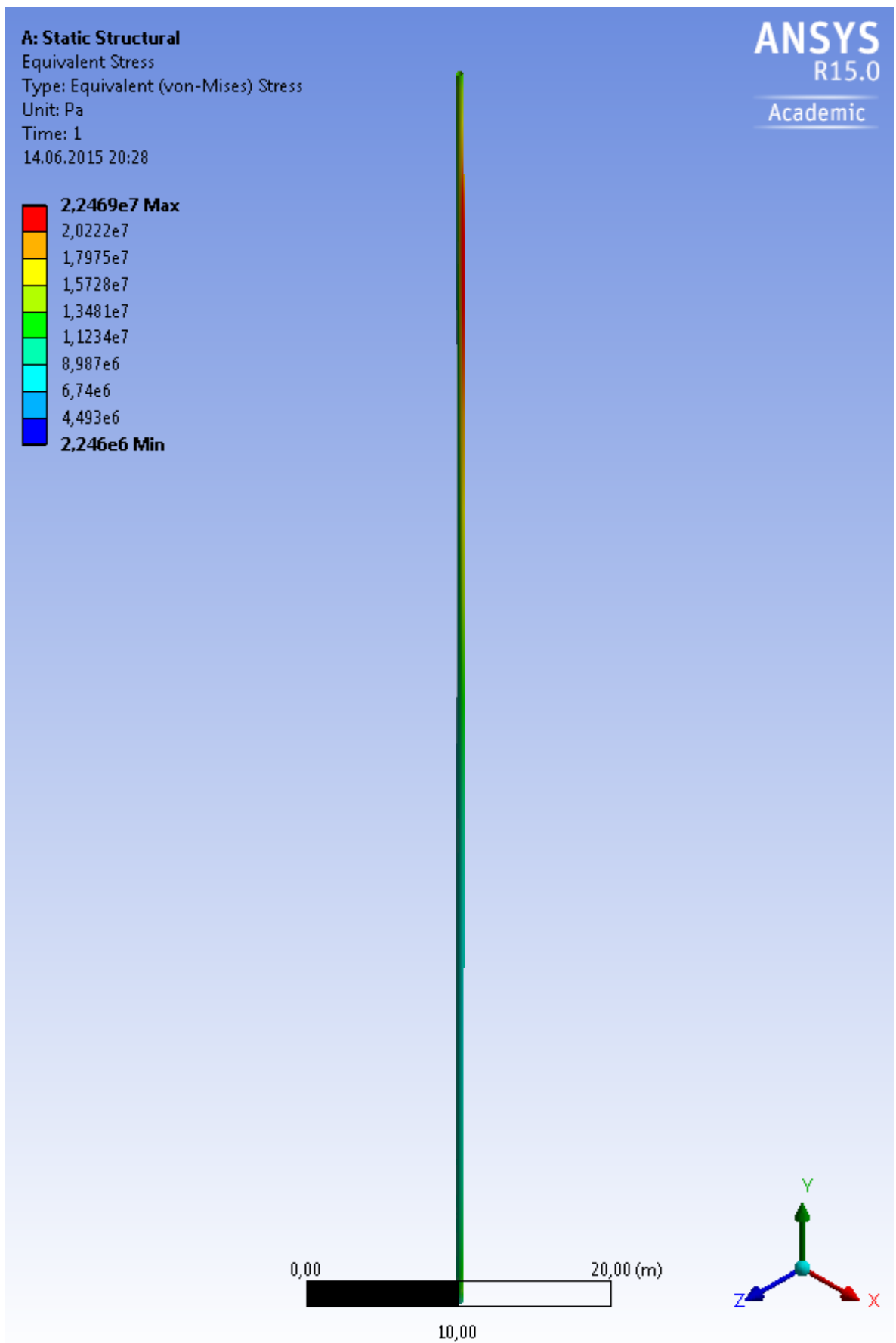


Figure 6-40. Von-Mises stress distribution in the 21 inch steel riser at the wave height of 2.5 m

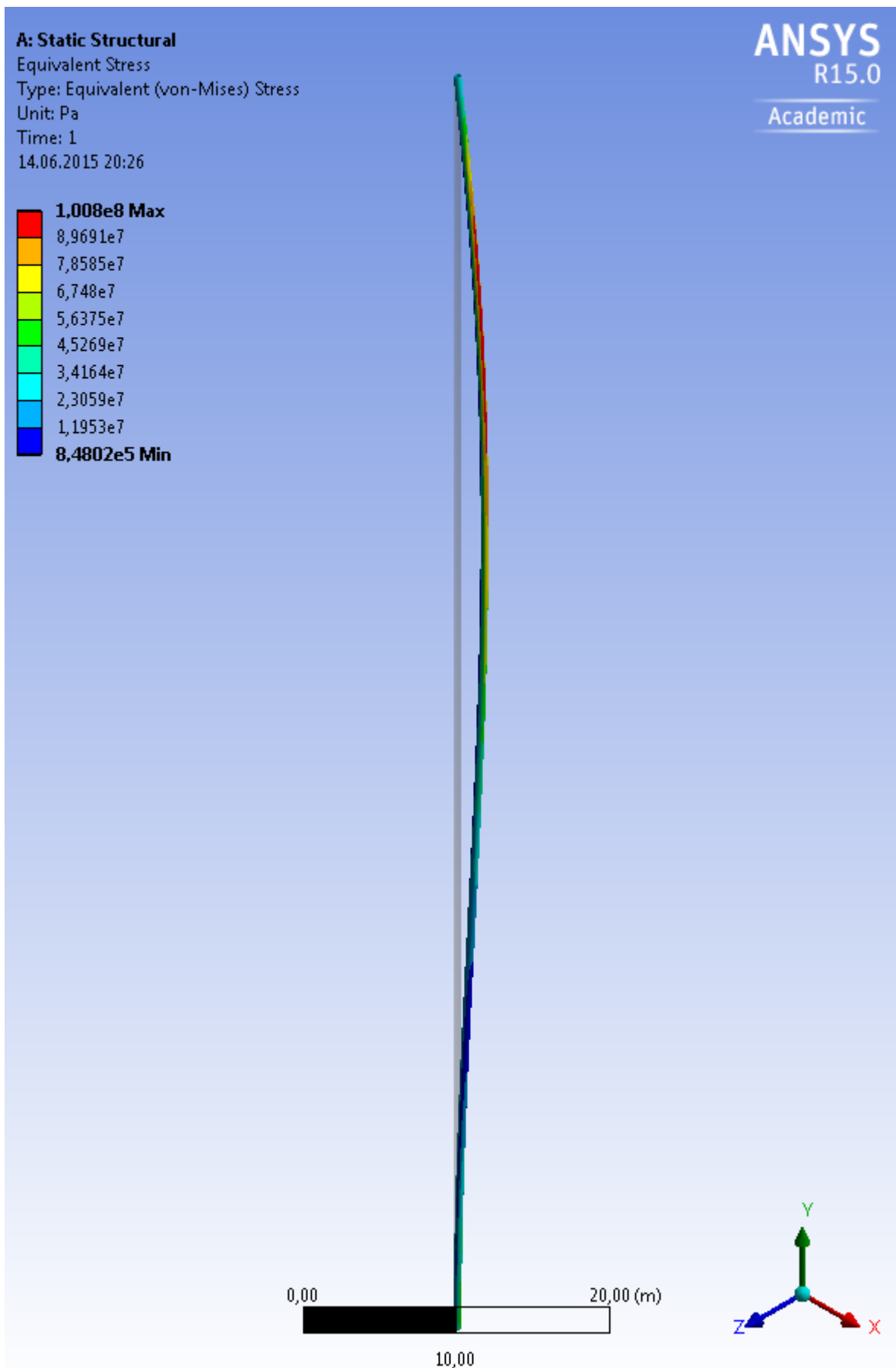


Figure 6-41. Von-Mises stress distribution in the 21 inch steel riser at the wave height of 8 m

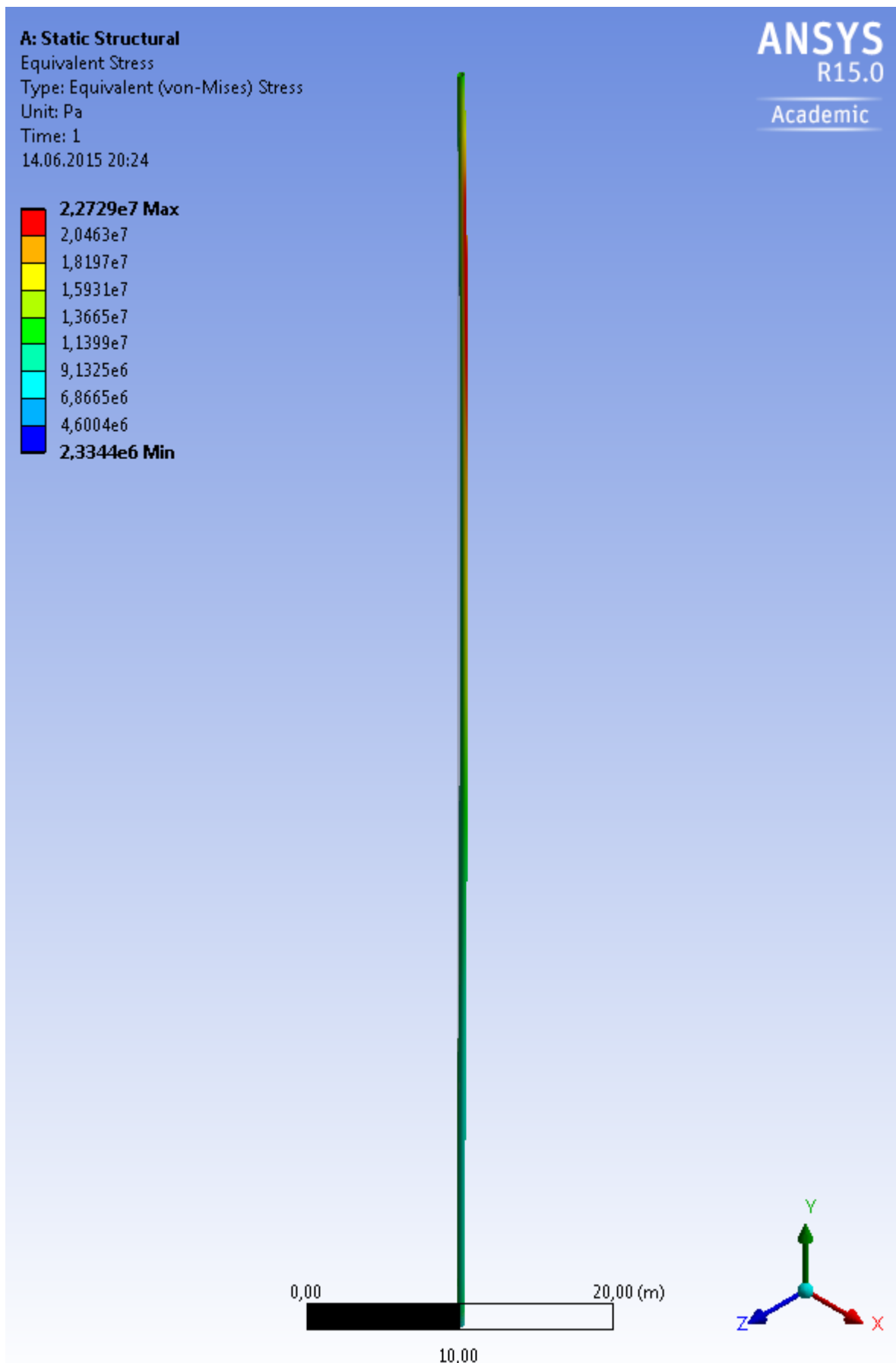


Figure 6-42. Von-Mises stress distribution in the 21 inch aluminum riser at the wave height of 2.5 m

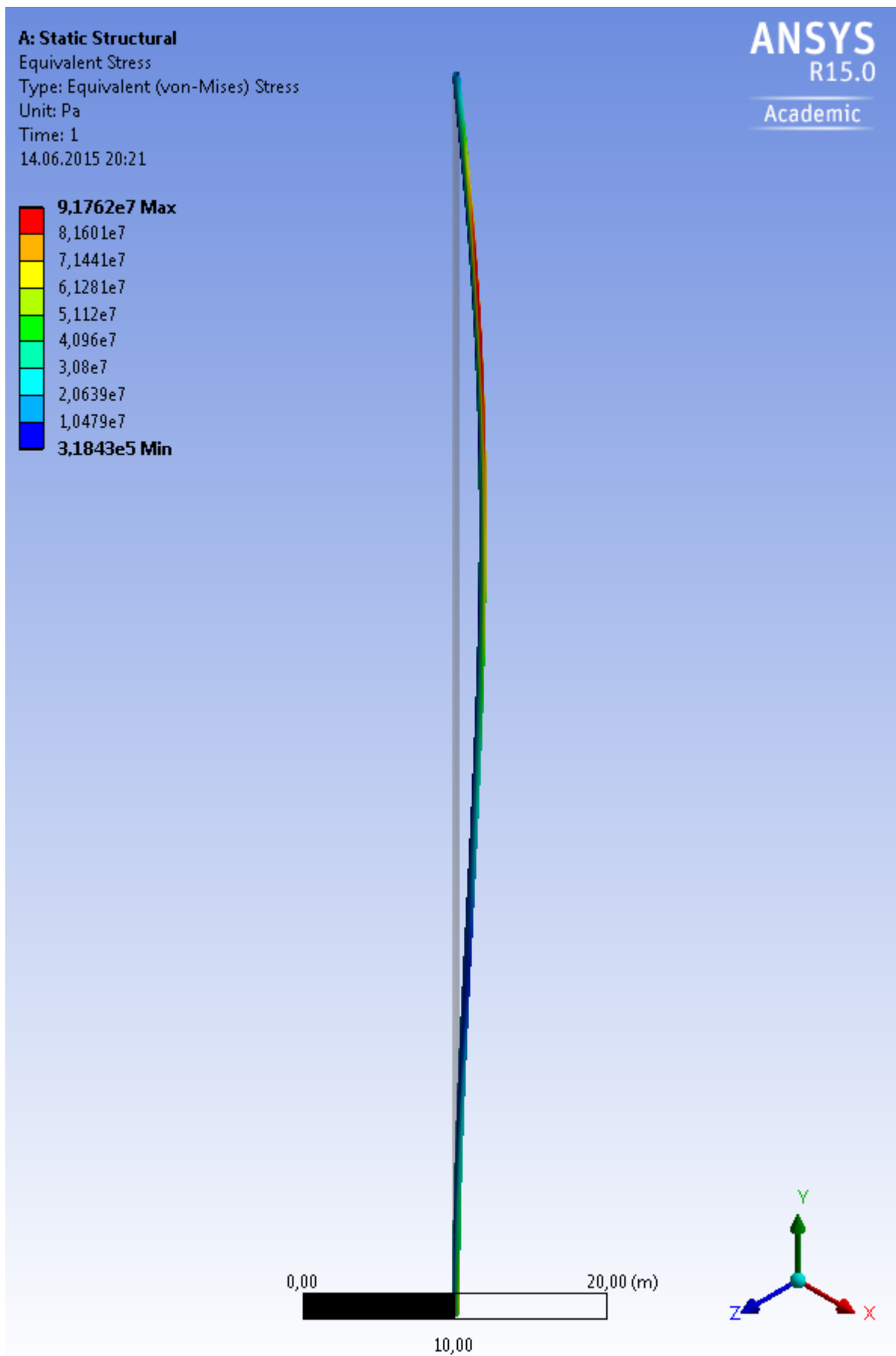


Figure 6-43. Von-Mises stress distribution in the 21 inch aluminum riser at the wave height of 8 m

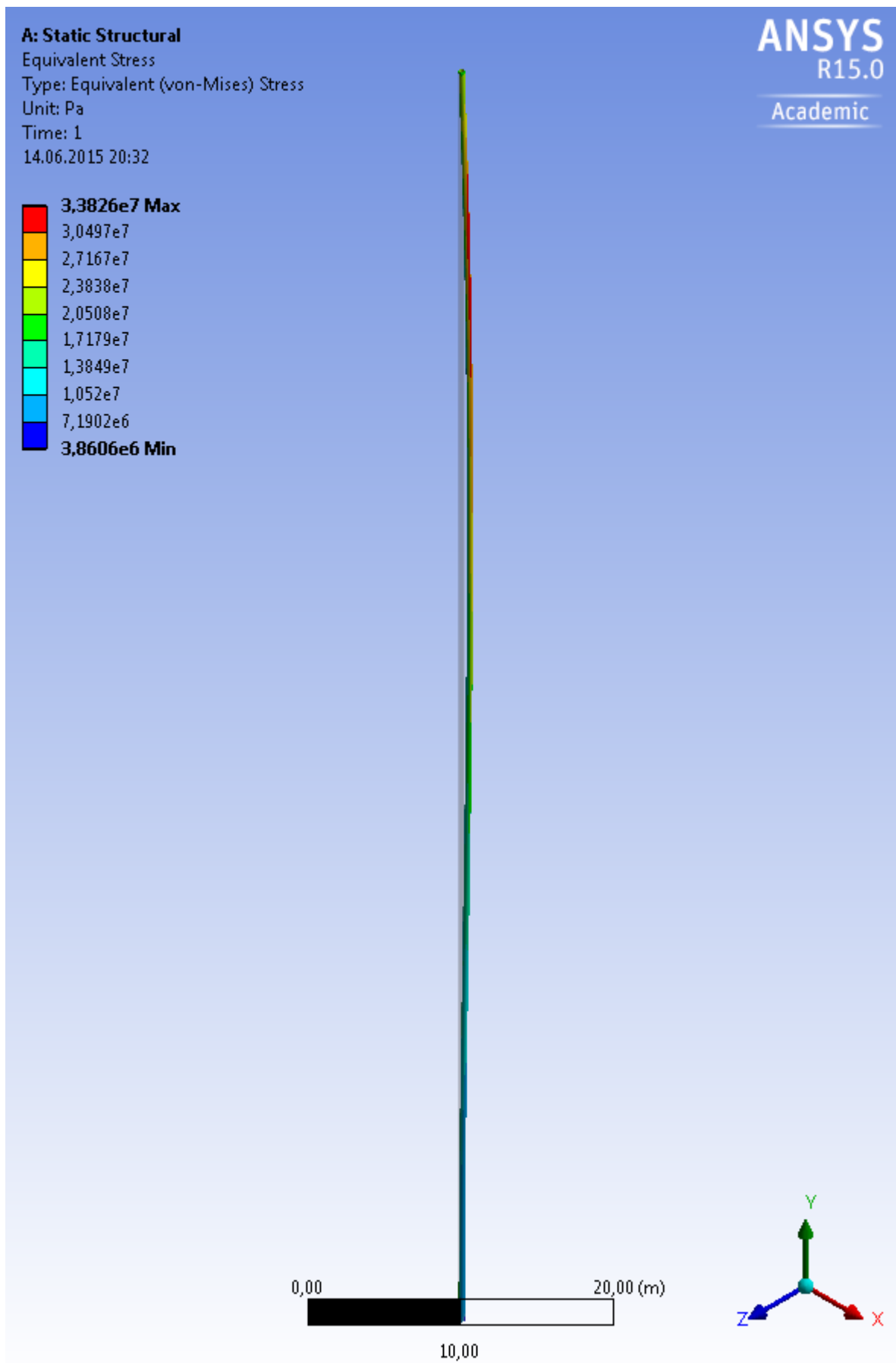


Figure 6-44. Von-Mises stress distribution in the 16 inch steel riser at the wave height of 2.5 m

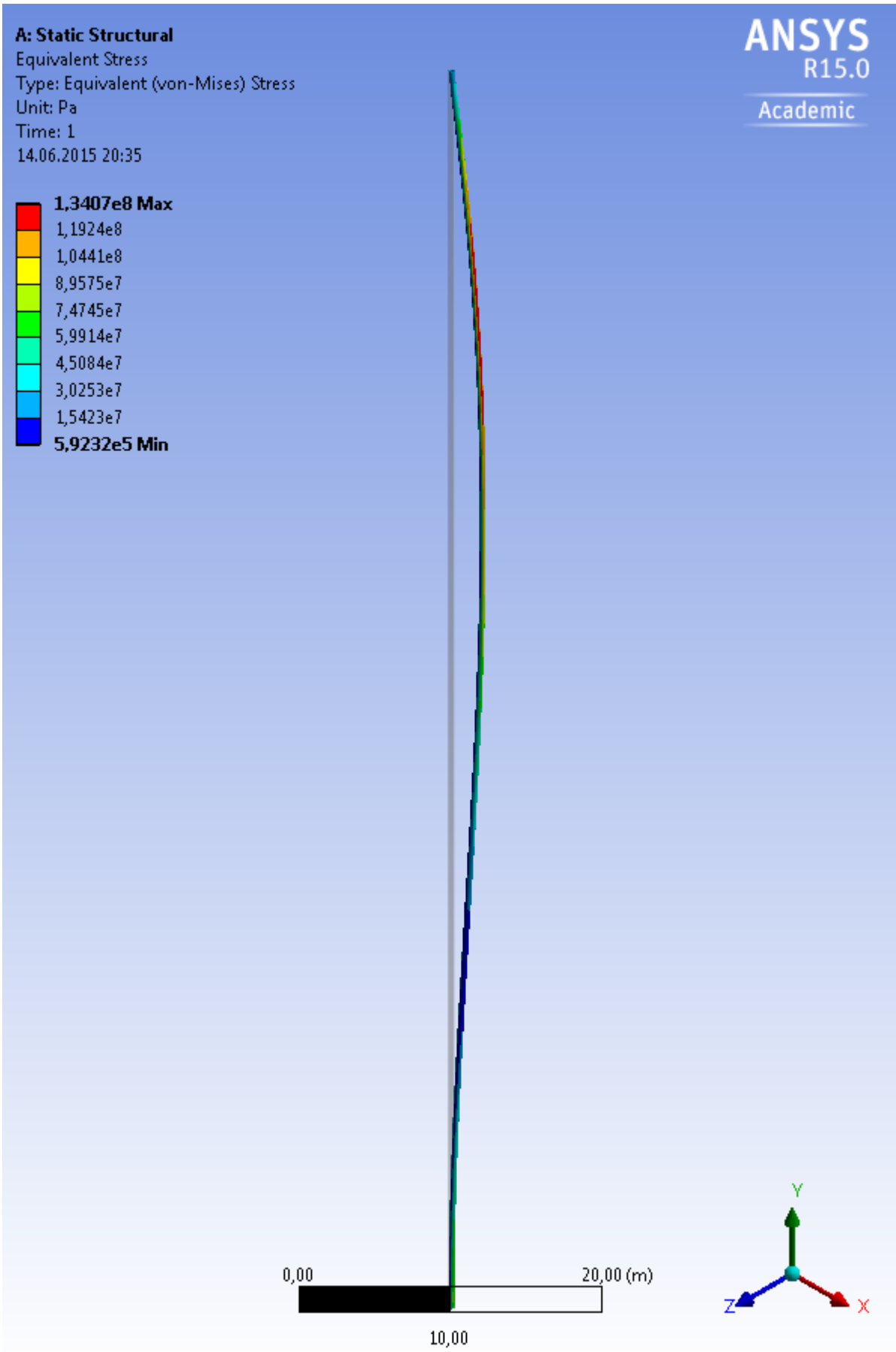


Figure 6-45. Von-Mises stress distribution in the 16 inch steel riser at the wave height of 8 m

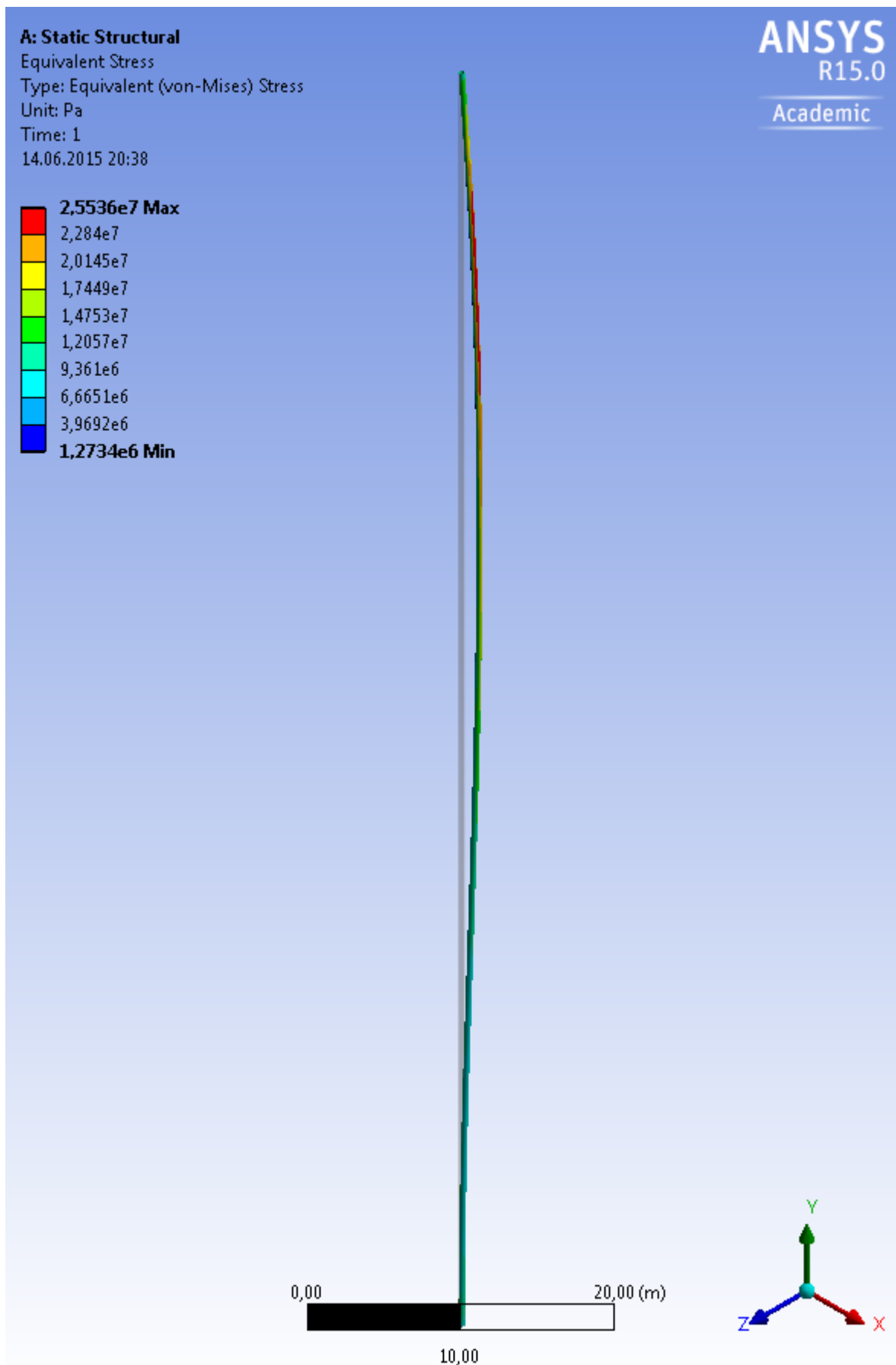


Figure 6-46. Von-Mises stress distribution in the 16 inch aluminum riser at the wave height of 2.5 m

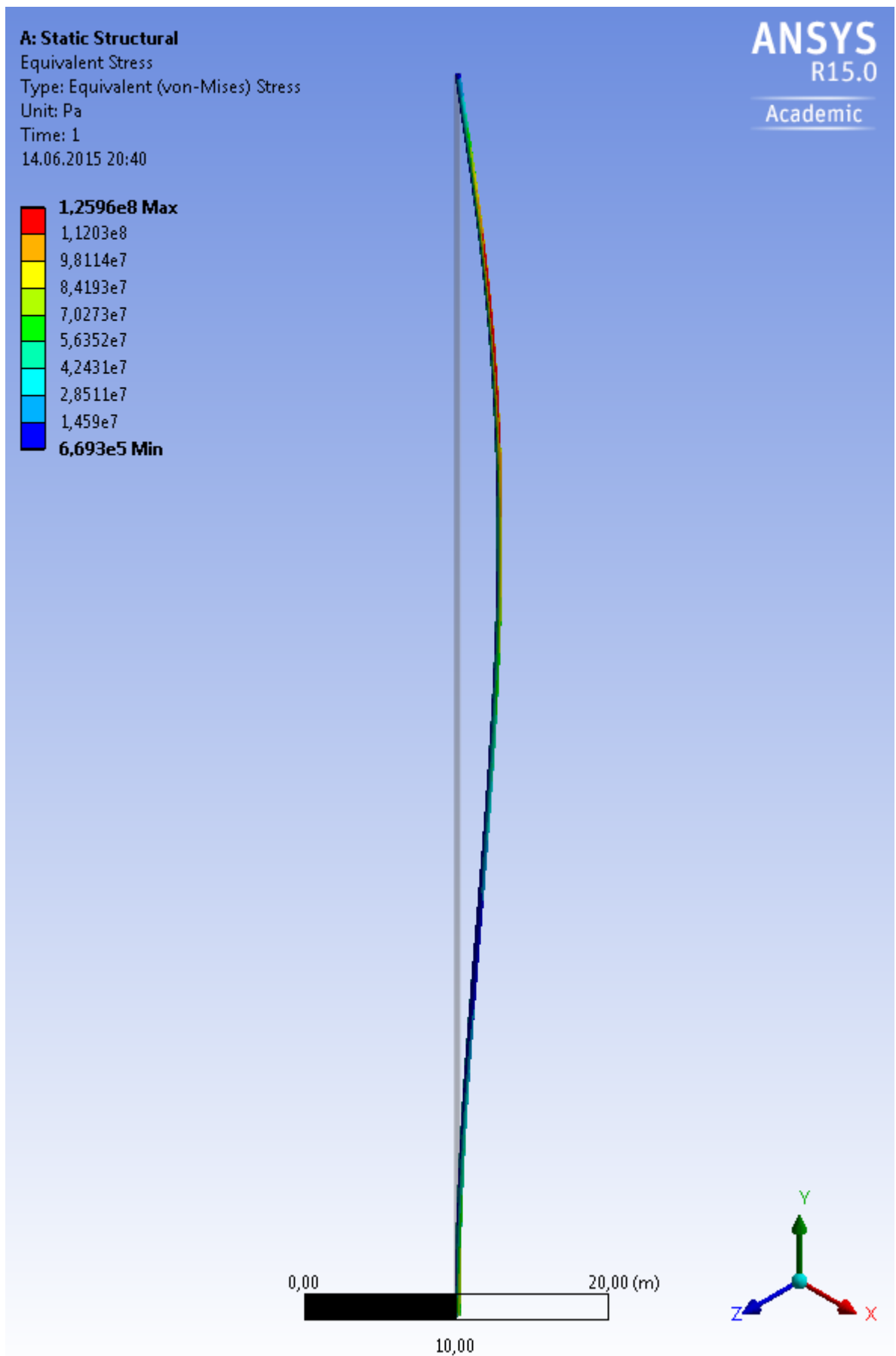


Figure 6-47. Von-Mises stress distribution in the 16 inch aluminum riser at the wave height of 8 m

7. SUMMARY AND CONCLUSIONS

The assessment and analysis of 16 inch and 21 inch risers were performed to examine their response and performance during drilling operations relevant to the arctic conditions of the Kara Sea.

The assessment of drilling risers and recommendations are based on limitation criterions from API RP 16Q, ISO 13624-1 and DNV-OS-F201 standards, which are described in Chapter 2 of the thesis.

The analysis results have shown that for all of the criteria, that need to be fulfilled, riser angles and stresses are the most critical technical requirements since they are limiting the operation of both risers, and especially the 16 inch riser. The density of the drilling fluid also becomes a limiting factor in the presence of extreme waves.

The burst check calculations were carried out for all risers according to DNV-OS-F201, by taking the drilling fluid with the heaviest density of 2037 kg/m^3 (17 ppg). As a result, it was verified that all riser configurations with different material properties are designed without any risk for the burst of the main riser pipe.

Therefore, summary of results and main conclusions of the Master thesis are the following:

- **Effect of the wave height on the effective tension**

The effective tension is dependent of the wave height, and increasing with increasing wave heights during simulation. Moreover, the effective top tension depends on the drilling fluid density. The tension is lower with light drilling fluid and gets higher when using heavy drilling fluid.

- **Effect of the wave height on the Von-Mises stress**

16 inch, 21 inch steel and 21 inch aluminum risers show satisfactory results except for the design wave height of 6 and 7 m. These wave heights led to anomalous behavior and produce unacceptable stresses in the risers due to the resonance effect. The response of steel risers also allows to conclude that careful assessment and design should be performed previous to the drilling operations, especially in challenging arctic conditions, with high safety margin requirements.

As expected, the conventional 21 inch riser has lower stresses for all types of the drilling fluid at all design wave heights.

- **Effect of the wave height on the maximum upper flex ball/joint angle**

The maximum angles for upper flex/ball joint of risers fulfilled the API and ISO requirements for allowable inclinations of the riser. However, the 16 inch aluminum riser with heavy drilling fluids (12, 14 and 17 ppg) is not capable to withstand the wave heights of 9 to 10 m, which are considered extreme conditions. Also, it is clear that maximum upper flex/ball joint angle is increasing with increasing wave height.

- **Effect of the wave height on the maximum lower flex ball/joint angle**

The maximum lower flex ball/joint angle of various risers fulfilled the requirements of API and ISO standards. Only the 16 inch aluminium riser with light drilling fluids (8.55 and 12 ppg) is not suitable for operations in extreme conditions with wave heights of 9 to 10 m. However, the 16 inch aluminium riser can be used when using the heavier drilling fluid (14 and 17 ppg) since it then becomes more stable and the maximum lower flex/ball joint angle gets within the allowable API limit.

The static analysis was performed in ANSYS Workbench 15.0. Riser configurations for modeling in ANSYS software are the same as used for the simulations in OrcaFlex. On the basis of analysis results it was concluded that the 16 inch and 21 inch steel risers have performed well in comparison with the 16 inch and 21 inch aluminum risers. However, aluminum risers can also be used for drilling operations in the Kara Sea since the disconnection mode can be activated during the worst-case scenario.

Since the dynamic analysis has shown the existence of the anomaly region for stresses in drilling risers OrcaFlex software can be highly recommended for the use during riser assessment. However, ANSYS software based on the well-known finite element method is also recommended to examine the distribution of stresses in riser walls and is considered to be a powerful tool giving precise and trustful results.

Recommendations and suggestions for the future research

The models built in ANSYS and OrcaFlex can be used as a basis for further research, preferably with real data for waves and sea current profile.

Further the soil and lower stack should be modeled in more detail since the apparent weight of LMRP and BOP stack was not specified during the modeling in OrcaFlex. In reality the variations in the bottom effective tension will be transferred to the lower flex/ball joint

initially, then to LMRP/BOP stack, and to wellhead finally. The wellhead will therefore be exposed to tension which can be very high depending on the bottom effective tension. Thus, this dynamic loading can cause the wellhead fatigue and assessment may need to be carried out prior to operations.

REFERENCES

1. API, *API RP 16Q - American Petroleum Institute - Recommended Practice for Design, Selection, Operation and Maintenance of Marine Drilling Riser Systems*. Washington, DC, USA, 1993.
2. ISO, *ISO 13624-1 Part 1: Design and operation of marine drilling riser equipment*. International Organization for Standardization, 2010.
3. DNV, *DNV-OS-F201 Dynamic Risers*. Det Norske Veritas, Hovik, Norway, 2010.
4. Bellarby, J., *Well Completion Design*. Elsevier, The Netherlands, 2009.
5. Hariharan, M. and R. Thethi. *Drilling Riser Management In Deepwater Environments*. The 7th International Oil & Gas Conference and Exhibition. New Delhi, India, 2007.
6. Bai, Y. and Q. Bai, *Subsea Engineering Handbook*. Gulf Professional Publishing, Waltham, MA, USA, 2012.
7. Sparks, C.P., *Fundamentals of marine riser mechanics: basic principles and simplified analyses*. PennWell Books, Tulsa, Oklahoma, USA, 2007.
8. Transocean, *Offshore Frontiers*. Houston, TX, USA, 2011.
9. *The Schlumberger Oilfield Glossary*.
http://www.glossary.oilfield.slb.com/en/Terms/b/bop_stack.aspx.
10. Rees, A. and D. Sharpe, *Drilling in Extreme Environments: Challenges and Implications for the Energy Insurance Industry*. Lloyds of London Report, UK, 2011.
11. Boresi, A.P., R.J. Schmidt, and O.M. Sidebottom, *Advanced Mechanics of Materials*. John Wiley & Sons, New York, USA, 1993.
12. Aadnoy, B.S., *Mechanics of Drilling*. Shaker, Germany, 2006.
13. Gudmestad, O.T., *Marine Technology and Operations: Theory and Practice* The University of Stavanger, Norway, 2014.
14. Thorogood, J.L., A.S. Train, and A.J. Adams, *Deep Water Riser System Design and Management*. IADC/SPE Drilling Conference – 39295. Dallas, TX, USA, 1998.
15. Blevins, R.D., *Applied Fluid Dynamics Handbook*. Van Nostrand Reinhold Company, New York, USA, 1984.
16. Feng., C.C., *The measurement of vortex induced effects in flow past stationary and oscillating circular and d-section cylinders*. The University of British Columbia, Canada, 1963.
17. Anagnostopoulos., P., *Flow-induced vibrations in engineering practice*. WIT Press, 1st edition, 2002.

18. Allen, D.W., *Vortex-Induced Vibration of Deepwater Risers*. Offshore Technology Conference – 8703. Houston, TX, USA, 1998.
19. Blevins, R.D., *Flow-induced vibration*. Krieger Publishing Company, New York, USA, 1994.
20. Zdravkovich, M., *Review and classification of various aerodynamic and hydrodynamic means for suppressing vortex shedding*. Journal of Wind Engineering and Industrial Aerodynamics, 1981.
21. Gudmestad, O.T., *Lecture notes on Marine Technology course at the University of Stavanger*. Stavanger, Norway, 2010.
22. Marchenko, N., *Russian Arctic Seas: The Navigation Conditions and Accidents*. Springer Science & Business Media, Berlin, Germany, 2012.
23. Oceans and Seas, *The Kara Sea*. <http://oceangid.blogspot.no/2013/04/karskoe-more.html>.
24. ISO, *ISO 19906: Petroleum and natural gas industries - Arctic offshore structures*. International Organization for Standardization, 2010.
25. Bulakh, M., O.T. Gudmestad, and A.B. Zolotukhin, *Strategy Of The Kara Sea Oil And Gas Field Development And Evaluation Of Economy Uncertainties*. ASME 2011 30th International Conference on Ocean, Offshore and Arctic Engineering. Rotterdam, The Netherlands, 2011.
26. Efimov, Y., et al., *Cluster Development of The Barents and Kara Seas HC Mega Basins From the Novaya Zemlya Archipelago*. Offshore Technology Conference – 24650. Houston, TX, USA, 2014.
27. Orcina, *OrcaFlex Manual - version 9.8a*. Cumbria, UK, 2012.
28. Aasen, J. A. and Aadnøy, B., *Three-dimensional well tubular design improves margins in critical wells*. Journal of Petroleum Science and Engineering, Elsevier B. V., The Netherlands, 2006.

APPENDIX A

BURST DNV-OS-F201 (2010) – 21 INCH STEEL RISER

Calculation Input Data

Outer Diameter, D	=	21	in	=	533,4	mm
Specific Minimum Yield Stress, $SMYS$	=	250	MPa	=	36259,4	Psi
Specific Minimum Tensile Strength, $SMTS$	=	400	MPa	=	58015,1	Psi
Yield stress temperature derating factor, $f_{y,temp}$	=	0	MPa	=	0	Psi
Tensile strength temperature derating factor, $f_{u,temp}$	=	0	MPa	=	0	Psi
Material strength factor, α_u	=	0,96				
Material resistance factor, γ_m	=	1,15				
Safety class resistance factor, γ_{SC}	=	1,26				
Water depth, d	=	100	m	=	328,1	ft
Starting elevation of internal fluid, h_0	=	27,5	m	=	90,2	ft
Internal fluid density, ρ_i	=	17	ppg	=	2036,6	kg/m ³
Seawater density, ρ_e	=	8,555	ppg	=	1025	kg/m ³
Maximum surface design pressure, p_d	=	0	MPa	=	0	Psi

Calculation Output Data

Yield stress, f_y	=	$(SMYS \cdot f_{y,temp}) \cdot \alpha_u$	=	240	MPa	=	34809,1	Psi
Tensile Strength, f_u	=	$(SMTS \cdot f_{u,temp}) \cdot \alpha_u$	=	384	MPa	=	55694,5	Psi
Height of internal fluid column, h	=	$d + h_0$	=	27,5	m	=	418,3	ft
Local internal design pressure, P_{ld}	=	$p_d + \rho_i \cdot g \cdot h$	=	2,55	MPa	=	369,5	Psi
Local incidental pressure, p_{li}	=	$p_{ld} + 0,1 \cdot p_d$	=	2,55	MPa	=	369,5	Psi
Local external pressure, p_e	=	$\rho_e \cdot g \cdot h$	=	1,28	MPa	=	185,9	Psi
Minimum required wall thickness without allowance and tolerances, t_l	=	$\frac{D}{\frac{4}{\sqrt{3}} \cdot \frac{\min\left(f_y; \frac{f_u}{1,15}\right)}{\gamma_m \gamma_{SC} (p_{li} - p_e)} + 1}$	=	1,76	mm	=	0,07	in

BURST DNV-OS-F201 (2010) – 16 INCH STEEL RISER

Calculation Input Data

Outer Diameter, D	=	16	in	=	406,4	mm
Specific Minimum Yield Stress, $SMYS$	=	250	MPa	=	36259,4	Psi
Specific Minimum Tensile Strength, $SMTS$	=	400	MPa	=	58015,1	Psi
Yield stress temperature derating factor, $f_{y, temp}$	=	0	MPa	=	0	Psi
Tensile strength temperature derating factor, $f_{u, temp}$	=	0	MPa	=	0	Psi
Material strength factor, α_u	=	0,96				
Material resistance factor, γ_m	=	1,15				
Safety class resistance factor, γ_{SC}	=	1,26				
Water depth, d	=	100	m	=	328,1	ft
Starting elevation of internal fluid, h_0	=	27,5	m	=	90,2	ft
Internal fluid density, ρ_i	=	17	ppg	=	2036,6	kg/m ³
Seawater density, ρ_e	=	8,555	ppg	=	1025	kg/m ³
Maximum surface design pressure, p_d	=	0	MPa	=	0	Psi

Calculation Output Data

Yield stress, f_y	=	$(SMYS \cdot f_{y,temp}) \cdot \alpha_u$	=	240	MPa	=	34809,1	Psi
Tensile Strength, f_u	=	$(SMTS \cdot f_{u,temp}) \cdot \alpha_u$	=	384	MPa	=	55694,5	Psi
Height of internal fluid column, h	=	$d + h_0$	=	27,5	m	=	418,3	ft
Local internal design pressure, P_{ld}	=	$p_d + \rho_i \cdot g \cdot h$	=	2,55	MPa	=	369,5	Psi
Local incidental pressure, p_{li}	=	$p_{ld} + 0.1 \cdot p_d$	=	2,55	MPa	=	369,5	Psi
Local external pressure, p_e	=	$\rho_e \cdot g \cdot h$	=	1,28	MPa	=	185,9	Psi
Minimum required wall thickness without allowance and tolerances, t_1	=	$\frac{D}{\frac{4}{\sqrt{3}} \cdot \frac{\min\left(f_y; \frac{f_u}{1.15}\right)}{\gamma_m \gamma_{SC} (p_{li} - p_e)} + 1}$	=	1,34	mm	=	0,05	in

APPENDIX B

MAIN RISER PIPE PROPERTIES CALCULATION – 21 INCH STEEL RISER

Calculation Input Data

$$\begin{aligned} \text{Pipe outer diameter, } D_o &= 0,533 \text{ m} = 21 \text{ in} \\ \text{Pipe inner diameter, } D_i &= 0,489 \text{ m} = 19,3 \text{ in} \\ \text{Modulus of elasticity, } E &= 207 \text{ GPa} \\ \text{Poisson ratio, } \nu &= 0,293 \end{aligned}$$

Calculation Output Data

$$\begin{aligned} \text{Wall thickness, } WT &= \frac{D_o - D_i}{2} = 0,02200 \text{ m} = 0,866 \text{ in} \\ \text{Cross-sectional area, } A_z &= \frac{\pi}{4} (D_o^2 - D_i^2) = 0,03530 \text{ m}^2 \\ \text{Moment of inertia, } I_x &= \frac{\pi}{64} (D_o^4 - D_i^4) = 0,00115 \text{ m}^4 \\ \text{Modulus of rigidity, } G &= \frac{E}{2(1+\nu)} = 80,05 \text{ GPa} \\ \text{Polar moment of inertia, } J_{zz} &= \frac{\pi}{32} (D_o^4 - D_i^4) = 0,00231 \text{ m}^4 \\ \text{Bending stiffness,} &= E \cdot I_x = 238,9 \cdot 10^3 \text{ kN} \cdot \text{m}^2 \\ \text{Axial stiffness,} &= E \cdot A_z = 7,307 \cdot 10^6 \text{ kN} \\ \text{Torsional stiffness,} &= G \cdot J_{zz} = 184,8 \cdot 10^3 \text{ kN} \cdot \text{m}^2 \end{aligned}$$

MAIN RISER PIPE PROPERTIES CALCULATION – 16 INCH STEEL RISER

Calculation Input Data

$$\begin{aligned} \text{Pipe outer diameter, } D_o &= 0,406 \text{ m} = 16 \text{ in} \\ \text{Pipe inner diameter, } D_i &= 0,368 \text{ m} = 14,5 \text{ in} \\ \text{Modulus of elasticity, } E &= 207 \text{ GPa} \\ \text{Poisson ratio, } \nu &= 0,293 \end{aligned}$$

Calculation Output Data

$$\begin{aligned} \text{Wall thickness, } WT &= \frac{D_o - D_i}{2} = 0,01900 \text{ m} = 0,748 \text{ in} \\ \text{Cross-sectional area, } A_z &= \frac{\pi}{4} (D_o^2 - D_i^2) = 0,02309 \text{ m}^2 \\ \text{Moment of inertia, } I_x &= \frac{\pi}{64} (D_o^4 - D_i^4) = 0,00043 \text{ m}^4 \\ \text{Modulus of rigidity, } G &= \frac{E}{2(1+\nu)} = 80,05 \text{ GPa} \\ \text{Polar moment of inertia, } J_{zz} &= \frac{\pi}{32} (D_o^4 - D_i^4) = 0,00087 \text{ m}^4 \\ \text{Bending stiffness,} &= E \cdot I_x = 89,7 \cdot 10^3 \text{ kN} \cdot \text{m}^2 \\ \text{Axial stiffness,} &= E \cdot A_z = 4,779 \cdot 10^6 \text{ kN} \\ \text{Torsional stiffness,} &= G \cdot J_{zz} = 69,4 \cdot 10^3 \text{ kN} \cdot \text{m}^2 \end{aligned}$$

MAIN RISER PIPE PROPERTIES CALCULATION – 21 INCH ALUMINIUM RISER

Calculation Input Data

$$\begin{aligned} \text{Pipe outer diameter, } D_o &= 0,533 \text{ m} = 21 \text{ in} \\ \text{Pipe inner diameter, } D_i &= 0,489 \text{ m} = 19,3 \text{ in} \\ \text{Modulus of elasticity, } E &= 70 \text{ GPa} \\ \text{Poisson ratio, } \nu &= 0,334 \end{aligned}$$

Calculation Output Data

$$\begin{aligned} \text{Wall thickness, } WT &= \frac{D_o - D_i}{2} = 0,02200 \text{ m} = 0,866 \text{ in} \\ \text{Cross-sectional area, } A_z &= \frac{\pi}{4}(D_o^2 - D_i^2) = 0,03530 \text{ m}^2 \\ \text{Moment of inertia, } I_x &= \frac{\pi}{64}(D_o^4 - D_i^4) = 0,00115 \text{ m}^4 \\ \text{Modulus of rigidity, } G &= \frac{E}{2(1+\nu)} = 26,24 \text{ GPa} \\ \text{Polar moment of inertia, } J_{zz} &= \frac{\pi}{32}(D_o^4 - D_i^4) = 0,00231 \text{ m}^4 \\ \text{Bending stiffness,} &= E \cdot I_x = 80,8 \cdot 10^3 \text{ kN} \cdot \text{m}^2 \\ \text{Axial stiffness,} &= E \cdot A_z = 2,471 \cdot 10^6 \text{ kN} \\ \text{Torsional stiffness,} &= G \cdot J_{zz} = 60,6 \cdot 10^3 \text{ kN} \cdot \text{m}^2 \end{aligned}$$

MAIN RISER PIPE PROPERTIES CALCULATION – 16 INCH ALUMINIUM RISER

Calculation Input Data

$$\begin{aligned} \text{Pipe outer diameter, } D_o &= 0,406 \text{ m} = 16 \text{ in} \\ \text{Pipe inner diameter, } D_i &= 0,368 \text{ m} = 14,5 \text{ in} \\ \text{Modulus of elasticity, } E &= 70 \text{ GPa} \\ \text{Poisson ratio, } \nu &= 0,334 \end{aligned}$$

Calculation Output Data

$$\begin{aligned} \text{Wall thickness, } WT &= \frac{D_o - D_i}{2} = 0,01900 \text{ m} = 0,748 \text{ in} \\ \text{Cross-sectional area, } A_z &= \frac{\pi}{4} (D_o^2 - D_i^2) = 0,02309 \text{ m}^2 \\ \text{Moment of inertia, } I_x &= \frac{\pi}{64} (D_o^4 - D_i^4) = 0,00043 \text{ m}^4 \\ \text{Modulus of rigidity, } G &= \frac{E}{2(1+\nu)} = 26,24 \text{ GPa} \\ \text{Polar moment of inertia, } J_{zz} &= \frac{\pi}{32} (D_o^4 - D_i^4) = 0,00087 \text{ m}^4 \\ \text{Bending stiffness,} &= E \cdot I_x = 89,7 \cdot 10^3 \text{ kN} \cdot \text{m}^2 \\ \text{Axial stiffness,} &= E \cdot A_z = 1,616 \cdot 10^6 \text{ kN} \\ \text{Torsional stiffness,} &= G \cdot J_{zz} = 22,7 \cdot 10^3 \text{ kN} \cdot \text{m}^2 \end{aligned}$$

APPENDIX C

21 INCH STEEL RISER and AUXILIARY LINES PROPERTIES

Length/joint =	22,86		m										
Riser material density =	7,85		ton/m ³										
Content density =	1,025		ton/m ³										
Seawater density =	1,025		ton/m ³										
Line Type	Outer Diameter		Wall Thickness		No. of Lines	Inner Diameter		Dry Weight	Content Weight	Submerged & Flooded Weight	Displacement (closed)		
	m	in	m	in		m	in					ton/m	ton/m
Main Pipe	0,533	21,0	0,022	0,875	1	0,4890	19,25	0,2771	0,1924	0,2409	0,2286		
Choke/Kill Line	0,165	6,50	0,02535	1,000	2	0,1143	4,500	0,0873	0,0105	0,0759	0,0219		
Booster Line	0,127	5,00	0,0127	0,500	1	0,1016	4,000	0,0358	0,0083	0,0311	0,0130		
Hydraulic Line	0,073	2,88	0,0071	0,280	2	0,0590	2,320	0,0116	0,0028	0,0101	0,0043		

16 INCH STEEL RISER and AUXILIARY LINES PROPERTIES

Length/joint =	22,86		m										
Riser material density =	7,85		ton/m ³										
Content density =	1,025		ton/m ³										
Seawater density =	1,025		ton/m ³										
Line Type	Outer Diameter		Wall Thickness		No. of Lines	Inner Diameter		Dry Weight	Content Weight	Submerged & Flooded Weight	Displacement (closed)		
	m	in	m	in		m	in					ton/m	ton/m
Main Pipe	0,406	16,0	0,019	0,75	1	0,3680	14,50	0,1812	0,1090	0,1576	0,1326		
Choke/Kill Line	0,127	5,00	0,016	0,625	2	0,0950	3,750	0,0438	0,0073	0,0381	0,0130		
Booster Line	0,102	4,00	0,0095	0,375	1	0,0830	3,250	0,0217	0,0055	0,0188	0,0084		
Hydraulic Line	0,089	3,50	0,0065	0,25	2	0,0760	3,000	0,0132	0,0046	0,0115	0,0064		

21 INCH ALUMINIUM RISER and AUXILIARY LINES PROPERTIES

Length/joint = 22,86 m
 Riser material density = 2,77 ton/m³
 Content density = 1,025 ton/m³
 Seawater density = 1,025 ton/m³

Line Type	Outer Diameter		Wall Thickness		No. of Lines	Inner Diameter		Dry Weight	Content Weight	Submerged & Flooded Weight	Displacement (closed)
	m	in	m	in		m	in				
Main Pipe	0,533	21,0	0,022	0,875	1	0,4890	19,25	0,0978	0,1924	0,0616	0,2286
Choke/Kill Line	0,165	6,50	0,02535	1,000	2	0,1143	4,500	0,0308	0,0105	0,0194	0,0219
Booster Line	0,127	5,00	0,0127	0,500	1	0,1016	4,000	0,0126	0,0083	0,0080	0,0130
Hydraulic Line	0,073	2,88	0,0071	0,280	2	0,0590	2,320	0,0041	0,0028	0,0026	0,0043

16 INCH ALUMINIUM RISER and AUXILIARY LINES PROPERTIES

Length/joint = 22,86 m
 Riser material density = 2,77 ton/m³
 Content density = 1,025 ton/m³
 Seawater density = 1,025 ton/m³

Line Type	Outer Diameter		Wall Thickness		No. of Lines	Inner Diameter		Dry Weight	Content Weight	Submerged & Flooded Weight	Displacement (closed)
	m	in	m	in		m	in				
Main Pipe	0,406	16,0	0,019	0,75	1	0,3680	14,50	0,0640	0,1090	0,0403	0,1326
Choke/Kill Line	0,127	5,00	0,016	0,625	2	0,0950	3,750	0,0154	0,0073	0,0097	0,0130
Booster Line	0,102	4,00	0,0095	0,375	1	0,0830	3,250	0,0076	0,0055	0,0048	0,0084
Hydraulic Line	0,089	3,50	0,0065	0,25	2	0,0760	3,000	0,0047	0,0046	0,0029	0,0064

APPENDIX D

MINIMUM TOP TENSION CALCULATION by API RP 16Q – 21 INCH STEEL RISER

Parameter	Description	Value			
$\rho_m, \text{kg/m}^3$	Drilling Fluid Weight Density	1025	1438	1678	2037
$\rho_w, \text{kg/m}^3$	Sea Water Weight Density	1025	1025	1025	1025
H_m, m	Drilling Fluid Column to point of consideration	119,3	119,3	119,3	119,3
H_w, m	Sea Water Column to point of consideration including storm surge and tide	93,8	93,8	93,8	93,8
H_{sw}, m	Sea Water Depth	100	100	100	100
$H_{LMRP+BOP}, \text{m}$	Height of LMRP + BOP Stack	8,5	8,5	8,5	8,5
H_{wh}, m	Height of the Wellhead	1,5	1,5	1,5	1,5
h_{TR-MSL}, m	Distance from Tensioner Ring to Mean Sea Level	10	10	10	10
H_{S+T}, m	Height of Storm Surge +Tide	3,8	3,8	3,8	3,8
$h_{RKB-MSL}, \text{m}$	Distance from RKB to Mean Sea Level	27,5	27,5	27,5	27,5
h_{RKB-ML}, m	Distance from RKB to Mud Line	2	2	2	2
L_r, m	Length of the Riser	100	100	100	100
$L_{r,sub}, \text{m}$	Submerged Riser Length	90	90	90	90
$\rho_{steel}, \text{kg/m}^3$	Riser material density	7850	7850	7850	7850
D_{ir}, m	Internal Diameter of the Riser	0,489	0,489	0,489	0,489
D_{or}, m	External Diameter of the Riser	0,533	0,533	0,533	0,533
$D_{i k/c}, \text{m}$	Internal Diameter of the Kill/Choke Line	0,1143	0,1143	0,1143	0,1143
$D_{i mb}, \text{m}$	Internal Diameter of the Mud Booster Line	0	0	0	0
A_r, m^2	Cross Sectional Area of Riser	0,035	0,035	0,035	0,035
A_i, m^2	Internal Cross Sectional Area of the Riser including auxiliary lines	0,208	0,208	0,208	0,208
f_{wt}	Submerged Weight Tolerance Factor (minimum value = 1.05 unless accurately weighed)	1,05	1,05	1,05	1,05
B_n	Net Lift of Buoyancy Material above the point of consideration	0	0	0	0
f_{bt}	Buoyancy Loss and Tolerance Factor resulting in elastic compression, long term water absorption, and manufacturing tolerance. (Maximum value = 0.96 unless accurately known by submerged weighing under compression at rated depth)	0,96	0,96	0,96	0,96
R_f	Reduction Factor Relating Vertical Tension at the Slip Ring to Tensioner Setting to account for fleet angle and mechanical efficiency (usually 0,9-0,95; 0,9 - non-drilling; 0,95 - drilling)	0,95	0,95	0,95	0,95
N	Number of Tensioners Supporting the Riser	12	12	12	12
n	Number of Tensioners Subject to Sudden Failure	1	1	1	1
W_s	Submerged Riser Weight with auxiliary lines above the point of consideration	39891,1	39891,1	39891,1	39891,1
T_{SRmin}, N	Minimum Slip Ring Tension	464288,2	564931,4	623416,6	710900,6
T_{min}, N	Minimum Required Top Tension	533153,9	648725,0	715885,0	816345,2

MINIMUM TOP TENSION CALCULATION by API RP 16Q – 16 INCH STEEL RISER

Parameter	Description	Value			
$\rho_m, \text{ kg/m}^3$	Drilling Fluid Weight Density	1025	1438	1678	2037
$\rho_w, \text{ kg/m}^3$	Sea Water Weight Density	1025	1025	1025	1025
$H_m, \text{ m}$	Drilling Fluid Column to point of consideration	119,3	119,3	119,3	119,3
$H_w, \text{ m}$	Sea Water Column to point of consideration including storm surge and tide	93,8	93,8	93,8	93,8
$H_{SW}, \text{ m}$	Sea Water Depth	100	100	100	100
$H_{LMRP+BOP}, \text{ m}$	Height of LMRP + BOP Stack	8,5	8,5	8,5	8,5
$H_{wh}, \text{ m}$	Height of the Wellhead	1,5	1,5	1,5	1,5
$h_{TR-MSL}, \text{ m}$	Distance from Tensioner Ring to Mean Sea Level	10	10	10	10
$H_{S+T}, \text{ m}$	Height of Storm Surge + Tide	3,8	3,8	3,8	3,8
$h_{RKB-MSL}, \text{ m}$	Distance from RKB to Mean Sea Level	27,5	27,5	27,5	27,5
$h_{RKB-ML}, \text{ m}$	Distance from RKB to Mud Line	2	2	2	2
$L_r, \text{ m}$	Length of the Riser	100	100	100	100
$L_{r,sub}, \text{ m}$	Submerged Riser Length	90	90	90	90
$\rho_{steel}, \text{ kg/m}^3$	Riser material density	7850	7850	7850	7850
$D_{ir}, \text{ m}$	Internal Diameter of the Riser	0,368	0,368	0,368	0,368
$D_{or}, \text{ m}$	External Diameter of the Riser	0,406	0,406	0,406	0,406
$D_{i \text{ k/c}}, \text{ m}$	Internal Diameter of the Kill/Choke Line	0,095	0,095	0,095	0,095
$D_{i \text{ mb}}, \text{ m}$	Internal Diameter of the Mud Booster Line	0	0	0	0
$A_r, \text{ m}^2$	Cross Sectional Area of Riser	0,023	0,046	0,046	0,046
$A_i, \text{ m}^2$	Internal Cross Sectional Area of the Riser including auxiliary lines	0,120	0,120	0,120	0,120
f_{wt}	Submerged Weight Tolerance Factor (minimum value = 1.05 unless accurately weighed)	1,05	1,05	1,05	1,05
B_n	Net Lift of Buoyancy Material above the point of consideration	0	0	0	0
f_{bt}	Buoyancy Loss and Tolerance Factor resulting in elastic compression, long term water absorption, and manufacturing tolerance. (Maximum value = 0.96 unless accurately known by submerged weighing under compression at rated depth)	0,96	0,96	0,96	0,96
R_f	Reduction Factor Relating Vertical Tension at the Slip Ring to Tensioner Setting to account for fleet angle and mechanical efficiency (usually 0,9-0,95; 0,9 - non-drilling; 0,95 - drilling)	0,95	0,95	0,95	0,95
N	Number of Tensioners Supporting the Riser	12	12	12	12
n	Number of Tensioners Subject to Sudden Failure	1	1	1	1
W_s	Submerged Riser Weight with auxiliary lines above the point of consideration	23658,8	23658,8	23658,8	23658,8
$T_{SRmin}, \text{ N}$	Minimum Slip Ring Tension	274589,3	332821,6	366661,2	417279,6
$T_{min}, \text{ N}$	Minimum Required Top Tension	315317,9	382187,5	421046,4	479172,8

**MINIMUM TOP TENSION CALCULATION by API RP 16Q – 21 INCH ALUMINIUM
RISER**

Parameter	Description	Value			
$\rho_m, \text{ kg/m}^3$	Drilling Fluid Weight Density	1025	1438	1678	2037
$\rho_w, \text{ kg/m}^3$	Sea Water Weight Density	1025	1025	1025	1025
$H_m, \text{ m}$	Drilling Fluid Column to point of consideration	119,3	119,3	119,3	119,3
$H_w, \text{ m}$	Sea Water Column to point of consideration including storm surge and tide	93,8	93,8	93,8	93,8
$H_{sw}, \text{ m}$	Sea Water Depth	100	100	100	100
$H_{LMRP+BOP}, \text{ m}$	Height of LMRP + BOP Stack	8,5	8,5	8,5	8,5
$H_{wh}, \text{ m}$	Height of the Wellhead	1,5	1,5	1,5	1,5
$h_{TR-MSL}, \text{ m}$	Distance from Tensioner Ring to Mean Sea Level	10	10	10	10
$H_{S+T}, \text{ m}$	Height of Storm Surge +Tide	3,8	3,8	3,8	3,8
$h_{RKB-MSL}, \text{ m}$	Distance from RKB to Mean Sea Level	27,5	27,5	27,5	27,5
$h_{RKB-ML}, \text{ m}$	Distance from RKB to Mud Line	2	2	2	2
$L_r, \text{ m}$	Length of the Riser	100	100	100	100
$L_{r,sub}, \text{ m}$	Submerged Riser Length	90	90	90	90
$\rho_{alumin}, \text{ kg/m}^3$	Riser material density	2700	2700	2700	2700
$D_{ir}, \text{ m}$	Internal Diameter of the Riser	0,489	0,489	0,489	0,489
$D_{or}, \text{ m}$	External Diameter of the Riser	0,533	0,533	0,533	0,533
$D_{i k/c}, \text{ m}$	Internal Diameter of the Kill/Choke Line	0,114	0,114	0,114	0,114
$D_{imb}, \text{ m}$	Internal Diameter of the Mud Booster Line	0	0	0	0
$A_r, \text{ m}^2$	Cross Sectional Area of Riser	0,035	0,035	0,035	0,035
$A_i, \text{ m}^2$	Internal Cross Sectional Area of the Riser including auxiliary lines	0,208	0,208	0,208	0,208
f_{wt}	Submerged Weight Tolerance Factor (minimum value = 1.05 unless accurately weighed)	1,05	1,05	1,05	1,05
B_n	Net Lift of Buoyancy Material above the point of consideration	0	0	0	0
f_{bt}	Buoyancy Loss and Tolerance Factor resulting in elastic compression, long term water absorption, and manufacturing tolerance. (Maximum value = 0.96 unless accurately known by submerged weighing under compression at rated depth)	0,96	0,96	0,96	0,96
R_f	Reduction Factor Relating Vertical Tension at the Slip Ring to Tensioner Setting to account for fleet angle and mechanical efficiency (usually 0,9-0,95; 0,9 - non-drilling; 0,95 - drilling)	0,95	0,95	0,95	0,95
N	Number of Tensioners Supporting the Riser	12	12	12	12
n	Number of Tensioners Subject to Sudden Failure	1	1	1	1
W_s	Submerged Riser Weight with auxiliary lines above the point of consideration	10235,5	10235,5	10235,5	10235,5
$T_{SRmin}, \text{ N}$	Minimum Slip Ring Tension	158820,6	259463,8	317949,0	405433,0
$T_{min}, \text{ N}$	Minimum Required Top Tension	182377,7	297948,9	365108,9	465569,0

**MINIMUM TOP TENSION CALCULATION by API RP 16Q – 16 INCH ALUMINIUM
RISER**

Parameter	Description	Value			
$\rho_m, \text{ kg/m}^3$	Drilling Fluid Weight Density	1025	1438	1678	2037
$\rho_w, \text{ kg/m}^3$	Sea Water Weight Density	1025	1025	1025	1025
$H_m, \text{ m}$	Drilling Fluid Column to point of consideration	119,3	119,3	119,3	119,3
$H_w, \text{ m}$	Sea Water Column to point of consideration including storm surge and tide	93,8	93,8	93,8	93,8
$H_{SW}, \text{ m}$	Sea Water Depth	100	100	100	100
$H_{LMRP+BOP}, \text{ m}$	Height of LMRP + BOP Stack	8,5	8,5	8,5	8,5
$H_{wh}, \text{ m}$	Height of the Wellhead	1,5	1,5	1,5	1,5
$h_{TR-MSL}, \text{ m}$	Distance from Tensioner Ring to Mean Sea Level	10	10	10	10
$H_{S+T}, \text{ m}$	Height of Storm Surge +Tide	3,8	3,8	3,8	3,8
$h_{RKB-MSL}, \text{ m}$	Distance from RKB to Mean Sea Level	27,5	27,5	27,5	27,5
$h_{RKB-ML}, \text{ m}$	Distance from RKB to Mud Line	2	2	2	2
$L_r, \text{ m}$	Length of the Riser	100	100	100	100
$L_{r.sub}, \text{ m}$	Submerged Riser Length	90	90	90	90
$\rho_{alumin}, \text{ kg/m}^3$	Riser material density	2700	2700	2700	2700
$D_{is}, \text{ m}$	Internal Diameter of the Riser	0,368	0,368	0,368	0,368
$D_{or}, \text{ m}$	External Diameter of the Riser	0,406	0,406	0,406	0,406
$D_{i.k/c}, \text{ m}$	Internal Diameter of the Kill/Choke Line	0,095	0,095	0,095	0,095
$D_{i.mb}, \text{ m}$	Internal Diameter of the Mud Booster Line	0	0	0	0
$A_r, \text{ m}^2$	Cross Sectional Area of Riser	0,023	0,046	0,046	0,046
$A_i, \text{ m}^2$	Internal Cross Sectional Area of the Riser including auxiliary lines	0,120	0,120	0,120	0,120
f_{wt}	Submerged Weight Tolerance Factor (minimum value = 1.05 unless accurately weighed)	1,05	1,05	1,05	1,05
B_n	Net Lift of Buoyancy Material above the point of consideration	0	0	0	0
f_{bt}	Buoyancy Loss and Tolerance Factor resulting in elastic compression, long term water absorption, and manufacturing tolerance. (Maximum value = 0.96 unless accurately known by submerged weighing under compression at rated depth)	0,96	0,96	0,96	0,96
R_f	Reduction Factor Relating Vertical Tension at the Slip Ring to Tensioner Setting to account for fleet angle and mechanical efficiency (usually 0,9-0,95; 0,9 - non-drilling; 0,95 - drilling)	0,95	0,95	0,95	0,95
N	Number of Tensioners Supporting the Riser	12	12	12	12
n	Number of Tensioners Subject to Sudden Failure	1	1	1	1
W_s	Submerged Riser Weight with auxiliary lines above the point of consideration	6070,5	6070,5	6070,5	6070,5
$T_{SRmin}, \text{ N}$	Minimum Slip Ring Tension	93420,9	151653,2	185492,8	236111,2
$T_{min}, \text{ N}$	Minimum Required Top Tension	107277,6	174147,2	213006,1	271132,5

APPENDIX E

E1. Current Profile

Since there is no any real data available on the current velocity in the Kara Sea therefore the current profile is chosen. The calculation of current velocities in OrcaFlex is carried out by employing the Power Law method that can be written as the following equation:

$$S = S_b + (S_f - S_b) \times ((Z - Z_b) / (Z_f - Z_b))^{1/Exponent} \quad (E1.1)$$

where

S_f current velocity at the sea surface;

S_b current velocity at the sea bottom;

Z_f water surface Z level;

Z_b Z level of the sea bottom directly below (X, Y);

Exponent is the power law exponent.

The current velocity varying over the sea water depth is shown in Table E-1. The maximum values of current velocity at the surface and sea bottom are taken from ISO 19906 standard. [24]

Depth (m)	Velocity (m/s)
0	1.0
20	0.58
40	0.346
60	0.238
80	0.204
100	0.2

Table E-1. Distribution of current velocity over the sea water depth

E2. Design of Waves

According to the method described in the NORSOK-003 standard the wave period is varied within the range:

$$\sqrt{6.5H_{100}} \leq T \leq \sqrt{11H_{100}} \quad (E2.2)$$

The wave heights were proposed due to an insufficient data on significant wave height and values are shown in Table E-2.

Wave Height, H_{100} (m)
1
2
3
4
5
6
7
8
9
10

Table E-2. Proposed wave heights

Thus,

1. $\sqrt{6.5 \cdot H_{1,100}} \leq T_1 \leq \sqrt{11 \cdot H_{1,100}} \rightarrow \sqrt{6.5 \cdot 1} \leq T_1 \leq \sqrt{11 \cdot 1} \rightarrow 2.5 \leq T_1 \leq 3.2 \rightarrow T_1 = 3$
2. $\sqrt{6.5 \cdot H_{2,100}} \leq T_2 \leq \sqrt{11 \cdot H_{2,100}} \rightarrow \sqrt{6.5 \cdot 2} \leq T_2 \leq \sqrt{11 \cdot 2} \rightarrow 3.6 \leq T_2 \leq 5 \rightarrow T_2 = 5$
3. $\sqrt{6.5 \cdot H_{3,100}} \leq T_3 \leq \sqrt{11 \cdot H_{3,100}} \rightarrow \sqrt{6.5 \cdot 3} \leq T_3 \leq \sqrt{11 \cdot 3} \rightarrow 4.4 \leq T_3 \leq 5.7 \rightarrow T_3 = 5$
4. $\sqrt{6.5 \cdot H_{4,100}} \leq T_4 \leq \sqrt{11 \cdot H_{4,100}} \rightarrow \sqrt{6.5 \cdot 4} \leq T_4 \leq \sqrt{11 \cdot 4} \rightarrow 5.1 \leq T_4 \leq 6.6 \rightarrow T_4 = 6$
5. $\sqrt{6.5 \cdot H_{5,100}} \leq T_5 \leq \sqrt{11 \cdot H_{5,100}} \rightarrow \sqrt{6.5 \cdot 5} \leq T_5 \leq \sqrt{11 \cdot 5} \rightarrow 5.7 \leq T_5 \leq 7.4 \rightarrow T_5 = 6$
6. $\sqrt{6.5 \cdot H_{6,100}} \leq T_6 \leq \sqrt{11 \cdot H_{6,100}} \rightarrow \sqrt{6.5 \cdot 6} \leq T_6 \leq \sqrt{11 \cdot 6} \rightarrow 6.2 \leq T_6 \leq 8.1 \rightarrow T_6 = 7$
7. $\sqrt{6.5 \cdot H_{7,100}} \leq T_7 \leq \sqrt{11 \cdot H_{7,100}} \rightarrow \sqrt{6.5 \cdot 7} \leq T_7 \leq \sqrt{11 \cdot 7} \rightarrow 6.7 \leq T_7 \leq 8.8 \rightarrow T_7 = 7$
8. $\sqrt{6.5 \cdot H_{8,100}} \leq T_8 \leq \sqrt{11 \cdot H_{8,100}} \rightarrow \sqrt{6.5 \cdot 8} \leq T_8 \leq \sqrt{11 \cdot 8} \rightarrow 7.2 \leq T_8 \leq 9.4 \rightarrow T_8 = 8$
9. $\sqrt{6.5 \cdot H_{9,100}} \leq T_9 \leq \sqrt{11 \cdot H_{9,100}} \rightarrow \sqrt{6.5 \cdot 9} \leq T_9 \leq \sqrt{11 \cdot 9} \rightarrow 7.6 \leq T_9 \leq 10 \rightarrow T_9 = 8$
10. $\sqrt{6.5 \cdot H_{10,100}} \leq T_{10} \leq \sqrt{11 \cdot H_{10,100}} \rightarrow \sqrt{6.5 \cdot 10} \leq T_{10} \leq \sqrt{11 \cdot 10} \rightarrow 8 \leq T_{10} \leq 10.5 \rightarrow T_{10} = 10$

Hence, the input data for waves is established to simulate a satisfactory representation of sea conditions for the riser analysis and results are presented in Table E-3.

Wave Height, H_s (m)	T₁ (s)	T₂ (s)
1	3	-
2	5	-
3	5	-
4	6	-
5	6	7
6	7	-
7	7	-
8	8	9
9	8	-
10	9	10

Table E-3. Design wave heights with associated periods

APPENDIX F

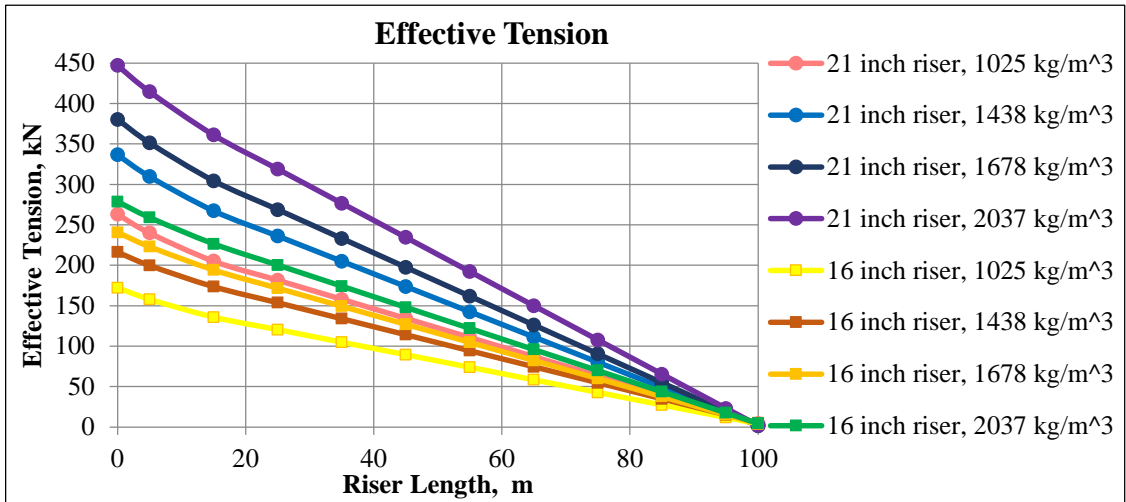


Figure F-1. Effective tension of steel risers at the wave height of 1 m and period of 3 s

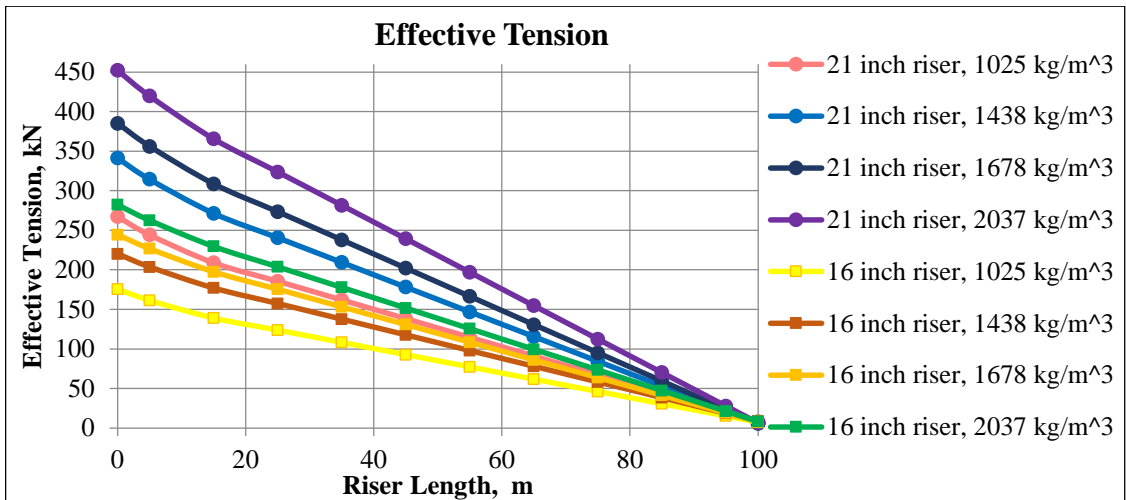


Figure F-2. Effective tension of steel risers at the wave height of 2 m and period of 5 s

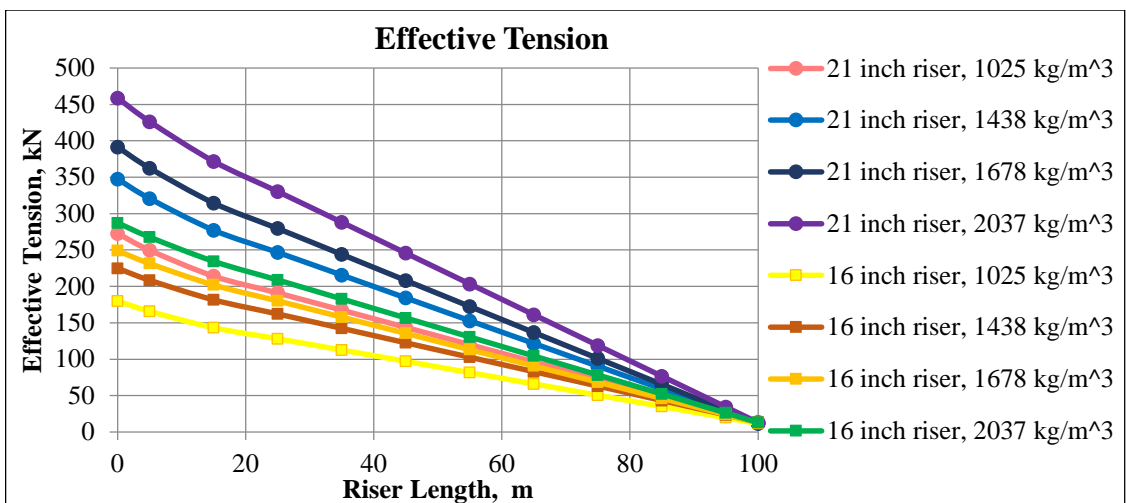


Figure F-3. Effective tension of steel risers at the wave height of 3 m and period of 5 s

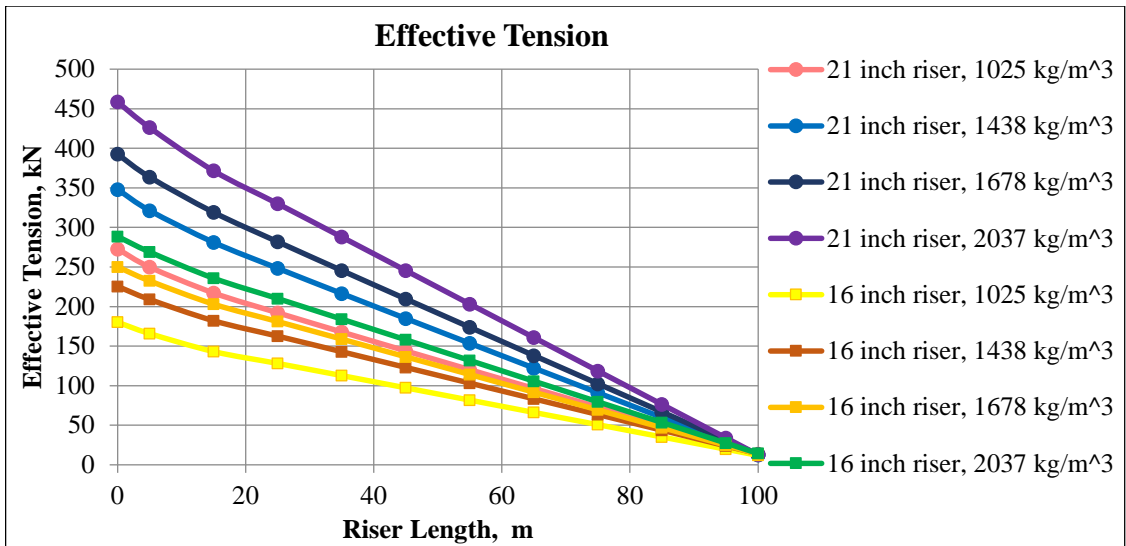


Figure F-4. Effective tension of steel risers at the wave height of 4 m and period of 6 s

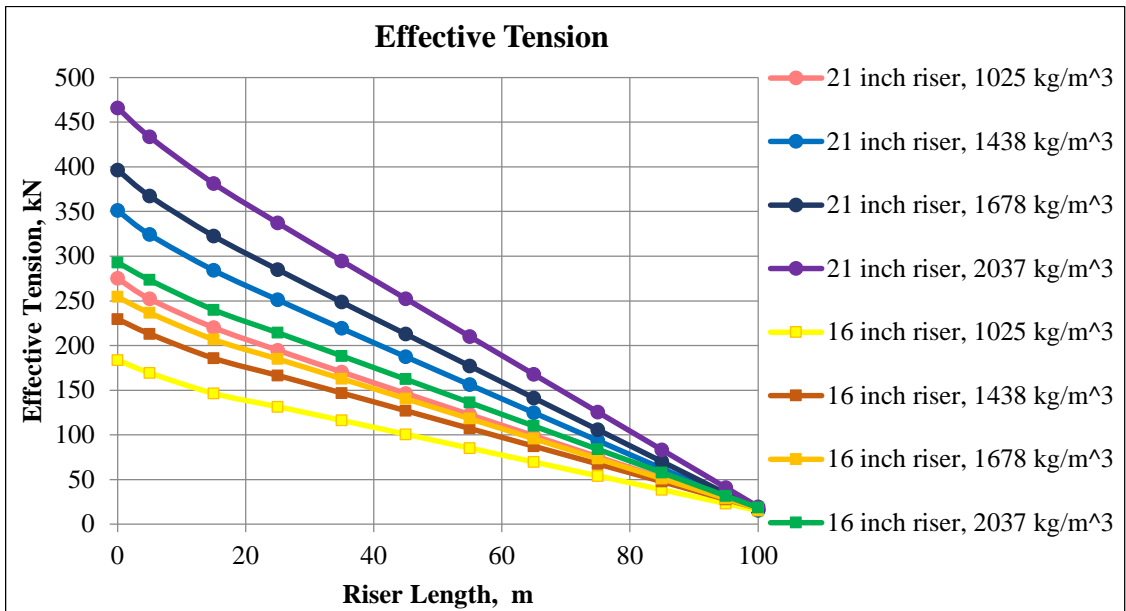


Figure F-5. Effective tension of steel risers at the wave height of 5 m and period of 6 s

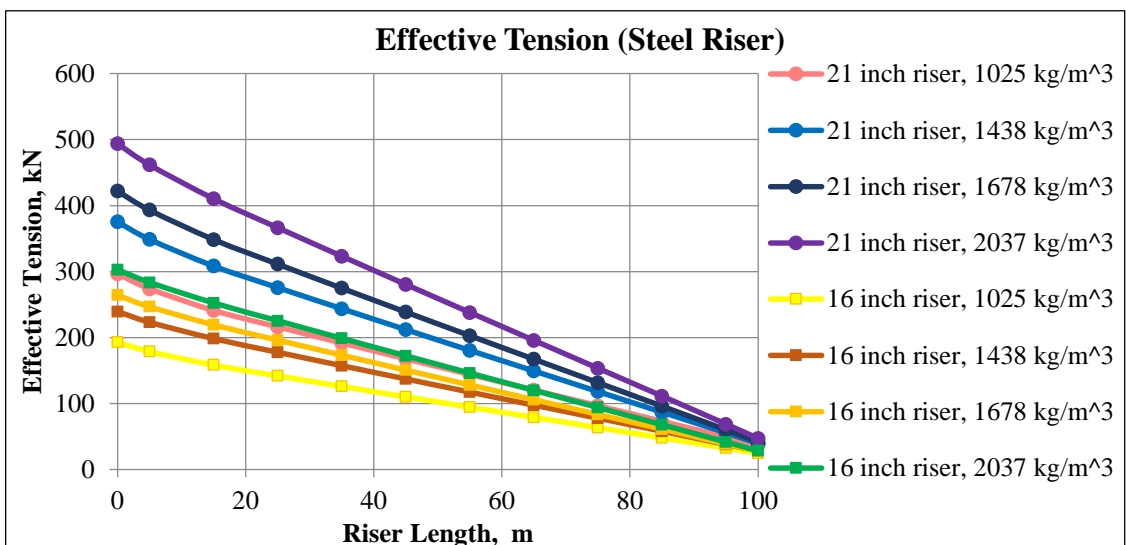


Figure F-6. Effective tension of steel risers at the wave height of 5 m and period of 7 s

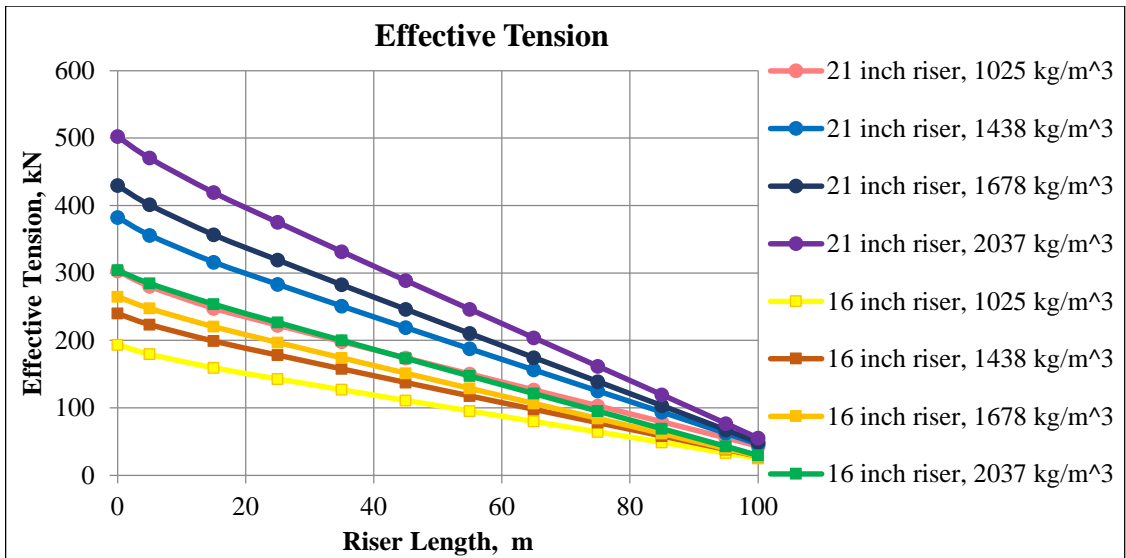


Figure F-7. Effective tension of steel risers at the wave height of 6 m and period of 7 s

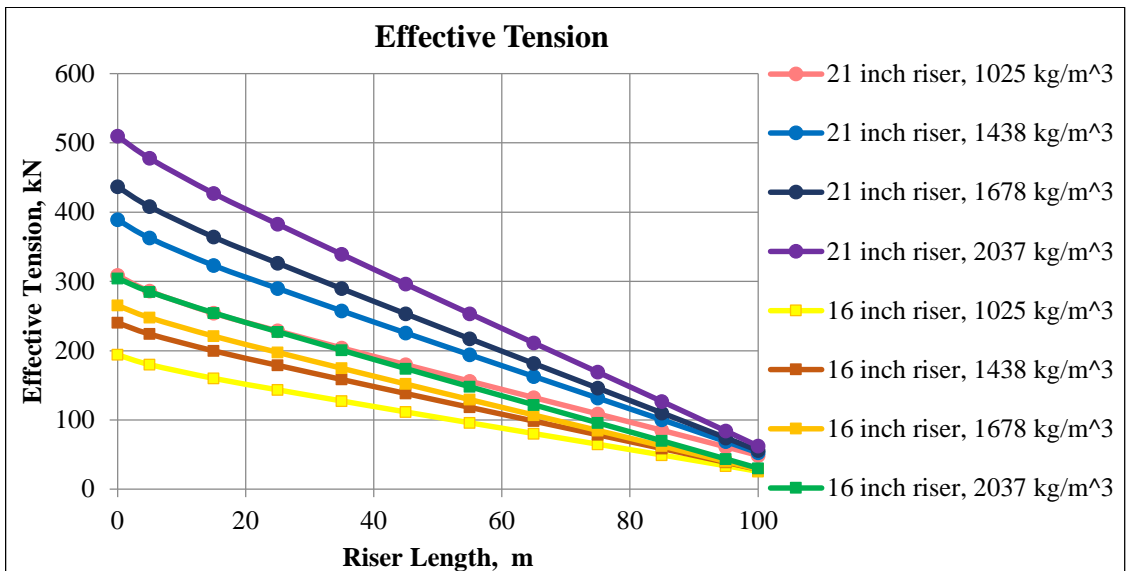


Figure F-8. Effective tension of steel risers at the wave height of 7 m and period of 7 s

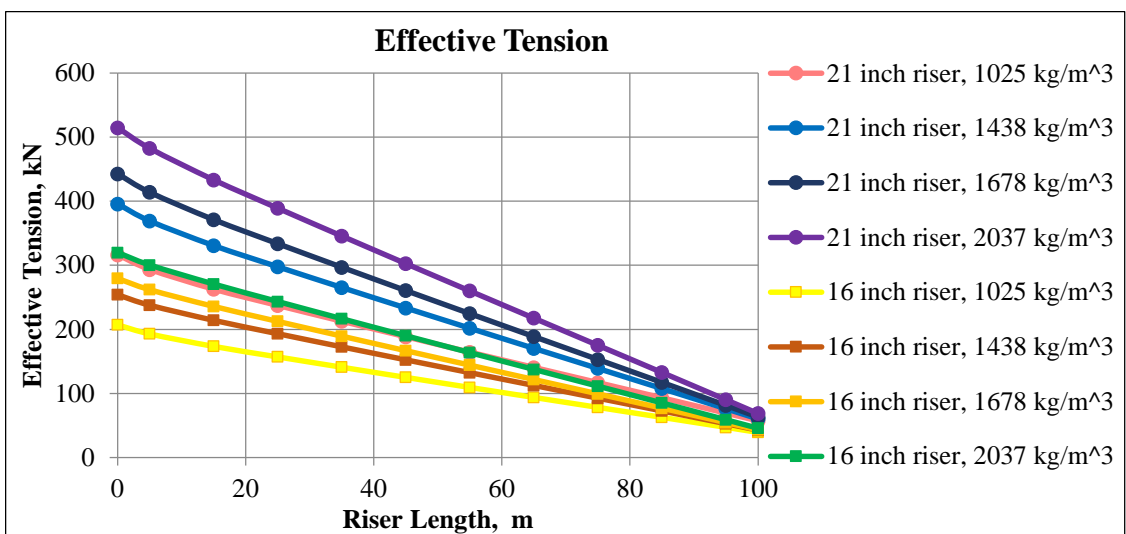


Figure F-9. Effective tension of steel risers at the wave height of 8 m and period of 8 s

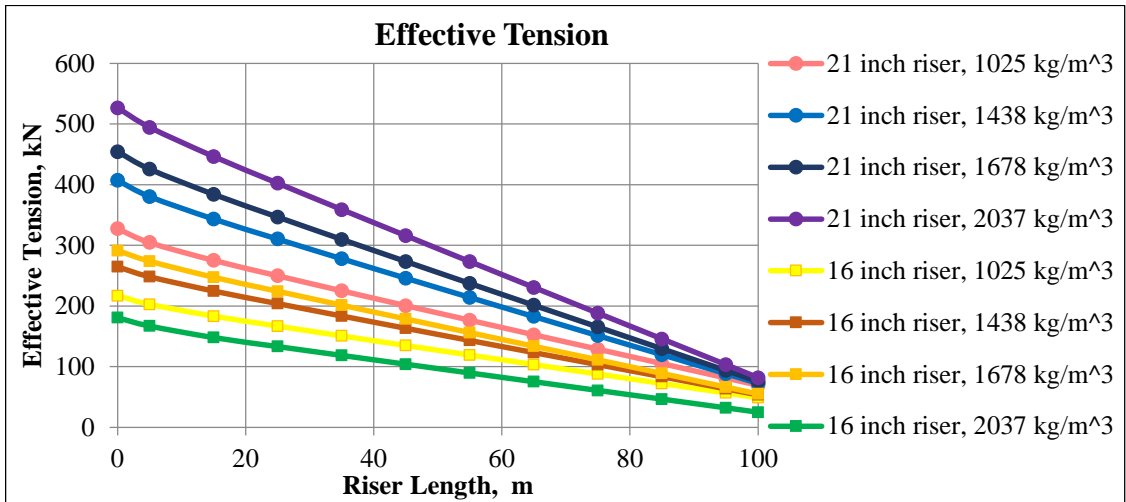


Figure F-10. Effective tension of steel risers at the wave height of 8 m and period of 9 s

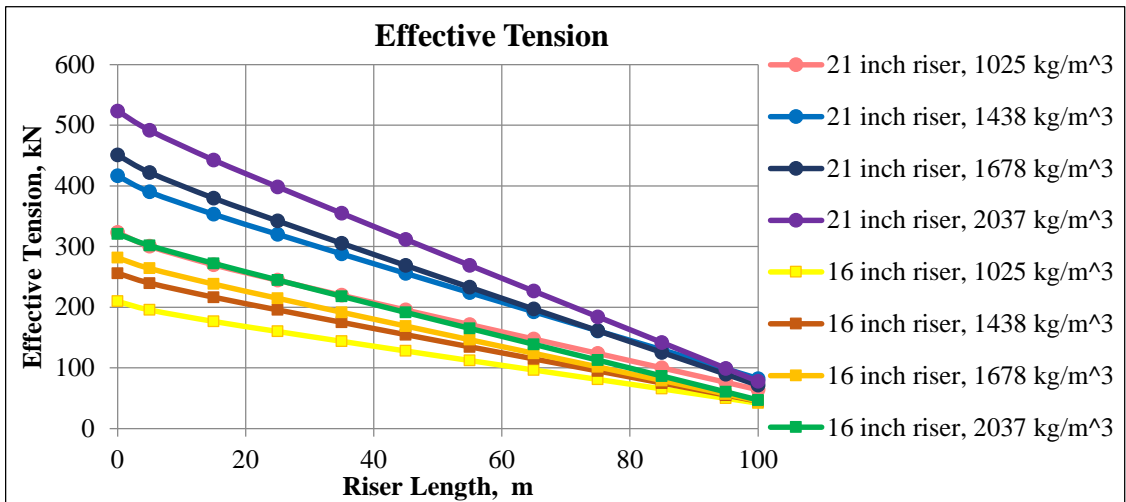


Figure F-11. Effective tension of steel risers at the wave height of 9 m and period of 8 s

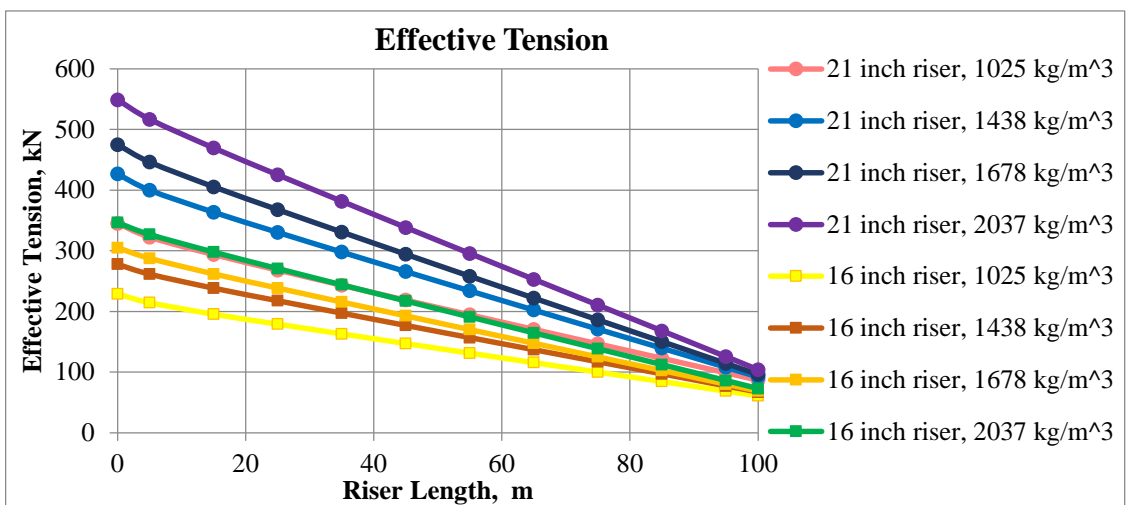


Figure F-12. Effective tension of steel risers at the wave height of 10 m and period of 9 s

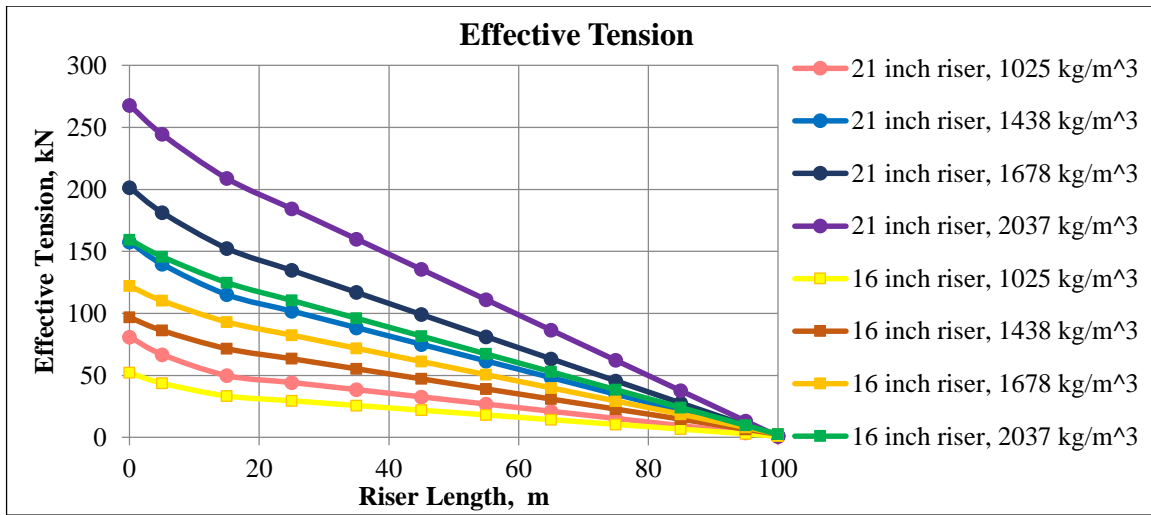


Figure F-13. Effective tension of aluminum risers at the wave height of 1 m and period of 3 s

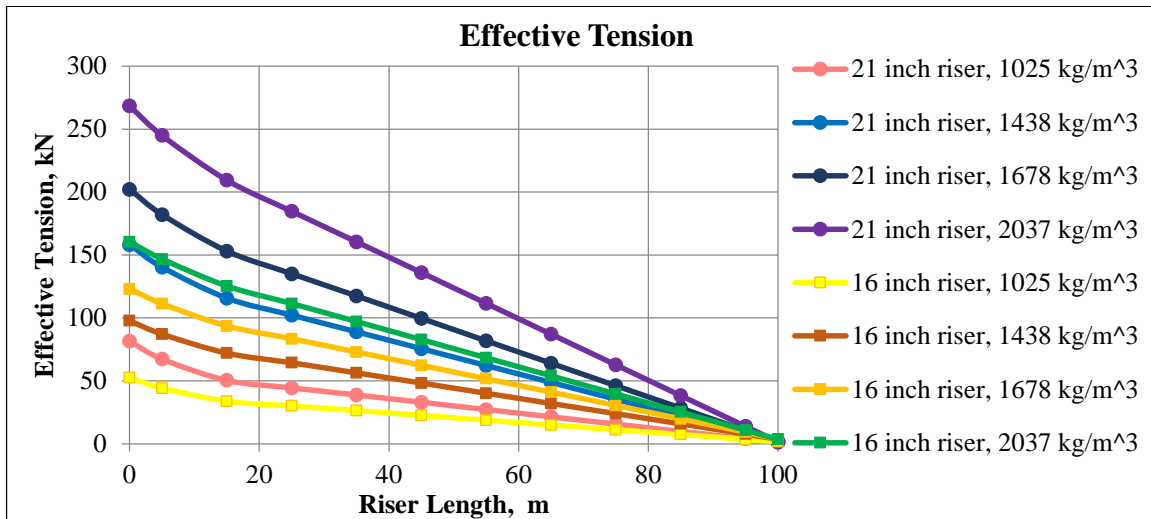


Figure F-14. Effective tension of aluminum risers at the wave height of 2 m and period of 5 s

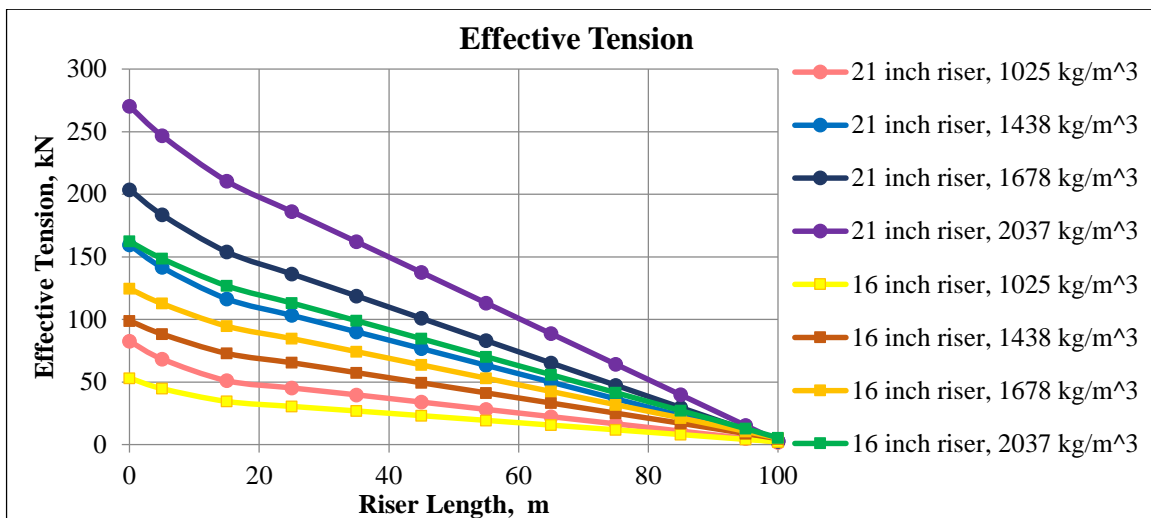


Figure F-15. Effective tension of aluminum risers at the wave height of 3 m and period of 5 s

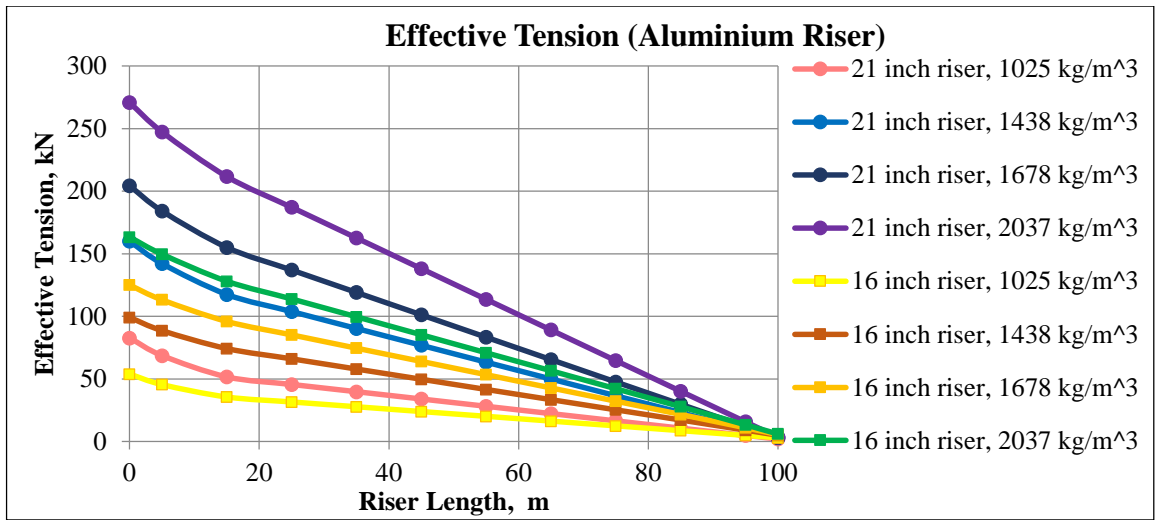


Figure F-16. Effective tension of aluminum risers at the wave height of 4 m and period of 6 s

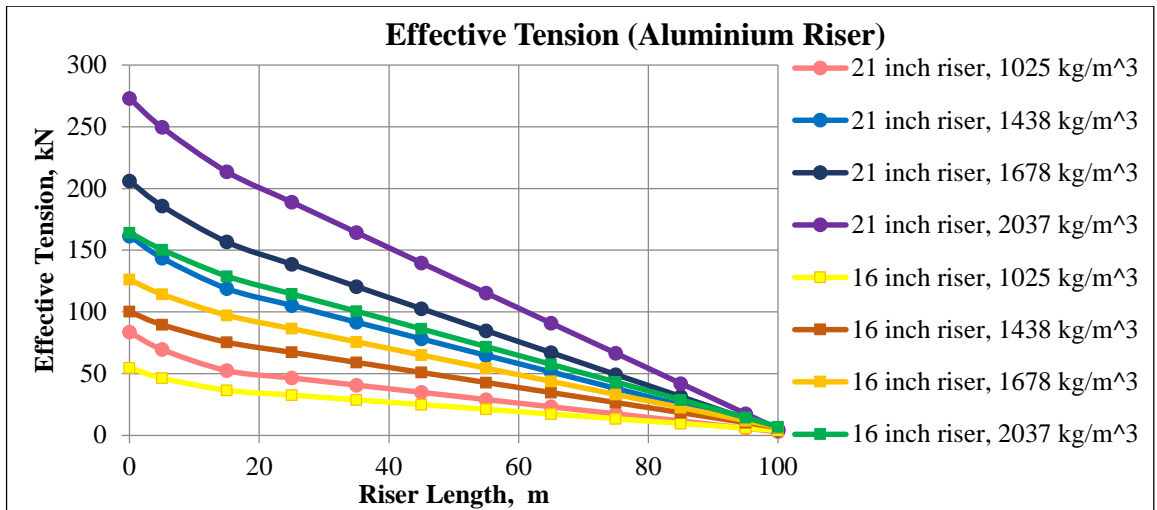


Figure F-17. Effective tension of aluminum risers at the wave height of 5 m and period of 6 s

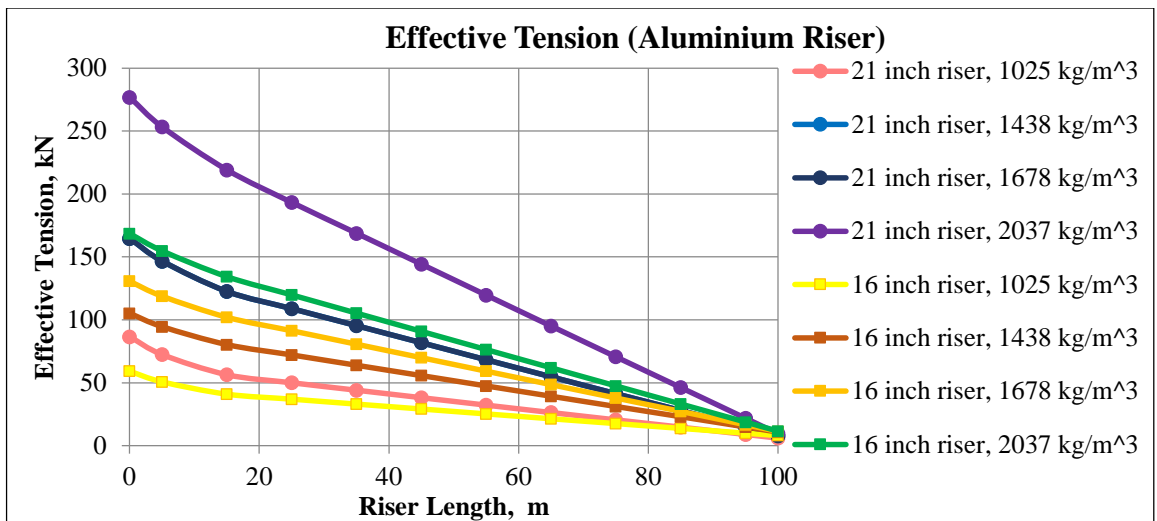


Figure F-18. Effective tension of aluminum risers at the wave height of 5 m and period of 7 s

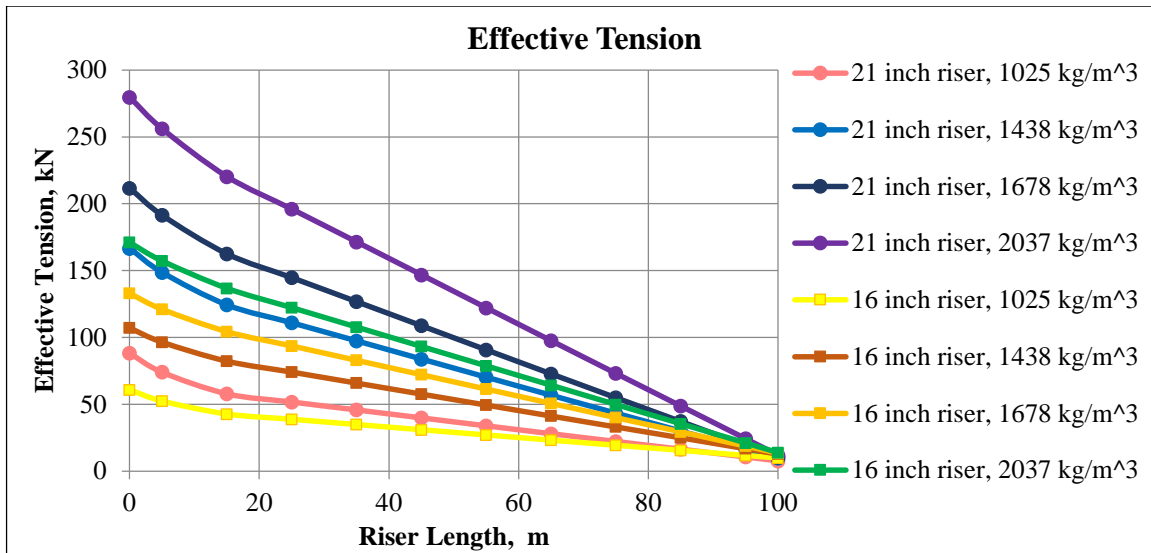


Figure F-19. Effective tension of aluminum risers at the wave height of 6 m and period of 7 s

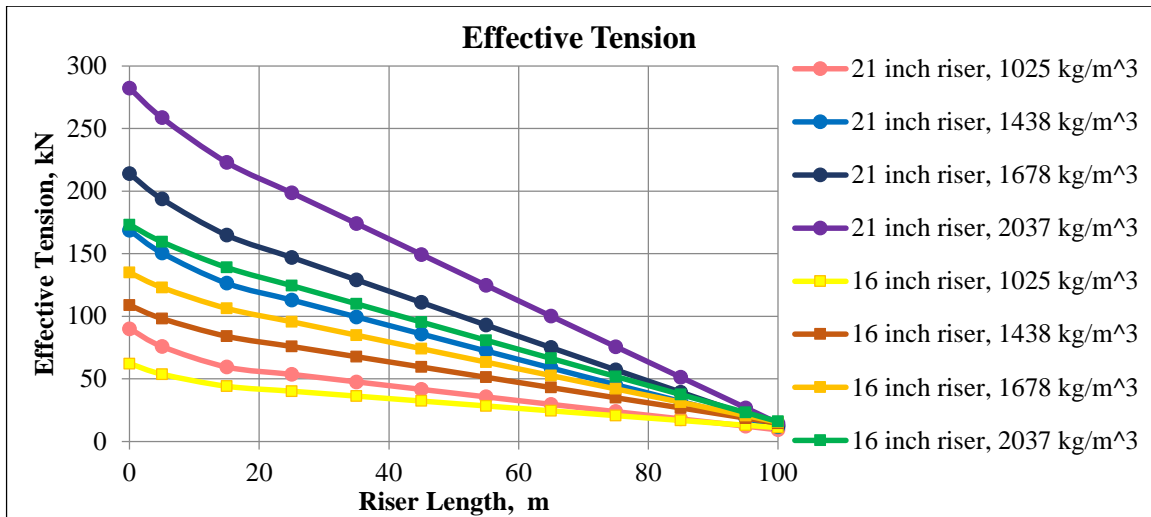


Figure F-20. Effective tension of aluminum risers at the wave height of 7 m and period of 7 s

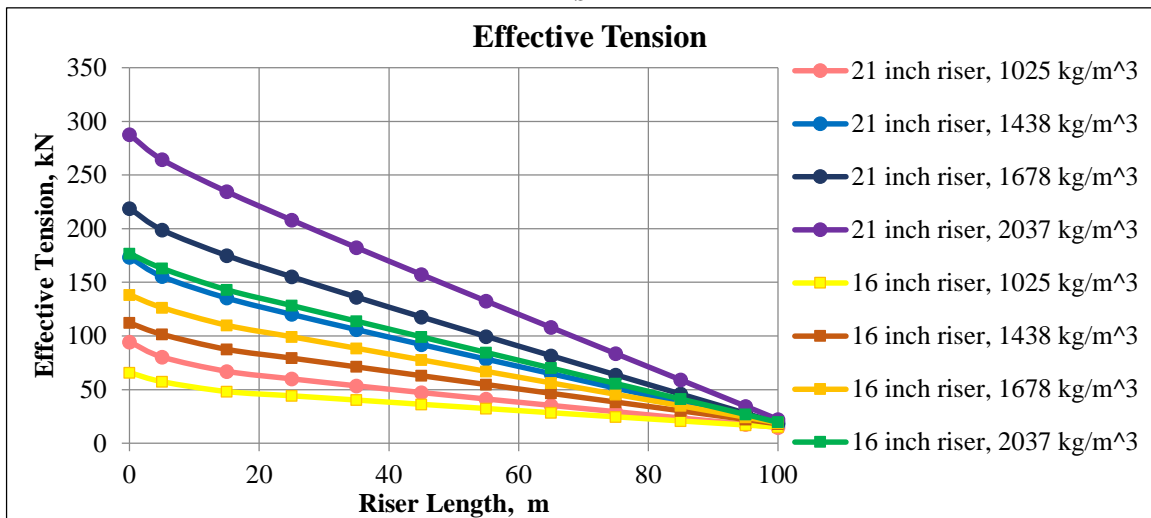


Figure F-21. Effective tension of aluminum risers at the wave height of 8 m and period of 8 s

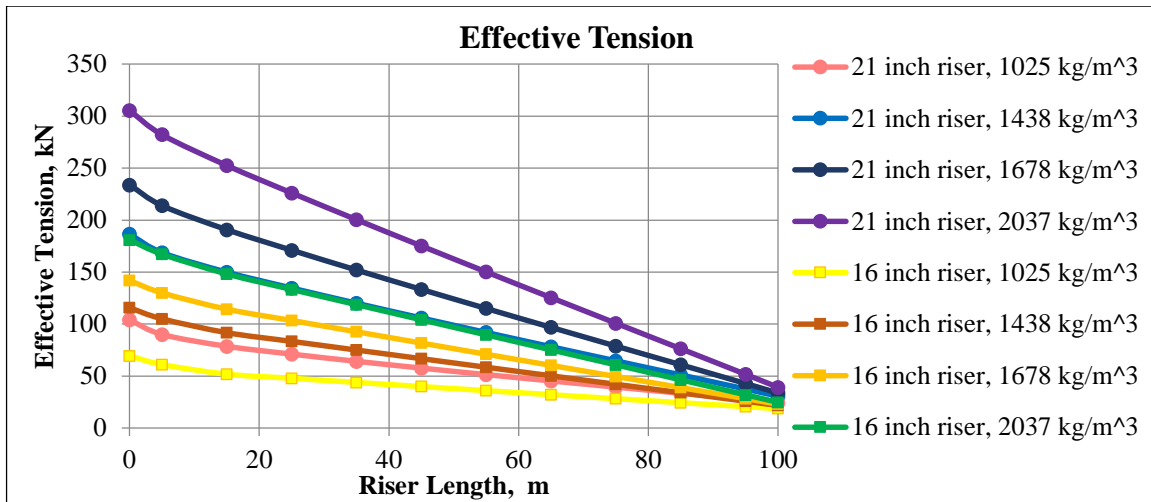


Figure F-22. Effective tension of aluminum risers at the wave height of 8 m and period of 9 s

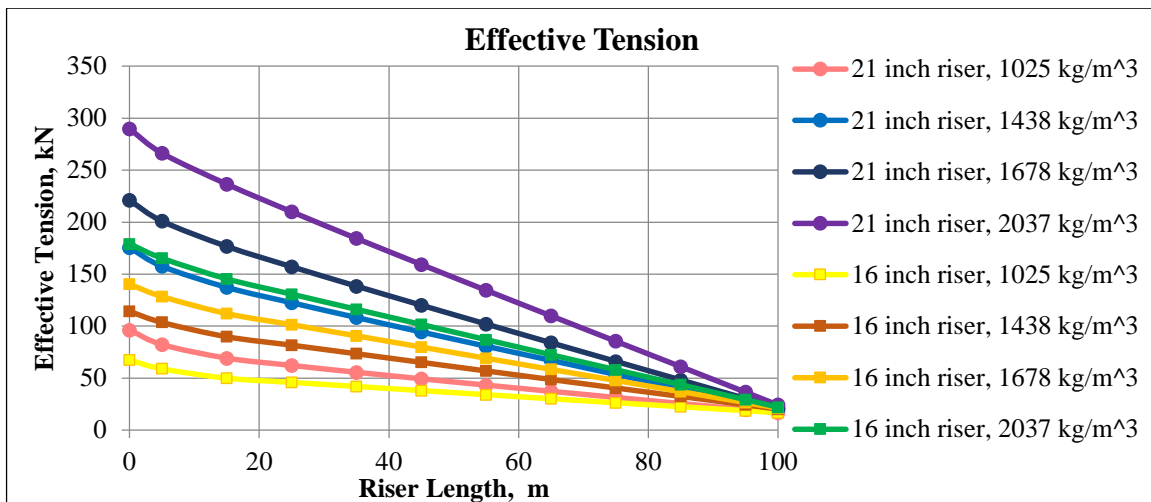


Figure F-23. Effective tension of aluminum risers at the wave height of 9 m and period of 8 s

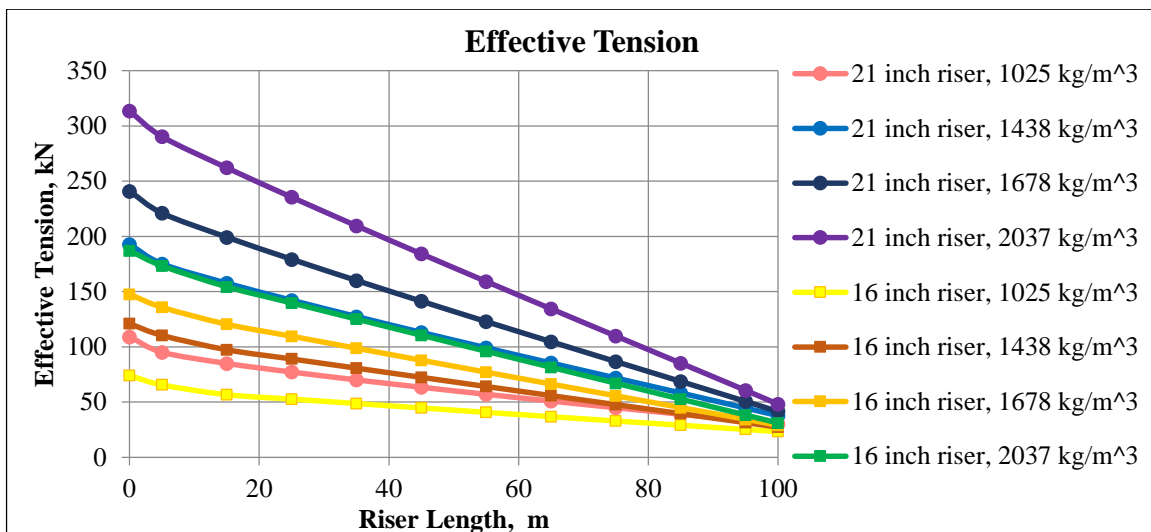


Figure F-24. Effective tension of aluminum risers at the wave height of 10 m and period of 9 s

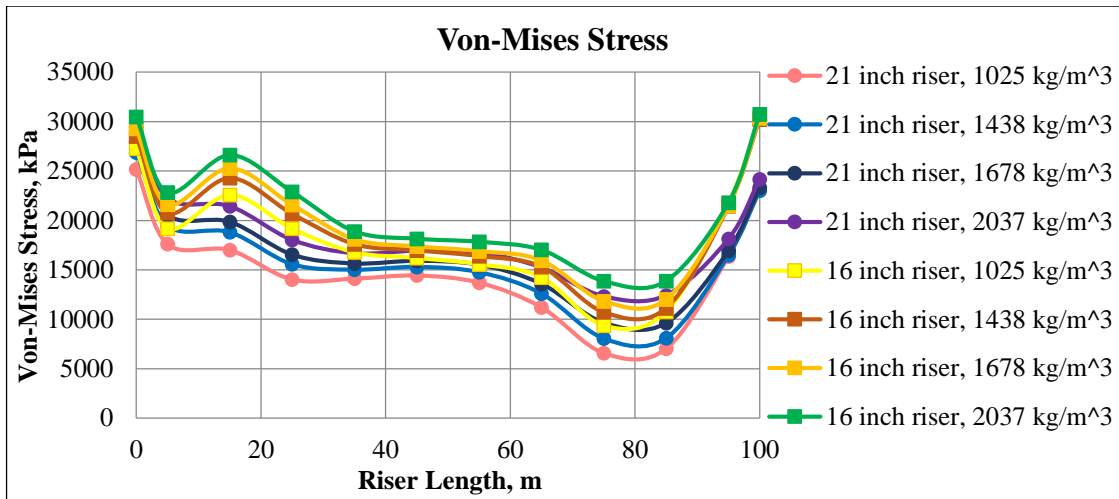


Figure F-25. Von-Mises stress of steel risers at the wave height of 1 m and period of 3 s (API and ISO limit is at 167500 kPa)

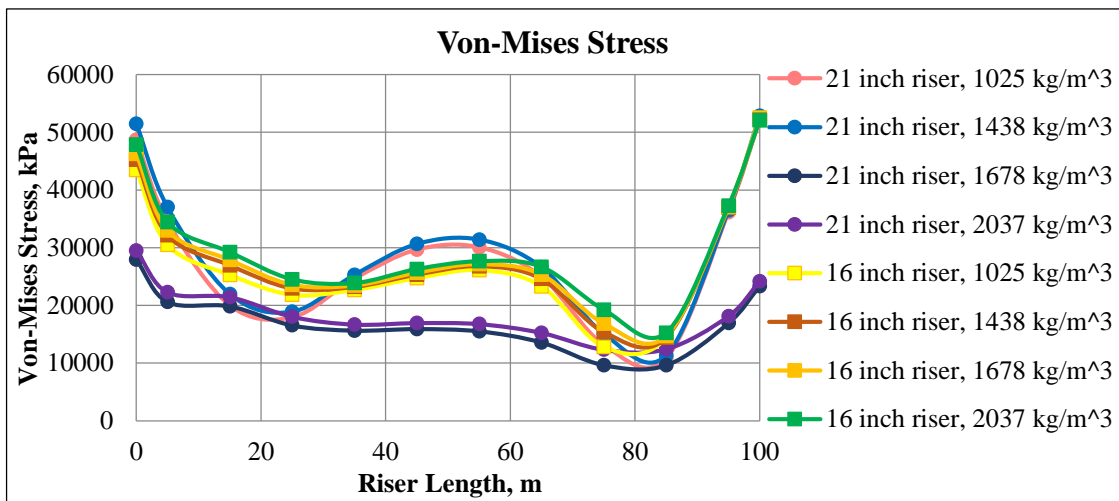


Figure F-26. Von-Mises stress of steel risers at the wave height of 2 m and period of 5 s (API and ISO limit is at 167500 kPa)

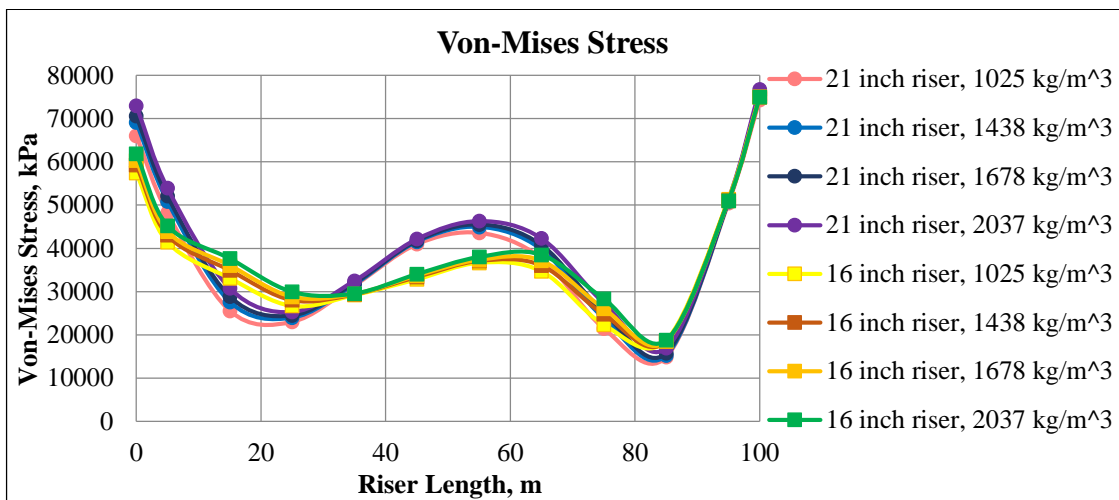


Figure F-27. Von-Mises stress of steel risers at the wave height of 3 m and period of 5 s (API and ISO limit is at 167500 kPa)

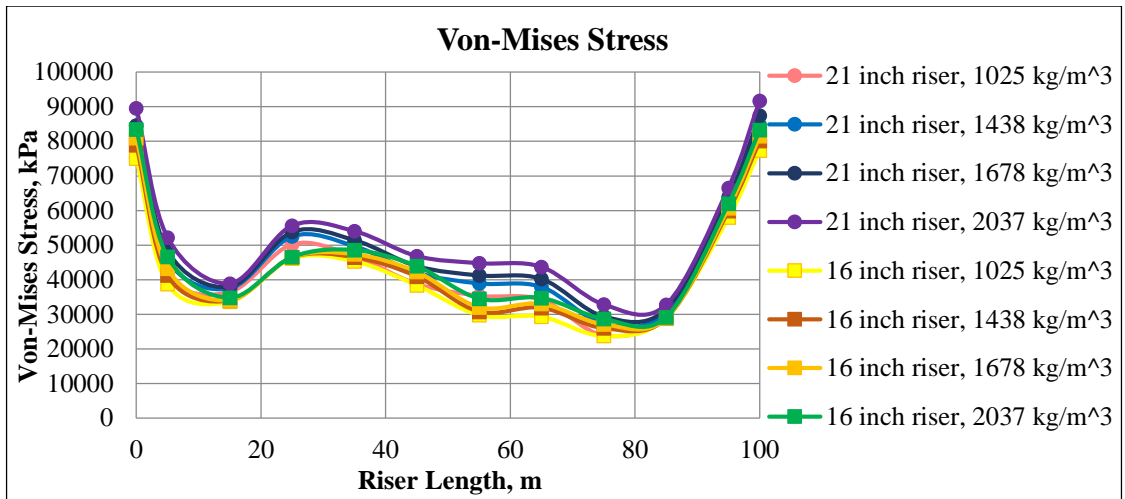


Figure F-28. Von-Mises stress of steel risers at the wave height of 4 m and period of 6 s (API and ISO limit is at 167500 kPa)

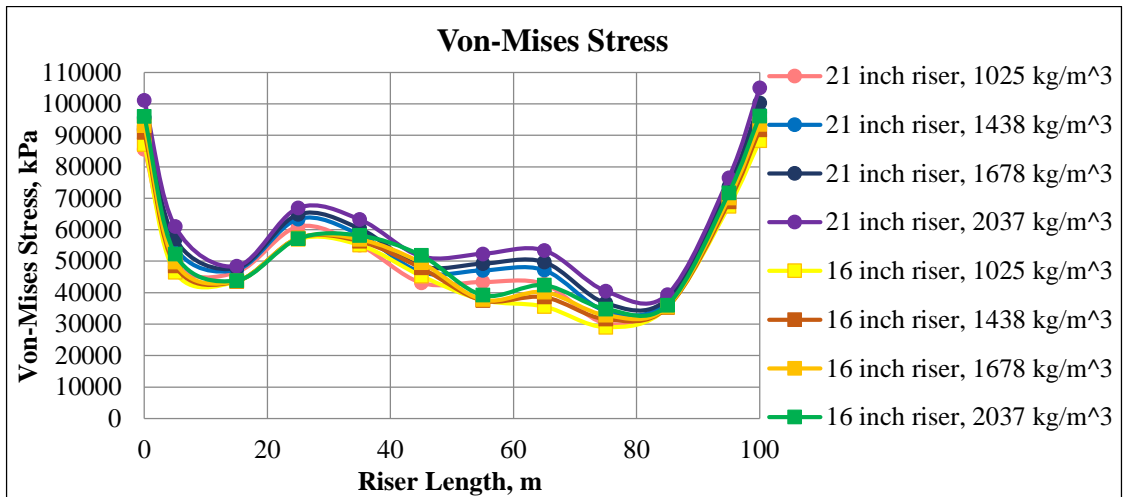


Figure F-29. Von-Mises stress of steel risers at the wave height of 5 m and period of 6 s (API and ISO limit is at 167500 kPa)

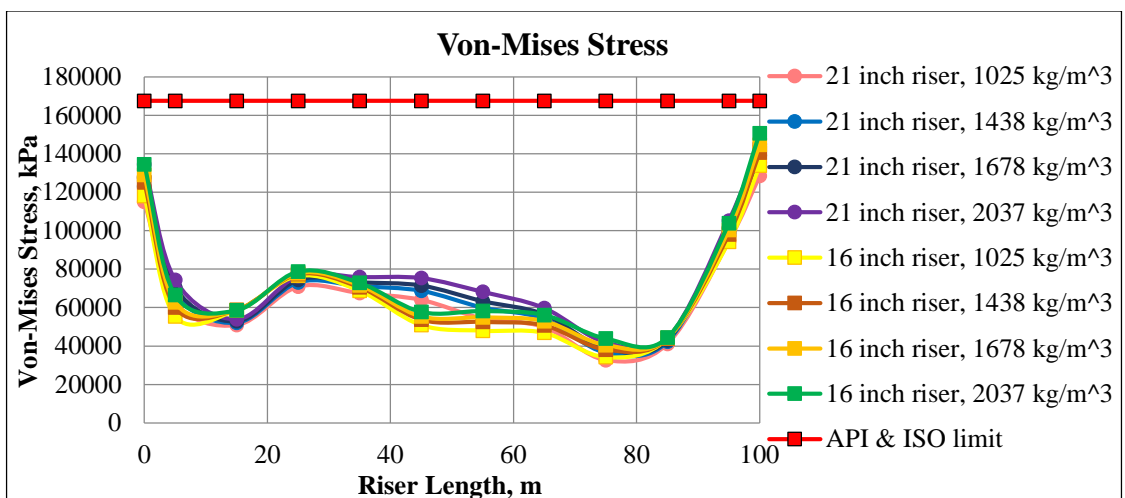


Figure F-30. Von-Mises stress of steel risers at the wave height of 5 m and period of 7 s

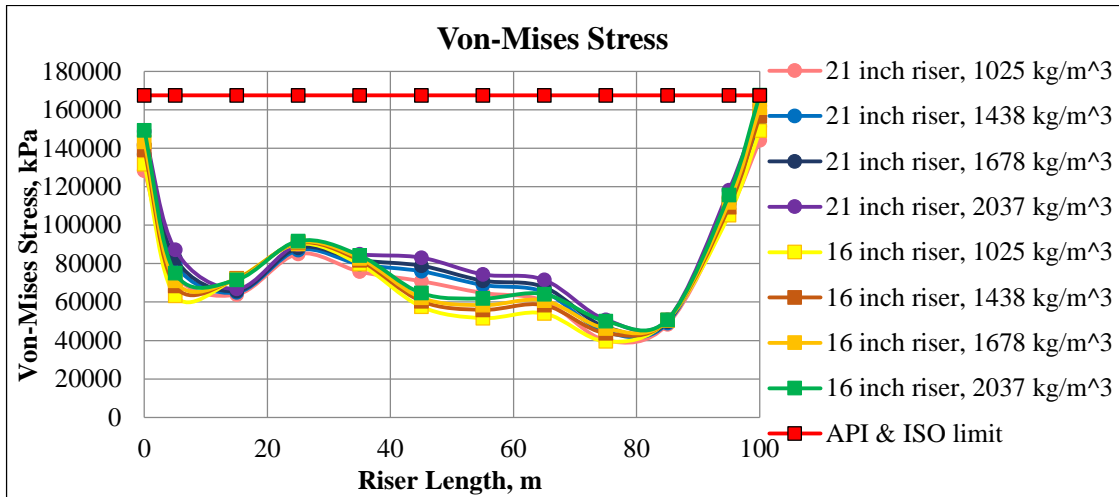


Figure F-31. Von-Mises stress of steel risers at the wave height of 6 m and period of 7 s

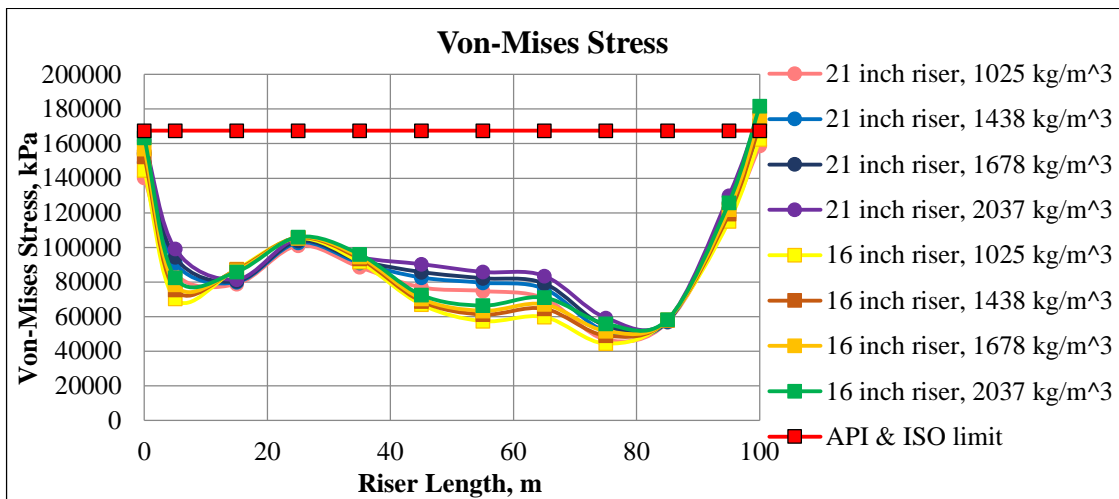


Figure F-32. Von-Mises stress of steel risers at the wave height of 7 m and period of 7 s

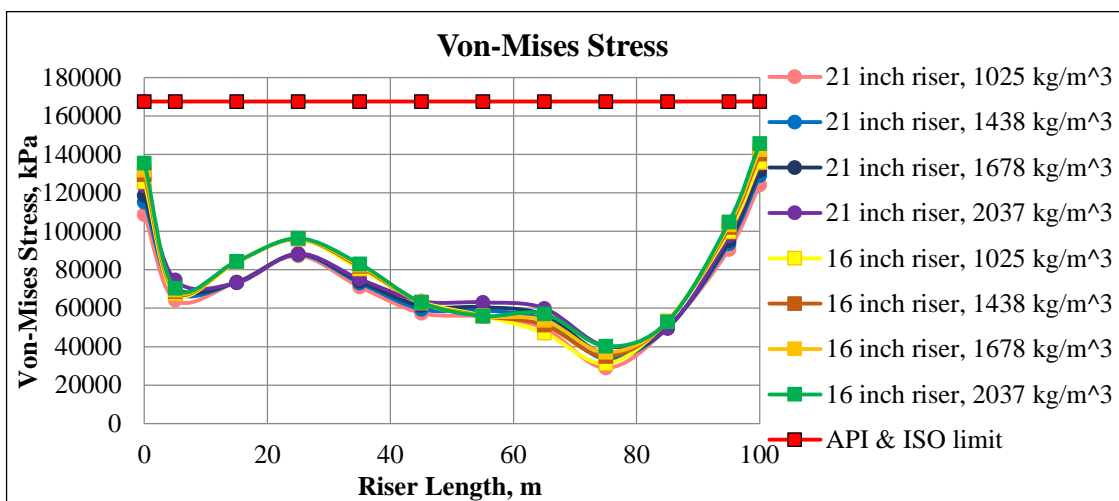


Figure F-33. Von-Mises stress of steel risers at the wave height of 8 m and period of 8 s

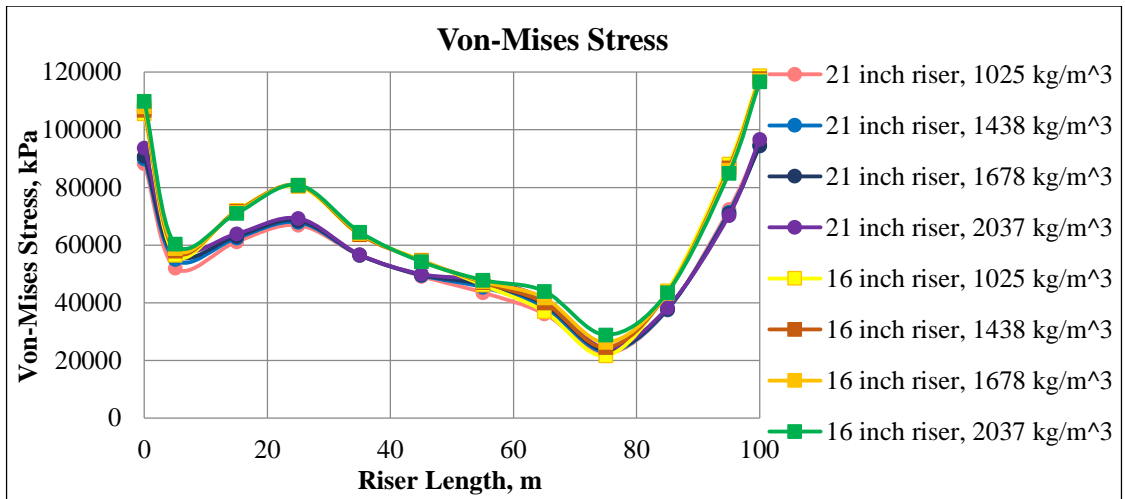


Figure F-34. Von-Mises stress of steel risers at the wave height of 8 m and period of 9 s (API and ISO limit is at 167500 kPa)

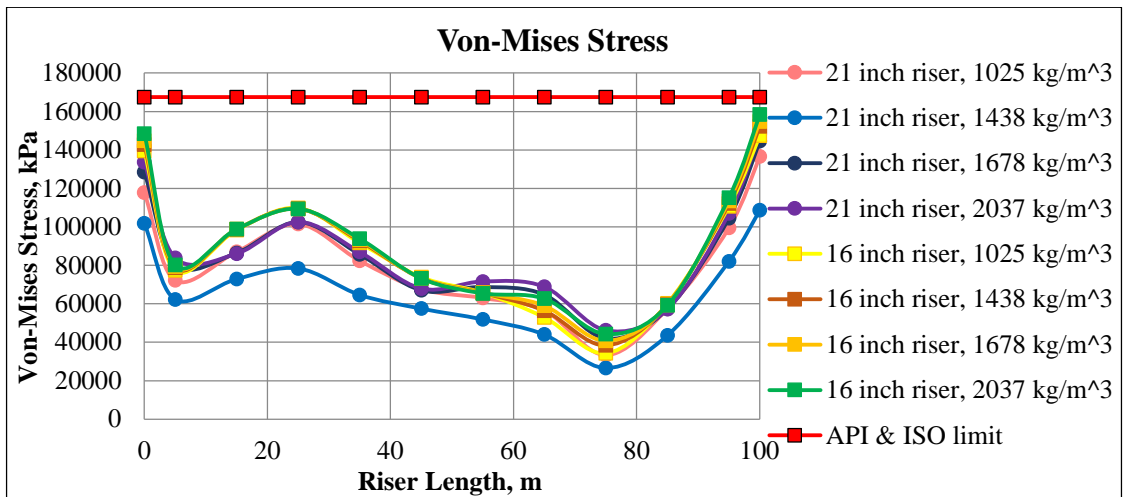


Figure F-35. Von-Mises stress of steel risers at the wave height of 9 m and period of 8 s

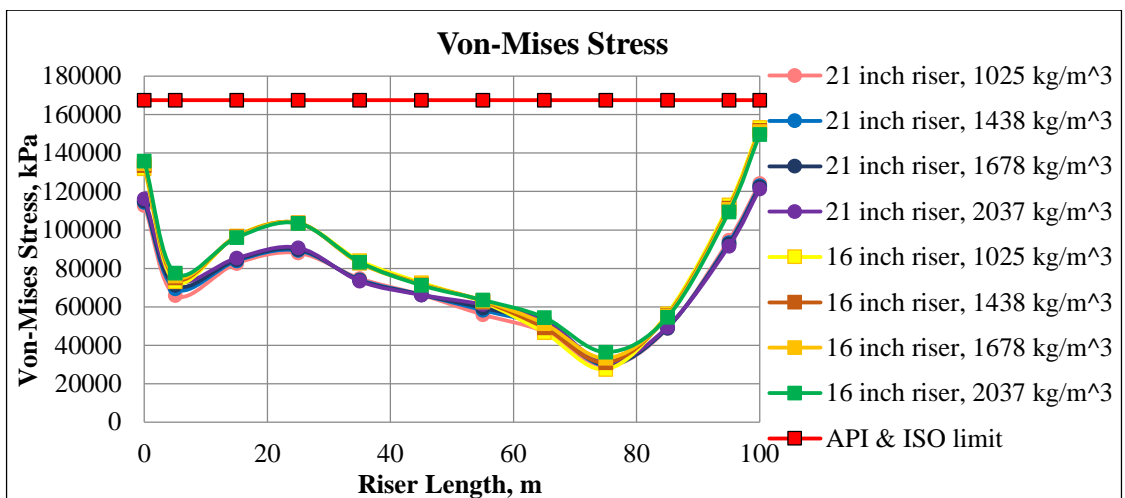


Figure F-36. Von-Mises stress of steel risers at the wave height of 10 m and period of 9 s

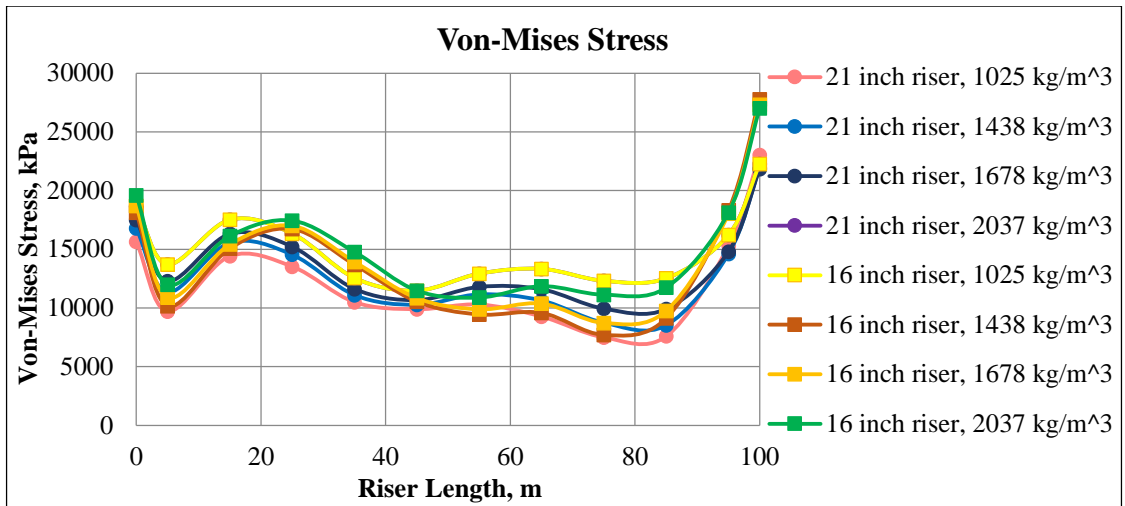


Figure F-37. Von-Mises stress of aluminum risers at the wave height of 1 m and period of 3 s (API and ISO limit is at 60300 kPa)

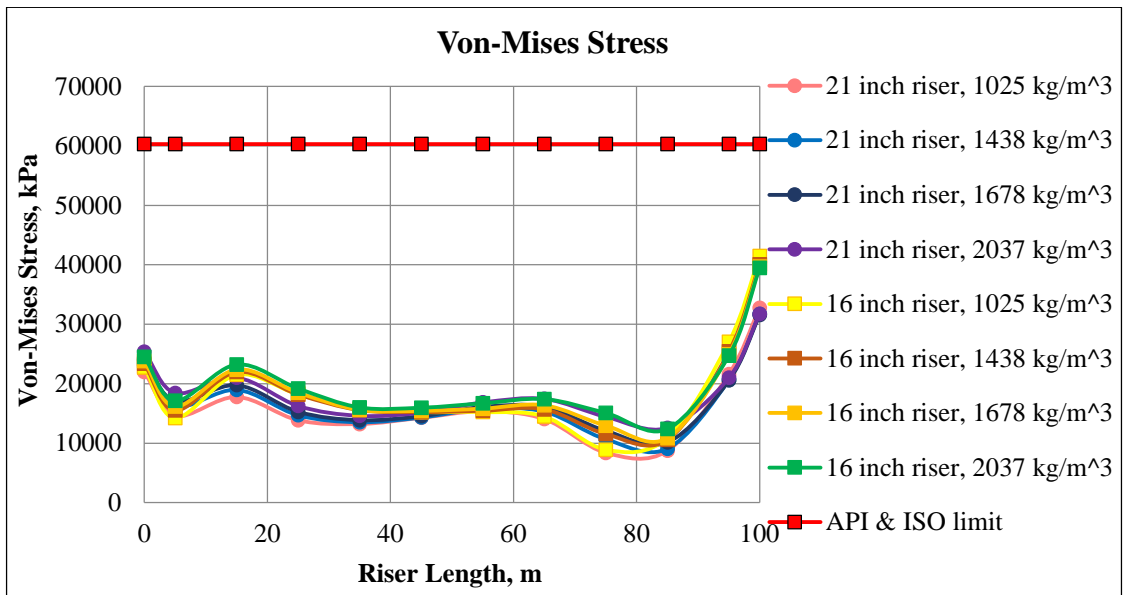


Figure F-38. Von-Mises stress of aluminum risers at the wave height of 2 m and period of 5 s

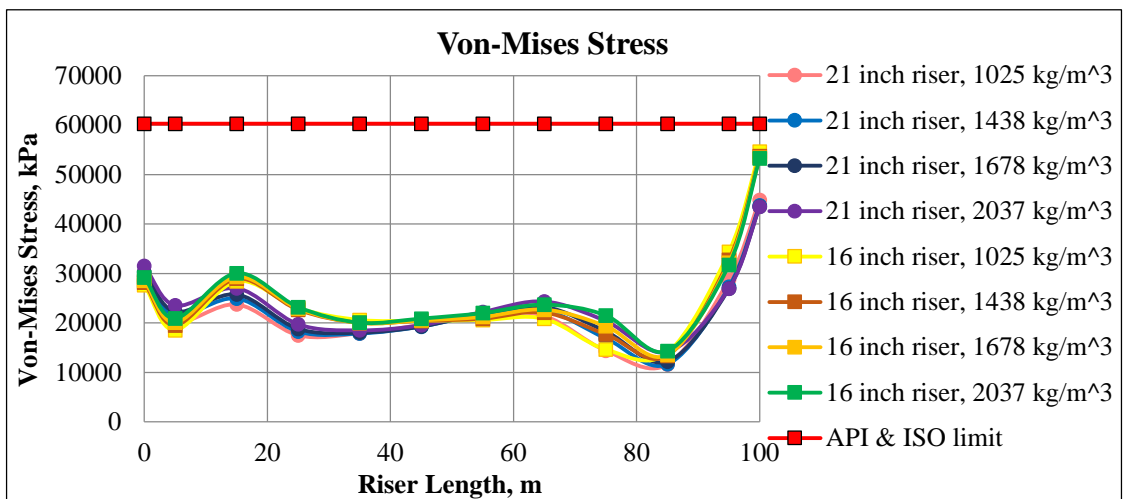


Figure F-39. Von-Mises stress of aluminum risers at the wave height of 3 m and period of 5 s

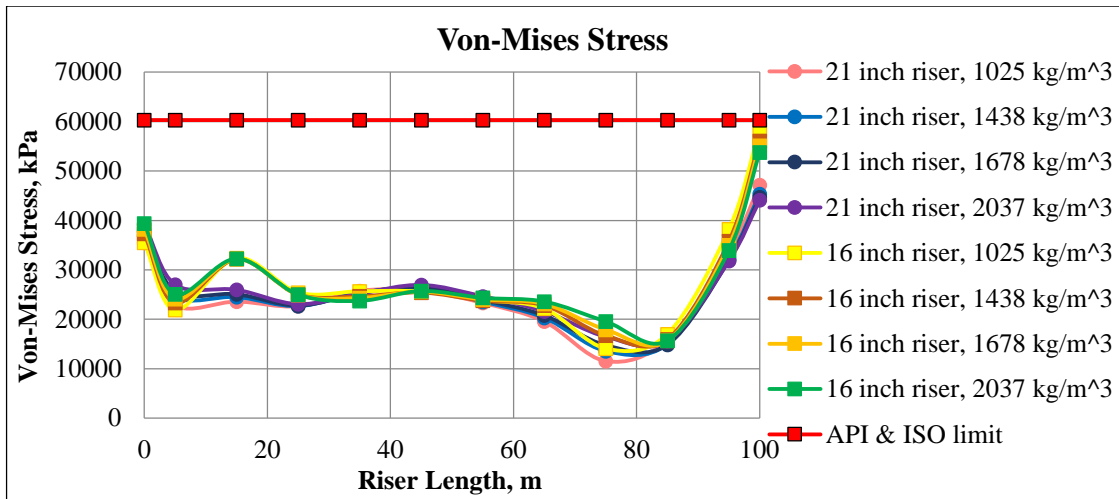


Figure F-40. Von-Mises stress of aluminum risers at the wave height of 4 m and period of 6 s

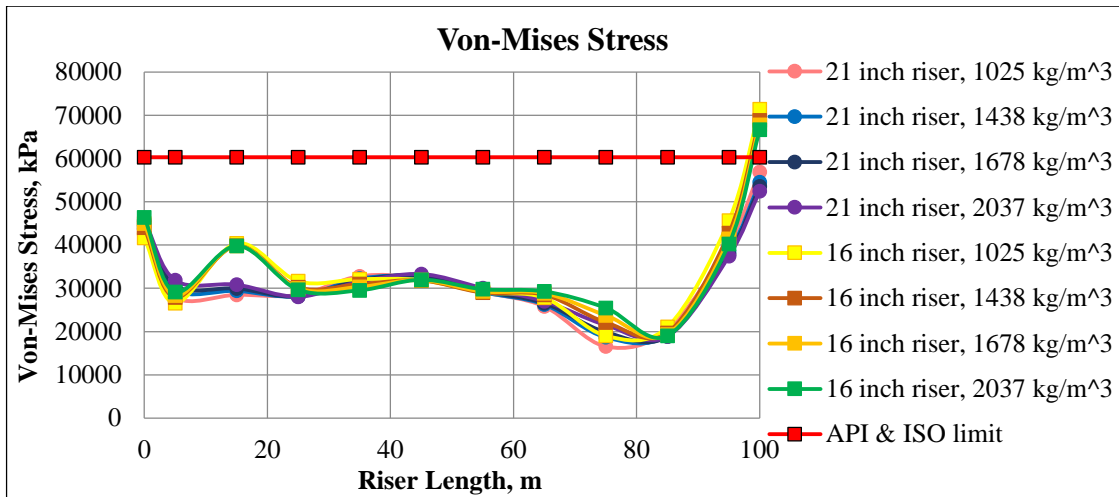


Figure F-41. Von-Mises stress of aluminum risers at the wave height of 5 m and period of 6 s

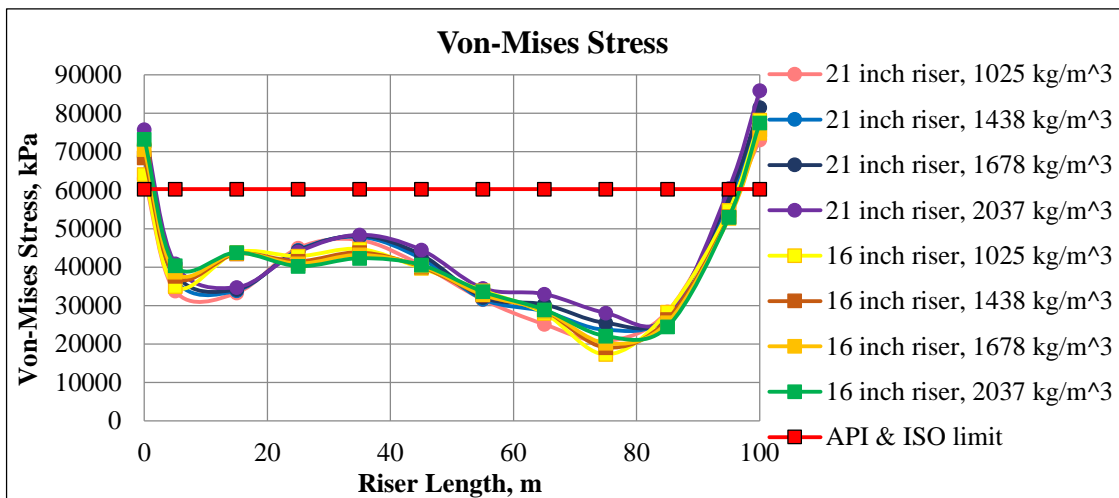


Figure F-42. Von-Mises stress of aluminum risers at the wave height of 5 m and period of 7 s

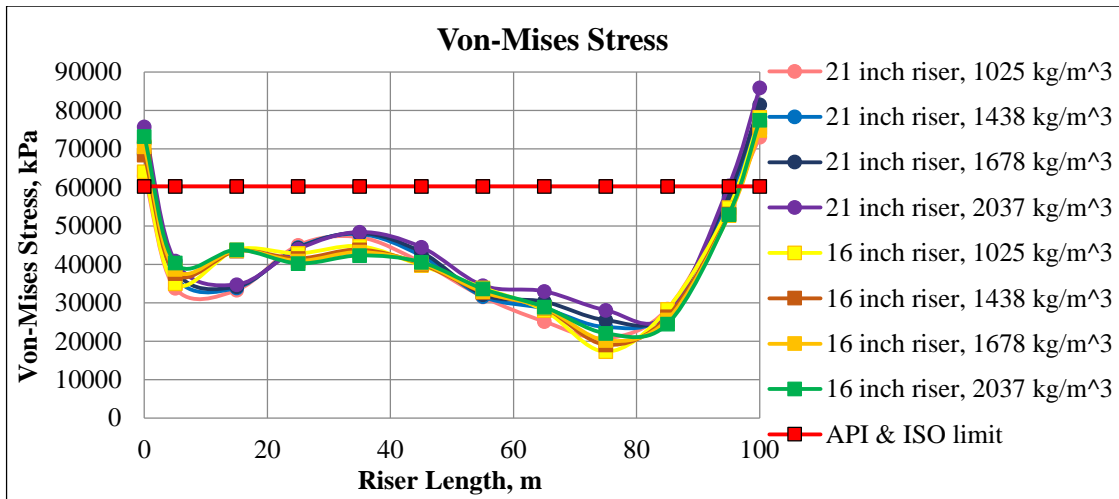


Figure F-43. Von-Mises stress of aluminum risers at the wave height of 6 m and period of 7 s

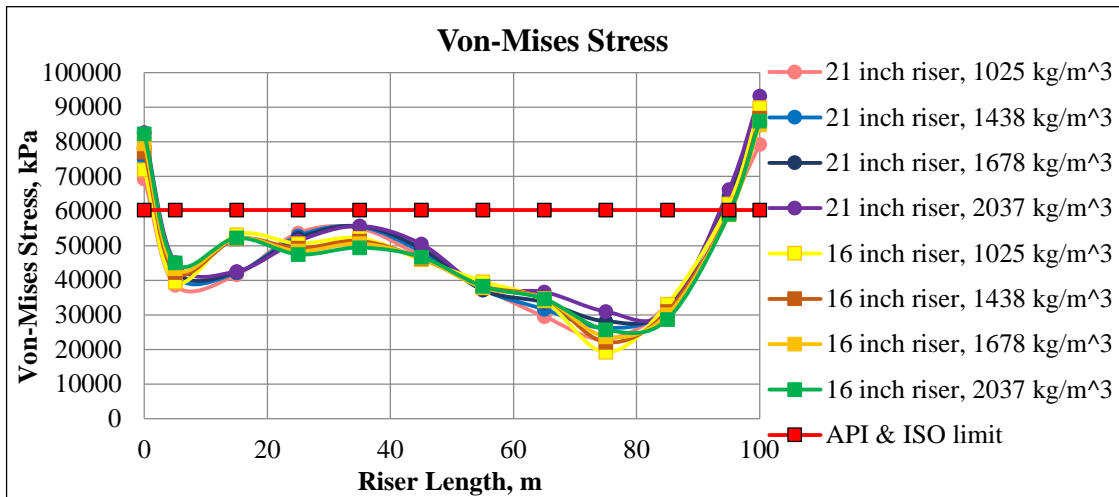


Figure F-44. Von-Mises stress of aluminum risers at the wave height of 7 m and period of 7 s

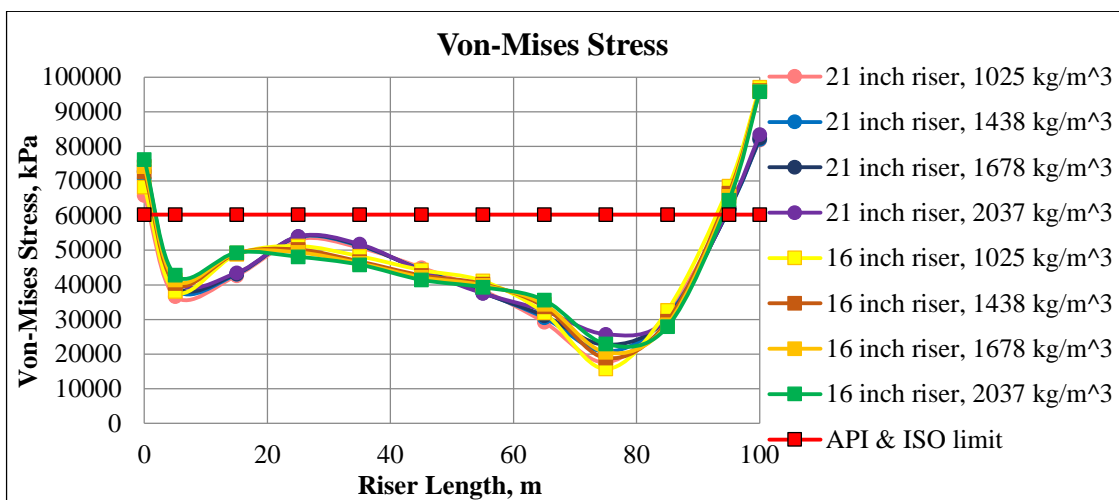


Figure F-45. Von-Mises stress of aluminum risers at the wave height of 8 m and period of 8 s

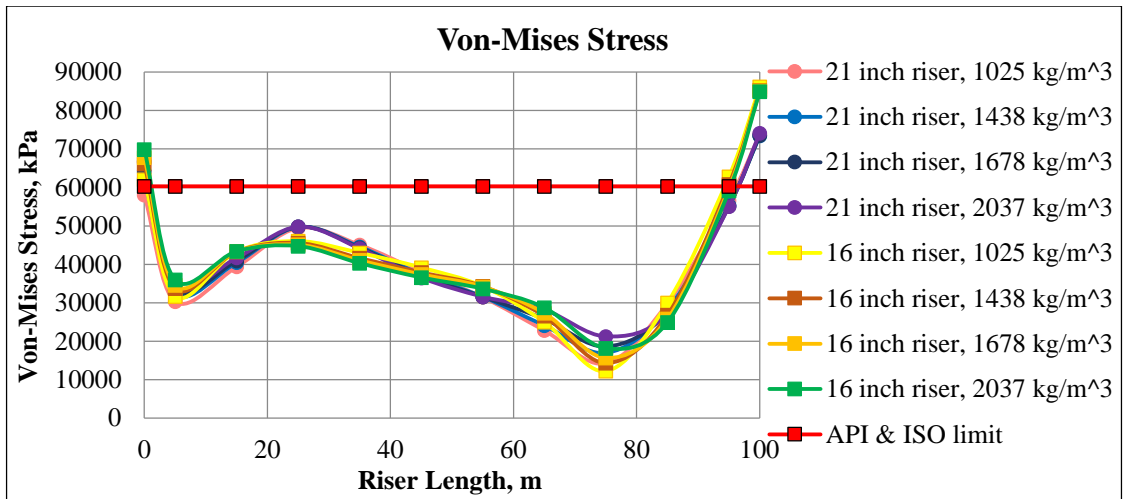


Figure F-46. Von-Mises stress of aluminum risers at the wave height of 8 m and period of 9 s

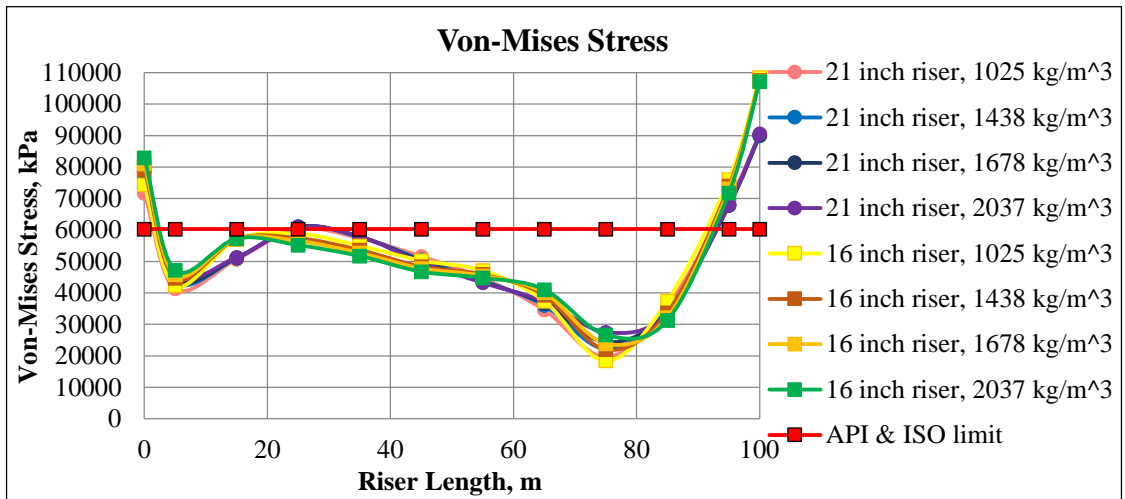


Figure F-47. Von-Mises stress of aluminum risers at the wave height of 9 m and period of 8 s

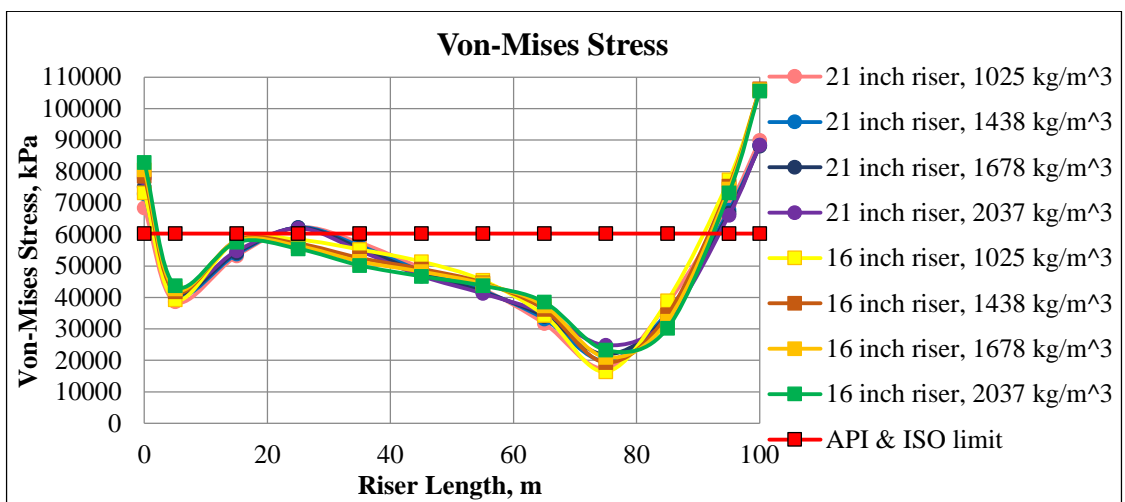


Figure F-48. Von-Mises stress of aluminum risers at the wave height of 10 m and period of 9 s

APPENDIX G

A detailed description of loads' calculations caused by current and waves are presented for various riser configurations in this Appendix. The calculations are based on the theory discussed in Chapter 4.5.3.

G1. Load calculations for 21 inch riser at the conditions of waves with height of 8 m

Input Data

Parameter	Designation	Value	Dimension
Wave height	H	8	m
Wave amplitude	ξ_0	4	m
Period	T	8	s
Water depth	d	100	m
Outer diameter of the riser	D	0.533	m
Water density	ρ	1025	kg/m^3
Standard gravity	g	9.81	m/s^2
Drag coefficient	C_D	1.05	
Mass coefficient	C_M	1.2	

Calculations

1. Wave amplitude:

$$\xi_0 = \frac{H}{2} = 4 \text{ m}$$

2. Wave length:

$$L = \frac{g \cdot T^2}{2\pi} = 100 \text{ m}$$

3. Angular velocity:

$$\omega = \frac{2\pi}{T} = 0.8 \text{ s}^{-1}$$

4. $k = \frac{2\pi}{L} = 0.063$

5. **Checking deep water criterion:**

$$\frac{d}{L} = 1 > 0.5 - \text{deep water area}$$

6. **Checking conditions for Morison's equation:**

$$\frac{D}{L} = 0.005 < 0.2$$

$$\frac{H}{L} = 0.08 \leq 0.14 - \text{non-breaking waves}$$

$$\frac{a}{D} < 0.2 \rightarrow a < 0.11$$

Assuming that the motion amplitude (a) for the drilling riser is negligible the Morison equation can be used safely to calculate the forces.

7. **Calculating the Keulegan-Carpenter number to check which term will dominate in the Morison equation:**

$$N_{KC} = \frac{\pi \cdot H}{D} = 15\pi$$

Hence, the drag term will be dominating in the equation.

8. **The Morison equation can be written as follows:**

$$F(t) = \int_{-d}^{\xi_0} \left(\rho \cdot \frac{\pi D^2}{4} \right) \cdot C_M \cdot \dot{u} dz + \int_{-d}^{\xi_0} \frac{1}{2} \cdot \rho \cdot C_D \cdot D \cdot u \cdot |u| dz$$

The equation can be solved using a graphical method when each contributing term is plotted on a timeline and the maximum force is found graphically.

9. **For deep water zone the horizontal velocity and acceleration can be presented as the following:**

$$u = \frac{\xi_0 g k}{\omega} e^{kz} \cdot \sin(\omega t), \quad \dot{u} = \xi_0 g k e^{kz} \cdot \cos(\omega t)$$

Therefore

$$F_M(t) = \int_{-d}^{\xi_0} \left(\rho \cdot \frac{\pi D^2}{4} \right) \cdot C_M \cdot \dot{u} dz = \int_{-d}^{\xi_0} \left(\rho \cdot \frac{\pi D^2}{4} \right) \cdot C_M \cdot \xi_0 g k e^{kz} \cdot \cos(\omega t) dz =$$

$$\begin{aligned}
&= \left(\rho \cdot \frac{\pi D^2}{4} \right) \cdot C_M \cdot \xi_0 g k \cdot \cos(\omega t) \left[\frac{e^{kz}}{k} \right]_{-d}^{\xi_0} = \\
&= \left(\rho \cdot \frac{\pi D^2}{4} \right) \cdot C_M \cdot \xi_0 g \cdot \cos(\omega t) [e^{k\xi_0} - e^{-kd}]
\end{aligned}$$

and

$$\begin{aligned}
F_D(t) &= \int_{-d}^{\xi_0} \frac{1}{2} \cdot \rho \cdot C_D \cdot D \cdot u \cdot |u| dz = \int_{-d}^{\xi_0} \frac{1}{2} \cdot \rho \cdot C_D \cdot D \cdot \left(\frac{\xi_0 g k}{\omega} e^{kz} \right)^2 \cdot \sin(\omega t) |\sin(\omega t)| dz = \\
&= \frac{1}{2} \cdot \rho \cdot C_D \cdot D \cdot \left(\frac{\xi_0 g k}{\omega} \right)^2 \cdot \sin(\omega t) |\sin(\omega t)| \int_{-d}^{\xi_0} e^{2kz} dz = \\
&= \frac{1}{2} \cdot \rho \cdot C_D \cdot D \cdot \left(\frac{\xi_0 g k}{\omega} \right)^2 \cdot \sin(\omega t) |\sin(\omega t)| \left[\frac{e^{2kz}}{2k} \right]_{-d}^{\xi_0} = \\
&= \frac{1}{4} \cdot \rho \cdot C_D \cdot D \cdot k \cdot \left(\frac{\xi_0 g}{\omega} \right)^2 \cdot \sin(\omega t) |\sin(\omega t)| [e^{2k\xi_0} - e^{-2kd}]
\end{aligned}$$

Finally, the expression for the total force calculation can be presented in the next form:

$$\begin{aligned}
F_{Total}(t) &= F_M(t) + F_D(t) = \left(\rho \cdot \frac{\pi D^2}{4} \right) \cdot C_M \cdot \xi_0 g \cdot \cos(\omega t) [e^{k\xi_0} - e^{-kd}] + \\
&+ \frac{1}{4} \cdot \rho \cdot C_D \cdot D \cdot k \cdot \left(\frac{\xi_0 g}{\omega} \right)^2 \cdot \sin(\omega t) |\sin(\omega t)| [e^{2k\xi_0} - e^{-2kd}]
\end{aligned}$$

- 10.** All derived expressions can now be plotted for a 2 s (and 10 s for illustration) wave period and the maximum force impact can be found afterwards.

It is important to notice that the integration is performed up to ξ_0 . This is a conservative simplification because in reality the maximum force occurs in a place between the wave crest and still water level for a given time period. That implies that to be theoretically correct the equation have to be solved for maximum force with variable upper-integration limit, varying from 0 to ξ_0 .

11.

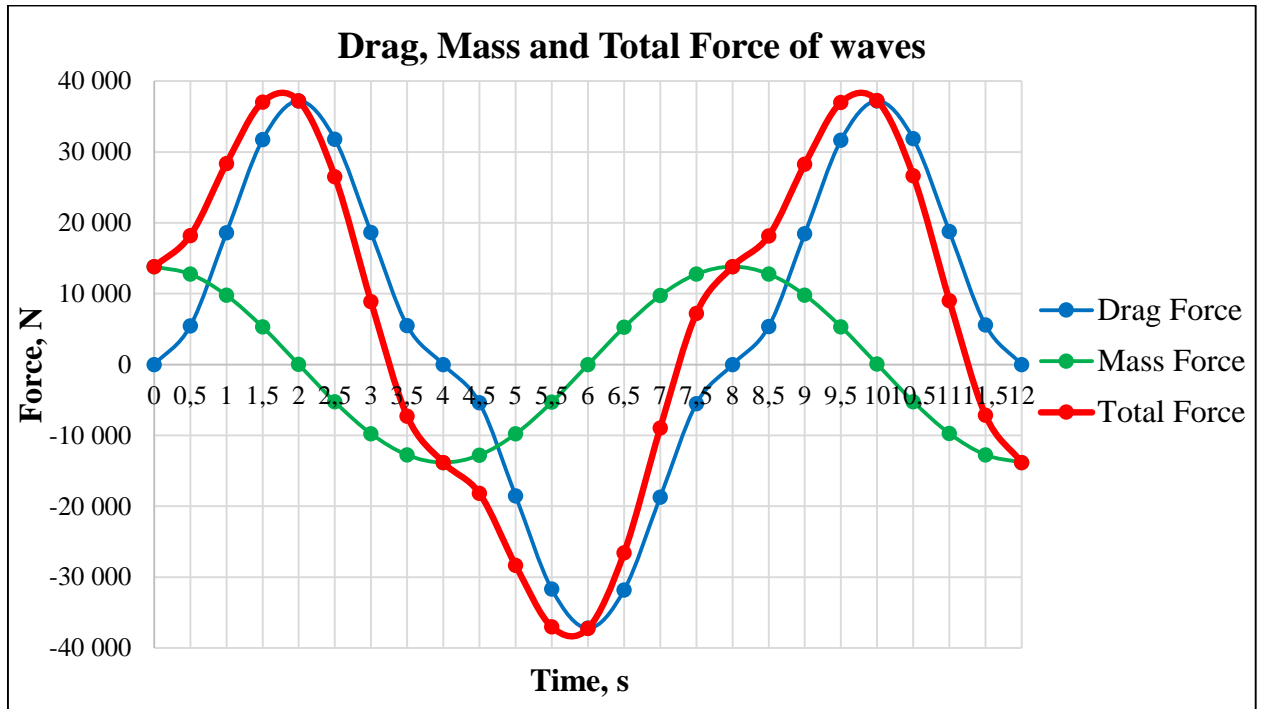


Figure G-1. Drag, Mass and Total Force of wave

The drag, mass and total forces are shown in Figure G-1 as a function of time. It can be observed from Figure the forces express negative values as well but the only positive values should be taken into account.

$$F_{Total} = 39\,000 \text{ N is at the maximum when } t \approx 1.9 \text{ s.}$$

12.

However, the maximum total force should also be defined and plotted as a function of the water depth. The water depth (z) varies from the top point at the wave crest ($\xi_0 = 4 \text{ m}$) to the depth at which the maximum total force has any observed impact ($F_{Total}(t = 1.9 \text{ s})$ is approximately equal to 0). The step of depth variation is chosen to be equal to 1 m since the size of the cell in the ANSYS model is specified as 1 m.

$$F_{Total}(t = 1.9, z) = F_M(t = 1.9, z) + F_D(t = 1.9, z) = \left(\rho \cdot \frac{\pi D^2}{4} \right) \cdot C_M \cdot \xi_0 g e^{kz} \cdot \cos(\omega t) + \frac{1}{2} \cdot \rho \cdot C_D \cdot D \cdot k \cdot \left(\frac{\xi_0 g k}{\omega} e^{kz} \right)^2 \cdot \sin(\omega t) \sin(\omega t)$$

13.

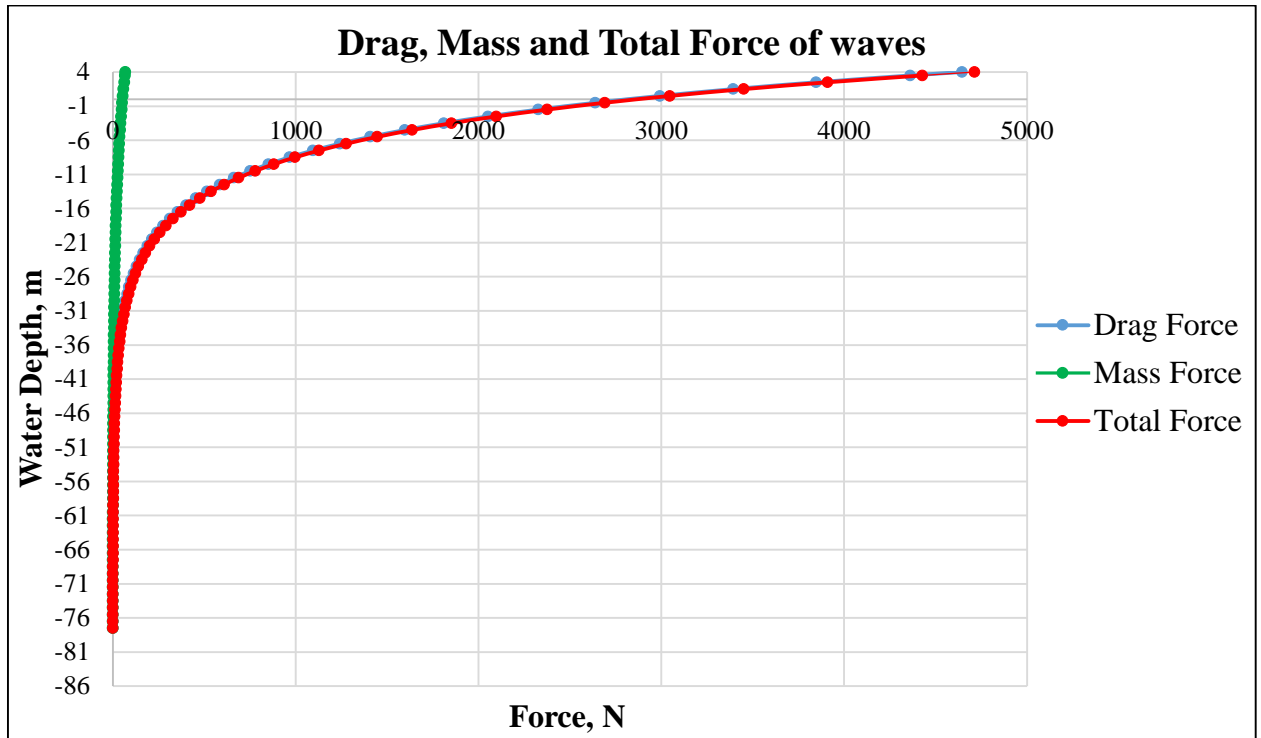


Figure G-2. Distribution of Drag, Mass and Total Force of wave over the water depth

The detailed calculations of forces are presented in Excel file on DVD.

Since the drilling riser is also exposed to the sea current therefore current forces should be determined in order to apply them on the riser structure in the ANSYS model. For calculation of forces acting on the riser at a constant current the only drag term is taken into consideration in the Morison equation. The distribution of the current velocity over the water depth can be found by the Power Law equation used in OrcaFlex (see Appendix E and Chapter 6.2.3).

Input Data

Parameter	Designation	Value	Dimension
Current velocity at the surface	S_0	1	m/s
Current velocity at the sea bottom	S_b	0.2	m/s
Water depth	d	100	m
Outer diameter of the riser	D	0.533	m
Water density	ρ	1025	kg/m^3
Standard gravity	g	9.81	m/s^2
Drag coefficient	C_D	1.05	
Power Law Exponent	<i>Exponent</i>	0.3	

Calculations

1. Current velocity:

$$S(z) = S_b + (S_f - S_b) \times ((z - z_b) / (z_f - z_b))^{1/Exponent}$$

where z varies from 0 to 90 m as the bottom end of the riser is located 10 m above the seabed.

2. Average velocity of the current:

$$S_{average} = \frac{S_n + S_{n+1}}{2}$$

3. Finally the drag force can be calculated using the following equation:

$$F_{Total} = F_D = \int_{z'-\Delta z}^{z'} f_D(z, t) dz = \int_{z'-\Delta z}^{z'} \frac{1}{2} \cdot \rho \cdot C_D \cdot D \cdot u \cdot |u| dz = \frac{1}{2} \cdot \rho \cdot C_D \cdot D \cdot u^2 \cdot \Delta z$$

where $u = S_{average}$

The step of the water depth variation (Δz) is equal to 1 m due to the cell length (1 m) in the mesh created on the riser structure.

4. The calculation results are presented in Table G-1.

Water Depth, z	Δz	Current Velocity, $S(z)$	Average Velocity of the Current, $S_{average}$	Drag Force, F_D
m	m	m/s	m/s	N
0	-	1,000	-	-
-1	1	0,974	0,987	279
-2	1	0,948	0,961	265
-3	1	0,923	0,935	251
-4	1	0,898	0,910	238
-5	1	0,874	0,886	225
-6	1	0,851	0,863	213
-7	1	0,828	0,840	202
-8	1	0,806	0,817	191
-9	1	0,784	0,795	181
-10	1	0,763	0,774	172
-11	1	0,742	0,753	163
-12	1	0,722	0,732	154
-13	1	0,703	0,713	146
-14	1	0,684	0,693	138
-15	1	0,665	0,675	131
-16	1	0,647	0,656	124
-17	1	0,630	0,639	117
-18	1	0,613	0,621	111

-19	1	0,596	0,605	105
-20	1	0,580	0,588	99
-21	1	0,565	0,572	94
-22	1	0,549	0,557	89
-23	1	0,535	0,542	84
-24	1	0,520	0,528	80
-25	1	0,507	0,514	76
-26	1	0,493	0,500	72
-27	1	0,480	0,487	68
-28	1	0,468	0,474	64
-29	1	0,455	0,462	61
-30	1	0,444	0,450	58
-31	1	0,432	0,438	55
-32	1	0,421	0,427	52
-33	1	0,411	0,416	50
-34	1	0,400	0,405	47
-35	1	0,390	0,395	45
-36	1	0,381	0,386	43
-37	1	0,371	0,376	41
-38	1	0,363	0,367	39
-39	1	0,354	0,358	37
-40	1	0,346	0,350	35
-41	1	0,338	0,342	34
-42	1	0,330	0,334	32
-43	1	0,323	0,327	31
-44	1	0,316	0,319	29
-45	1	0,309	0,312	28
-46	1	0,303	0,306	27
-47	1	0,296	0,299	26
-48	1	0,290	0,293	25
-49	1	0,285	0,288	24
-50	1	0,279	0,282	23
-51	1	0,274	0,277	22
-52	1	0,269	0,272	21
-53	1	0,265	0,267	20
-54	1	0,260	0,262	20
-55	1	0,256	0,258	19
-56	1	0,252	0,254	18
-57	1	0,248	0,250	18
-58	1	0,244	0,246	17
-59	1	0,241	0,243	17
-60	1	0,238	0,239	16
-61	1	0,235	0,236	16
-62	1	0,232	0,233	16
-63	1	0,229	0,230	15
-64	1	0,227	0,228	15

-65	1	0,224	0,225	15
-66	1	0,222	0,223	14
-67	1	0,220	0,221	14
-68	1	0,218	0,219	14
-69	1	0,216	0,217	14
-70	1	0,214	0,215	13
-71	1	0,213	0,214	13
-72	1	0,211	0,212	13
-73	1	0,210	0,211	13
-74	1	0,209	0,210	13
-75	1	0,208	0,208	12
-76	1	0,207	0,207	12
-77	1	0,206	0,206	12
-78	1	0,205	0,206	12
-79	1	0,204	0,205	12
-80	1	0,204	0,204	12
-81	1	0,203	0,203	12
-82	1	0,203	0,203	12
-83	1	0,202	0,202	12
-84	1	0,202	0,202	12
-85	1	0,201	0,202	12
-86	1	0,201	0,201	12
-87	1	0,201	0,201	12
-88	1	0,201	0,201	12
-89	1	0,201	0,201	12
-90	1	0,200	0,200	12

Table G-1. Drag force calculations

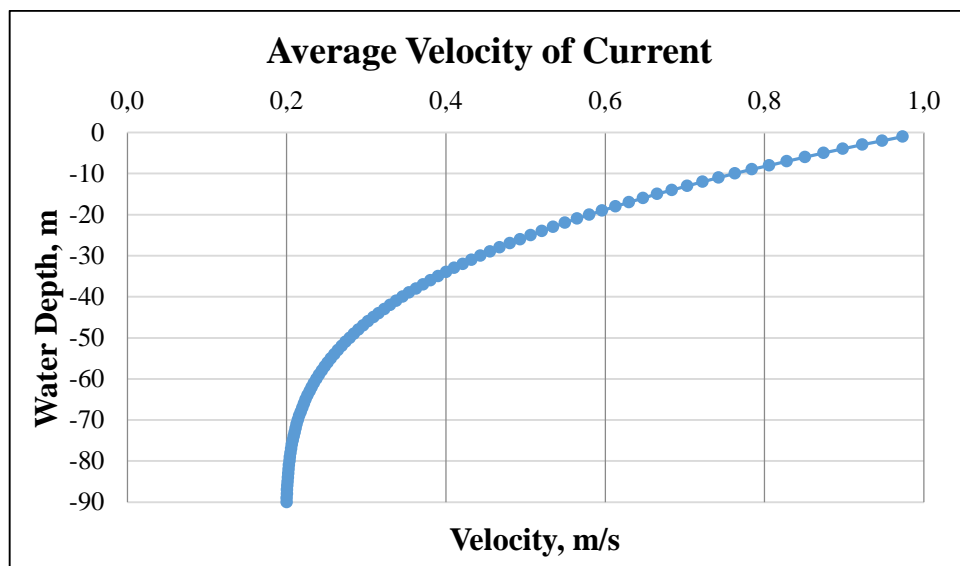


Figure G-3. Average velocity of the current over the water depth

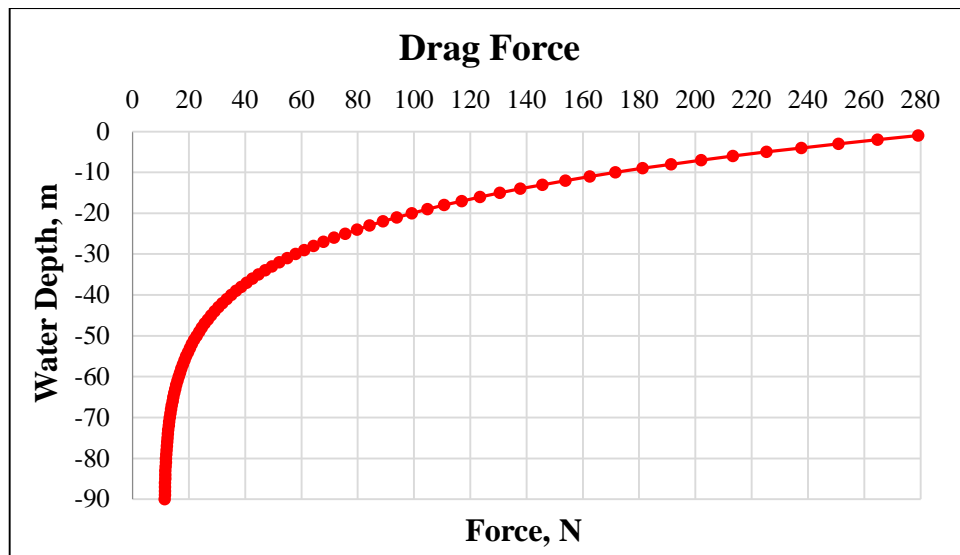


Figure G-4. Distribution of the Drag Force over the water depth

The detailed calculations of the drag force for the case of the 21 inch riser can be found in Excel file on DVD.

G2. Load calculations for 16 inch riser at the conditions of waves with height of 2.5 m

Input Data

Parameter	Designation	Value	Dimension
Wave height	H	2.5	m
Wave amplitude	ξ_0	1.25	m
Period	T	5	s
Water depth	d	100	m
Outer diameter of the riser	D	0.406	m
Water density	ρ	1025	kg/m^3
Standard gravity	g	9.81	m/s^2
Drag coefficient	C_D	1.05	
Mass coefficient	C_M	1.2	

Calculations

1. Wave amplitude:

$$\xi_0 = \frac{H}{2} = 1.25 \text{ m}$$

2. Wave length:

$$L = \frac{g \cdot T^2}{2\pi} = 39.03 \text{ m}$$

3. Angular velocity:

$$\omega = \frac{2\pi}{T} = 1.3 \text{ s}^{-1}$$

4. $k = \frac{2\pi}{L} = 0.161$

5. Checking deep water criterion:

$$\frac{d}{L} = 2.561 > 0.5 \text{ - deep water area}$$

6. Checking conditions for Morison's equation:

$$\frac{D}{L} = 0.01 < 0.2$$

$$\frac{H}{L} = 0.064 \leq 0.14 \text{ - non - breaking waves}$$

$$\frac{a}{D} < 0.2 \rightarrow a < 0.08$$

Assuming that the motion amplitude (a) for the drilling riser is negligible the Morison equation can be used safely to calculate the forces.

7. Calculating the Keulegan-Carpenter number to check which term will dominate in the Morison equation:

$$N_{KC} = \frac{\pi \cdot H}{D} = 6\pi$$

Hence, the both the drag and mass term will be presented in the equation.

8. The Morison equation can be written as follows:

$$F(t) = \int_{-d}^{\xi_0} \left(\rho \cdot \frac{\pi D^2}{4} \right) \cdot C_M \cdot \dot{u} dz + \int_{-d}^{\xi_0} \frac{1}{2} \cdot \rho \cdot C_D \cdot D \cdot u \cdot |u| dz$$

The equation can be solved using the graphical method when each contributing term is plotted on the timeline and the maximum force is found graphically.

9. For deep water zone the horizontal velocity and acceleration can be presented as the following:

$$u = \frac{\xi_0 g k}{\omega} e^{kz} \cdot \sin(\omega t), \quad \dot{u} = \xi_0 g k e^{kz} \cdot \cos(\omega t)$$

Therefore

$$\begin{aligned} F_M(t) &= \int_{-d}^{\xi_0} \left(\rho \cdot \frac{\pi D^2}{4} \right) \cdot C_M \cdot \dot{u} dz = \int_{-d}^{\xi_0} \left(\rho \cdot \frac{\pi D^2}{4} \right) \cdot C_M \cdot \xi_0 g k e^{kz} \cdot \cos(\omega t) dz = \\ &= \left(\rho \cdot \frac{\pi D^2}{4} \right) \cdot C_M \cdot \xi_0 g k \cdot \cos(\omega t) \left[\frac{e^{kz}}{k} \right]_{-d}^{\xi_0} = \\ &= \left(\rho \cdot \frac{\pi D^2}{4} \right) \cdot C_M \cdot \xi_0 g \cdot \cos(\omega t) \left[e^{k\xi_0} - e^{-kd} \right] \end{aligned}$$

and

$$\begin{aligned}
F_D(t) &= \int_{-d}^{\xi_0} \frac{1}{2} \cdot \rho \cdot C_D \cdot D \cdot u \cdot |u| dz = \int_{-d}^{\xi_0} \frac{1}{2} \cdot \rho \cdot C_D \cdot D \cdot \left(\frac{\xi_0 g k}{\omega} e^{kz} \right)^2 \cdot \sin(\omega t) \sin(\omega t) dz = \\
&= \frac{1}{2} \cdot \rho \cdot C_D \cdot D \cdot \left(\frac{\xi_0 g k}{\omega} \right)^2 \cdot \sin(\omega t) \sin(\omega t) \int_{-d}^{\xi_0} e^{2kz} dz = \\
&= \frac{1}{2} \cdot \rho \cdot C_D \cdot D \cdot \left(\frac{\xi_0 g k}{\omega} \right)^2 \cdot \sin(\omega t) \sin(\omega t) \left[\frac{e^{2kz}}{2k} \right]_{-d}^{\xi_0} = \\
&= \frac{1}{4} \cdot \rho \cdot C_D \cdot D \cdot k \cdot \left(\frac{\xi_0 g}{\omega} \right)^2 \cdot \sin(\omega t) \sin(\omega t) \left[e^{2k\xi_0} - e^{-2kd} \right]
\end{aligned}$$

Finally, the expression for the total force calculation can be presented in the next form:

$$\begin{aligned}
F_{Total}(t) &= F_M(t) + F_D(t) = \left(\rho \cdot \frac{\pi D^2}{4} \right) \cdot C_M \cdot \xi_0 g \cdot \cos(\omega t) \left[e^{k\xi_0} - e^{-kd} \right] + \\
&+ \frac{1}{4} \cdot \rho \cdot C_D \cdot D \cdot k \cdot \left(\frac{\xi_0 g}{\omega} \right)^2 \cdot \sin(\omega t) \sin(\omega t) \left[e^{2k\xi_0} - e^{-2kd} \right]
\end{aligned}$$

10. All derived expressions can now be plotted for a 6 s (and 11 s for illustration) wave period and the maximum force impact can be found afterwards.

It is important to notice that the integration is performed up to ξ_0 . This is a conservative simplification because in reality the maximum force occurs in a place between the wave crest and still water level for a given time period. That implies that to be theoretically correct the equation have to be solved for maximum force with variable upper-integration limit, varying from 0 to ξ_0 .

11.

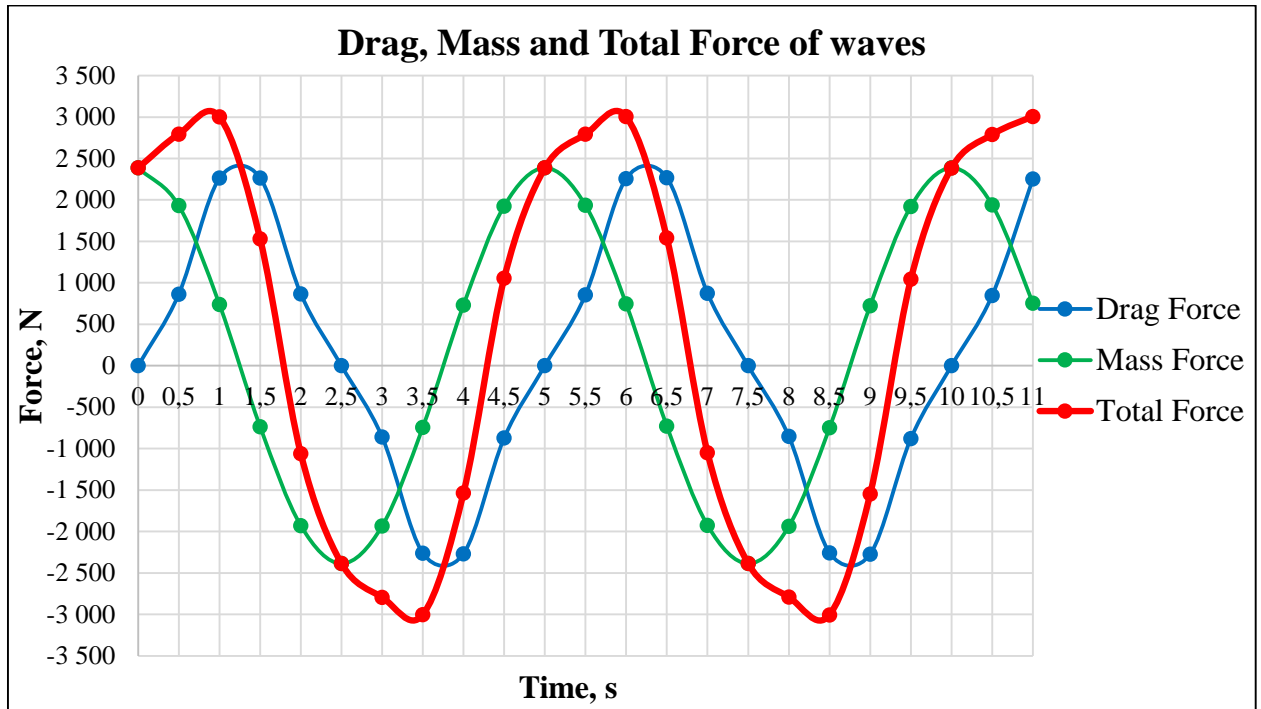


Figure G-5. Drag, Mass and Total Force of wave

The drag, mass and total forces are shown in Figure G-5 as a function of time. It can be observed from Figure the forces express negative values as well but the only positive values should be taken into account.

$$F_{Total} = 3100 \text{ N is at the maximum when } t \approx 0.9 \text{ s.}$$

12.

However, the maximum total force should also be defined and plotted as a function of the water depth. The water depth (z) varies from the top point at the wave crest ($\zeta_0 = 1.25 \text{ m}$) to the depth at which the maximum total force has any observed impact ($F_{Total}(t = 0.9 \text{ s})$ is approximately equal to 0). The step of depth variation is chosen to be equal to 1 m since the size of the cell in the ANSYS model is specified as 1 m.

$$F_{Total}(t = 0.9, z) = F_M(t = 0.9, z) + F_D(t = 0.9, z) = \left(\rho \cdot \frac{\pi D^2}{4} \right) \cdot C_M \cdot \xi_0 g e^{kz} \cdot \cos(\omega t) +$$

$$+ \frac{1}{2} \cdot \rho \cdot C_D \cdot D \cdot k \cdot \left(\frac{\xi_0 g k}{\omega} e^{kz} \right)^2 \cdot \sin(\omega t) \sin(\omega t)$$

13.

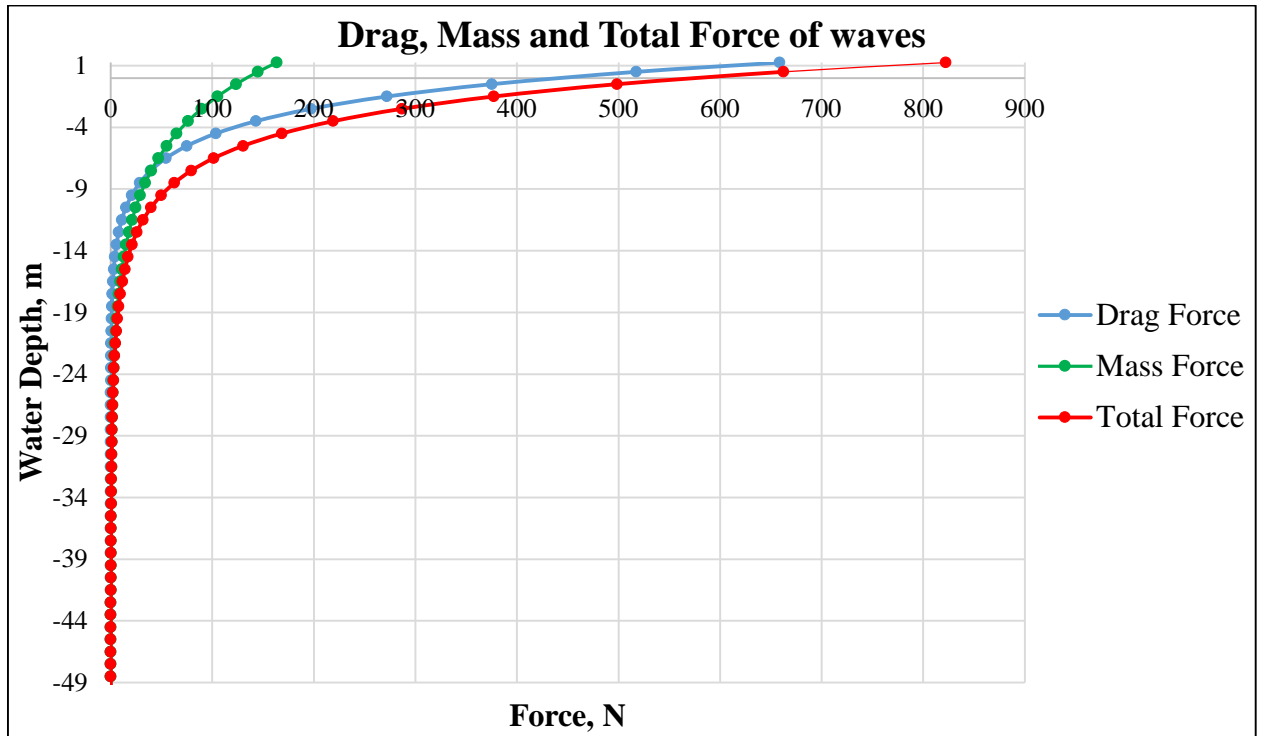


Figure G-6. Distribution of Drag, Mass and Total Force of wave over the water depth

The detailed calculations of forces are presented in Excel file on DVD.

Since the drilling riser is also exposed to the sea current therefore current forces should be determined in order to apply them on the riser structure in the ANSYS model. For calculation of forces acting on the riser at a constant current the only drag term is taken into consideration in the Morison equation. The distribution of the current velocity over the water depth can be found by the Power Law equation used in OrcaFlex (see Appendix E and Chapter 6.2.3).

Input Data

Parameter	Designation	Value	Dimension
Current velocity at the surface	S_0	1	m/s
Current velocity at the sea bottom	S_b	0.2	m/s
Water depth	d	100	m
Outer diameter of the riser	D	0.406	m
Water density	ρ	1025	kg/m^3
Standard gravity	g	9.81	m/s^2
Drag coefficient	C_D	1.05	
Power Law Exponent	<i>Exponent</i>	0.3	

Calculations

1. Current velocity:

$$S(z) = S_b + (S_f - S_b) \times ((z - z_b) / (z_f - z_b))^{1/Exponent}$$

where z varies from 0 to 90 m as the bottom end of the riser is located 10 m above the seabed.

2. Average velocity of the current:

$$S_{average} = \frac{S_n + S_{n+1}}{2}$$

3. Finally the drag force can be calculated using the following equation:

$$F_{Total} = F_D = \int_{z'-\Delta z}^{z'} f_D(z, t) dz = \int_{z'-\Delta z}^{z'} \frac{1}{2} \cdot \rho \cdot C_D \cdot D \cdot u \cdot |u| dz = \frac{1}{2} \cdot \rho \cdot C_D \cdot D \cdot u^2 \cdot \Delta z$$

where $u = S_{average}$

The step of the water depth variation (Δz) is equal to 1 m due to the cell length (1 m) in the mesh created on the riser structure.

4. The calculation results are presented in Table G-2.

Water Depth, z	Δz	Current Velocity, $S(z)$	Average Velocity of the Current, $S_{average}$	Drag Force, F_D
m	m	m/s	m/s	N
0	-	1,000	-	-
-1	1	0,974	0,987	213
-2	1	0,948	0,961	202
-3	1	0,923	0,935	191
-4	1	0,898	0,910	181
-5	1	0,874	0,886	172
-6	1	0,851	0,863	163
-7	1	0,828	0,840	154
-8	1	0,806	0,817	146
-9	1	0,784	0,795	138
-10	1	0,763	0,774	131
-11	1	0,742	0,753	124
-12	1	0,722	0,732	117
-13	1	0,703	0,713	111
-14	1	0,684	0,693	105
-15	1	0,665	0,675	99
-16	1	0,647	0,656	94
-17	1	0,630	0,639	89
-18	1	0,613	0,621	84

-19	1	0,596	0,605	80
-20	1	0,580	0,588	76
-21	1	0,565	0,572	72
-22	1	0,549	0,557	68
-23	1	0,535	0,542	64
-24	1	0,520	0,528	61
-25	1	0,507	0,514	58
-26	1	0,493	0,500	55
-27	1	0,480	0,487	52
-28	1	0,468	0,474	49
-29	1	0,455	0,462	47
-30	1	0,444	0,450	44
-31	1	0,432	0,438	42
-32	1	0,421	0,427	40
-33	1	0,411	0,416	38
-34	1	0,400	0,405	36
-35	1	0,390	0,395	34
-36	1	0,381	0,386	32
-37	1	0,371	0,376	31
-38	1	0,363	0,367	29
-39	1	0,354	0,358	28
-40	1	0,346	0,350	27
-41	1	0,338	0,342	26
-42	1	0,330	0,334	24
-43	1	0,323	0,327	23
-44	1	0,316	0,319	22
-45	1	0,309	0,312	21
-46	1	0,303	0,306	20
-47	1	0,296	0,299	20
-48	1	0,290	0,293	19
-49	1	0,285	0,288	18
-50	1	0,279	0,282	17
-51	1	0,274	0,277	17
-52	1	0,269	0,272	16
-53	1	0,265	0,267	16
-54	1	0,260	0,262	15
-55	1	0,256	0,258	15
-56	1	0,252	0,254	14
-57	1	0,248	0,250	14
-58	1	0,244	0,246	13
-59	1	0,241	0,243	13
-60	1	0,238	0,239	13
-61	1	0,235	0,236	12
-62	1	0,232	0,233	12
-63	1	0,229	0,230	12
-64	1	0,227	0,228	11

-65	1	0,224	0,225	11
-66	1	0,222	0,223	11
-67	1	0,220	0,221	11
-68	1	0,218	0,219	10
-69	1	0,216	0,217	10
-70	1	0,214	0,215	10
-71	1	0,213	0,214	10
-72	1	0,211	0,212	10
-73	1	0,210	0,211	10
-74	1	0,209	0,210	10
-75	1	0,208	0,208	9
-76	1	0,207	0,207	9
-77	1	0,206	0,206	9
-78	1	0,205	0,206	9
-79	1	0,204	0,205	9
-80	1	0,204	0,204	9
-81	1	0,203	0,203	9
-82	1	0,203	0,203	9
-83	1	0,202	0,202	9
-84	1	0,202	0,202	9
-85	1	0,201	0,202	9
-86	1	0,201	0,201	9
-87	1	0,201	0,201	9
-88	1	0,201	0,201	9
-89	1	0,201	0,201	9
-90	1	0,200	0,200	9

Table G-2. Drag force calculations

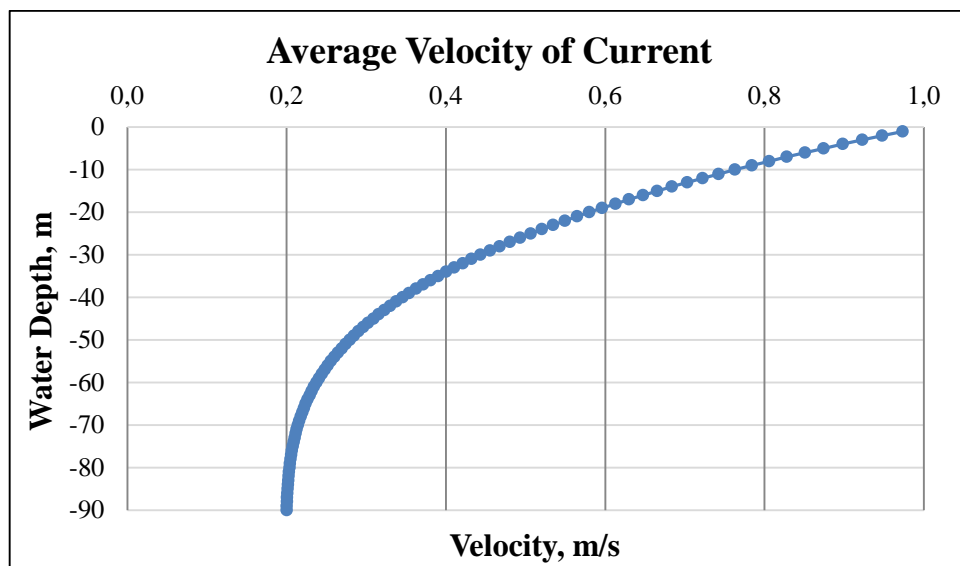


Figure G-7. Average velocity of the current over the water depth

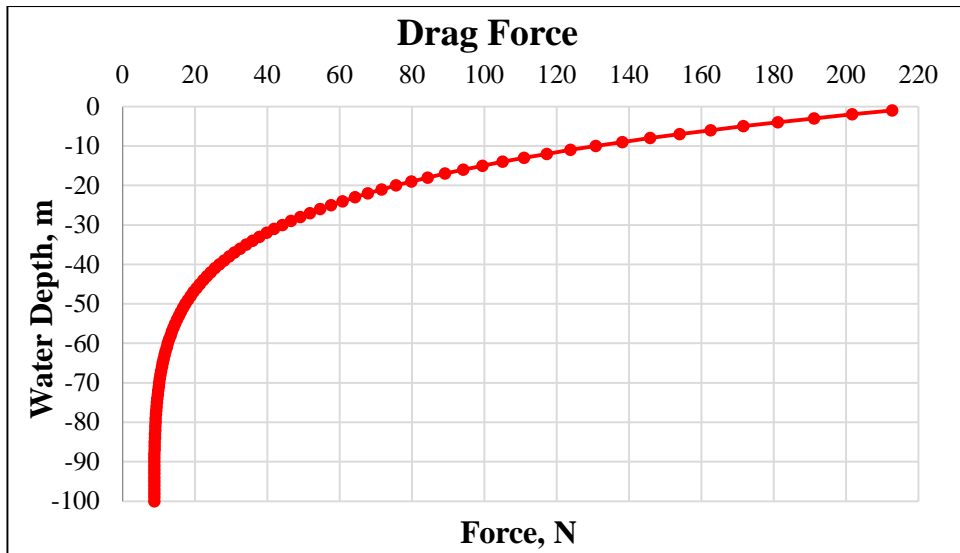


Figure G-8. Distribution of the Drag Force over the water depth

The detailed calculations of the drag force for the case of the 16 inch riser can be found in Excel file on DVD.

G3. Load calculations for 16 inch riser at the conditions of waves with height of 8 m

Input Data

Parameter	Designation	Value	Dimension
Wave height	H	8	m
Wave amplitude	ξ_0	4	m
Period	T	8	s
Water depth	d	100	m
Outer diameter of the riser	D	0.406	m
Water density	ρ	1025	kg/m^3
Standard gravity	g	9.81	m/s^2
Drag coefficient	C_D	1.05	
Mass coefficient	C_M	1.2	

Calculations

1. **Wave amplitude:**

$$\xi_0 = \frac{H}{2} = 4 \text{ m}$$

2. **Wave length:**

$$L = \frac{g \cdot T^2}{2\pi} = 100 \text{ m}$$

3. **Angular velocity:**

$$\omega = \frac{2\pi}{T} = 0.8 \text{ s}^{-1}$$

4. $k = \frac{2\pi}{L} = 0.063$

5. **Checking deep water criterion:**

$$\frac{d}{L} = 1 > 0.5 \text{ - deep water area}$$

6. Checking conditions for Morison's equation:

$$\frac{D}{L} = 0.004 < 0.2$$

$$\frac{H}{L} = 0.08 \leq 0.14 \text{ - non - breaking waves}$$

$$\frac{a}{D} < 0.2 \rightarrow a < 0.08$$

Assuming that the motion amplitude (a) for the drilling riser is negligible the Morison equation can be used safely to calculate the forces.

7. Calculating the Keulegan-Carpenter number to check which term will dominate in the Morison equation:

$$N_{KC} = \frac{\pi \cdot H}{D} = 19.7\pi$$

Hence, the drag will be dominating in the equation.

8. The Morison equation can be written as follows:

$$F(t) = \int_{-d}^{\xi_0} \left(\rho \cdot \frac{\pi D^2}{4} \right) \cdot C_M \cdot \dot{u} dz + \int_{-d}^{\xi_0} \frac{1}{2} \cdot \rho \cdot C_D \cdot D \cdot u \cdot |u| dz$$

The equation can be solved using the graphical method when each contributing term is plotted on the timeline and the maximum force is found graphically.

9. For deep water zone the horizontal velocity and acceleration can be presented as the following:

$$u = \frac{\xi_0 g k}{\omega} e^{kz} \cdot \sin(\omega t), \quad \dot{u} = \xi_0 g k e^{kz} \cdot \cos(\omega t)$$

Therefore

$$\begin{aligned} F_M(t) &= \int_{-d}^{\xi_0} \left(\rho \cdot \frac{\pi D^2}{4} \right) \cdot C_M \cdot \dot{u} dz = \int_{-d}^{\xi_0} \left(\rho \cdot \frac{\pi D^2}{4} \right) \cdot C_M \cdot \xi_0 g k e^{kz} \cdot \cos(\omega t) dz = \\ &= \left(\rho \cdot \frac{\pi D^2}{4} \right) \cdot C_M \cdot \xi_0 g k \cdot \cos(\omega t) \left[\frac{e^{kz}}{k} \right]_{-d}^{\xi_0} = \\ &= \left(\rho \cdot \frac{\pi D^2}{4} \right) \cdot C_M \cdot \xi_0 g \cdot \cos(\omega t) \left[e^{k\xi_0} - e^{-kd} \right] \end{aligned}$$

and

$$\begin{aligned}
F_D(t) &= \int_{-d}^{\xi_0} \frac{1}{2} \cdot \rho \cdot C_D \cdot D \cdot u \cdot |u| dz = \int_{-d}^{\xi_0} \frac{1}{2} \cdot \rho \cdot C_D \cdot D \cdot \left(\frac{\xi_0 g k}{\omega} e^{kz} \right)^2 \cdot \sin(\omega t) \sin(\omega t) dz = \\
&= \frac{1}{2} \cdot \rho \cdot C_D \cdot D \cdot \left(\frac{\xi_0 g k}{\omega} \right)^2 \cdot \sin(\omega t) \sin(\omega t) \int_{-d}^{\xi_0} e^{2kz} dz = \\
&= \frac{1}{2} \cdot \rho \cdot C_D \cdot D \cdot \left(\frac{\xi_0 g k}{\omega} \right)^2 \cdot \sin(\omega t) \sin(\omega t) \left[\frac{e^{2kz}}{2k} \right]_{-d}^{\xi_0} = \\
&= \frac{1}{4} \cdot \rho \cdot C_D \cdot D \cdot k \cdot \left(\frac{\xi_0 g}{\omega} \right)^2 \cdot \sin(\omega t) \sin(\omega t) \left[e^{2k\xi_0} - e^{-2kd} \right]
\end{aligned}$$

Finally, the expression for the total force calculation can be presented in the next form:

$$\begin{aligned}
F_{Total}(t) &= F_M(t) + F_D(t) = \left(\rho \cdot \frac{\pi D^2}{4} \right) \cdot C_M \cdot \xi_0 g \cdot \cos(\omega t) \left[e^{k\xi_0} - e^{-kd} \right] + \\
&+ \frac{1}{4} \cdot \rho \cdot C_D \cdot D \cdot k \cdot \left(\frac{\xi_0 g}{\omega} \right)^2 \cdot \sin(\omega t) \sin(\omega t) \left[e^{2k\xi_0} - e^{-2kd} \right]
\end{aligned}$$

10. All derived expressions can now be plotted for a 2 s (and 10 s for illustration) wave period and the maximum force impact can be found afterwards.

It is important to notice that the integration is performed up to ξ_0 . This is a conservative simplification because in reality the maximum force occurs in a place between the wave crest and still water level for a given time period. That implies that to be theoretically correct the equation have to be solved for maximum force with variable upper-integration limit, varying from 0 to ξ_0 .

11.

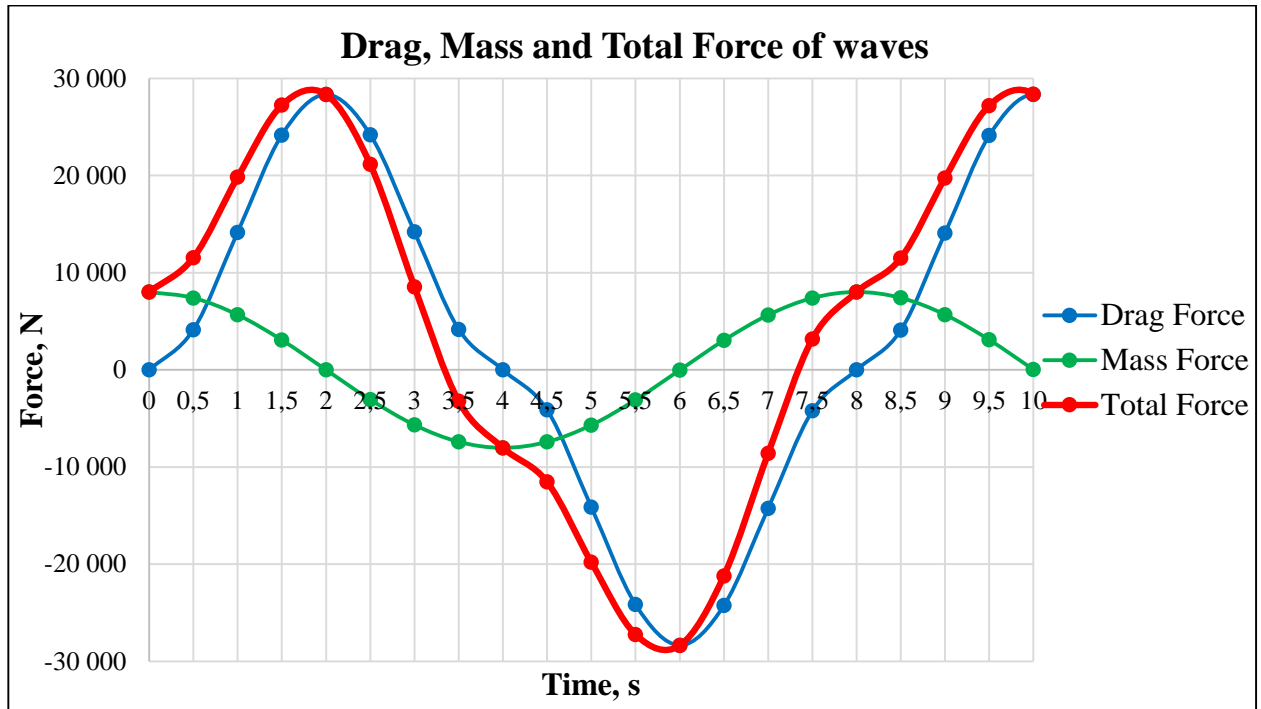


Figure G-9. Drag, Mass and Total Force of wave

The drag, mass and total forces are shown in Figure G-9 as a function of time. It can be observed from Figure the forces express negative values as well but the only positive values should be taken into account.

$$F_{Total} = 29\,000 \text{ N is at the maximum when } t \approx 1.9 \text{ s.}$$

12.

However, the maximum total force should also be defined and plotted as a function of the water depth. The water depth (z) varies from the top point at the wave crest ($\xi_0 = 4 \text{ m}$) to the depth at which the maximum total force has any observed impact ($F_{Total}(t = 1.9 \text{ s})$ is approximately equal to 0). The step of depth variation is chosen to be equal to 1 m since the size of the cell in the ANSYS model is specified as 1 m.

$$F_{Total}(t = 1.9, z) = F_M(t = 1.9, z) + F_D(t = 1.9, z) = \left(\rho \cdot \frac{\pi D^2}{4} \right) \cdot C_M \cdot \xi_0 g e^{kz} \cdot \cos(\omega t) + \frac{1}{2} \cdot \rho \cdot C_D \cdot D \cdot k \cdot \left(\frac{\xi_0 g k}{\omega} e^{kz} \right)^2 \cdot \sin(\omega t) \sin(\omega t)$$

13.

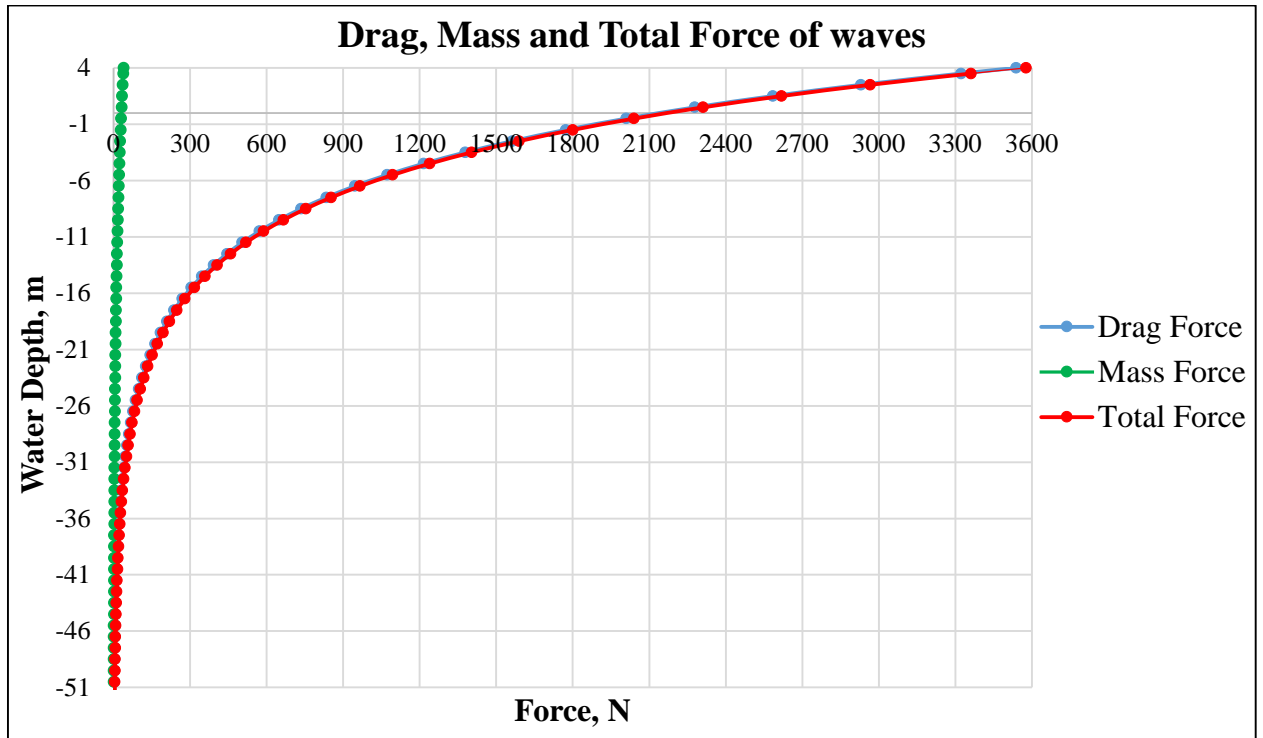


Figure G-10. Distribution of Drag, Mass and Total Force of wave over the water depth

The detailed calculations of forces are presented in Excel file on DVD.

Since the drilling riser is also exposed to the sea current therefore current forces should be determined in order to apply them on the riser structure in the ANSYS model. The drag forces in case of 16 inch riser operated in the presence of waves with height of 8 m are the same as in the previous Appendix G-2.